Final report: HI-EPS

-Highly integrated electric propulsion system

ENS Journalnr.: 64009-0218

Project consortium:

Aalborg University

Serenergy

Lithium-Balance

Cemtec

Preface

This report documents the results obtained in the HI-EPS project funded by the EUDP 2009-II program under the contract 64009-0218 during the period from January 2010 to December 2012. The project partners were Aalborg University (project manager), Serenergy, Lithium-Balance and Cemtec.

The project vision was to solve the last two inherent problems faced by electric vehicles; A short range and a long recharging time. This was achieved by the development of a highly integrated power propulsion system (HI-EPS) consisting of; an efficient methanol fuel cell system and a lithium-ion battery pack including an advanced battery managing system (BMS). This enables electric vehicles to have a range of at least 600 km pr. charge and a refueling ability similar to gasoline fuelled vehicles. By using methanol as fuel the obstacles towards market introduction caused by the low energy density and infrastructure problems associated with hydrogen is circumvented.

The main report presents key results and conclusion. Further details can be found in the appendices in the form of scientific publications, technical reports and marketing material.

Summary and conclusion

The original project idea was to develop an integrated propulsion system consisting of a battery pack with battery management system and a fuel cell system for range extension. Serenergy and Lithium-Balance would offer this product to the automotive industry as an integrated unit. This idea was pursued in the first phases of the project and a system PID and communication concept was successfully developed. However, during later phases of the project this concept turned out to be difficult to sell and it was not possible to find a suitable demonstration partner for the unit. The main reason is that most car manufacturers have either their own battery system and are interested in the range extender alone or they have only an interest in the battery system. For this reason it was decided to pursue separate marketing and sales channels for each of the two parts individually.

These difficulties lead to the decision that the demonstration phase of the project was changed from collaboration with the car industry and integration into a commercial or pre-commercial vehicle to laboratory testing and demonstration. This also allowed much more focus to be put on the technology development and testing to be done under well-defined conditions without excessive practical vehicle integration efforts.

With these changes in scope, the project has successfully developed the key technologies that were planned in the original project. A 5 kW methanol fueled range extender system based on a liquid cooled high temperature PEM fuel cell was developed and tested at Serenergy. The reformer and the fuel cell stack designs were developed through this project in synergy with amongst others the COBRA project. The fact that a complete new liquid cooled fuel cell stack was developed constitutes a substantial extension of the original ambition and scope that was to use an existing air cooled stack design. Lithium-Balance developed a new BMS system that can be certified to automotive standards including diagnostics features and a modular design.

The integrated battery system coupled with the range extender was successfully demonstrated in June/July 2012. Subjected to a simulated power consumption profile of the electric Mitsubishi iMev during a New European Drive Cycle (NEDC), it was verified that a range of 600 km can be achieved.

Serenergy has initiated activities with Daimler, AUDI and HYUNDAI where the fuel cell range extender will be implemented in test and demonstration vehicles. In parallel with these activities, the fuel cell system is further developed in the COBRA-II project. The battery management system is further developed by Lithium-Balance in collaboration with FIAT and PORSCHE and with financial support from the EUDP program. The commercial launch is planned to take place in November 2013 at the EVS conference in Barcelona and production is expected to start in the first quarter of 2014.

Technical achievements

The project was realized through a number of work packages (WP) ranging from overall system design and control through development of subsystems to individual components. The results of each work package are described below with additional details in the appendices.

WP2: System Layout (**AAU**, SER, LIBA)

The objective of this work package was to develop the overall system layout. An existing model that simulates the energy flow from batteries and fuel cell system during a given drive cycle was further developed and extended to include the fuel cell range extender. The model simulations provide the link between the vehicle technical specifications, a given drive cycle, and the power consumption of the vehicle. The performance of a given propulsion system can be assed when subjected to the predicted power consumption of the vehicle to estimate driving range, maximum speed, efficiency and so on. Alternatively, the power consumption can be used with an electronic load connected to a real propulsion system to emulate the performance in a real vehicle. Both applications were pursued in the projects. The initial work focused on selection of appropriate range extender and battery pack sizes. Subsequently, a specific propulsion system was set up in the laboratory and tested when subjected to the calculated power consumption pattern. This procedure is schematically illustrated in Figure 1.

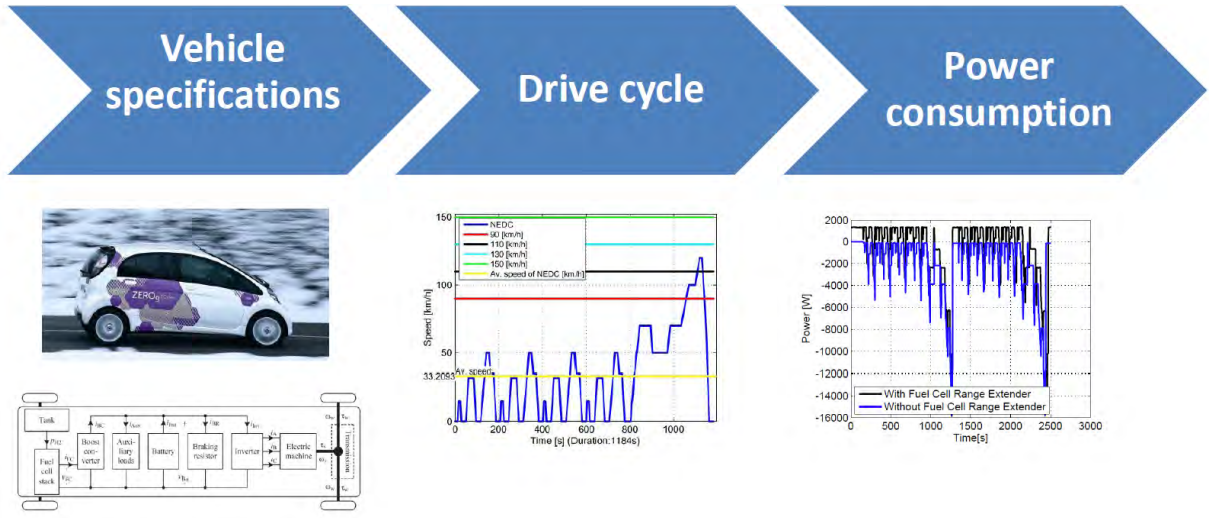

Figure 1 Vehicle simulation procedure

The demonstration activities were focused around a small city vehicle and the Mitsubishi iMEV was used as an example as fairly detailed specifications were available for this car. The New European Drive Cycle (NEDC) was used to determine the power consumption. To size the range extender and the battery pack the following criteria were used.

1. The range extender should deliver the average power consumption during the drive cycle which will ensure that the driving range is only limited by the size of the fuel tank.
2. The battery pack should be able to deliver the peak power required during the high speed driving part of the drive cycle and during accelerations.

The peak power encountered during the simulated drive cycle was 48 kW and the average power consumption was 5 kW. To meet the peak power demand would require a too large battery pack to be economically feasible within the project budget. Therefore the entire system was scaled down by a factor of 3 leading to a 16 kWh battery pack and a 1.7 kW range extender system.

Further details on the vehicle simulations and a number of simulation results are presented in a scientific paper published in IEEE Transactions on Vehicle Technology (see appendix 1).

The laboratory testing of the described system was conducted at Serenergy in June 2012. A schematic of the test setup is shown in Figure 2.

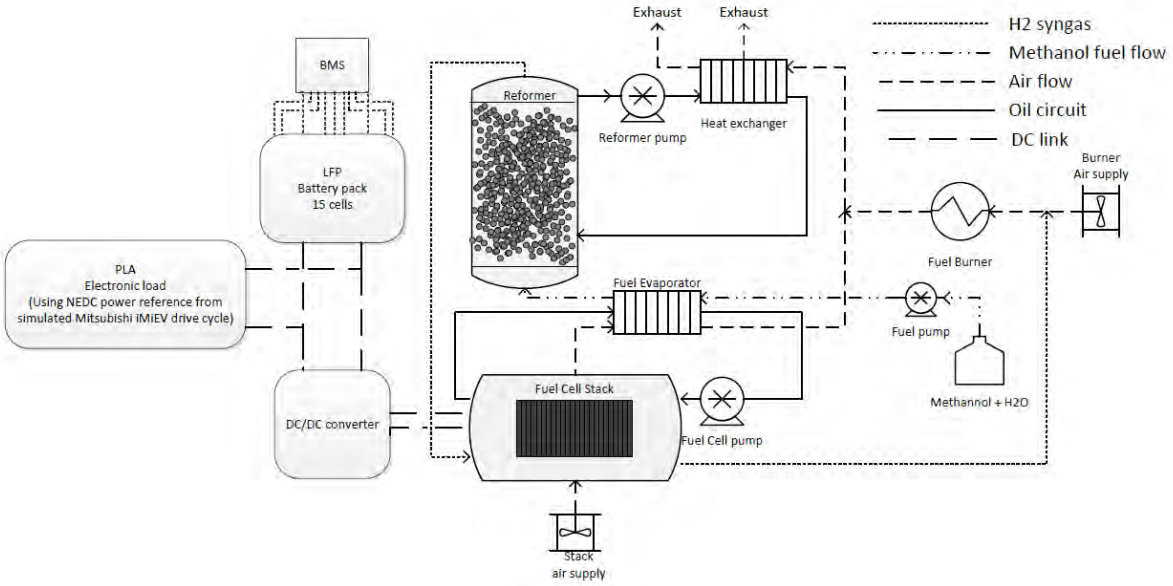

Figure 2 Schematic of the HI-EPS battery and range extender system.

For practical reasons a 5 kW range extender was used but with the power output limited to 1.7 kW as mentioned above. The measured power consumptions/productions during two drive cycles with and without the fuel cell range extender enabled are shown in Figure 3.

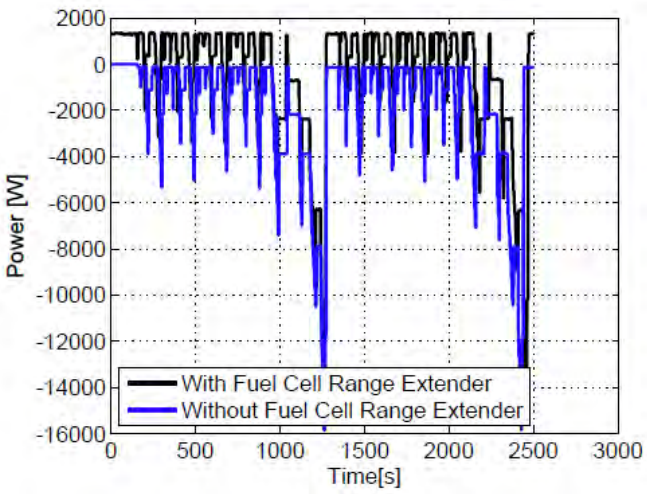

Figure 3 Measured power consumption and production with and without range extender.

The simulated drive cycle based upon which the range extender was sized included regeneration of braking power. This was not possible to include during the laboratory experiments for which reason the average power consumption during the drive cycle exceeded the fixed range extender power. This caused a slightly decreasing battery voltage during the experiments. Except for this minor issue, the laboratory testing demonstrated the feasibility of the system and proved that the desired driving range can be met. During the experiments the system efficiency was measured and the result is shown in Figure 4. Two curves are included; one showing the stack efficiency and one showing calculated system efficiency where the auxiliary power consumption from balance of plant components is accounted for.

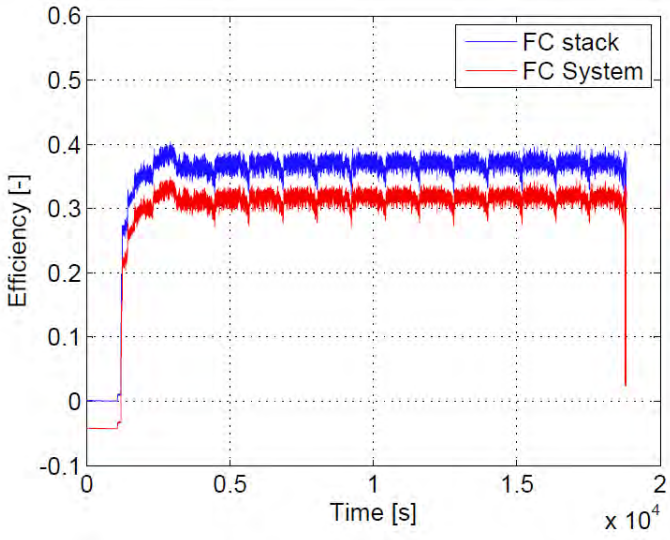

Figure 4 Measured range extender electric efficiency during drive cycles.

As seen, the system electric efficiency was around 32% which is considered fully acceptable given the fact that a prototype system was used for the tests and that it was operated at 33% of the rated power. Further details about the tests can be found in appendix 2 that contains a scientific paper submitted for publication in the International Journal of Hydrogen Energy.

As a final remark on the system efficiency it should be noted that an essential advantage of using the range extender coupled with the battery pack, in addition to the extended range, is the ability to utilize the waste heat. The waste heat can be used to heat the passenger compartment and the battery pack when needed. This heat should otherwise have been supplied by the batteries or another external heat source. Therefore it can be argued that it is reasonable to define a CHP efficiency of the range extender system when part of the waste heat is utilized. For a 10 kW range extender this leads to a graph as shown in Figure 5.

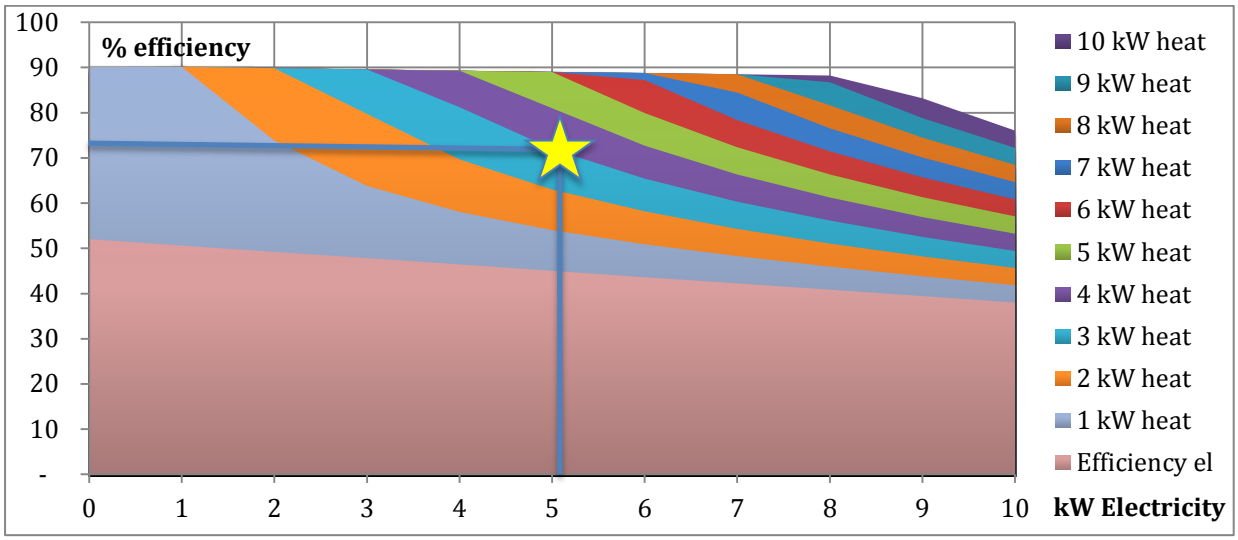

Figure 5 Map of range extender CHP efficiency based on full or partial utilization of waste heat.

As seen, a total efficiency of 70-80% is obtainable when there is a heating demand. Further discussion of the waste heat utilization is given in the market analysis report included in appendix 3.

WP3: Reformer optimization (**AAU**, SER)

An updated reformer (generation 2.0) was designed, manufactured and tested. The main design criteria with respect to physical parameters were; low weight, high durability and low production costs. Concerning the performance, the key parameters were; reduced operating temperature, reduced steam to carbon ratio and minimum CO production.

Testing carried out on a previously developed 350W system with an integrated methanol reformer gave very important input for design of a reformer for the 5 kW system. A problem regarding degradation of the reformer catalyst and corrosion of metal structures in reformer related components was seen. This meant that focus at the early stages was on pre-design material tests. This involved reformer catalyst tests, with a special focus on methanol slip rates and surface treatment of aluminum structures. In short it was learned that the reformer catalyst bed/cavity had to be larger than initially expected i.e. the space velocity was reduced.

The reformer in the 350W system is milled from an aluminum block. The use of fins milled in aluminum gives great heat transfer properties from the burner air, into the reformer bed where it is needed. A new approach is taken for the first generation reformer for the larger system. To reduce weight and increase durability the reformer design is a standard shell and tube structure made of thin walled stainless steel tubing. The fairly complex tubular design is manufactured by a German partner that excels in welding stainless steel tubes. Similar processes are used by the same manufacturer for the automotive industry, which shows that despite the complex nature of the design, it is possible to manufacture at a low cost.

The removal of the fins and change of material to stainless steel decreases heat transfer but this is compensated for by using liquid, instead of air, heating. The same liquid used in the fuel cell will be used to heat the reformer. The reformer catalyst is placed in the small, inner tubes, while heating fluid is pumped through the outer shell to provide heat for the reaction. The methanol/water mix is provided in a superheated vapor state in one end of the reactor and the hydrogen rich product flows from the other end. This approach removes the need for electric pre-heating of the reformer as it can be heated with the liquid, which is heated in the burner.

Reformate quality is also a very important parameter. The liquid heating approach will result in closer to isothermal operation of the reformer, making it possible to ensure low CO levels in the reformate gas. Temperature increases at the outlet of the reformer was previously seen to result in higher CO concentrations. Decreased methanol slip will be achieved and maintained throughout the module's lifetime by increasing the volume of catalyst per watt produced. The small reformer has 0.23mL/W produced, whereas the new reformer design has 0.42mL/W. The first prototype of the reformer and a detailed outline is presented in Figure 6**Error! Reference source not found.**.

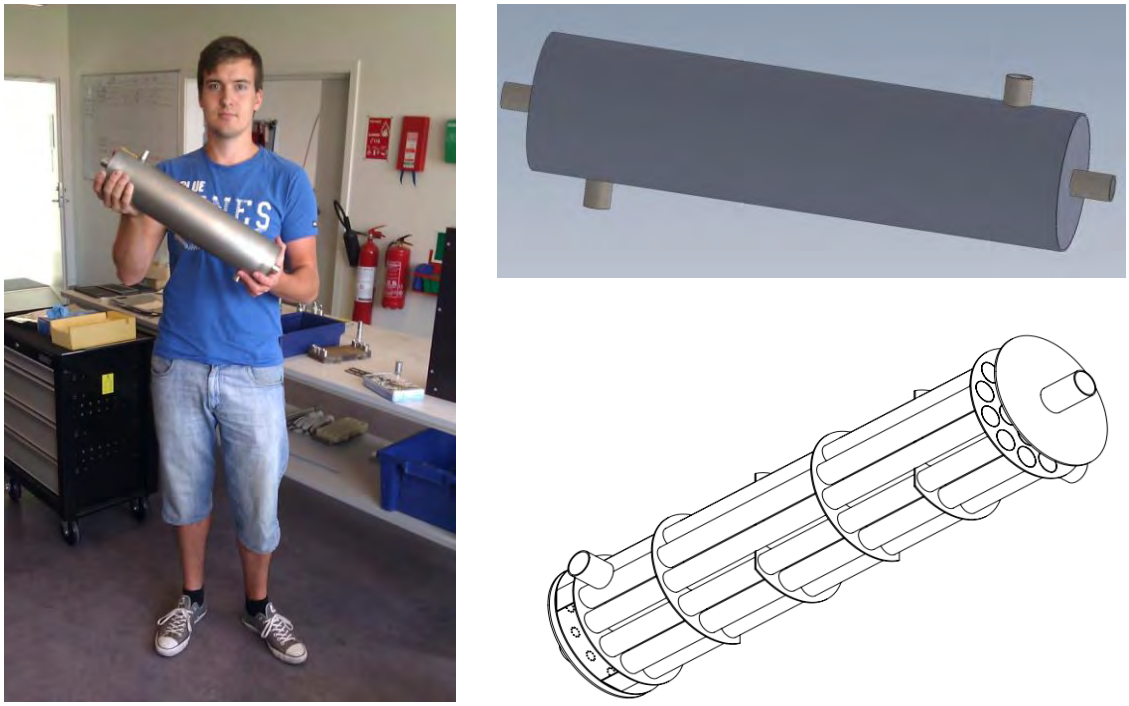

Figure 6 Photo and outline drawings of the developed 5 kW methanol reformer.

The prototype was thoroughly tested covering a range of operating temperatures and steam-to-carbon ratios. The testing was performed both at Serenergy and at AAU. The test setup at AAU is shown in Figure 7.

Figure 7 Reformer test setup at AAU.

In parallel with the testing a detailed Computational Fluid Dynamics (CFD) model of the reformer was developed accounting for the fluid flow, heat and mass transfer as well as the reforming process. An outline of the CFD model is shown in Figure 8.

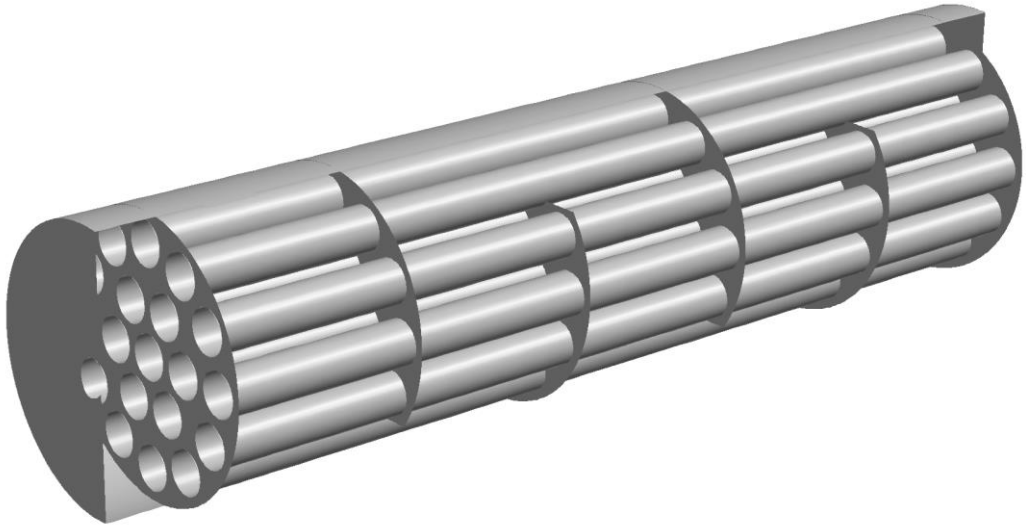

Figure 8 Outline of the computational fluid dynamics model of the methanol reformer.

The model predicts the methanol steam reforming process and gives detailed insight into the methanol conversion process as well as the carbon monoxide formation. As an example, a contour plot of predicted carbon monoxide is presented in Figure 9.

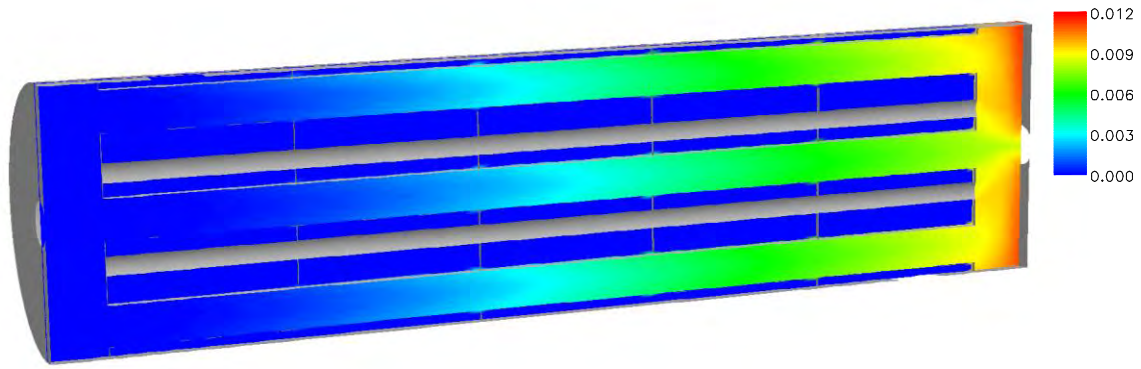

Figure 9 Mole fraction of carbon monoxide at the reactor center plane.

The model predictions were compared to the measurements performed using the setups described above. Overall very good agreement between measurements and model prediction was found as seen from Figure 10 showing the carbon monoxide concentration in the reformate versus fuel flow.

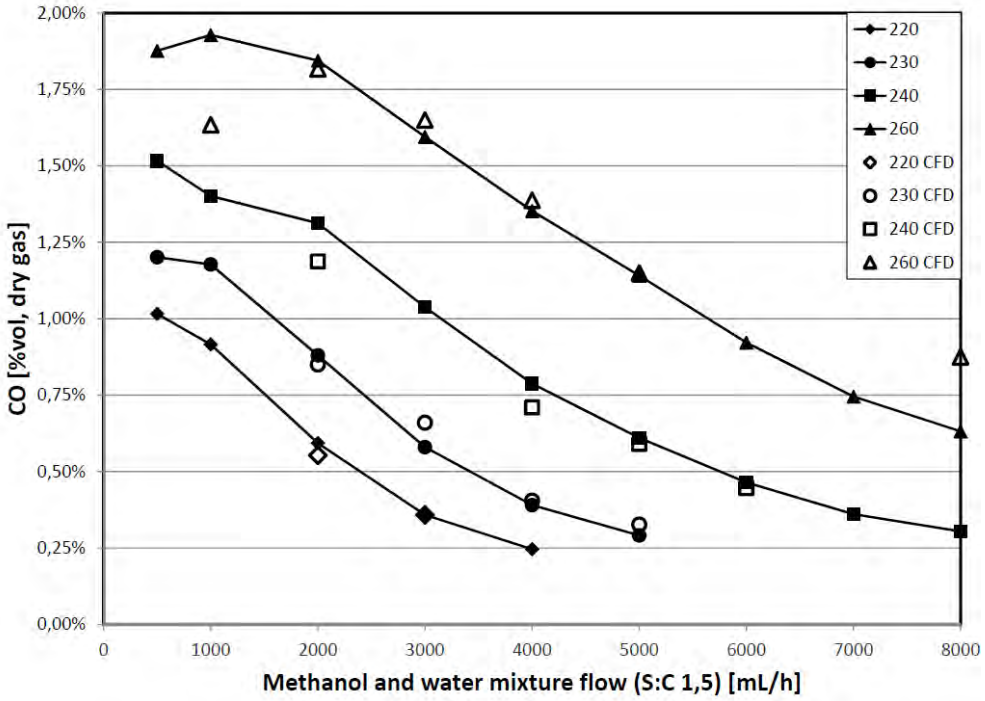

Figure 10 Measured and predicted CO concentration versus fuel flow rate and temperature.

With the developed model operational parameters as well as geometry design parameters could be studied without having to manufacture the reformer. As an example, the influence from steam-to-carbon was analyzed by comparing axial methanol and carbon monoxide profiles at steam-to-carbon ratios of 1.2 and 1.5. The result is shown in Figure 11.

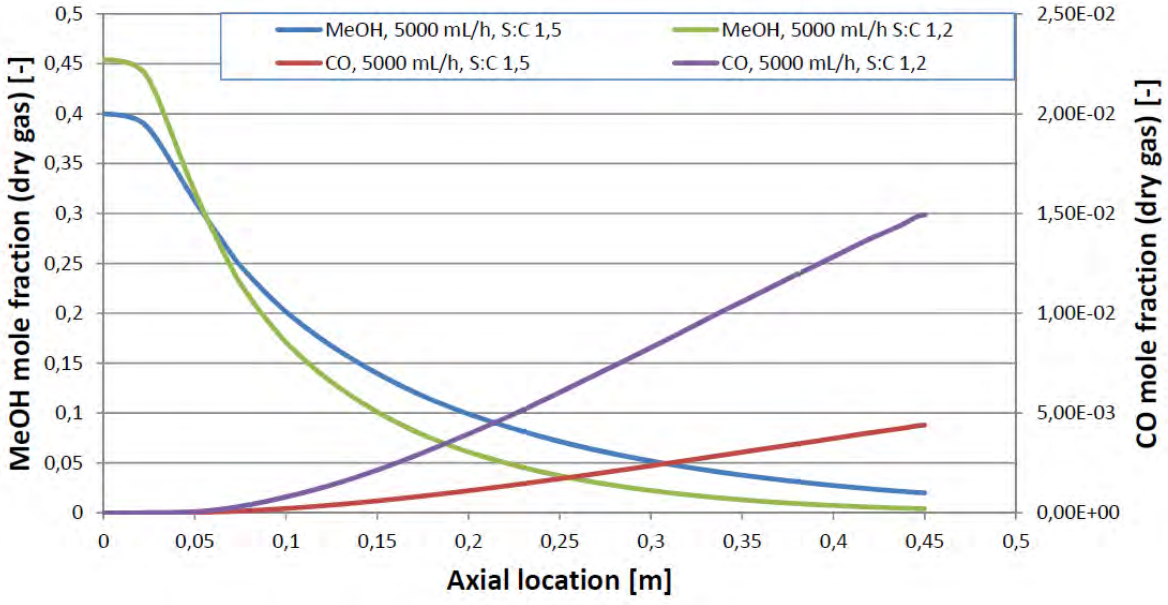

Figure 11 Axial methanol and CO profiles versus steam-to-carbon ratio.

Further details about the CFD model and the model prediction can be found in appendix 4.

WP4: Fuel cell stack optimization (**SER**, AAU)

The original intention was to use an existing stack design based on air cooling and further develop the design in the HI-EPS project with particular focus on the bipolar plates and the sealing. However, it was decided to develop a completely new stack design based on liquid cooling as it offers several advantages for larger fuel cell powers including better temperature control and decreased air flow through the cathode. The stack development was a joint effort with the COBRA project with the main focus of the HI-EPS project being on the bipolar plates and the sealing concept and materials.

In Figure 12 below, the CAD design of the new fuel cell stack can be seen. The stack is composed of 165cm2 cells, much larger than the 45cm2 used in the air cooled stack. For each cell there are two plates and one Membrane Electrode Assembly (MEA). The plates distribute the reactants for the electrochemical reaction and the coolant. In both ends of the stack extra stiff endplates are mounted; in order keep an even pressure across the whole 165cm2, furthermore pipes and current collectors are connected to these plates as can be seen in the pictures below. The CAD drawing shows the concept for a full length (120 cell) stack while an assembled 20 cell stack can be seen in the photograph.

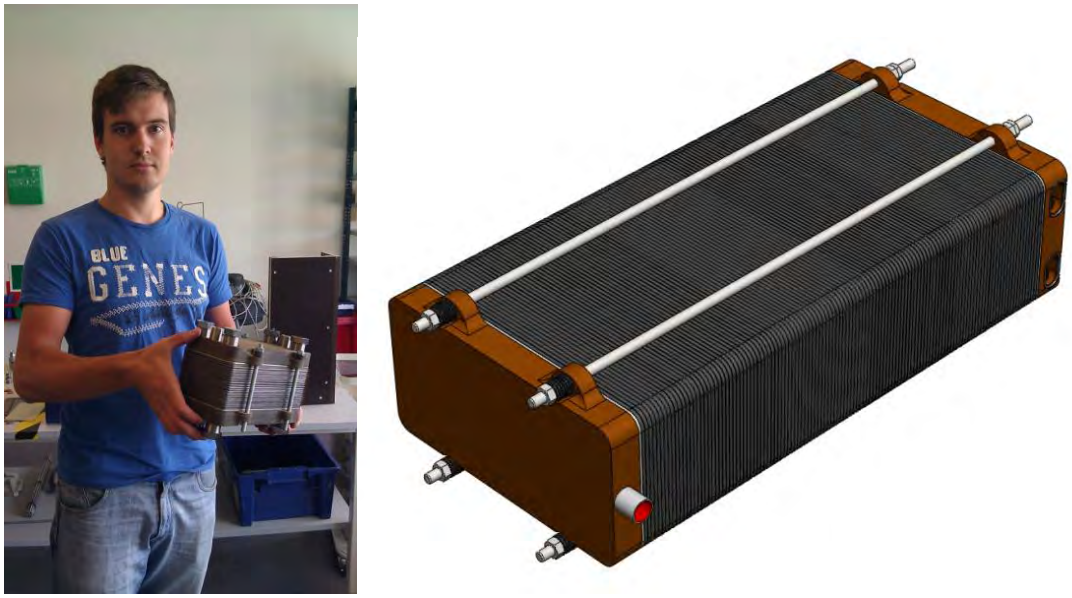

Figure 12 The developed liquid cooled stack concept.

WP4a: New bipolar plates

The objective of this work package was to develop lighter and cheaper bipolar plates with improved durability. Traditionally graphite based bipolar plates have been applied for PEM fuel cells. Graphite based plates have good properties with regards to low electrical resistance, high corrosion resistance and good thermal properties. However graphite plates can be difficult and expensive to manufacture within the necessary tolerances, furthermore they can in some cases have problems with low mechanical strength and high porosity. The latter is suspected to result in faster performance degradation of the fuel cell stack.

Because of the above mentioned problems it is relevant to do a survey of the currently available plate materials for HTPEM fuel cell stacks. In Figure 13 below a framework for material selection is presented. As it is seen two overall categories have been investigated; composite plates and metal plates. Composite plates are typically a combination of graphite and a polymer binder, but in some cases other materials can be added such as metal powder.

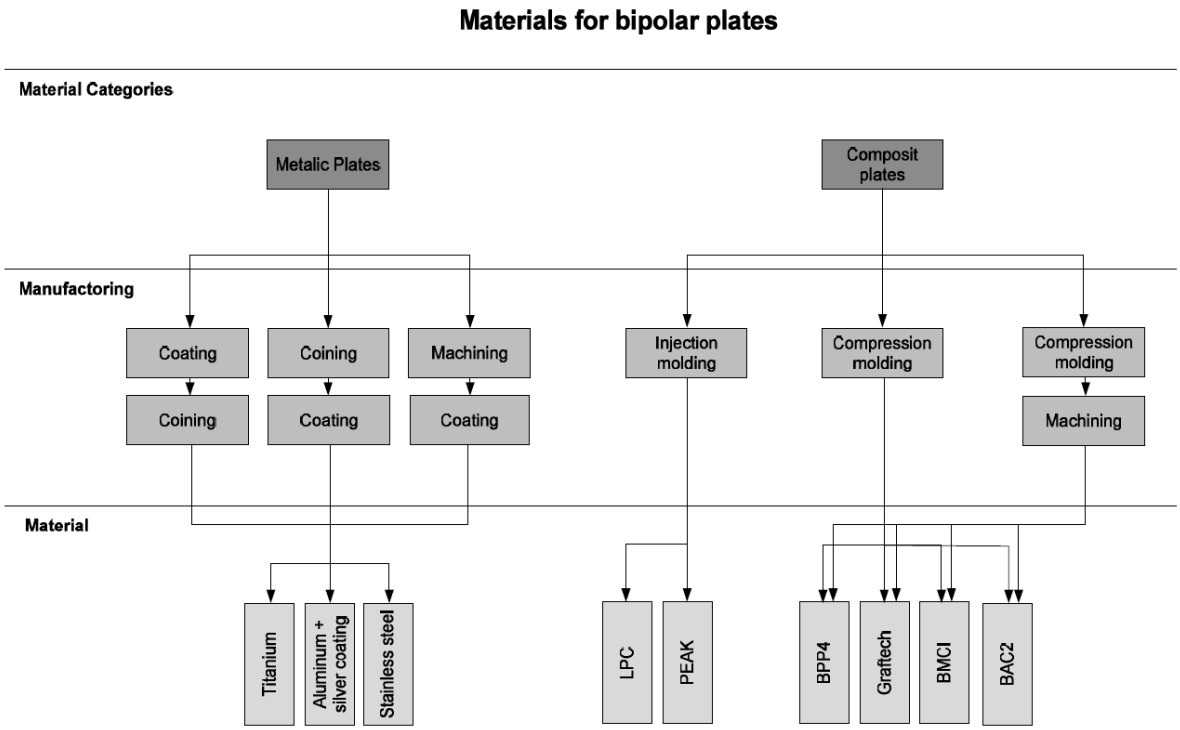

Figure 13 Outline of material screening process.

As mentioned above bipolar plate materials, need to excel with respect to certain material properties. The reason for this is the fuel cell operating conditions which are defined below:

- Temperature: -20C to 180C
- Current densities: up to 2 A/cm2
- Humidity: High
- Chemical and acid compatibility:
    - High concentration of phosphoric acid
    - Coolant: Oil, Ester or Alcohol based

As it is seen these conditions are quit harsh, thus finding suitable plate material is challenging.

While metals generally are good engineering materials and are manufacturable by many different and effective methods, they typically suffer from corrosion problems. Especially in fuel cell environments, it has proven difficult to find long lasting metals, alloys, coating or combinations hereof. The typical issue is the combination of corrosive chemicals, high electrode potentials and the reducing atmosphere on the anode side and the oxidizing atmosphere on the cathode side. Making it inherently difficult to find protective surfaces for metals and alloys.

Aluminum has good thermal and electrical properties; furthermore it is fairly cheap and easy to machine or shape in e.g. a coining process. However a major drawback of aluminum is that it corrodes very easy in the harsh fuel cell environment, thus aluminum needs a coating in order to withstand the conditions in a HTPEM fuel cell. Coating with a silver layer could possibly protect the aluminum. Besides from the coating process the metal plates need to be shaped, either by a coining process or a machining process. Coining can possibly be performed before or after the coating process, whether the coating is done before or after can influence tolerances and costs. If a coining process is used this can offer low costs in large/medium scale manufacturing, while machining is cost effective at small numbers.

At Serenergy aluminum plates with silver coating have been tested as an potential metallic material. The tests were conducted ex-situ in concentrated phosphoric acid. The tests have shown that even with the silver coating the plates have corrosion problems. Thus current coating technology needs further development.

Properties like electrical and thermal conductivity are important parameters for the fuel cell performance. In the table below, these properties are compared for some of the investigated materials.

	Electrical Conductivity [S/cm]		Thermal Conductivity [W/mk]	
	In-plane	Through-plane	In-plane	Through-plane
BPP 4	200	41.7	-	20
BMC 955	80	45	46,2	19,2
Grafcell	1429	33	275	5
Aluminum (pure)	≈375000	≈375000	≈230	≈230
Titanium (pure)	≈74000	≈74000	≈20	≈20
Stainless Steel (316)	≈13500	≈13500	≈15	≈15

To summarize, a survey of bipolar plate materials for HTPEM fuel cells was made focusing on two material categories; composites and metals. Their independent advantages with respect to material properties and manufacturing methods were discussed based on data sheets and tests. Finding the right materials can significantly reduce cost, and significantly improve lifetime and performance of fuel cell products, thus future work is important. Additional discussion of the screening is available in appendix 5.

WP4b: Sealing for fuel cells

Both the liquid channel and the air/hydrogen channels need to be sealed. For the liquid channel it is not important to be able to dissassemble the plates again whereas with the hydrogen/air supply channels it is necessary to be able to access the membrane. This means that gluing solutions have been tested for the liquid plates and more traditional gasketing solutions have been tested for the hyrdogen/air side.

A number of different seal methods have tested. The list includes:

- Acryl CPT
- Glass reinforced acryl CPT
- Fluorosilicone

- Viton
- Loctite
- Sifel
- Epoxy

The materials were exposed to a suit of potential cooling liquids in addition to phosphoric acid, air and elevated temperatures as summarized in the table below:

Compatibility Test	Acryl	Flour Silicone	RAMP Silicone A (white)	RAMP Silicone B (black)	FKM (various grades)	Confidential liquid side gasket
TEG	Fair	n/a	Moderate	Moderate	Good-Fair	n/a
Paratherm NF	Poor	n/a	Poor	Poor	Good	n/a
DOW CAL 10 (EG w. Additive)	Poor	Good	n/a	n/a	n/a	n/a
Addinol XW15	Good	Good	n/a	n/a	n/a	n/a
Calflo AF	Poor	Good	n/a	n/a	n/a	n/a
MEG	Moderate	Good	n/a	n/a	n/a	n/a
DEG	Moderate	Good	n/a	n/a	n/a	n/a
H3PO4 (80%)	Poor	Poor	Poor	Poor	Good-Poor	n/a
Air (170ºC)	Poor	n/a	n/a	n/a	n/a	n/a
Operation in a stack	yes	no	no	no	yes	yes

The environment that the gasket material is exposed to in the fuel cell is harsh and requires a special material composition to continue functioning through the fuel cell's lifetime. After a long search promising gasket materials have been identified both on the gas and liquid sides of the cell and testing continues with them.

Three materials were qualified for testing in operating stacks. Current activities with gasket materials revolve around long term testing in a stack and improvement of production procedures with possible suppliers. Further details are enclosed as appendix 6.

WP5: Battery pack optimization (**LIBA**, AAU, SER)

In the HI-EPS project, Lithium Balance has developed a new battery management system (BMS) that can be certified to fulfill automotive standards for control systems and electronics used in mass produced cars in terms of vibration, EMC and temperature performance. This BMS is to be used with lithium-ion battery packs primarily in electric and hybrid vehicles, but will also be applicable in industrial machines, ships, trains and power storage systems such as for photo voltaic or grid batteries. The charging and discharging algorithm developed for the HI-EPS unit is described in appendix 7.

Cooperation with automotive manufacturers

Many OEMs and their suppliers have expressed an interest in Lithium Balance developing such an automotive certified BMS, and some of them have contributed to the design and prototypes developed in the HI-EPS project. Initially SAAB and their battery manufacturer Boston Power were

involved in the concept design, and they were intended to test the BMS in battery packs and in vehicles during the project. However, due to subsequent financial problems at SAAB, their EV project was stopped as well as their contribution to the BMS development project. Later Fisker Automotive and their battery manufacturer SK Innovation took over this role, and provided input during the development of the prototype, and they also intended to participate in the test of the new BMS. Unfortunately, Fisker also ran into financial difficulties and had to stop the cooperation with Lithium Balance. However, in spite of not being able to test the developed BMS in actual vehicles in cooperation with automotive OEMs their input to the requirements, design and prototype phases have been invaluable.

The n-BMS concept

The n-BMS concept and prototype developed in the HI-EPS project is for a modular and flexible platform that can be used:

- with any lithium ion battery chemistry
- in any application from 3-1000V
- at very low cost
- has full redundancy so it continues to operate and shuts down the battery safely in case of an accident
- has a measurement accuracy is within 3mV
- with one temperature sensor per cell and
- measures SOC and SOH accurate per cell – not just at pack level – to make SOC calculations much more accurate and provide better state of health information.

The modular concept is quite unique, as much of the intelligence has been distributed from a central control board to the individual cell monitoring boards. All communication between boards is done with the automotive grade communication protocol CAN-BUS. The larger processor on each monitoring board is larger and more powerful than normally seen and effectively makes the monitoring board work as an individual BMS that can take decisions and act independently from the other boards in the system. The purpose is to ensure multiple redundancies where individual boards can take over from others, if they should fail or loose communication. This concept has been named the “networked BMS” or in short the n-BMS.

More details are presented in the n-BMS Power Point presentation in appendix 8.

WP6: Certification (**SER**, LIBA)

The objective of this work package was to ensure a continuous focus on the ability to have the final unit approved according to the highest automotive standards. This concerns the selection of components for the unit as well as the design of electronics and control algorithms.

Due to the change in scope away from an integrated system including both batteries/BMS and fuel cell range extender it was decided to focus the certification activities on the BMS as it was considered more mature.

The results of these tests performed by DELTA according to selected automotive standards are included in appendix 9. Although the tests at DELTA revealed problems in meeting some of the tests, the BMS is considered able to meet these requirements after minor modifications.

WP7: Market analysis (**Cemtec**, SER, LIBA, AAU)

A detailed screening and analysis of the market for the HI-EPS unit was be carried out. A procedure to quantify the cost/benefit of replacing ordinary Internal Combustion Engine (ICE) driven vehicles with HI-EPS drive train was developed based on a range of parameters. Based on this procedure it is possible to evaluate whether the introduction of the HI-EPS in a certain vehicle and/or in a certain geographic area is feasible from an economical point of view.

Initially, market segmentation was performed based on the grouping into categories used by the Danish car importers. In each segment the cost was broken down to identify the cost associated with having a combustion engine in the vehicle. In this context, the taxation of internal combustion engine driven cars is associated with the engine as a battery electric car is exempted from taxation. From this analysis it was found that the engine cost constitutes the largest share of the total car cost in the luxury segment.

For each of the segments the most probable usage pattern was identified ranging from almost entirely in city driving for the small car to predominantly freeway driving for the luxury class. These usage pattern provided inputs for the drive cycle analysis in WP2.

Although the luxury car seems to have the pricing that leaves the highest amount for the battery and range extender system it was still decided to focus the further analysis on the small car class. This is mainly due to the fact that it is likely to drive in a city drive cycle with low average speed allowing a small fuel cell system to be used and large benefits from the battery/fuel cell hybridization. For the luxury cars that drive mostly at sustained high speed, the fuel cell would be required to deliver a very large average power and there would be little benefit from the battery as a buffer. Hence the small car class was chosen for further studies.

Much more details on the market study and segmentation can be found in appendix 3.

WP8: Marketing & planning of next steps (**LIBA**, SER, AAU, Cemtec)

Since the initial development of the HI-EPS concept much has been learned in terms of technology, market approach and adoption towards key customers.

Furthermore the two collaborating companies have refined and developed a unique go to market strategy regarding the automotive market that is somewhat different than the initial ideas early in the HI-EPS project.

Although a strong focus on automotive applications remains, a deeper understanding of market and suitable approach has led to a step wise plan where niche and industrial applications will build mass, price optimization and development towards the end automotive market.

The above has led to fragmented and distributed approach where there has been developed a roadmap for each technology and related company.

Battery management system roadmap

During the HI-EPS project it was not possible to find a common customer for Serenergy and Lithium Balance in order for us to test the combined fuel cell and battery power storage system in one car. The mutual test of the integrated system was therefore conducted as a laboratory test at Aalborg University, whereas the two companies have attempted to find individual customers for the vehicle test.

For Lithium Balance the purpose of the project was to develop a Battery Management System (BMS) that will fulfill the future requirements of automotive customers for control electronics used on mass produced vehicles. This impacts both the functionality of the BMS and the international standards that the product should fulfill. No current and commercially available BMS on the market fulfills the requirements needed to achieve automotive certification. Some Automotive OEMs or tier 1 suppliers (e.g. BMW, FEV, Continental) have such automotive graded BMS in-house – but only available for own use or for the automotive OEM's with high volume production EV programs. These platforms are typically developed specifically for one car model and will cost the customer at least 10 mDKK for development per car model. They are therefore expensive, inflexible and not commercially available for any other than the largest OEMs.

With the BMS developed in this project Lithium Balance's strategy is to make the first commercially available automotive grade BMS platform – a modular and flexible platform that can be used with any battery, in any application from 3-1000V and at very low cost. In the project it has been possible to make a conceptual design for such an automotive grade BMS and implement this in a single 3-48V BMS module prototype. The requirements for the proposed automotive grade BMS was developed with input from SAAB/GM, AVL, Magna, Fisker Automotive and the battery suppliers Boston Power and SK Innovation.

It was first expected that it would be possible to test the actual prototypes in cooperation with SAAB, but before the prototype development could begin, SAAB went into financial difficulties. Soon after the cooperation with Fisker Automotive started instead, and even though the prototypes were finished this time (early 2012), Fisker also had to put the project on hold at their end due to financial difficulties. It has therefore not been possible to test the new BMS prototype in actual vehicles.

The prototypes were developed with layout assistance from Flextronics, who also manufactured the prototypes. These were tested by DELTA in accordance with the automotive standards and requirements, and the tests confirmed that the design and prototype indeed fulfills the functionality requirements needed for an automotive grade BMS. This concluded the BMS development activities in the HI-EPS project.

During the project several automotive OEMs and battery manufacturers have expressed great interest in the product – especially the smaller OEMs such as Brilliance, SAIC, and HK Motors in Asia. For this reason and as a result of the very successful prototype development and test conducted in Hi-EPS, Lithium Balance therefore decided to apply for a new project grant from EUDP in the autumn 2012, and the grant was confirmed December 2012. This new project will run 2013-2014 and two Automotive OEM's Porsche and Fiat, have agreed to participate in this project to provide further input and test prototypes and integrate the first systems in a demonstration vehicle.

The goals of this proposed project is therefore to finalize the development of the automotive grade BMS. This includes:

- establishing the necessary procedures to fulfill the relevant automotive standards for development, test and production
- develop the full BMS system according to the standards and to achieve flexibility up to 1000V
- comprehensive test and validation in-house, at Delta and at Porsche and Fiat in order to have the BMS certified according to automotive standards
- conduct long term demonstration in electric vehicles at Lithium Balance and Fiat to document long term performance and benefits
- prepare and start the market launch where one German OEM already has committed to purchase 50 systems for a test fleet of vehicles in 2013

Commercial launch is planned to take place at the EVS conference in Barcelona November 2013, and production is expected to commence in first quarter of 2014.

Fuel cell roadmap

The following roadmap outlines the roadmap towards a market introduction of the Reformed Methanol Fuel cell RMFC – range extender.

The below illustrated roadmap outlines the initiated and planned activities that will follow the HI EPS project. Furthermore activities on vehicle and fuel cell level concurrently and in direct succession of the HIEPS project.

In early stages of the concept development the below will be refined and planned in combination with the strategy processes on national and international level.

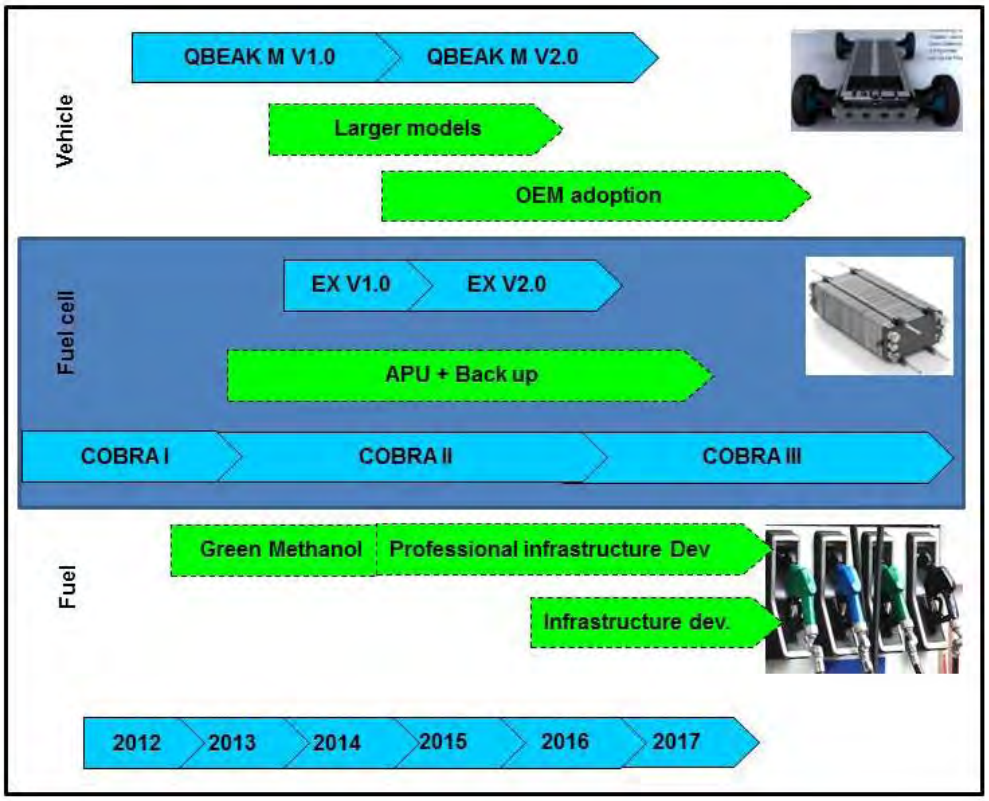

Road map activities

The roadmap is based on the "COBRA" development platform for RMFC and the Danish based QBEAK EV development platform as a carrier for the immediate RMFC platform for demonstration and niche markets, this work is currently on-going in the "MECC" project. Furthermore activities are under development in on the fuel infrastructure under "Green Methanol" a collaborative project with participation of infrastructure providers and operators.

Concurrently with the above work is being done with and for large vehicle OEM on an initial basis to demonstrate and clarify the technology track. The roadmap is continuously updated as it is directed primarily on a case by case situation with OEM's that is the key to large scale deployment.

Expected market development

The Below figure from the IEA Blue Map scenario shows the projected accumulated sales within the BEV and PHEV area where the range extender will take a share between 1-3%

IEA BLUE map scenarie for globalt salg af plug-in hybridbiler og elbiler, 2010-2050. Årligt salg, millioner biler.

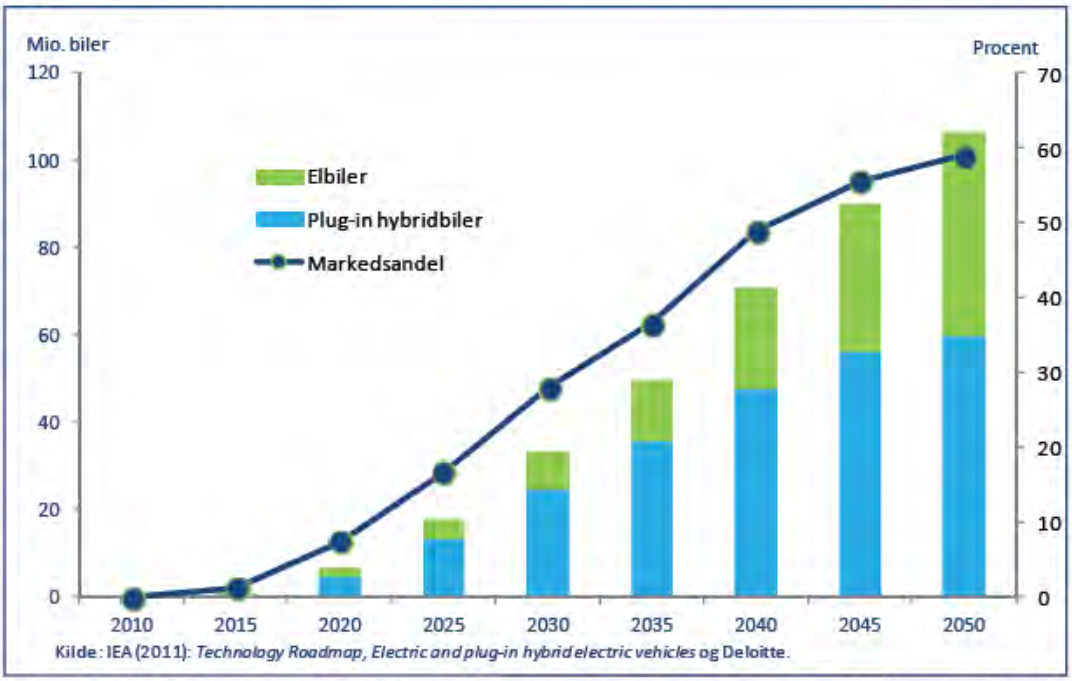

Kilde: IEA (2011): *Technology Roadmap, Electric and plug-in hybrid electric vehicles* og Deloitte.

Note: IEA BLUE map scenarie bygger på en antagelse om en reduktion i udledningen af drivhusgasser frem til 2050 på 50 procent.

Appendix 1

Paper published in: IEEE TRANSACTIONS ON VEHICULAR TECHNOLOGY, VOL. 62, NO. 1, JANUARY 2013

"Evaluation of Fuel-Cell Range Extender Impact on Hybrid Electrical Vehicle Performance"

Evaluation of Fuel-Cell Range Extender Impact on Hybrid Electrical Vehicle Performance

Hans-Christian B. Jensen, Erik Schaltz, *Member, IEEE*, Per Sune Koustrup, Søren Juhl Andreasen, and Søren Knudsen Kær

***Abstract*—The use of electric vehicles (EVs) is advantageous because of zero emission, but their market penetration is limited by one disadvantage, i.e., energy storage. Battery EVs (BEVs) have a limited range, and their batteries take a long time to charge, compared with the time it takes to refuel the tank of a vehicle with an internal combustion engine (ICE). Fuel cells (FCs) can be added to an EV as an additional energy source. These are faster to refill and will therefore facilitate the transition from vehicles running on fossil fuel to electricity. Different EV setups with FC strategies are presented and compared. The results of the setups are presented by range, efficiency, and price. These show the negative effect on the range when purpose-designed setups are driven above the design requirement as the range drops considerably. The simulations also showed the necessity of good FC control when driving in start/stop city cycles. Simulations with the New European Driving Cycle (NEDC) showed that efficiency fell by at least 15% for the FC hybrid EV (FCHEV) when compared with BEVs.**

***Index Terms*—Battery electric vehicle (BEV), fuel cell (FC), fuel-cell hybrid electric vehicle (FCHEV), methanol, range extender (RE).**

NOMENCLATURE

α	Angle of the driving surface [rad].
$\eta_{\mathrm{Bat,cha}}$	$= 0.95$. Charging efficiency [–].
ω_e	Angular frequency of the stator [rad/s].
ω_w	Angular velocity of the wheels [rad/s].
ω_s	Shaft angular velocity of an electric machine [rad/s].
ϕ_{EM}	Power factor angle [rad].
ρ_{air}	$= 1.2041$. Air density of dry air at 20 [°C] [kg/m^3].
τ_t	Traction torque [N · m].
τ_w	Torque of each driving wheel [N · m].
τ_s	Shaft torque of the electric machine [N · m].
τ_e	Electromechanical torque [N · m].
τ_c	Coulomb torque [N · m].
A_{front}	Front area [m^2].
B_v	Viscous friction coefficient [N·m·s/rad].
BEV	Battery electric vehicle. Vehicle runs on charged batteries.
c_{rr}	Tire rolling resistance coefficient [–].
C_{drag}	Aerodynamic drag coefficient [–].
$\mathrm{DoD}_{\mathrm{Bat}}$	Depth of discharge [–].
$\mathrm{DoD}_{\mathrm{Bat,ini}}$	Initial depth of discharge [–].
f_t	Traction force of the vehicle [N].
f_I	Inertial force of the vehicle [N].
f_{rr}	Rolling resistance force of the wheels [N].
f_g	Gravitational force of the vehicle [N].
f_n	Normal force of the vehicle [N].
f_{aero}	Force due to wind resistance [N].
FC	Fuel cell.
FCEV	FC electric vehicle. The energy source for the powertrain is the FC stacks.
FCHEV	FC hybrid electric vehicle. This setup has more than one energy source.
g	$= 9.81$. Free-fall acceleration [m/s^2].
G	Gear ratio of differential [–].
i_d	D-axis current [A].
i_q	Q-axis current [A].
$\hat{I}_p$	Peak phase current [A].
i_{Inv}	Inverter input current [A].
HVAC	Heating, ventilation, and air conditioning.
Hybridization factor	$P_{\mathrm{FC}}/P_{\mathrm{FC}} + P_{\mathrm{Bat}}$.
$i_{\mathrm{Bat,cell}}$	Battery cell current [A].
$i_{\mathrm{Bat,eq,cell}}$	Equivalent battery cell current [A].
i_{BC}	Output current of the boost converter [A].
i_{FC}	Input current of the boost converter [A].
ICE	Internal combustion engine.
J_s	Shaft moment of inertia [kg · m^2].
k	Peukert number [–].
L_d	D-axis inductance [H].
L_q	Q-axis inductance [H].
M_{car}	Mass of the vehicle [kg].
m_i	Modulation index [–].
NEDC	New European Driving Cycle.
p_{EM}	Electric input power [W].
$p_{Q,\mathrm{Inv}}$	Power loss of one switch [W].
$p_{D,\mathrm{Inv}}$	Power loss of one diode [W].
p_t	Traction power [W].
p_s	Shaft power of electric machine [W].
$P = n_{\mathrm{Poles}}$	Number of poles [#].
p_{Inv}	Inverter input power [W].

Manuscript received March 8, 2012 revised July 13, 2012; accepted August 8, 2012. Date of publication September 13, 2012; date of current version January 14, 2013. This work was supported by the Danish Energy Technology Development and Demonstration Program under a Highly Integrated Electric Propulsion System project grant. The review of this paper was coordinated by Mr. D. Diallo.

H.-C. B. Jensen, E. Schaltz, S. J. Andreasen, and S. K. Kær are with the Department of Energy Technology, 9220 Aalborg, Denmark (e-mail: hcj@et.aau.dk).

P. S. Koustrup is with Intelligent Cells, 8000 Aarhus, Denmark.

Color versions of one or more of the figures in this paper are available online at http://ieeexplore.ieee.org.

Digital Object Identifier 10.1109/TVT.2012.2218840

P_{BC}	Output power of the boost converter [W].
$P_{\mathrm{Loss,\,BC}}$	Power loss of the boost converter [W].
PMSM	Permanent-magnet synchronous machine.
R_{BC}	Resistance of the switch and the diode [Ω].
R_s	Stator phase resistance [Ω].
$R_{Q,\,\mathrm{Inv}}$	Inverter switch resistance [Ω].
$R_{D,\,\mathrm{Inv}}$	Inverter diode resistance [Ω].
r_w	Wheel radius [m].
$R_{\mathrm{Bat,\,cell,\,dis}}$	Inner battery cell resistance during discharge mode [Ω].
$R_{\mathrm{Bat,\,cell,\,cha}}$	Inner battery cell resistance during charge mode [Ω].
RE	Range extender.
$\mathrm{SoC_{Bat}}$	Battery state-of-charge [–].
V_{Bat}	Battery voltage [V].
$V_{Q,\,\mathrm{th,\,Inv}}$	Inverter switch threshold voltage [V].
$V_{D,\,\mathrm{th,\,Inv}}$	Inverter diode threshold voltage [V].
$\hat{V}_p$	Peak phase voltage [V].
v_{car}	Velocity of the vehicle [m/s].
v_{wind}	Headwind speed [m/s].
v_d	D-axis voltage [V].
v_q	Q-axis voltage [V].
$v_{\mathrm{Bat,\,cell}}$	Battery cell voltage[V].
$v_{\mathrm{Bat,\,int,\,cell}}$	Internal battery cell voltage [V].
$V_{\mathrm{th,\,BC}}-$	Threshold voltage of the switch and the diode [V].
$\dot{v}_{\mathrm{car}}$	Acceleration of the vehicle [$\mathrm{m/s^2}$].

I. Introduction

In Europe, there is a growing demand for greener vehicles; this demand that is expected to increase significantly, particularly as stricter laws on emissions, which are planned, are put into force. The goal of these restrictions points toward zero particle emission and CO_2 reductions; therefore, it is not surprising that there is also a rise in the need for cleaner energy sources, which have zero emission. Electric vehicles (EVs) are one solution to the ever-growing demands for greener vehicles as they are highly efficient, produce zero emission, are silent, and can be furthermore used for power regulation by a grid operator. However, the Achilles' heel of EVs is the storage of electric energy, and before this is solved, EVs are reduced to households with two cars and primarily used for local travel. The second problem with EVs compared with vehicles with an ICE is shifted cost; therefore, the cost is shifted from operating cost to buying cost. Hence, an EV is more expensive to buy but costs less to operate than a comparably sized ICE vehicle [1, p. 5].

The problem with energy storage is divided into limited driving range and long charging time. These issues are coupled as they are both centered on the battery package of the car, but charging time can also be caused by the electric grid that supplies the power. The analysis of the electric grid will not be included in this paper.

One solution that is considered to solve the energy storage problem in EVs is FCs. FCs are one of these alternative energy sources [2], which are used more and more, due to their increasing reliability (numbers are presented in [3]) and cost effectiveness (price development for FCs is shown in [4]). EVs with FCs are divided into either BEVs with an FC RE or FCHEVs. The difference between the two vehicle setups is the hybridization factor and their usage. REs are more used as a backup power source, and their purpose is to extend the range when needed. FCHEVs run mainly on FCs, and the power available from the FCs is therefore higher than for REs. The focus of this paper is to illustrate the advantages and disadvantages of including FCs as an RE or as a primary source of electric power.

Both EV types, i.e., REs and FCHEVs, compared in this paper include a battery pack, which is used to start up the FC system and to power the vehicle until the FC has obtained the operating temperature. The complexity of both the FCHEV model and the BEV model is adjusted so that it is able to estimate properly the energy consumption of an EV [5]–[7], but it also defines many of the different components that it contains, e.g., transmission, electric machines, power electronics, and batteries.

This paper present a simulation model of an EV with a battery pack and a simple FC-stack model. This paper will also analyze four design setups and present a comparison of BEVs and FCHEVs. A vehicle that will be primarily used in cities has low requirements for a sustained top speed, but the demands for energy are high as the vehicle has to carry enough energy for a minimum of two full working days of 8 h. This is approximately 600 km, which is why the possibility to refuel is of interest. The next vehicle setup is for intercity driving. The maximum allowed top speed on such roads is either 80 or 90 km/h, depending on the country. A sustained top speed of 90 km/h for 600 km was chosen. If a car can sustain a speed of 110 km/h, it will be of no threat to other drivers and sufficient for limited driving on motorways. A range of 500 km per refueling at 110 km/h was chosen for the third setup. The last setup is fully operable on motorways. Most countries has a limit of 130 km/h on motorways. A minimum range of 400 km at 130 km/h was chosen. This is more than 3 h of continuous driving of which reason the driver will probably be in need for a small coffee break anyway. The range requirements are clarified in Section III-B.

The selection of each component (electric machines, power electronics, batteries, etc.,) of the power system is optimized for the setup requirement. The vehicle setups are designed to fulfill a driving cycle that consists of city, road, and motorway driving.

II. Nonlinear Vehicle Modeling

A. Architecture

There are no limitation in the architecture of EVs [8], but the standard setup contains one to four electric dc or ac machines. Further options include: gearboxes or direct drives, high or low battery voltages, one- or three-phase charging, etc. The architecture used in this paper is the most common for EVs and resembles the architecture used for vehicles with an ICE. This architecture is shown in Fig. 1.

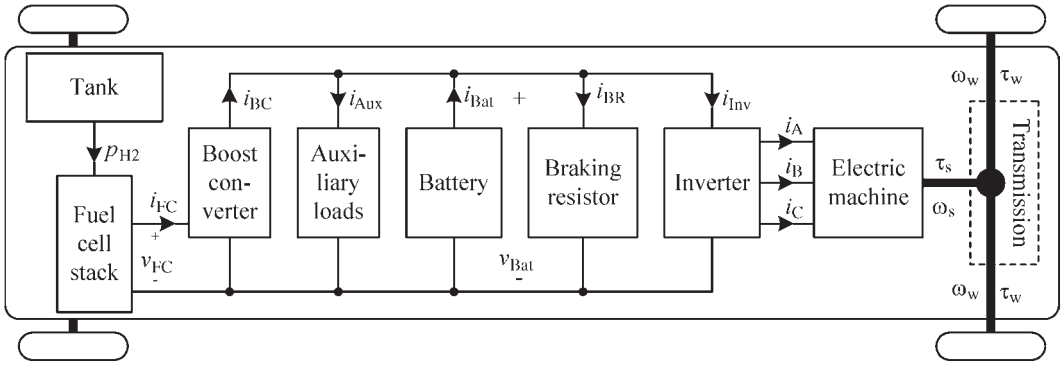

Fig. 1. General FCEV architecture.

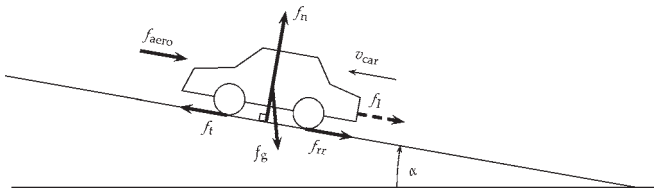

Fig. 2. Free-body diagram of (thick arrows) forces acting on the EV.

The functions of the different components included in the architecture overview shown in Fig. 1 are as follows. Torque to the wheels is supplied through a differential with a gear ratio that converts the maximum rotation speed of the motor to the top speed of the EV. The motor of the vehicle is a three-phase electric ac machine. The dc from the power source is converted into three phases by the inverter, which also controls the torque and speed of the ac machine. The battery supplies the vehicle with electrical power. Auxiliary loads are a simple model of electrical losses used by lighting systems, comfort systems, safety systems, etc. The boost converter makes it possible to transfer power from the FC stack to the high-voltage side of the battery. The braking resistor removes excessive power generated from either the motor during braking or from the FC when the power need changes faster than that which the FC is capable.

B. Force Model

The EV is exposed to the forces from the electric machine (f_t), gravity (f_g), aerodynamic resistance (f_{aero}), rolling resistance (f_{rr}), and inertial effect (f_I). These forces affect the vehicle in different directions and sizes, where the size depends on different variables, whereas the directions are more constant. The directions of the different forces are shown in Fig. 2.

The sum of the presented forces describes how the vehicle behaves. The sum is called the traction force of a vehicle, and if the directions in Fig. 2 are used, then the traction force can be described by the following [9]:

$$f_t = \underbrace{M_{\text{car}}\dot{v}_{\text{car}}}_{f_I} + \underbrace{M_{\text{car}} \cdot g}_{f_g} \cdot \sin(\alpha) + \overbrace{\underbrace{M_{\text{car}} \cdot g \cdot \cos(\alpha)}_{f_{\text{rr}}} \cdot c_{\text{rr}}}^{f_n} + \underbrace{\frac{1}{2}\rho_{\text{air}} C_{\text{drag}} A_{\text{front}} (v_{\text{car}} + v_{\text{wind}})^2}_{f_{\text{aero}}} \tag{1}$$

$$c_{\text{rr}} = 0.01\left(1 + \frac{3.6}{100} v_{\text{car}}\right). \tag{2}$$

TABLE I
AVERAGE POWER LEVEL OF THE AUXILIARY LOADS OF THE VEHICLE. THE VALUES ARE ADOPTED FROM [9]–[11]

Radio	52 [W]
HVAC	489 [W]
Lights	316 [W]
Total p_{Aux}	857 [W]

C. Auxiliary Loads

A modern car has basic safety features such as lights, wipers, and a horn, but cars are also equipped with comfort features such as a radio, heat, and air conditioning. All of these are in some degree expected to be in an EV if it has to replace a standard vehicle with an ICE. Not all of these electric loads generate a constant load, e.g., the power consumption of the climate system strongly depend on the internal and external temperatures.

When analyzing EVs, it is important to include also the losses, which are due to auxiliary components, as they are part of the daily usage of the vehicles. To make analysis results comparable, the average values suggested in Table I are used.

D. Transmission

The torque, angular velocity, and power of the drive shaft connected to the wheels, which are shown in Fig. 1, are given by the following:

$$\tau_t = f_t r_w \tag{3}$$

$$\tau_w = \frac{\tau_t}{2} \tag{4}$$

$$\omega_w = \frac{v_{\text{car}}}{r_w} \tag{5}$$

$$p_t = f_t v_{\text{car}}. \tag{6}$$

The same variables are derived for the drive shaft connected to the electric ac machine. The efficiency of the differential of the transmission system is assumed to be constant with the value of $\eta_{\text{TS}} = 0.95$ [9]. Hence, the shaft torque, angular velocity, and power are as follows:

$$\tau_s = \begin{cases} \eta_{\text{TS}} \frac{\tau_t}{G}, & p_t < 0 \\ \frac{\tau_t}{\eta_{\text{TS}} G}, & p_t \geq 0 \end{cases} \tag{7}$$

$$\omega_s = G\omega_w \tag{8}$$

$$p_s = \tau_s \omega_s. \tag{9}$$

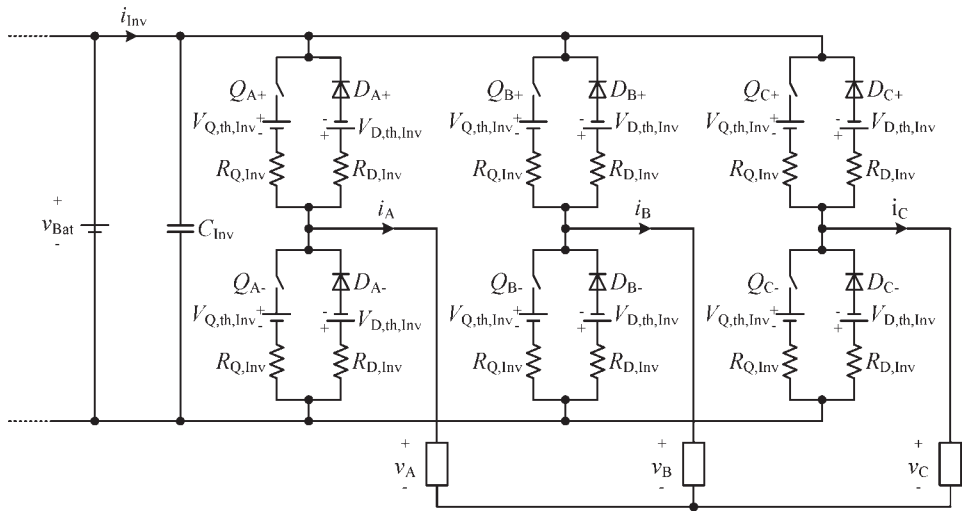

Fig. 3. Circuit diagram of the inverter.

E. Electric Machine

The PMSM is selected due to its high power density and high efficiency. The model of an electric machine is divided into an electric part and a mechanical part. The electric part of the PMSM is modeled in the DQ-frame, i.e.,

$$v_d = R_s i_d + L_d \frac{di_d}{dt} - \omega_e L_q i_q \tag{10}$$

$$v_q = R_s i_q + L_q \frac{di_q}{t} + \omega_e L_d i_d + \omega_e \lambda_{pm} \tag{11}$$

$$p_{\text{EM}} = \frac{3}{2}(v_d i_d + v_q i_q). \tag{12}$$

The mechanical part of the PMSM is modeled as follows:

$$\tau_e = J_s \frac{d\omega_s}{dt} + B_v \omega_s + \tau_c + \tau_s \tag{13}$$

$$p_s = \tau_s \omega_s. \tag{14}$$

The last part of the model is the coupling between the electric part and the mechanical part, which is given by

$$\tau_e = \frac{3}{2}\frac{n_{\text{Poles}}}{2}\left(\lambda_{pm} i_q + (L_d - L_q) i_d i_q\right) \tag{15}$$

$$\omega_e = \frac{n_{\text{Poles}}}{2}\omega_s. \tag{16}$$

F. Inverter

The inverter used in the vehicle model is a three-phase inverter. The circuit diagram of such inverter is shown in Fig. 3. The inverter converts power between the ac/electric machine side (with phase voltages v_A, v_B, and v_C) and the dc/battery side by turning on and off switches Q_{A+}, Q_{A-}, Q_{B+}, Q_{B-}, Q_C, and Q_{C-}. The switches has an on-resistance $R_{Q,\,\text{Inv}}$. The diodes in parallel of each switch are creating a path for the motor currents during the deadtime, i.e., the time where both switches in one branch are nonconducting to avoid a shoot-through.

Since the inverter is a converter from dc to three-phase ac and the conversion is not used in the model as both sides in the model of the inverter are calculated as power, the inverter model is simplified as a power loss through the inverter. The average power losses of one switch $p_{Q,\,\text{Inv}}$ and one diode $p_{D,\,\text{Inv}}$ in Fig. 3 during one fundamental period are [12] as follows:

$$p_{Q,\,\text{Inv}} = \left(\frac{1}{8} + \frac{m_i}{3\pi}\right) R_{Q,\,\text{Inv}} \hat{I}_p^2 + \left(\frac{1}{2\pi} + \frac{m_i}{8}\cos(\phi_{\text{EM}})\right) V_{Q,\,\text{th,\,Inv}} \hat{I}_p \tag{17}$$

$$p_{D,\,\text{Inv}} = \left(\frac{1}{8} - \frac{m_i}{3\pi}\right) R_{D,\,\text{Inv}} \hat{I}_p^2 + \left(\frac{1}{2\pi} - \frac{m_i}{8}\cos(\phi_{\text{EM}})\right) V_{D,\,\text{th,\,Inv}} \hat{I}_p \tag{18}$$

$$m_i = \frac{2\hat{V}_p}{V_{\text{Bat}}}. \tag{19}$$

Assuming that the threshold voltage drop of the switches and diodes are equal, i.e., $V_{\text{th,\,Inv}} = V_{Q,\,\text{th,\,Inv}} = V_{D,\,\text{th,\,Inv}}$, and that the resistances of the switches and diodes are also equal, i.e., $R_{\text{Inv}} = R_{Q,\,\text{Inv}} = R_{D,\,\text{Inv}}$, the total power loss of the inverter is given by

$$P_{\text{Inv,\,loss}} = 6\left(P_{Q,\,\text{Inv}} + P_{D,\,\text{Inv}}\right) = \frac{3}{2} R_{\text{Inv}} \hat{I}_p^2 + \frac{6}{\pi} V_{\text{th,\,Inv}} \hat{I}_p. \tag{20}$$

The component connected to the output of the inverter is the electric motor; hence, the output power of the inverter is equal to the motor input power p_{EM}. This results in the following equations for inverter power and efficiency:

$$p_{\text{Inv}} = v_{\text{Bat}} i_{\text{Inv}} = p_{\text{EM}} + p_{\text{Inv,\,loss}}. \tag{21}$$

G. Battery

The battery is a necessity not only for EVs but also for vehicles with an ICE as they drive the power for the start-up and emergency systems. The size of the battery pack varies depending on the vehicle that they supply, as does the type of

TABLE II
DATA SHEET SPECIFICATIONS OF SAFT VL 37570 LI-ION BATTERY

Maximum voltage	$V_{\mathrm{Bat,max,cell}}$	4.2 [V]
Nominal voltage	$V_{\mathrm{Bat,nom,cell}}$	3.7 [V]
Minimum voltage	$V_{\mathrm{Bat,min,cell}}$	2.5 [V]
1 hour capacity	$Q_{1,\mathrm{cell}}$	7 [Ah]
Nominal 1 [h] discharge current	$I_{\mathrm{Bat},1,\mathrm{cell}}$	7 [A]
Maximum pulse discharge current	$I_{\mathrm{Bat,max,cell}}$	28 [A]

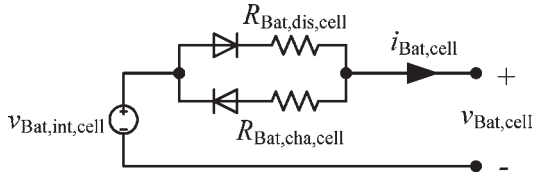

Fig. 4. Electric equivalent circuit diagram of a battery cell.

battery. The battery model parameters used are based on a Saft VL 37570 lithium-ion cell [13]. The specifications are listed in Table II.

1) Electric Model: The model of the battery is a steady-state model, i.e., the dynamic behavior is not included, and it is based on the electric equivalent circuit diagram, which is shown in Fig. 4.

As shown in Fig. 4, the model consists of an internal voltage source and two inner resistances that are used for charging and discharging. The two diodes in the figure are ideal and only have symbolic meaning for the model, i.e., they shift between the charging and discharging resistances. Discharging currents are treated as positive currents, and charging currents are then negative.

The cell voltage in the model is calculated by

$$v_{\mathrm{Bat,cell}} = \begin{cases} v_{\mathrm{Bat,int,cell}} - R_{\mathrm{Bat,cell,dis}} i_{\mathrm{Bat,cell}}, & i_{\mathrm{Bat,cell}} \geq 0 \\ v_{\mathrm{Bat,int,cell}} - R_{\mathrm{Bat,cell,cha}} i_{\mathrm{Bat,cell}}, & i_{\mathrm{Bat,cell}} < 0. \end{cases} \tag{22}$$

The value of the inner voltage source and that of the two resistances in the model depend on the DoD of the battery. The values for the battery model are obtained by the curves given in the data sheet of the Saft battery cell. The voltage source and the resistances are approximated by the tenth-order polynomials found in [14, p. 8].

2) Battery Capacity Model: The changes in the SoC and the DoD are calculated by integrating the current drawn from or delivered to the battery. The formulas to calculate $\mathrm{SoC_{Bat}}$ and $\mathrm{DoD_{Bat}}$ are as follows:

$$\mathrm{DoD_{Bat}} = \mathrm{DoD_{Bat,ini}} + \int \frac{i_{\mathrm{Bat,eq,cell}}}{Q_{\mathrm{Bat},1,\mathrm{cell}}} dt \tag{23}$$

$$\mathrm{SoC_{Bat}} = 1 - \mathrm{DoD_{Bat}}. \tag{24}$$

The equivalent battery cell current used to calculate the SoC and the DoD is defined as [7], [14]

$$i_{\mathrm{Bat,eq,cell}} = \begin{cases} I_{\mathrm{Bat},1,\mathrm{cell}} \left(\frac{i_{\mathrm{Bat,cell}}}{I_{\mathrm{Bat},1,\mathrm{cell}}} \right)^k, & i_{\mathrm{Bat,cell}} \geq 0 \\ \eta_{\mathrm{Bat,cha}} i_{\mathrm{Bat,cell}}, & i_{\mathrm{Bat,cell}} < 0 \end{cases} \tag{25}$$

$$k = \begin{cases} 1, & i_{\mathrm{Bat,cell}} \leq I_{\mathrm{Bat},1,\mathrm{cell}} \\ 1.125, & i_{\mathrm{Bat,cell}} > I_{\mathrm{Bat},1,\mathrm{cell}}. \end{cases} \tag{26}$$

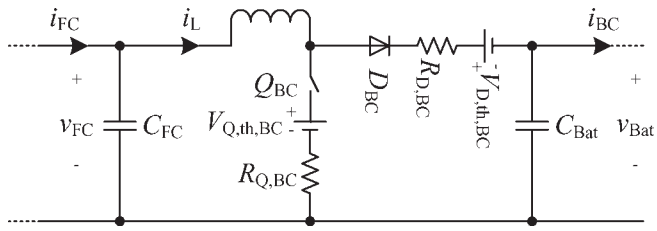

Fig. 5. Electric circuit diagram of the boost converter.

The Peukert number k has two different values, depending on the amplitude of the discharge current. For currents higher than the nominal 1-h discharge current $I_{\mathrm{Bat},1,\mathrm{cell}}$, the capacity is reduced.

H. Boost Converter

The boost converter increases the voltage on the FC side to the level of the battery on the other side. The electric circuit diagram of the boost converter is shown in Fig. 5.

The function of the boost converter is to convert the voltage of the FC to the same level as the battery. These values are not used in the simulation model. Hence, the model of the boost converter is reduced to an equation, which calculates the losses in the boost converter. The losses in the boost converter are due to switch resistance $R_{Q,\mathrm{BC}}$, diode resistance $R_{D,\mathrm{BC}}$, and threshold voltages $V_{Q,\mathrm{th,BC}}$ and $V_{D,\mathrm{th,BC}}$. The losses are approximated by assuming that the resistances and threshold voltages of switch Q_{BC} and diode D_{BC} are equal, i.e., $R_{\mathrm{BC}} = R_{Q,\mathrm{BC}} = R_{D,\mathrm{BC}}$ and $V_{\mathrm{th,BC}} = V_{Q,\mathrm{th,BC}} = V_{D,\mathrm{th,BC}}$. The power transfer equations of the boost converter are therefore given by

$$P_{\mathrm{FC}} = V_{\mathrm{FC}} i_{\mathrm{FC}} = P_{\mathrm{BC}} + P_{\mathrm{loss,BC}} \tag{27}$$

$$P_{\mathrm{BC}} = V_{\mathrm{Bat}} i_{\mathrm{BC}} \tag{28}$$

$$P_{\mathrm{loss,BC}} = R_{\mathrm{BC}} i_{\mathrm{FC}}^2 + V_{\mathrm{th,BC}} i_{\mathrm{FC}}. \tag{29}$$

I. FC RE System

The FC RE converts the chemical energy available in the inlet anode and cathode gases of the FC stack into electrical power and heat, which are both usable by the vehicle for traction and cabin heating. Different fuel types are available, with the most common being hydrogen, which is stored either as compressed gas in a metal hydride tank or as cryogenic liquid. Using hydrogen as a fuel involves volumetric challenges for many applications and reliance on the development of a new fuel distribution system. For these reasons, fuel reforming is an interesting alternative to enable the use of liquid fuels, such as methanol and ethanol, which can be produced from renewable sources and handled much like existing fuels for automotive applications [15], [16]. High-temperature polymer electrolyte membrane (HTPEM) FCs are ideal candidates for these type of systems because of their robustness to impurities in the inlet gases and to high temperatures, which enable more convenient cooling and system design [17]–[21].

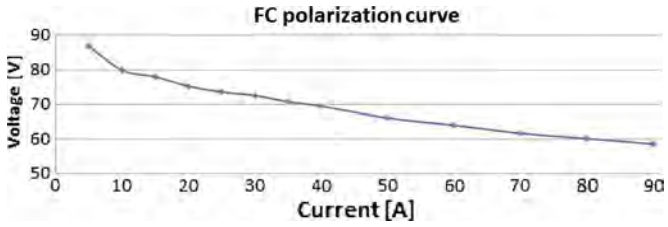

Fig. 6. FC-stack polarization curve.

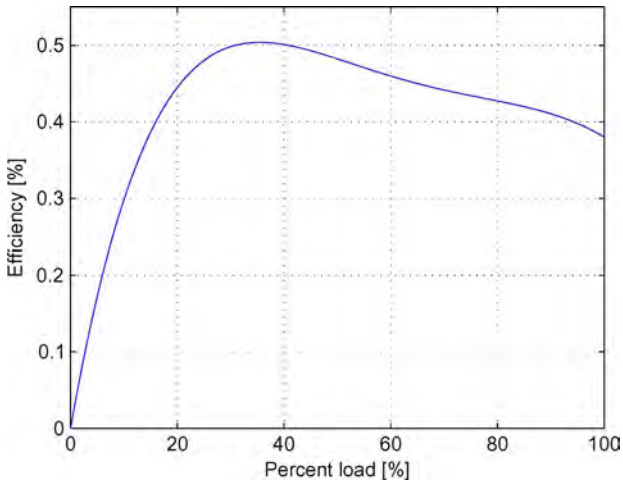

Fig. 7. Efficiency curve of the FC stack and the reformer.

The FC system on which the model parameters are based on is a 5-kW HTPEM FC stack developed by Serenergy [22]. The FC system contains an evaporator where a 1.5-steam-to-carbon-ratio methanol-and-water mixture is pumped through, heat evaporated, and superheated. Afterward, this fuel flow enters a chemical reactor, which is a methanol reformer that converts the steam-based methanol-and-water mixture into a hydrogen-rich gas, containing traces of CO, CO_2, and water. This hydrogen-rich gas is sent directly to the anode of a HTPEM FC stack, where it is converted into electrical energy. The FC-stack polarization curve, which expresses the electrical performance of the FC stack, is in the model approximated by a polynomial expression at the ideal operating temperature, which is shown in Fig. 6. The consumed methanol fuel flow is calculated based on the current drawn in the FCs and the energy required to support the hydrogen production.

Some general conditions and constraints are applied to the simulation: Start-up time T_{startup} is set to 10 min, and a current change limitation Δi_{FC} of 0.15 A/s during start-up and 1.5 A/s during normal operation has been set to avoid various unwanted operating conditions for the FC system, which reduce the lifetime. The general conditions chosen can be optimized for individual applications, as well as other types of FC systems and control strategies.

The model of the methanol in the tank is based on energy and equivalent mass. The calculated used energy is then multiplied with the efficiency polynomial to calculate the remaining energy and remaining methanol in mass as the mass affects the force model in Section II-B. The efficiency polynomial depicted in Fig. 7 contains the loss to the reformer and the efficiency of the FC.

The balance of plant for the FC stack is calculated using the aforementioned efficiency polynomial and the air blower loss of 35 W per kilowatt produced [23]. The energy needed to heat each cell is defined as 3.125 Wh/cell and can either be the electric energy or the energy density of the amount of used methanol during start-up.

1) Energy Manager: The energy manager in this setup is a logic-based system with six rules. The rules in the energy manager are defined by physical limitations and boundaries of the FC stack and the battery pack. The reference to the energy manager is current, and there is no SoC reference to keep the batteries at a perfect value as this would cause more start/stop cycles of the FC, which are slow and cause wearing of the FC. Another method could be a system with two references, i.e., current and SoC. The six rules are as follows.

- Start-up time T_{startup} is 10 min from the desire to use the RE for current to be drawn from the FC. This will be the prestart-up phase.
- During the heating phase, the energy used will be 3.125 Wh/cell.
- After shutdown, the start-up phase has to be redone from the prestart-up phase.
- During the start-up phase, the change in current Δi_{FC} is limited to 0.15 A/s.
- During the operation phase, the change in current Δi_{FC} is limited to 1.5 A/s.
- Vehicle is to shutdown at a SoC of 21%.

III. Simulation Model

Earlier, the models of each component of the power system and forces in the EV were explained. These models are combined into a single inverse model, which composes the main parts of the simulation model. The complete implementation in the Matlab/Simulink environment is shown in Fig. 8. The complete EV model includes the model of the forces acting on the vehicle (wind, gravity, rolling resistance, etc.,) and the individual components of the powertrain, i.e., transmission, an electric machine, an inverter, a battery, and a boost converter. The input to the simulation model is a driving cycle (examples will be presented in Section III-A), and the output of the model is all the currents, voltages, power, torque, etc., of the vehicle.

The driving cycle inputs are used to calculate the needed force. The force and the vehicle speed are then used to calculate the electric-motor angular velocity and torque. These are then used to calculate the peak current and power on the motor. Together with the voltage on the bus, the inverter current is calculated. The braking resistor uses all the currents on the bus and the maximum charge current to calculate the battery current. From the battery current, the battery model calculates the battery voltage, $\mathrm{SoC}_{\mathrm{Bat}}$, and the maximum charge current. The boost converter model requires the bus voltage and the FC power and current. The energy management strategy uses most of the system information to calculate the FC current. The FC then takes this information to calculate the remaining methanol and the output voltage and power. The remaining blocks calculate, respectively, the loss from the auxiliary loads and the FC support systems (balance of plant loss).

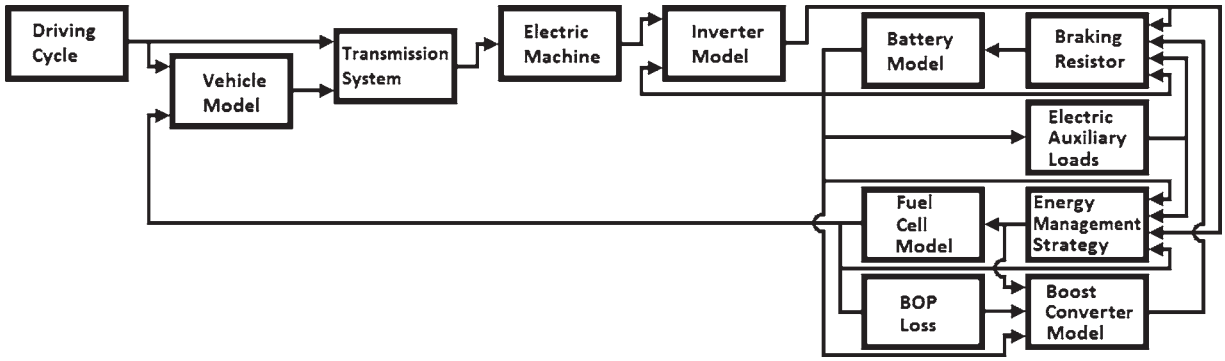

Fig. 8. Matlab/Simulink implementation of the FCHEV.

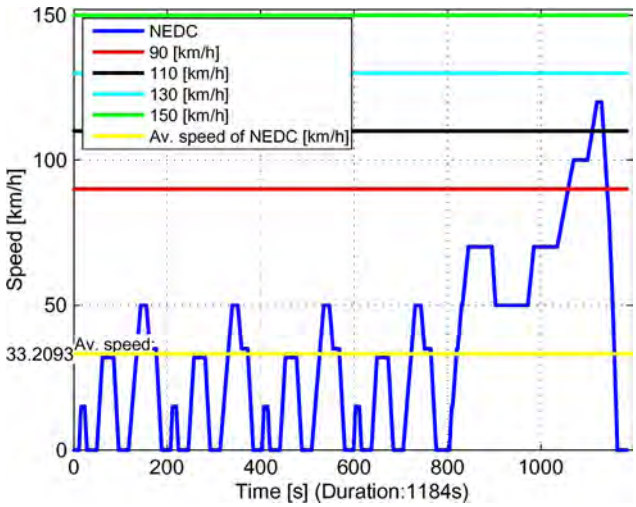

Fig. 9. Driving cycles used for the different EV setups.

TABLE III
RANGE OBTAINED WITH EACH DRIVING CYCLE RUNNING THE LENGTH OF NEDC

Driving cycle				
NEDC	90	110	130	150
10.93 [km]	29.6 [km]	36.18 [km]	42.76 [km]	49.33 [km]

A. Driving Cycles

Five different driving cycles are used to simulate the vehicle range. These are NEDC and constant motorway speeds of 90, 110, 130, and 150 km/h. The different driving cycles are shown in Fig. 9. As the NEDC driving cycle is more complex than the constant motorway driving cycles, the average speed is calculated (≈33 km/h) and plotted in the figure.

To compare the driving cycles further, the range achieved at the different driving cycles during the time (hence, driving cycle for 1184 s) that it takes to complete the NEDC is listed in Table III.

B. Setup Parameters

A simulation model of an EV requires several parameters, which are defined by the environment, the vehicle, and the driving cycle. The environment parameters wind speed v_{wind} and road angle α have been set to zero for horizontal driving with no wind, which gives the best comparison parameters.

TABLE IV
DESIGN RANGE REQUIREMENTS FOR THE FOUR SETUPS

Range Extender	150 [km] @ NEDC
90 FCHEV	600 [km] @ 90 [km/h]
110 FCHEV	500 [km] @ 110 [km/h]
130 FCHEV	400 [km] @ 130 [km/h]

The driving cycle varies according to the test and the setup requirements.

The setup requirements are presented in Table IV.

The range values in Table IV are used to define the size of the battery pack and the FC stack. The RE setup has a fixed FC-stack size, which follows the size of Serenergy's 5-kW RE, whereas the battery size is designed; therefore, the vehicle gets the same range as the original Mitsubishi iMiev when it drives the same driving cycle [24]. The other three setups [1, p. 61] are designed without fixed sizes and with the purpose of having the smallest battery size possible, while still obtaining the range from the range in Table IV. The battery size requirement is that it can support the velocity needed until the FC has finished the start-up procedure, which is 10 min for both the RE and the FCs.

The vehicle parameters (size, weight, drag coefficient, etc.,) are obtained from a Mitsubitshi iMiev [24]. The iMiev is already an EV; therefore, the parameters are valid for a comparison of EVs. There are some differences such as the nominal bus voltage, which is set to 600 V. The vehicle mass is Curb weight with a 100-kg driver. Car performance, such as top speed and acceleration, is used to calculate the motor size. The motor is designed for peak and continuous torque requirements, where the peak torque is only obtained for a period of 30 s. The requirement for the peak torque is given by the vehicle acceleration from 0 to 100 km/h in 15.9 s. The requirement for continuous torque is given by the top speed of 150 km/h.

The batteries are rarely able to provide a SoC of 100%, and the SoC decreases over time. To include this aging effect in the simulation model, the estimated maximum is 90%, and due to lifetime expectancy of the batteries, there is a minimum SoC of 21%. This minimum is protection against deep discharge, and for this reason, some battery makers increase their guarantee if the batteries are always kept above this lower limit. Hence, the usage is only 69% of the total capacity.

The setup parameters of the four setups are found in an iterative process. The iterative process consists of a two-step loop, where the first step consists of defining vehicle parameters.

TABLE V
DESIGNED EV SETUPS USED FOR SIMULATION. MOTOR SIZE IS SPECIFIED IN CONTINUOUS POWER

Set-up	Vehicle Mass [kg]	Drive System [L]	Battery [Wh]
Range Extender	1349	121	17371
90 FCHEV	1452	344	14476
110 FCHEV	1508	397	17371
130 FCHEV	1623	496	23161

Set-up	Fuel Cell [W]	Motor [W]	Methanol Tank [L]
Range Extender	6021	90829	8
90 FCHEV	47514	107776	93
110 FCHEV	62043	109611	81
130 FCHEV	85014	114184	73

The second step is to simulate the setup with a desired drive cycle and to record if the obtained range is as desired for the drive cycle. If the range obtained is not the desired range, then the process is redone with different vehicle parameters. The parameters are entered into the model and simulated using the Matlab/Simulink model depicted in Fig. 8, and once the outputs of the Matlab/Simulink model fulfill the requirements for the design of the parameters, then they are accepted and used in all of the test cases listed earlier.

The main parameters found for the four setups are listed in Table V.

The mass of the four setups do vary, and the last two setups are above the gross vehicle weight (1450 kg), which will result in further strengthening of bumpers, chassis, brakes, etc., and, thereby, increased weight. This extra weight due to strengthening is disregarded for comparison purposes. Another reason is that it might be solved by a different power (FC/battery) supply choice or a realistic start for motorway driving cycles.

IV. TEST RESULTS

The four EV setups are simulated with the five different driving cycles presented earlier. Each of these 20 combinations is simulated for three FC situations. The first situation is with an empty methanol tank, which indicates the emergency range, without the use of the FC. The difference between the two remaining situations is how the FC is heated during start-up. The classical method is with an electrical heater placed in the FC, and the energy to run the heater comes from the batteries. The second method is available for FCs with reformer systems, and the energy is obtained chemically using the energy contained in the methanol.

The test results are presented in three parts: The first part contains the range results, the second part presents the power usage results, and the last part presents the efficiency results.

A. Range Results

The range simulation results are presented in Table IX and shown in Fig. 10.

The chemical heating FC method obtains a longer range as higher efficiency is obtained than for the electrical heating FC method. The heated simulations have a longer range for driving cycles that are equal to or with smaller energy consumption than

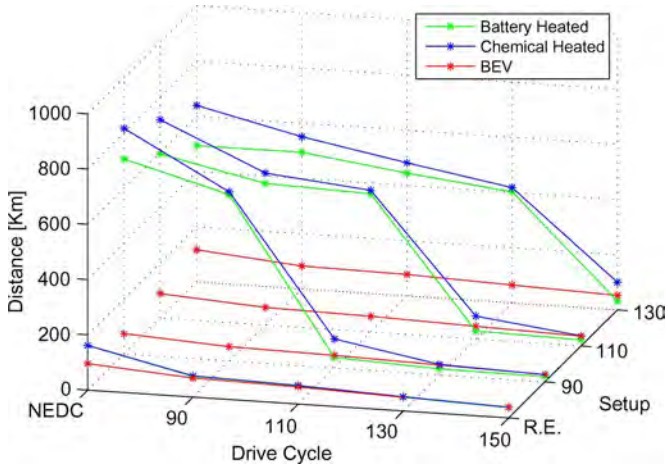

Fig. 10. Range of the setups in the different driving cycles.

TABLE VI
REMAINING METHANOL (IN LITERS) IN ELECTRICAL HEATING SIMULATIONS

Set-up	Driving cycle				
	NEDC	90	110	130	150
Range Extender	0	≈ 7	≈ 7.5	≈ 8	≈ 8
90 FCHEV	0	0	≈ 92	93	93
110 FCHEV	0	0	0	$\approx$81	81
130 FCHEV	0	0	0	0	$\approx$73

designed. Hence, the vehicle setup with a RE was designed for NEDC, and only this driving cycle has an improved range over the simulation with an empty methanol tank. The 90 FCHEV setup designed for 90 km/h has better range results for the NEDC driving cycle and 90 motorway driving cycles. This trend continues for the other two setups. In the simulations with the chemical heating tests, all except the 90 FCHEV at 150 km/h provide a longer range than for the empty simulations. The 90 FCHEV at the 150-km/h simulation last closes to 10 min.

The range results obtained are not always the maximum range that the vehicle is able to obtain, as the vehicle is sometimes able to continue at reduced speeds because there is still methanol left in the tank during these simulations. This would be valid for daily operation, but this is not included in these simulations. The remaining methanol in the simulations is presented in Table VI.

The remaining methanol can be converted to the range at reduced speeds, and the reduced speed is defined by the size of the FC. If the power is high, then the reduced top speed will also be high.

B. Energy Usage Results

The energy usage results indicate the amount of power needed to move the car by 1 km. The results are presented in Table VII, where the first column and the bottom row contain the mean of the other columns or rows.

The empty simulations and the RE setup both have below average and the lowest energy usage results of all FC situations and setups, but they have, respectively, no used heating energy and the lowest weight. The heated energy per kilometer is

TABLE VII
MEAN USAGE SETUP (IN WATTHOURS PER KILOMETER)

Set-up	Fuel cell simulation			
	Average	Empty	Chemical	Electrical
Range Extender	255	241	262	262
90 FCHEV	305	251	322	342
110 FCHEV	309	256	322	350
130 FCHEV	316	267	324	357
Average	296	254	307	328

TABLE VIII
BEV AND PREHEATED RESULTS

Set-up	Fuel cell simulation: Empty				
	NEDC	90	110	130	150
Range Extender	97%	99%	99%	99%	99%
90 FCHEV	97%	99%	99%	99%	99%
110 FCHEV	97%	99%	99%	99%	99%
130 FCHEV	97%	99%	99%	99%	99%
Set-up	Fuel cell simulation: Chemical				
	NEDC	90	110	130	150
Range Extender	92%	97%	97%	97%	97%
90 FCHEV	74%	89%	87%	83%	79%
110 FCHEV	76%	89%	89%	86%	80%
130 FCHEV	77%	90%	89%	89%	86%

higher than the average, which is mainly due to energy used for heating and the increased mass of the methanol. The chemical heating method has better performance than the electrical heating method, but this is due to two observations: less weight due to methanol used for heating and a longer driving range before running out of energy on the battery. In all chemical heating simulations, the FC stack passed the heating phase.

C. Power Electronics and Braking Resistor Efficiency Results

The power electronics and the braking resistor consist of the boost converter, the braking resistor, and the inverter, and they transfer electricity between the motor, the power sources, and the auxiliary components. The efficiency of the power electronics can indicate if the setup is close to the optimal or far from it as the power electronics are similar for all the setups. Hence, the difference in efficiency is caused by factors outside the power electronics.

The efficiency results for the EV running only on a battery and while being chemically heated are presented in Table VIII and calculated as follows:

$$\eta = \frac{P_{\mathrm{EM}} + P_{\mathrm{AUX}}}{P_{\mathrm{FC}} + P_{\mathrm{Bat}}}. \tag{30}$$

The empty efficiency results show the performance of the inverter and the combined performance of the braking resistor and the inverter. The constant speed tests indicate the efficiency of the inverter to be 99% and the efficiency of the (loss of the) braking resistor and the inverter to be 97% during NEDC.

The chemical heating FC simulations show that the RE setup has an almost constant efficiency of 97% at constant speeds, whereas there is more variation in the other setups. The other setups have, at their designed velocities, efficiency of 89% with increasing efficiency at lower velocities, where the highest is 90% for the 130 FCHEV going at a constant 90 km/h. When going faster, the efficiency drops to 79% for the 90 FCHEV going at a constant 150 km/h. In the NEDC driving cycle, the efficiency drops even further to the range of 74%–92%. The results show that the FC has problems following the power needed for the NEDC, which caused the SoC of the batteries to cycle close to full capacity.

V. CONCLUSION

The vehicle setups proposed in this paper have demonstrated how the setups fulfill the design requirement and deliver improved results in drive cycles with a lower range. (The range is shown in Table IX.)

It is proven that, when exceeding the design requirement, the range drops to roughly half, whereas the FCHEV setups drop to 5%–8% for the electrically heated FC stack and to 18%–27% for the chemically heated FC stack. These diminishing range results do not take into account the range obtainable with reduced velocity as remaining methanol has an impact on these results (shown in Table VI). The remaining methanol is equal to the unused energy, which could be converted to range.

Table VI, which shows the worst electrically heated simulation results, highlights the fact that there is not enough time to begin the FC stack before the batteries are empty. The vehicle therefore runs at the desired speed for less than 10 min. In these tests, the batteries run out of energy and can therefore not heat up the fuel stack to the desired temperature. Consequently, the vehicle is unable to continue on reduced velocity.

Chemical heating can resolve the problem of heating the FC stack when the battery is depleted of energy. It can also obtain a longer range when compared with electrical heating, due to higher efficiency in the former. However, the chemical heating process can have a longer start-up time and can be more expensive.

The power electronics and braking resistor efficiency results indicate that the FCs are not controlled to optimize variable load cycles, e.g., NEDC. The results highlight that a potential efficiency gain of at least 15% can be obtained with better FC control. In the remaining drive cycles, the power electronics have efficiency of at least 89%.

The power consumption per kilometer and overall efficiency are better in the simulations with an empty tank compared with the other simulations. The average power consumption per kilometer is 253.59, 307.45, and 327.88 Wh/km for the empty tank, chemical heating, and electrical heating simulations, respectively. The different vehicle setups have the following average usage. The RE has 255.03 Wh/km. The 90 and 110 FCHEV setups resemble each other with 305.21 and 309.33 Wh/km, respectively. The 130 FCHEV setup has larger usage of 315.66 Wh/km, which, percentagewise, cannot be explained only by the increased mass but is considered since the mass affects the motor size, which then again increases the power source.

The iMiev has space for four passengers, and the boot capacity is 235 L; however, when there are two passengers in the car, the luggage space increases to 860 L. Hence, each of the four setups is possible, but only the first setup guarantees transportation of four passengers.

TABLE IX
RANGE RESULTS

Set-up	Fuel cell simulation	Driving cycle				
		NEDC	90	110	130	150
Range Extender	Electrical	160.85 [km]	75.33 [km]	65.27 [km]	50.23 [km]	37.71 [km]
90 FCHEV	Electrical	706.16 [km]	601.93 [km]	37.71 [km]	21.78 [km]	19.08 [km]
110 FCHEV	Electrical	593.8 [km]	512.6 [km]	500.13 [km]	28.64 [km]	21.92 [km]
130 FCHEV	Electrical	493.42 [km]	494.78 [km]	444.55 [km]	401.88 [km]	32.21 [km]
Range Extender	Chemical	161.48 [km]	76.85 [km]	66.95 [km]	51.78 [km]	39.21 [km]
90 FCHEV	Chemical	816.75 [km]	611.78 [km]	105.29 [km]	38.13 [km]	26.54 [km]
110 FCHEV	Chemical	717.63 [km]	549.53 [km]	512.81 [km]	82.73 [km]	36.58 [km]
130 FCHEV	Chemical	639 [km]	550.78 [km]	482.01 [km]	417.16 [km]	100.33 [km]
Range Extender	Empty	95.61 [km]	68.95 [km]	61.69 [km]	49.54 [km]	38.71 [km]
90 FCHEV	Empty	73.92 [km]	51.83 [km]	45.81 [km]	36.11 [km]	27.25 [km]
110 FCHEV	Empty	88.07 [km]	63.33 [km]	56.81 [km]	45.86 [km]	35.92 [km]
130 FCHEV	Empty	116.42 [km]	82.88 [km]	77.61 [km]	64.46 [km]	52.71 [km]

This configuration does not take into account the possibility of placing any of the equipment in the motor compartment in the rear or in the space used by the old battery pack, which is under the floor [24]. The sizes of these compartments are unknown, but all the setups tested are possible and not just theoretical setups.

The advantages for the FCHEV setups are as follows:

1) longer normal operation range (more than four times on highway driving cycles);
2) faster refilling;
3) the main vehicle operates in the same way as a vehicle with an ICE.

Advantages for the BEV with a RE are as follows:

1) better efficiency;
2) better energy-to-kilometer ratio;
3) smaller drive train in both volume and weight;
4) In the second vehicle, it cannot be replaced with an ICE as none of the setups used in the simulations could run on FCs alone. This is demonstrated by the fact that no simulation with this setup used up all the methanol; however, as a second vehicle, it fulfills the requirement of having a lower price.

VI. FUTURE WORK

If a new standard driving cycle for start-up and entry to the motorway is obtained, then a redesign of the vehicle setups would give a more precise result of the actual range, which the average driver would obtain.

Other Li-ion battery models based on actual tests give more diversity and/or better simulations.

A motor designed specifically for the driving cycle rather than the vehicle requirements would yield better efficiency results.

An improved FC control strategy would yield improved efficiency results in city driving.

REFERENCES

[1] *A Portfolio of Power-trains for Europe: A Fact-Based Analysis—The Role of Battery Electric Vehicles, Plug-In Hybrids and Fuel Cell Electric Vehicles*, New York: McKinsey, 2012,Tech. Rep.
[2] M. Pehnt, "Life-cycle assessment of fuel cell stacks," *Int. J. Hydrogen Energy*, vol. 26, no. 1, pp. 91–101, Jan. 2001.
[3] G. Tian, S. Wasterlain, D. Candusso, F. Harel, D. Hissel, and X. Francois, "Identification of failed cells inside pemfc stacks in two cases: Anode/cathode crossover and anode/cooling compartment leak," *Int. J. Hydrogen Energy*, vol. 35, no. 7, pp. 2772–2776, Apr. 2010.
[4] *Fuel Cell Technologies Program*, U.S. Department of Energy (DOE), Washington, DC, 2011. [Online]. Available: http://www1.eere.energy.gov/hydrogenandfuelcells/pdfs/accomplishments.pdf
[5] F. Mapelli, D. Tarsitano, and M. Mauri, "Plug-in hybrid electric vehicle: Modeling, prototype realization, and inverter losses reduction analysis," *IEEE Trans. Ind. Electron.*, vol. 57, no. 2, pp. 598–607, Feb. 2010.
[6] D. W. Gao, C. Mi, and A. Emadi, "Modeling and simulation of electric and hybrid vehicles," *Proc. IEEE*, vol. 95, no. 4, pp. 729–745, Apr. 2007.
[7] E. Schaltz, "Design of a fuel cell hybrid electric vehicle drive system," Ph.D. dissertation, Dept. Energy Technol., Aalborg Univ., Aalborg, Denmark, 2010.
[8] C. C. Chan, A. Bouscayrol, and K. Chen, "Electric, hybrid, and fuel-cell vehicles: Architectures and modeling," *IEEE Trans. Veh. Technol.*, vol. 59, no. 2, pp. 589–598, Feb. 2010.
[9] M. Ehsani, Y. Gao, and A. Emadi, *Modern Electric, Hybrid Electric, and Fuel Cell Vehicles—Fundamentals, Theory, and Design*, 1st ed. Boca Raton, FL: CRC, 2005.
[10] A. Emadi, *Handbook of Automotive Power Electronics and Motor Drives*, 1st ed. New York: Taylor & Francis, 2005.
[11] S. M. Lukic and A. Emadi, "Performance analysis of automotive power systems: Effects of power electronic intensive loads and electrically-assisted propulsion systems," in *Proc. IEEE VTC*, 2002, vol. 3, pp. 1835–1839.
[12] F. Casanellas, "Losses in PWM inverters using igbts," *Proc. Inst. Elect. Eng.—Elect. Power Appl.*, vol. 141, no. 5, pp. 235–239, Sep. 1994.
[13] Saft, *Saftbatteries*, 2010. [Online]. Available: http://www.saftbatteries.com
[14] S. Soylu, Ed., *Electric Vehicles—Modelling and Simulations*. Rijeka, Croatia: Intech, 2011.
[15] S. H. Jensen, X. Sun, S. D. Ebbesen, R. Knibbe, and M. Mogensen, "Hydrogen and synthetic fuel production using pressurized solid oxide electrolysis cells," *Int. J. Hydrogen Energy*, vol. 35, no. 18, pp. 9544–9549, Sep. 2010.
[16] C. Graves, S. D. Ebbesen, M. Mogensen, and K. S. Lackner, "Sustainable hydrocarbon fuels by recycling CO_2 and H_2O with renewable or nuclear energy," *Renew. Sustain. Energy Rev.*, vol. 15, no. 1, pp. 1–23, Jan. 2011.
[17] J. Zhang, Z. Xie, J. Zhang, Y. Tang, C. Song, T. Navessin, Z. Shi, D. Song, H. Wang, D. P. Wilkinson, Z.-S. Liu, and S. Holdcroft, "High temperature PEM fuel cells," *J. Power Sources*, vol. 160, no. 2, pp. 872–891, Oct. 2006.
[18] S. J. Andreasen, J. R. Vang, and S. K. Kær, "High temperature pem fuel cell performance characterisation with CO and CO_2 using electrochemical impedance spectroscopy," *Int. J. Hydrogen Energy*, vol. 36, no. 16, pp. 9815–9830, Aug. 2011.
[19] S. J. Andreasen, L. Ashworth, I. N. M. Remon, and S. K. Kær, "Directly connected series coupled HTPEM fuel cell stacks to a li-ion battery DC bus for a fuel cell electrical vehicle," *Int. J. Hydrogen Energy*, vol. 33, no. 23, pp. 7137–7145, Dec. 2008.
[20] S. J. Andreasen, J. L. Jespersen, E. Schaltz, and S. K. Kær, "Characterisation and modelling of a high temperature PEM fuel cell stack using electrochemical impedance spectroscopy," *Fuel Cells*, vol. 9, no. 4, pp. 463–473, Aug. 2009.

[21] G. Avgouropoulos, J. Papavasiliou, M. K. Daletou, J. K. Kallitsis, T. Ioannides, and S. Neophytides, "Reforming methanol to electricity in a high temperature PEM fuel cell," *Appl. Catalysis B, Environ.*, vol. 90, no. 3/4, pp. 628–632, Aug. 2009.
[22] *Serenergy*, Dec. 2011. [Online]. Available: http://www.serenergy.dk/
[23] S. J. Andreasen, "Design and control of high temperature PEM fuel cell system," Ph.D. dissertation, Dept. Energy Technol., Aalborg Univ., Aalborg, Denmark, 2009.
[24] Mitsubishi, *Mitsubishi iMiEV elbiler—Teknik*, 2011. [Online]. Available: http://www.imiev.dk/mitsubishi-elbiler-teknik.aspx

Hans-Christian B. Jensen was born in Copenhagen, Denmark, in 1975. He received the M.Sc. and Ph.D. degrees in automation and control engineering from the Department of Control Engineering, Aalborg University, Aalborg, Denmark, in 2000 and 2003, respectively.

Since 2010, he has been a Postdoctoral Researcher with the Department of Energy Technology, Aalborg University. His research interests include the analysis, modeling, design, fault detection, automation, and control of fuel-cell stacks and electric vehicles.

Erik Schaltz (S'05–M'06) was born in Viborg, Denmark, in 1981. He received the M.Sc. and Ph.D. degrees in electrical engineering from the Department of Energy Technology, Aalborg University, Aalborg, Denmark, in 2005 and 2010, respectively.

Since 2009, he has been with the Department of Energy Technology, Aalborg University, where he is currently an Associate Professor. His research interests include the analysis, modeling, design, and control of power electronics; electric machines; and energy storage devices, including batteries, fuel cells, hybrid electric vehicles, and thermoelectric generators.

Per Sune Koustrup received the M.Sc. degree in international business from Aarhus School of Business, Aarhus University, Aarhus, Denmark, in 2006 and the Ph.D. degrees in electric vehicles and range extenders and in advanced energy system analysis on the energy PLAN model from Aalborg University, Aalborg, Denmark, in 2011 and 2012, respectively.

He is currently with Intelligent Cells, Aarhus, Denmark.

Søren Juhl Andreasen was born in Aalborg, Denmark, in 1981. He received the M.Sc. degree in mechanical engineering with specialization in electromechanical system design and the Ph.D. degree from Aalborg University, in 2005 and 2009, respectively.

In 2012, he was appointed Associate Professor with Aalborg University. He is involved in research concerning applied electrochemical impedance spectroscopy on fuel cells and lithium-ion batteries for electrical vehicle traction. His main research interests include theoretical and experimental analysis and the control of fuel-cell systems with a special focus on high-temperature polymer-electrolyte-membrane fuel cells and methanol reformer systems.

Søren Knudsen Kær was born in Brønderslev, Denmark, in 1972. He received the M.Sc. degree in mechanical engineering and the Ph.D. degree from Aalborg University, Aalborg, Denmark, in 1996 and 2001, respectively.

In 1999, he was a Visiting Researcher with Lawrence Livermore National Laboratories, Livermore, CA. In 2001, he was a Postdoctoral Fellow with Brigham Young University, Provo, UT. In 2006, he initiated the Hydrogen and Fuel Cell Academy: a doctoral school within Aalborg University with participation from the Technical University of Denmark. In 2007, he was appointed Professor with Aalborg University with a grant from the Obel Foundation. He started a fuel-cell research program, where he is currently the Head of 15 researchers. His main research interests include computational fluid dynamics modeling of fuel cells and reformer reactors and thermodynamic modeling of fuel-cell systems.

Appendix 2

Paper submitted to: International Journal of Hydrogen Energy

"Test of Hybrid Power System for Electrical Vehicles Using a Lithium-Ion Battery Pack and a Reformed Methanol Fuel Cell Range Extender"

Test of Hybrid Power System for Electrical Vehicles Using a Lithium-Ion Battery Pack and a Reformed Methanol Fuel Cell Range Extender

Søren Juhl Andreasen[1,a], *Leanne Ashworth*[b], *Simon Sahlin*[a]

Hans-Christian Becker Jensen[a] *and Søren Knudsen Kær*[a]

[a] Department of Energy Technology, Aalborg University, Pontoppidanstræde 101,DK-9220 Aalborg East, Denmark ,[1] sja@et.aau.dk

[b] Serenergy A/S, Majsmarken 1,DK-9500 Hobro, Denmark

Abstract

This work presents the proof-of-concept of an electric traction power system with a high temperature polymer electrolyte membrane fuel cell range extender, usable for automotive class electrical vehicles. The hybrid system concept examined, consists of a power system where the primary power is delivered by a lithium ion battery pack. In order to increase the run time of the application connected to this battery pack, a high temperature PEM (HTPEM) fuel cell stack acts as an on-board charger able to charge a vehicle during operation as a series hybrid. Because of the high tolerance to carbon monoxide, the HTPEM fuel cell system can efficiently use a liquid methanol/water mixture of 60%/40%, as fuel instead of compressed hydrogen, enabling potentially a higher volumetric energy density.

In order to test the performance of such a system, the experimental validation conducted uses a down-sized version of the battery pack used in the Mitsubishi iMiEV, which is subjected to power cycles derived from simulations of the vehicle undergoing multiple New European Drive Cycles (NEDC).

1 Introduction

Powering automotive vehicles using electric energy enables the use of different types of hybrid electrical configurations for increasing the fuel efficiency and reducing emissions. Battery electric vehicles powered 100% by batteries show good well-to-wheel efficiencies, but are still suffering from short range and long charging times. Fuel cell range extenders is one way of improving the driving range of electric vehicles using series or parallel hybrid configurations, where a fuel cell system efficiently charges the vehicle battery pack. Depending on the desired performance of the vehicle, the power provided by the battery system and fuel cell can be balanced, this work examines a system with a battery pack delivering the primary power, with a fuel cell charger that offers a smaller constant charge on the battery pack during driving.

Different fuel cell system solutions exist, the main differences depend on the fuel used. High temperature PEM fuel cells offer the possibility of using liquid fuels such as methanol, due to the high operating temperatures (160-180^{o}C). The methanol is converted to a hydrogen rich gas with CO_2 and traces of CO, and the increased operating temperatures allow these fuel cells to tolerate much higher CO concentrations than Nafion-based fuel cells. The increased tolerance to CO also enables the use of reformer systems with less hydrogen cleaning steps and requirements for hydrogen purity, reducing the complexity of the reformer systems. Using hydrogen containing CO, affects the steady-state as well as dynamic electrical performance of the fuel cell, but stable operation is still possible with concentrations up to 3% [1, 2, 3]. The typical polymer used in HTPEM fuel cells is polybenzimidazole (PBI), doped with phosphoric acid for proton conduction removing some of the disadvantages of Nafion-based low temperature PEM fuel cells that require the presence of liquid water for proton conduction.

Using liquid fuels such as methanol removes the high volume demands of compressed hydrogen storages, simplifies refueling, and enables the use of existing fuel distribution systems. Recent studies show the capabilities and advantages of using methanol reformer systems [4, 5, 6].

2 Experimental setup

This work demonstrates the use of a methanol fuelled fuel cell range extender for an originally battery electric vehicle. The Mitsubishi iMiEV is taken as an example of a commercially available small city car. The authors did not have the vehicle available for experimental characterization of power consumption versus drive pattern instead it was calculated using a mathematical drive cycle simulation program [7]. The New European Drive Cycle (NEDC) was used as input for these simulations. The details of the drive cycle simulations, the battery pack, and the fuel cell system are given in subsequent sections but in summary a 11 kWh battery pack was used in combination with 1.6 kW of fuel cell range extender power.

The system tested in this work includes a HTPEM fuel cell stack. The fuel for the stack is supplied by methanol steam reforming, and a DC/DC converter controls the fuel cell stack charging of the lithium-ion battery pack. In order to ensure safe operation this battery pack is monitored by a Battery Management System (BMS). A diagram of the test system is shown in figure 1.

The control system used was an EtherCAT (Ethernet for control automation technology) from Beckhoff.

The control and data acquisition of the fuel cell and reformer system is handled by an EtherCAT

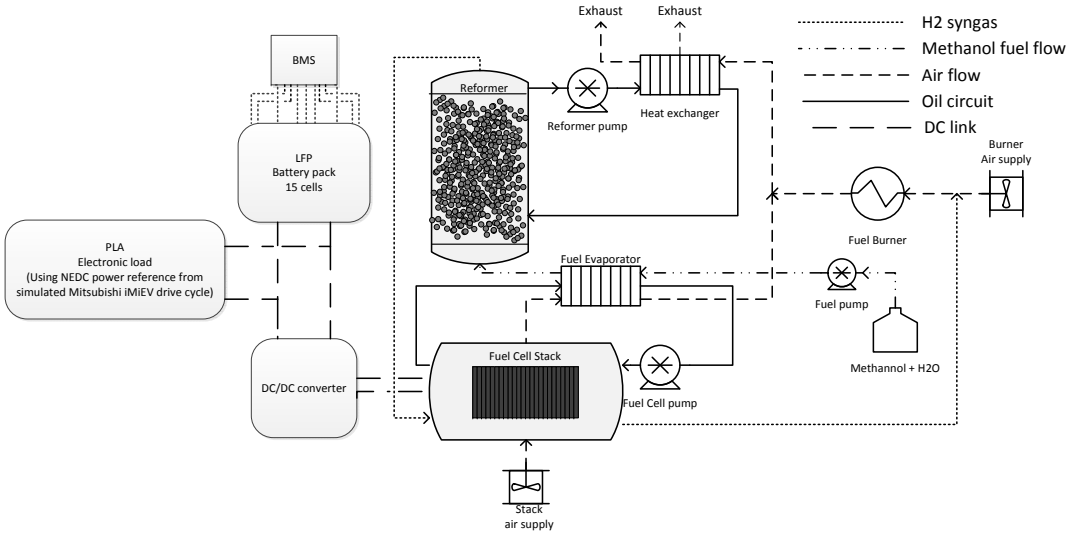

Figure 1: Schematic of the system setup including the primary components and connections.

(Ethernet for control automation technology) from Beckhoff. An EK1100 coupler was connected with a number of I/O terminals for measuring and actuating all sensors and BOP components. The EK1100 was connected to a PC running TwinCat and Labview. The control and data acquisition systems were programmed in a Labview virtual interface (VI). The battery management system logs the data of each battery cell every 1000ms. The emulation of the drive cycle on the vehicle is handled by a National Instruments USB-6215 and a Labview VI, that produces analog reference signals to the Amrel PLW25K-600-600 water cooled electronic load. The electronic load is only able to sink current, which means that regenerative breaking is disregarded in these experiments and conclusions.

2.1 Drive cycle emulation

In order to test the concept of using the proposed HTPEM fuel cell system topology, as a range extender in an electrical automotive applications, the Mitsubishi iMiEV is chosen as a case study. The main parameters used in the simulations can be found in table 1.

Parameter	Value	Unit
Weight (w/o power train)	1035	[kg]
Frontal area	2.17	[m^2]
Drag coefficient	0.24	[-]

Table 1: Main vehicle input parameters.

The power requirements for completing a sequence of New European Drive Cycles have been found

by using the simulation model described in [7]. The velocity profile for the NEDC can be seen in figure 2. The resulting power reference output by the model is down-scaled to match the maximum current of the reduced battery pack. The fuel cell power was chosen to match approximately the average power required to complete the NEDC. The same down-scale factor was then used for the fuel cell system and the battery pack. The fact that regenerative breaking could not be realized in the experimental setup and the startup of the fuel cell was disregarded in the simulation caused the battery pack SoC to decrease slightly during the experiments. This can be seen from figure 11. The used power profile has a maximum peak power of 16kW and the stack power supplies the average power required to complete the drive cycle, approximately one third of the rated 5 kW i.e. the fuel cell range extender is set to deliver a constant power of 1.6 kW when connected.

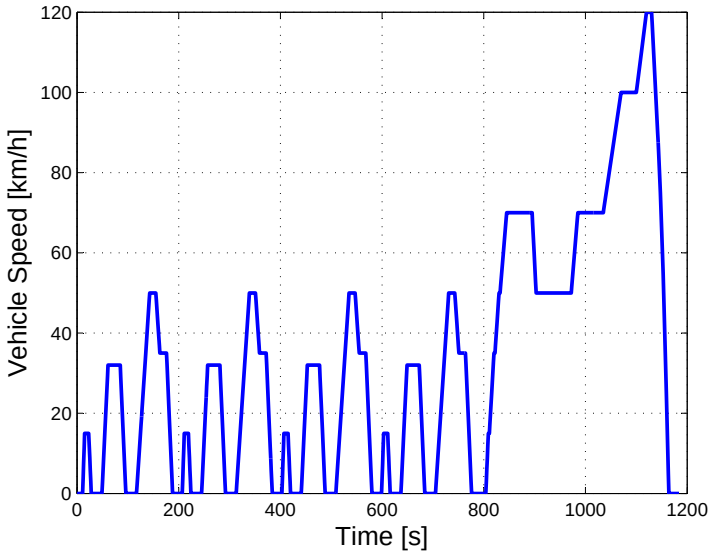

Figure 2: Velocity profile of New European Drive Cycle (NEDC).

In the following, the main components: Fuel cell stack, Methanol Reformer and Battery pack, and the different subsystems involved will be described in more detail.

2.2 Fuel Cell Stack

The fuel cell stack used is the Serenergy S165L-120, a 120 cell, liquid cooled, using a thermal oil such as tri-ethylene-glycol. The fuel cells used are Celtec P1000 with an active area of 165 cm^2 and their inherent high tolerance to CO concentrations of up to 2-3%. A picture of the fuel cell stack can be seen in figure 3.

The fuel cell stack is rated to an output power of 5kW, and a polarization curve can be seen in figure 4. To control and condition the power delivered by the fuel cell stack a DC/DC buck converter

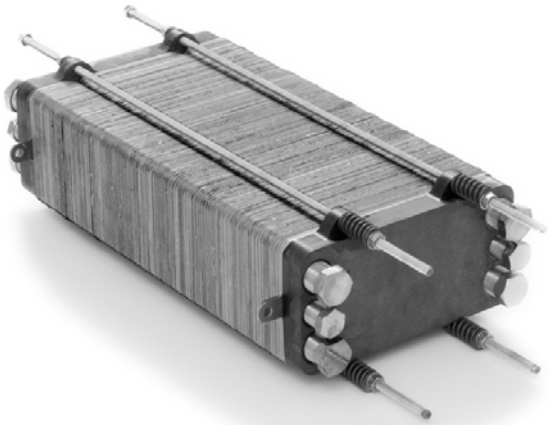

Figure 3: 5 kW high temperature PEM fuel cells stack, Serenergy S165L-120.

(DCDC72/50/8000) from Zahn Electronics inc. is used.

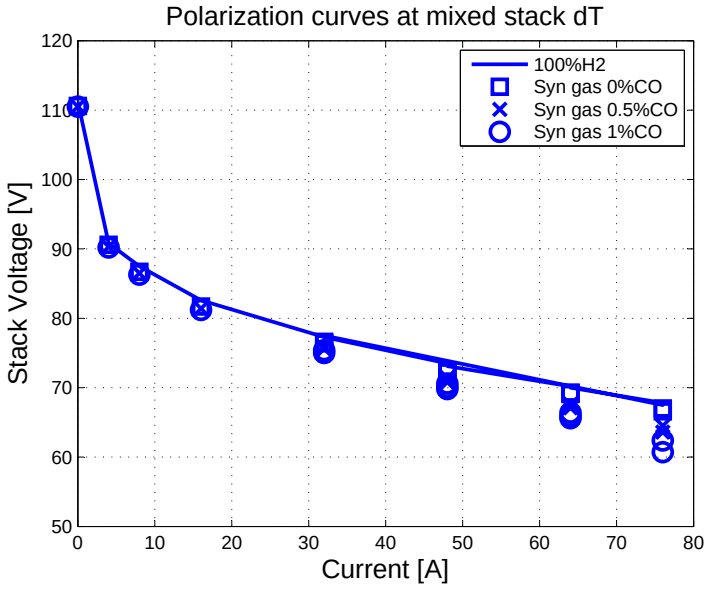

Figure 4: Polarization curves of 120 cell stack using different gas compositions. At an average stack temperature of 160^{o}C.

2.3 Methanol Reformer

The methanol reformer is designed as a tube-in-tube heat exchanger, the reformer part is filled with a BASF Selectra RP60 pellet based CuZn reformer catalyst. Equation 1 and 2 summarize the reactions that dominate the steam reforming within the operating conditions.

$$CH_3OH + H_2O \quad \leftrightarrow \quad 3H_2 + CO_2(49.5kJ/mol) \tag{1}$$

$$CO + H_2O \quad \leftrightarrow \quad H_2 + CO_2(-41kJ/mol) \tag{2}$$

The overall reaction is endothermic and heat is added to the reformer using an integrated oil heating of the catalyst bed. Heat is supplied externally to the oil from a catalytic burner running on the waste anode gas from the fuel cell stack. Figure 5 shows an example of the measured output gas composition as a function of fuel flow at 240^{o}C. For methanol reformers using this catalyst this is the typical gas quality; CO concentration increases with increasing temperatures, and residual unconverted methanol decreases with these increasing temperatures.

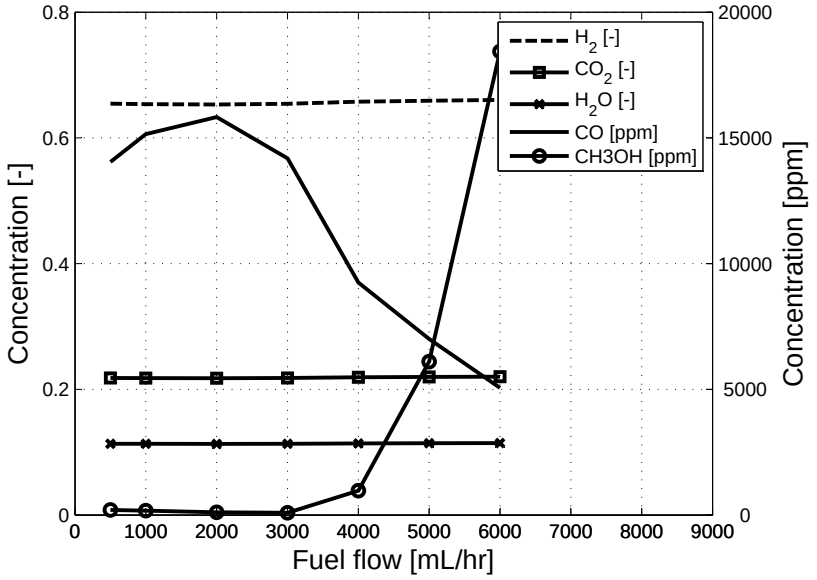

Figure 5: Output gas composition of the methanol reformer as a function reformer input flow at 240 ^{o}C.

2.4 Battery pack

The full power system has been designed as a scaled down version of the power system for the Mitsubishi iMiEV which originally has a 16 kWh battery pack. The battery pack used in these experiments is approximately 11 kWh and the power consumption used in the tests is scaled by 2/3, which is the ratio between the original motor size and the simulated motor size. The batteries used are Thundersky LFP400AHA, 400 Ah cells, and the battery pack consists of 15 series connected cells. To ensure safe

battery charging and discharging a BMS and relay box from Lithium Balance A/S is mounted to monitor and in case of emergency disconnect the battery pack. The BMS consists of a local monitoring unit LMU connecting each cell voltage to the BMS and monitoring the voltages and relaying information via CAN bus to the battery management control unit BCMU that handles decision making, data logging and system monitoring of the battery pack. The BCMU also controls the charging and balancing of the battery cells and can be used to monitor pack temperature, estimate state-of-charge and detect current leakage and insulation faults. For monitoring larger battery packs additional LMUs can be added to the system and connected to the common CAN communication protocol (se figure 6)

Figure 6: Lithium Balance Battery Management System, one BCMU and LMU shown in picture.

3 Experimental results

In order to evaluate the use of the proposed system as a range extender for automotive applications, a scaled down system test is conducted on the mentioned fuel cell / battery power system using an electronic load to emulate the drive cycle and compare the performance with and without the fuel cell range extender system. In the following, the experimental results are analyzed addressing each individual part of the traction power system:

- Battery pack
- Fuel cell stack
- Reformer system

3.1 Battery

The battery pack voltage is at 50V at the start of the experiment, as can be seen on figure 7. At the middle of the initial NEDC the fuel cell and reformer system heating is completed, and the system starts delivering power to the battery pack. During this time the battery pack supplies all the electrical power for the traction power. After the first sequence is completed, the DC/DC converter starts charging the batteries with the fuel cell stack. Positive currents indicate that energy is flowing to the battery pack, and it is clear from figure 7, that during the periods of idling in the drive cycle, the battery pack is charged with all the available fuel cell current in that operating point, approximately 21.5A.

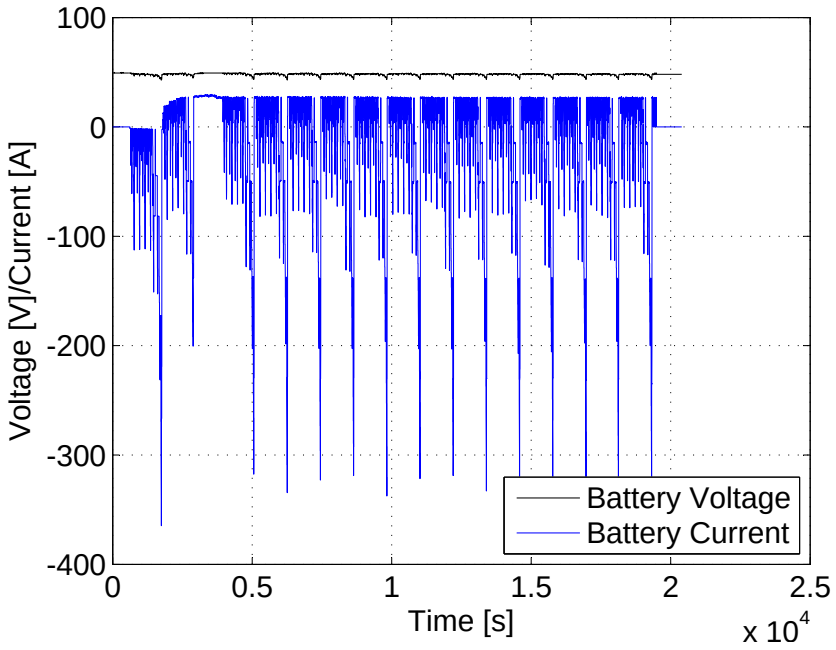

Figure 7: Graph of the battery pack voltage and current during drive cycles emulation.

In the initial drive cycle with fuel cell stack connected, the fuel cell current slightly increases as the system is heating and reaching the steady state temperature. Generally the addition of the fuel cell stack can be seen as the current load profile being shifted towards a smaller average current drawn from the battery pack. In real life driving, the overall effect on the range of the vehicle will depend very much on the type of drive cycle experienced by the vehicle. The drive cycles only slowly discharges the battery, it can be seen that the battery voltage, which has an initial value of 50V, decreases continuously down to 48.1V, where the tests are stopped. As mentioned above, the fuel cell system was designed to deliver the average power consumption of the drive cycle and the voltage should remain constant. However, as the heating phase consumes energy from the battery pack and regenerative breaking power is not included in the experiments, there is a slight voltage drop during the experiments.

Looking closer at one single drive cycle, which is visible in figure 8, the system voltage can be seen.

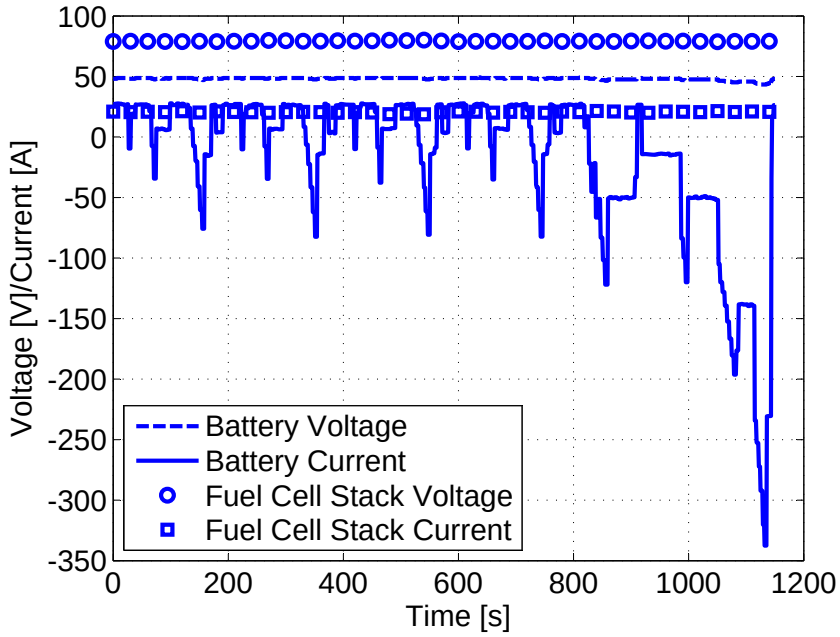

Figure 8: Graph of the battery pack voltage and current during emulation of a single drive cycle.

The battery voltage is kept somewhat constant, even with a slight increase, because of the range extender, but as the drive cycle in the final highway driving profile exceeds the average power provided by the fuel cell stack, a more rapid decreasing voltage, and hereby state-of-charge is experienced. The fuel cell voltage and current are kept stable even though the battery current is fluctuating because of the controlled power drawn via the DC/DC converter.

3.2 Fuel Cell Stack

The graph in figure 9 shows the power drawn from the battery pack, and the power delivered from the fuel cell system. It is clearly seen that fuel cell stack, as it heats, increases the power delivered to the batteries, this is due to the increasing performance of the fuel cell system with increasing temperatures.

Because the DCDC converter is set to a constant output voltage matching the desired charging voltage of the battery pack. This means that the increase seen in power is due to a combination of the fuel cell stack slowly getting a more uniform temperature distribution and producing a higher voltage at the same current load point. The reformer exhibits a similar start-up phenomenon and after some time the output composition is at the desired values. The stack power settles at $\approx$1.6kW, and only has slight changes during the course of each NEDC, at some high current peaks the internal control system of

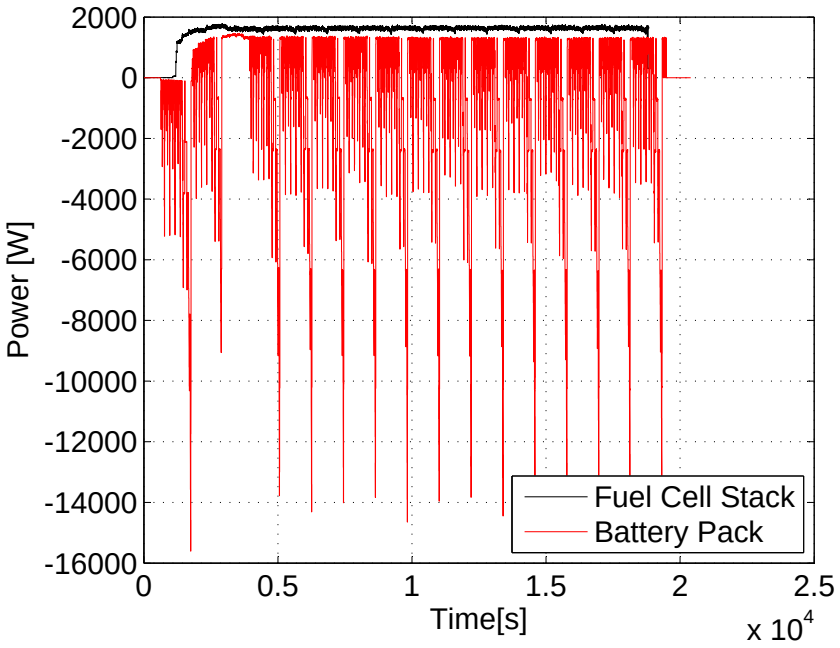

Figure 9: Graph of the power produced / consumed in the system during drive cycles emulation.

converter lags behind resulting in a slight fall in fuel cell power. The fuel cell stack voltage and current throughout the experiment settles after a few minutes of operating time to a voltage of 79.5V and a current of 21.5A.

3.3 Discussion

Even though the difference between the stack power used to constantly charge the battery pack (1.6kW), and the maximum power peaks of the drive cycle (16kW) are quite different in magnitude; the potential driving range is drastically altered which can be seen in figure 10. In figure 10, the measured power profile of two different tests using two NEDCs, one with the fuel cell range extender, and one without the fuel cell range extender is compared. A negative power is when current is drawn from the battery pack, and a positive power is when the battery pack is charged.

The main difference is that the power profile file measured with the range extender is superpositioned slightly by the power produced by the fuel cell system. By integrating the power profiles, the energy consumed can be calculated and compared in order to evaluate the effect of the onboard fuel cell charging system. Figure 11 shows the measured energy consumption of the battery pack during the two drive cycles imposed on the battery pack with and without the fuel cell range extender.

In the duration of the two sets of drive cycles, the result in the measurement running on pure battery

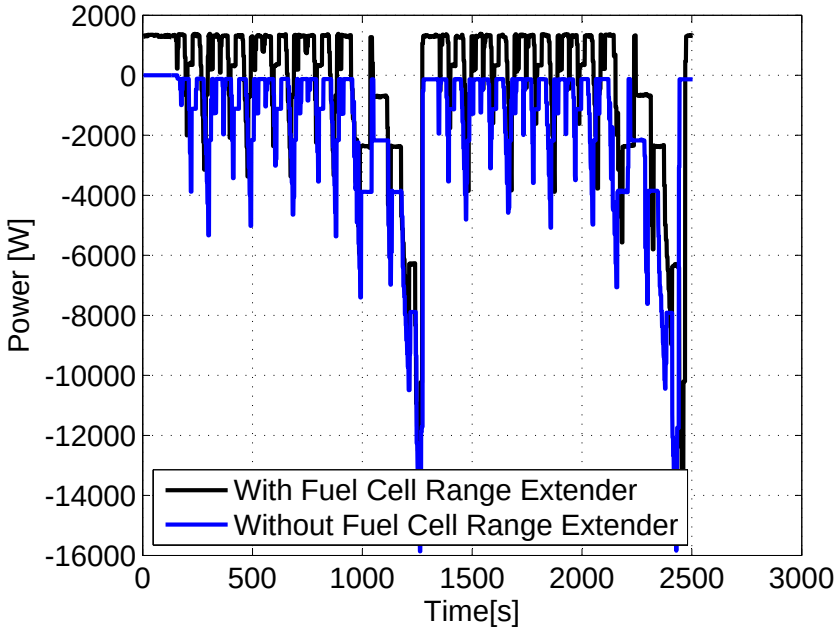

Figure 10: Power comparison of two experiments conducted using two NEDCs ; one with the fuel cell range extender, and one without.

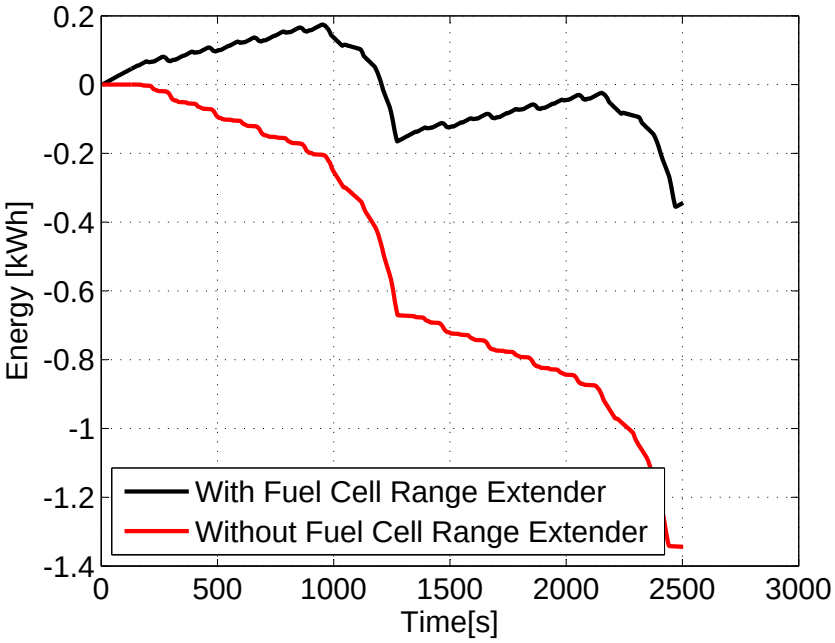

Figure 11: Energy consumption as a function of time with and without the fuel cell range extender.

energy, without the range extender is -1.35 kWh. The energy balance of the measurements of drive cycles with the fuel cell range extender results in a total consumption of -0.35 kWh, adding 1 kWh additionally, enabling a vehicle to potentially drive further. Adding the additional regenerative power

will of course also affect the final results, which depends a lot on the balance between available battery capacity, fuel cell power and average power consumption of the vehicle in question. In a similar way the results will also be affect by range extender control strategy, the energy and time used to heat the system. Whether the system is started up using electrical energy from the battery pack or chemical energy from the direct combustion of the methanol fuel, also plays a role. The considerations have not been analyzed in this work but, a few studies are available in the area of HTPEM fuel cell system heating strategies [8, 9].

In order to make a proper calculation of the full system efficiency of the fuel cell system, it is vital to know the power consumption of the balance of plant. A series of measurements have been conducted of each of the main contributors to the BOP power consumption. The BoP components included are: cathode blower, FC pump, reformer pump, burner blower, cooling radiator fan, PLC, anode valves, fuel pump, temperature controller and support electronics. Furthermore an efficiency of the BoP power supply of 95% is included. The power BoP power consumption can be seen as a function of delivered FC power in figure 12.

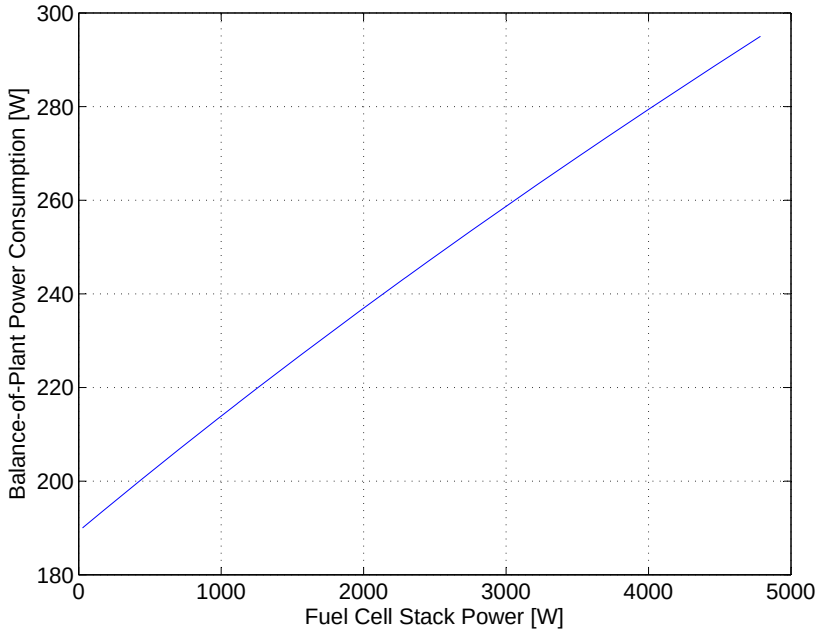

Figure 12: Balance-of-Plant power consumption as a function of fuel cell stack power.

Including the BoP power consumption the total system efficiency can be calculated as shown in Eq. 3.

$$\eta_{System} = \frac{P_{Electric}}{P_{Chemical}} = \frac{U_{FC} \cdot I_{FC}}{\dot{m}_{CH_3OH} \cdot LHV_{CH_3OH}} \tag{3}$$

In figure 13 the measured fuel cell stack and total system efficiency is show in the duration of the 15 drive cycles shown in figure 9.

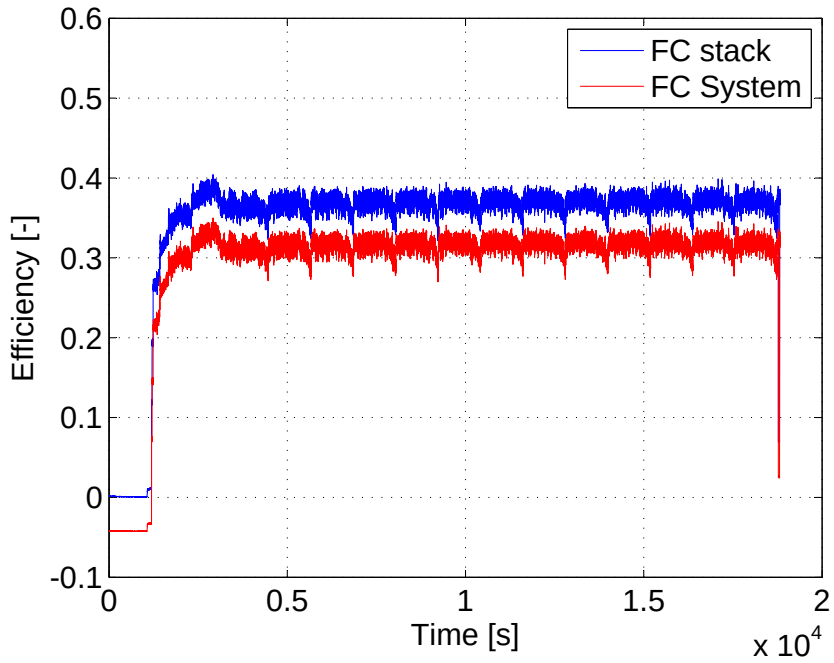

Figure 13: Graph of the fuel cell voltage and current during a single drive cycle emulation.

Because the fuel cell system is operating at constant temperature and constant current, the efficiency is steady throughout the course of the experiment. The short downward spikes seen on the efficiency occur during the rapid acceleration current spikes of the drive cycle, because of the internal voltage control of the DC/DC converter. The steady average efficiency of the fuel cell stack is 36.8% and for the total system it is 31.5%.

4 Conclusions

The concept of using a HTPEM fuel cell system fuelled by steam reformed methanol as a range extender in an electrical vehicle has been analyzed experimentally in this work on a scaled hybrid electrical system using emulated NEDCs based on a vehicle simulation model. Disregarding the absence of regenerative breaking, that potentially also is available to increase the run time of the battery pack during the drive cycle, the fuel cell acts as a stable and efficient range extender and significantly increases the run time and range of the power system. Depending of the actual driving profile of the application or vehicle in question the balance between battery and fuel cell power can of course be optimized. This work has experimentally demonstrated the use of a liquid cooled HTPEM fuel cell stack in a hybrid

electric system usable in vehicle applications.

5 Future work

In order to further detail the performance gain of using fuel cell range extenders, measurements on more integrated systems is needed. Furthermore other more realistic driving cycles should be used in order to fully determine the needed size of the range extender to a given application, and the total driving range increase gained. Because the system is working at elevated temperatures, additional information on the energy consumption of system heating is needed. The time required to heat the system will also play an important role in determining when the system is to be turned on and off, and which type of applications are of particular interest.

6 Acknowledgements

We gratefully acknowledge the financial support from the EUDP program and the Danish Energy Agency.

References

[1] Jianlu Zhang, Zhong Xie, Jiujun Zhang, Yanghua Tang, Chaojie Song, Titichai Navessin, Zhiqing Shi, Datong Song, Haijiang Wang, David P. Wilkinson, Zhong-Sheng Liu, and Steven Holdcroft. High temperature PEM fuel cells. *Journal of Power Sources*, 160:872–891, 2006.

[2] N. Wagner and E. Gülzow. Change of electrochemical impedance spectra during CO poisoning of the Pt and Pt-Ru anodes in a membrane fuel cell (PEFC). *Electrochemica Acta*, 48:3899–3907, 2004.

[3] Søren Juhl Andreasen, Jakob Rabjerg Vang, and Søren Knudsen Kær. High temperature PEM fuel cell performance characterisation with CO and CO2 using electrochemical impedance spectroscopy. *International Journal of Hydrogen Energy*, 36:9815–9830, 2011.

[4] Chao Pan, Ronghuan He, Qingfeng Li, Jens O. Jensen, Niels J. Bjerrum, Henrik A. Hjulmand, and Anders B. Jensen. Integration of high temperature PEM fuel cells with a methanol reformer. *Journal of Power Sources*, 145:392–398, 2005.

[5] Wei We and Che-Chuan Pai. Control of a heat-integrated proton exchange membrane fuel cell system with methanol reforming. *Journal of Power Sources*, 194:920–930, 2009.

[6] Rong-Fang Horng. Transient behaviour of a small methanol reformer for fuel cell during hydrogen production after cold start. *Energy Conversion and Management*, 46:1193–1207, 2005.

[7] Hans-Christian Becker Jensen, Erik Schaltz, Per Sune Koustrup, Søren Juhl Andreasen, and Søren Knudsen Kær. Evaluation of Fuel Cell Range Extender Impact on Hybrid Electrical Vehicle Performance. *IEEE Transactions on Vehicular Technology*, 62:50–60, 2013.

[8] Søren Juhl Andreasen and Søren Knudsen Kær. Modelling and evaluation of heating strategies for high temperature polymer electrolyte membrane fuel cell stacks. *International Journal of Hydrogen Energy*, 33:4655–4664, 2008.

[9] L. Jörissen J. Scholta, M. Messerschmidt and Ch. Hartnig. Externally cooled high temperature polymer electrolyte membrane fuel cell stack. *Journal of Power Sources*, 190:83–85, 2009.

List of Figures

List of Tables

Appendix 3

Market analysis report

Highly Integrated Electric Propulsion System

Enabling electric vehicles a range, refuelling time and comfort level similar to a gasoline vehicle by using li-ion batteries and a methanol HTPEM fuel cell range extender controlled by an advanced BMS

Final Project Report, WP7
EUDP project journal number: 64009-0218
Report Editor: Aalborg University

Utilizing heat from the fuel cells for heating-up the batteries and the cabin can result in a combined TTW heat-and-power efficiency above 80 % in cold weather for class A and B cars.

Source:
http://3.bp.blogspot.com/_7LQxj656qB0/TLh2TIlv_eI/AAAAAAAAJOA/Op4rnUnEPRM/s1600/2011+Citroen+C-Zero+20.jpg

Contents

Figures

Tables

Pictures

WP7: Market analysis

In this section a *Screening*, *Segmentation*, *Definition of representative segments & vehicles* and an *Analysis of the market for the HI-EPS unit* will be carried out. In the sub-section;

- "Screening" an overview of different types of vehicles will be presented and defined
- "Segmentation" the vehicle group "Cars" will be divided into 9 segments and a basic cost analysis of the cost pr. kW engine in different types of cars will be carried out.
- "Definition of representative segments & vehicles" three segments and three cars that represent these segments will be presented and analysed.
- "Technical assumptions" the technical assumptions that influence the power and energy-needs from batteries, fuel cells and energy-carriers are listed.
- "Analysis of the market for the HI-EPS unit" cost/benefit analyses based on the technical requirements are made.

By having made such an analysis one can evaluate whether the introduction of the HI-EPS in a certain vehicle and/or in a certain application is feasible from an economical point of view or not. Finally further recommendations and critique of the results are listed.

Screening

In order to analyse different vehicle types it is necessary to get an overview of which types exist. According to Statistics Denmark more than 4 million vehicles where on the roads in Denmark by January the 1st 2011.[1] In the table below the 4 million vehicles are divided into seven official groups. The groups are cars, busses, light duty vehicles (LDVs), heavy-duty vehicles (HDVs), mopeds and motorcycles, tractors and no motor. When excluding vehicles without motors there where 2.966.198 vehicles in Denmark by January the 1st 2011.

Table 1 – Number of vehicles in Denmark by January the 1st 2011

Vehicle type	No. of units	%	No. of analysis'
Cars	2.163.676	72.9	3
Busses	14.496	0.5	0
Light Duty Vehicles	441.455	14.9	0
Heavy Duty Vehicles*	42.712	1.4	0
Mopeds and motorcycles**	203.608	6.9	0
Tractors	97.911	3.3	0
No motor***	1.035.534	-	-
Total	4.001.732	-	-
Total with motor	2.966.198	100	3

* Trucks 28.480 + semi-stretch blockers (sættevognstrækkere) 12.891 + fire and rescue vehicles 1.341.
** Motorbikes 148.766 + moped 45 54.842.
*** Trailers up to 2 tons 815.517, trailers over 2 tons 42.053, semitrailers (sættevogne) 35.200, caravans 142.764.

In this analysis focus will be on "cars". With 73 % of all motorised vehicles in Denmark this is by far the biggest vehicle class. It has been decided to make three analyses in order to cover "cars" in a relatively comprehensive way.

[1] http://www.dst.dk/pukora/epub/Nyt/2011/NR138.pdf

Of special interest for HTPEM fuel cells are vehicles that;

- Run for as many hours in a row as possible (since it takes time to start-up the FC, the longer it runs the better in terms of lifetime)
- Runs at as low an average speed as possible (thereby decreasing the size measured in KW that the FC should be and thereby keeping the investment cost at a reasonable level)
- Can utilise as much of the waste-heat as possible (the waste-heat from a HTPEM fuel cell 1) is in a well-defined air stream and 2) comes at a high temperature meaning that it is easy to utilise a high part of the heat for heating and/or cooling purposes)
- Are used in areas where clean air is highly appreciated (urban vs. country)

Vehicles with these attributes are especially interesting not only because HTPEM fuel cells are strong in such applications but also because the two main competing technologies Internal Combustion Engines (ICE) and batteries are weak in applications with these attributes.

- ICEs e.g. have a poor efficiency at low loads (equal to low speeds), a poor efficiency when accelerating (change in loads) and are polluting.
- Batteries e.g. are poor at delivering energy for a long time (due to poor energy-density compared to gasoline and other liquid energy-carriers) and are poor at delivering heat (due to their high efficiency).

Vehicles with a perfect technological fit with the above listed attributes include city-busses and city-delivery-vans- and trucks. This analysis will however focus on cars. It is strongly recommended to make further analysis' regarding city-busses and city-delivery-vans- and trucks.

Segmentation

An official EU definition of car segments does not exist, but the EU-commission has on several occasions classified vehicles onto different segments when treating merger & acquisition cases between the major car manufacturers.[2] In the table below the different market segments according to the EU-commission and the Danish classification used by The Danish Car importers is seen in the first and the second column. In the third column the market share for the different car segments in Denmark for 2010 is seen.[3] In the fourth column the three most sold models for each class are listed.

[2] http://en.wikipedia.org/wiki/Euro_Car_Segment, http://ec.europa.eu/competition/mergers/cases/decisions/m416_en.pdf, http://ec.europa.eu/competition/mergers/cases/decisions/m1406_en.pdf,

[3] http://www.bilimp.dk/press/content.asp?id=361, Bilsalget i december 2010,18.1.2011, Chefkonsulent Tejs Lausten Jensen, 09-dec 10.

Table 2 – Car segments the associated market shares and the most sold models

EU-commission	Denmark	Market share (%)	3 most sold models, 2010
A - mini cars	lille klasse	47.21	**Toyota Aygo**, Chevrolet Spark, Opel Corsa
B - small cars			
C - medium cars	mellemklasse 1	21.44	**Ford Focus**, VW Golf, Hyundai I30
D - large cars	mellemklasse 2	15.17	**Toyota Avensis**, Ford Mondeo, Opel Insignia
E - executive cars	stor klasse	2.34	**Mercedes E-klasse**, BMW 5-serie, Audi A6
F - luxury cars	Luksus	0.07	**Jaguar XF**, Audi A8, Mercedes-Benz CLS
S - sport coupés	Sport	0.11	**Mazda MX-5**, Aston Martin Vantage, Lexus IS
M - multi cars	MPV	10.38	**Renault Scenic**, Citroen C4 Picasso, Ford C-Max
J - sport utility cars (incl. off-road vehicles)	øvrige	3.24	**Hyundai ix35**, Mitsubishi Outlander, Skoda Yeti
	el-biler	0.03	FIAT Fiorino, Tesla Roadster, FIAT Micro-VETT
	(livsstilsbiler)	(-)	Mini, Alfa Romeo Mito, Citroen DS3

Basic cost analysis

A basic cost analysis regarding the price pr. kW paid for engines as of today with and without taxes in Denmark will is carried out below. Based on the analysis's three segments will be defined for further analysis.

An analysis for all the 9 segments was to be carried out. In Denmark the class A and B are however merged (hereafter termed class A/B and A/B) of which reason the 9 segments are reduced to 8 segments. The most popular car from each segment, in terms of numbers sold in Denmark in 2010, will represent the segment in question. These vehicles are marked with bold in the above table. The vehicles will in order to be consistent and whenever possible be the cheapest model with 5 doors and with manual transmission (M/T).

This obviously results in a lot of bias since the cheapest model is not always the most popular one and is therefore not necessarily a good representation of that model. Gasoline engines are e.g. in general cheaper that diesel engines and this analysis is therefore expected to favourite gasoline engines over diesel engines. Furthermore one specific car is obviously not a representative represent of the specific segment. In order to have a more precise picture of the different segments one should include e.g. the 10 most popular vehicles in a weighted average for each segment. Due to resource reasons and due to fact that precise information's regarding the customers chooses of drive-train etc. are not publically available it has been decided to keep the analysis' at this relatively simple level. It is however believed that a simple analysis like the one below results in relative precise and highly useful information's.

Of special interest is the price customers are paying for the ICE before and after tax and VAT. In order to compare prices of different engines - prices are standardized and measured in €/kW. Since there are no registration tax on Battery Electric Vehicles (BEV) in Denmark (and only VAT has to be paid) it is considered not to the cars itself but the ICE that is being taxed.

Since there are no registration tax on Battery Electric Vehicles in Denmark
It is not the car itself that is taxed – It is the ICE.

Because of this one should obviously calculate what the tax is on the engine rather than on the car. Since the overall taxation on vehicles are often higher than 100 %, then the taxation on ICE's are expected to be several times higher. The cost of the engine (defined as engine, gearbox, coolant-loop etc.) as a fraction of the total cost of the car varies greatly and it depends on a number of factors. In this analysis it has however been assumed that 30 % of the cost of the new cars analysed origins from the engine. When a flat rate of 30 % for the cost of the engine is assumed then a price from 41 to 84 €/kW engine, as seen in the figure below, can be calculated.

Figure 1 – Estimation of price pr. kW engine before taxes

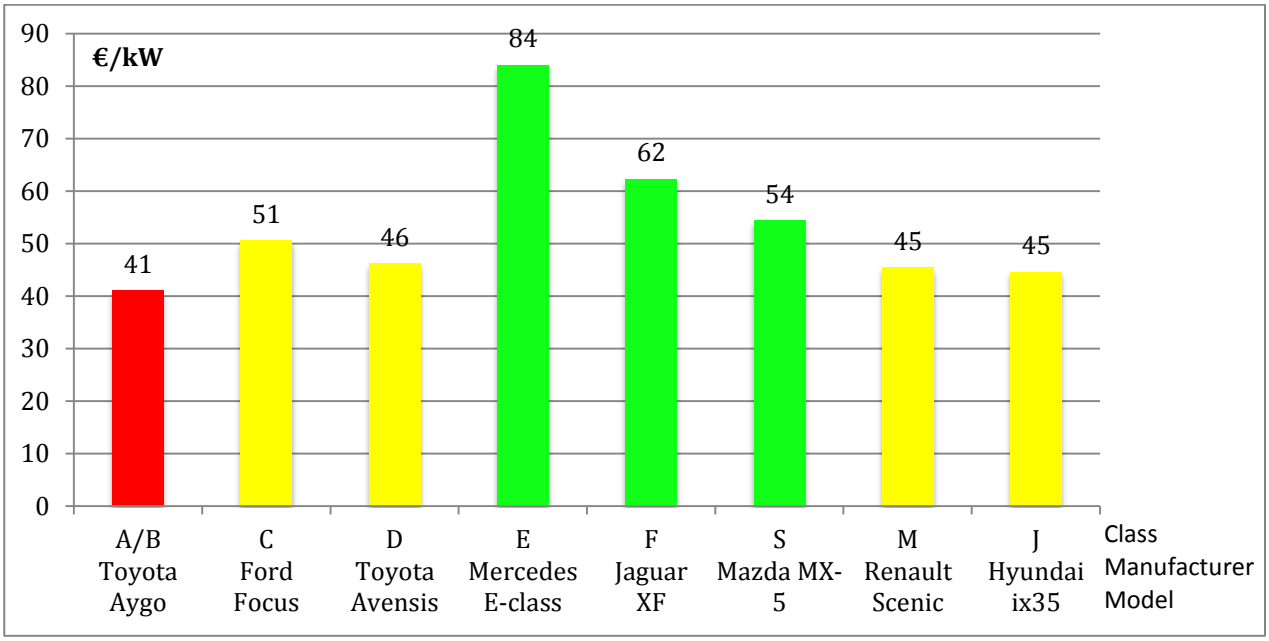

Based on the price pr. kW the 9 segments are divided into three different price groups, where red is the least and green is the most attractive entry-point from a HI-EPS point of view. Note that the colouring is only based on the price pr. kW. The segments are as follows;

- The lowest price pr. kW is paid for engines in class A and B (41 €/kW, red)
- A medium price pr. kW is paid for engines in class C, D, M and J (45 – 51 €/kW, yellow)
- The highest price pr. kW is paid for engines in class E, F and S (54 – 84 €/kW, green).

The classes E (executive), F (luxury) and S (sport) are very small in terms of numbers of sales. In combination they accounted for as little as 2.5 % of the Danish car market in 2010 and 6 % of the European market.[4]

Based on the preliminary analysis it is assumed that the current cost pr. kW for 90 % or more of the car-sales in Europe range from app. 40 to app. 50 €/kW and that the price pr. kW for certain niche markets can be more than 80 €/kW.

[4] http://www.zeroemissionvehicles.eu/uploads/Power_trains_for_Europe.pdf p. 16

In order to see if even higher prices pr. kW can be obtained for special supercars the most expensive Mercedes E-class was analysed. The list price of the Mercedes E 63 AMG in Denmark is kr. 2.245.700 (~ 300.000 €) and the motor can produce 386 kW. When analysed in the spreadsheet a price of 76 €/kW before tax is the result. That indicates that prices pr. kW are not in general higher for super-cars compared with E-class cars. The difference between the most expensive motor pr. kW and the cheapest is a factor of 2.05 (84 €/kW/ 41 €/kW).

All car-markets are influenced and regulated by politics in one way or another – It is just a matter of how and how much it is regulated by politics. The political influence and regulation differs greatly from country to country. Even countries like Germany and the United States regulate the use and sale of vehicles in different ways. In Germany (and rest of EU) there is e.g. high taxes on fuel and in the United States the use of Light-Duty Vehicles are exempted for certain taxes and electric vehicles are allowed to use the fast-lanes on the free-ways.

Below the results of an analysis showing what Danish customers pay pr. kW after tax is presented. In the figure below it is seen that prices pr. kW ranges from 125 to 590 €/kW. Not only has the price pr. kW increased dramatically (between 205 and 651 %), the difference between the most heavily taxed motor and the least taxed motor has also increased. The difference between the most expensive motor pr. kW and the cheapest has increased from a factor 2.05 to a factor of 4.72 (590 €/kW/ 125 €/kW).

Figure 2 – Estimation of price pr. kW motor after taxes

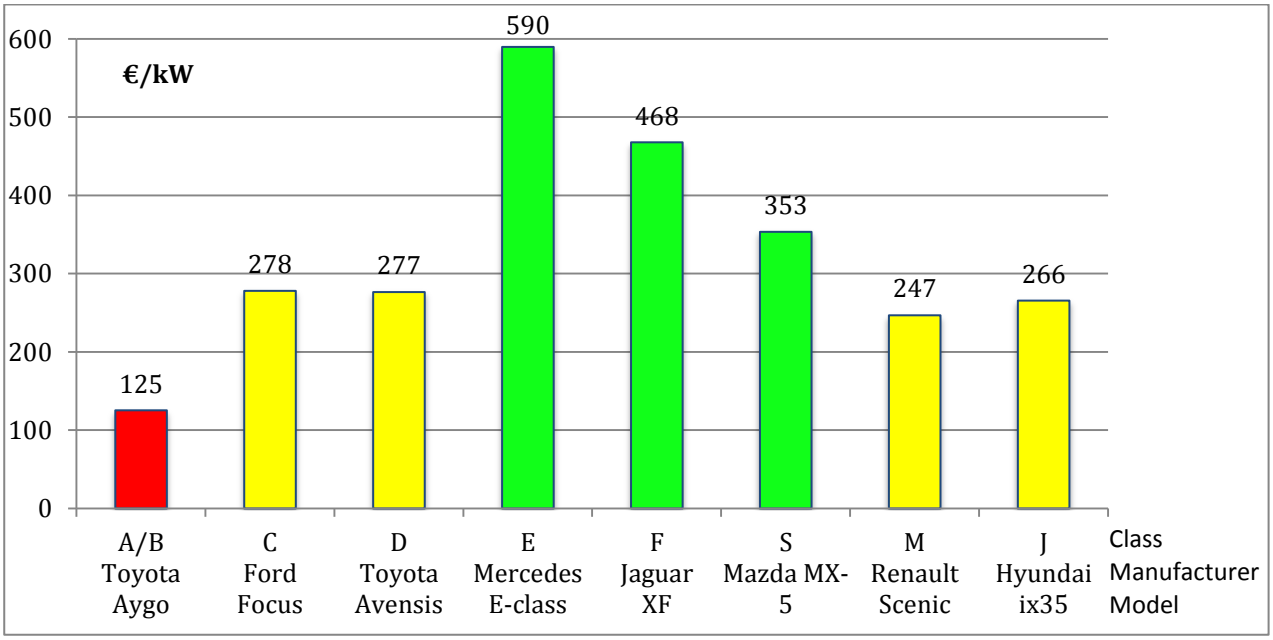

The Danish taxation rules thereby ceterus paribus makes it more financial attractive to implement the HI-EPS module in big and expensive vehicles such as the classes E, F and S compared to smaller and less expensive classes such as A, B, C, D, M and J. This is seen in the figure below where not only does the classes E, F and S have the highest overall prices, they also have the highest taxation pr. kW (ranging from 299 to 506 €/kW).

Figure 3 – Estimation of price pr. kW and Danish taxation pr. kW

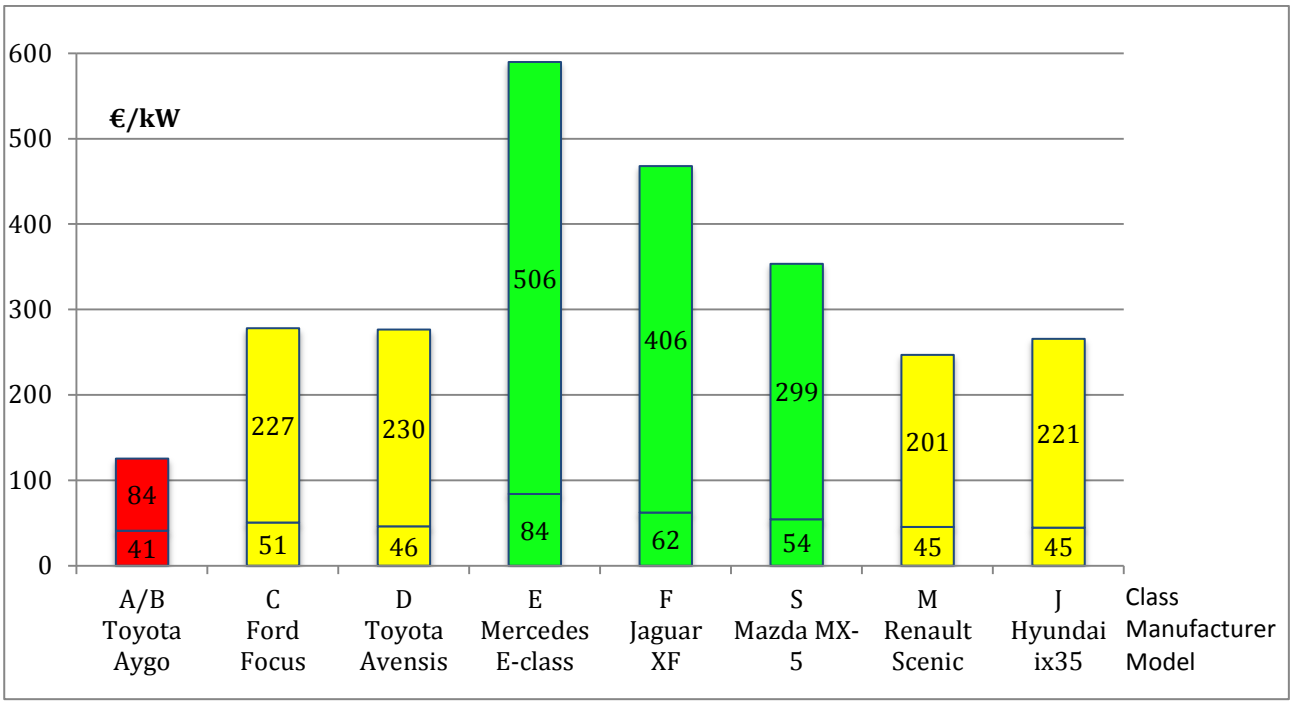

The engines are taxed between 205 and 651 % for Toyota Aygo and Jaguar XF respectively. The classes;

- A and B have a price pr. kW between below 200 € incl. taxes
- C, D, M and J have a price pr. kW between 200 and 300 € incl. taxes
- E, F and S have a price pr. kW above 300 € incl. taxes

It is concluded that engines in the car classes C, D, M and J are more expensive than engines in classes A and B, and that engines in the E, F and S classes are more expensive than engines in classes C, D, M and J pr. kW. Prices pr. kW before taxes can cost up to double as much for classes E, F and S compared to the classes A and B. From a cost-pr.-kW-engine point of view there seems to be three clear and well-defined segments – a cheap, a medium and a premium segment.

The cheap segment covers the classes A and B. It is most often small, simple and mass produced engines with well-known and well-tested technologies. Most often the engines run on gasoline. The medium segment covers the classes C, D, M and J. The technologies used are often newer than compared to classes A and B. There are a wide variety of engine sizes and both gasoline and diesel is popular. The premium segment is where new technologies are most often introduced. These engines are high performers in terms of durability, efficiency, torque, power-density and overall quality. The motors are most often produced in smaller numbers than for classes A, B, C, D, M and J.

Definition of representative segments & vehicles

Based on the findings in the *Basic cost analysis* it has been decided to analyse one car from each of the cheap, medium and premium segments. This has the advantage that it largely simplifies the number of analyses needed, and therefore deeper analyses than would otherwise be possible for each of the segments can therefore be carried out. It is believed that three analyses will give a

decent covering of the car-market and will provide the necessary knowledge in order to evaluate where first to commercialise the HI-EPS units.

Cheap segment - Urban driving

In many ways segment A and B are quite similar. Both segments cover small and cheap vehicles that cover the lower end of the market. In combination these two segments covers 47.2 % of the Danish market measured in sales numbers (2010) and 29 % of the European market (2008).[5]

It has been decided that the Battery Electric Vehicle (BEV) tripling's Mitsubishi iMiEV, Citroen Zero and Peugeot Ion will represent the A and B class (referred to as Mitsubishi iMiEV). The Mitsubishi iMiEV has been chosen of a number of reasons. It is available on the Danish roads as of 2011, it is made by two of the major car manufacturers in collaboration (Japanese Mitsubishi and French PSA) and it is widely regarded as one of the best and most competitive electric cars in the A and B segment. One could also have chosen e.g. the Nissan LEAF. The Nissan LEAF is however in most aspects a bigger car. It has a higher top speed (145 km/h versus 130 km/h for the Mitsubishi iMiEV), it is heavier, it has a bigger motor, it has a faster acceleration and it is more expensive. Since as clear a picture of the A/B segment is wanted as possible the team behind this report have deliberately gone for the smallest and cheapest of the major competitors in the A/B segment. The Mitsubishi iMiEV is furthermore most likely to be classified in the A segment, whereas the Nissan LEAF is to be classified in the B segment.

Many of the smallest vehicles are primarily used in cities where they drive at relatively low speeds, with many short accelerations and braking's, for relatively short distances and quite often serve as the family's second or third car. Since these vehicles will primarily be used in cities it has been defined that these vehicles as minimum have to sustain the NEDC and a continuous speed of minimum 90 km/h. A continuous top speed of 90 km/h means that the car can be used on freeways. Not that it will be comfortable to drive at this low speed on motorways, but it is possible to do so without being in danger. The minimum range is defined to be 600 km.[6] Obviously it happens that gasoline powered city cars use the motorways. Therefore electric powered city cars should also be able to use motorways for shorter trips. Of this reason electric city cars have to have a decent top speed and to sustain it for a minimum of range. The minimum top speed is defined to be 130 km/h and the range at this speed is defined to be at least 60 km.[7] The most important characteristics regarding the energy & power requirements for city cars are seen in the table below.

Table 3 – Minimum needed energy and power related features for a city car

Description	SI unit	number	Primarily energy/power from
Minimum continuous speed	- , km/h	NEDC, 90	Power from FC
Minimum range at continuous speed	km	600	Energy from FC
Minimum top speed	km/h	130	Power from batteries
Minimum range at top speed	km	60	Energy from batteries

[5] http://www.zeroemissionvehicles.eu/uploads/Power_trains_for_Europe.pdf p. 16
[6] http://www.europabio.org/Biofuels%20reports/well-to-wheel.pdf table 2.2.1
[7] Assuming a start SoC of 1 and an end SoC of 0.2 for a new battery and a auxiliary-use of 857 W.

The users of a car as the one defined in the table above can e.g. be home-helpers working in bigger cities. The above listed energy & power requirements for city cars are the vehicle and application specific assumptions. The technical assumptions of each type of vehicle will be listed later in the report.

Medium segment – Extra urban driving

Segment C, D, M and J covers medium class vehicles, which are normally heavier and more powerful than the cars in segment A and B. In combination these four segments covers 36.6 % of the Danish market measured in sales numbers (2010) and 65 % of the European market (2008).[8]

The twin Plug in Hybrid Electric Vehicles (PHEV) Chevrolet Volt and Opel Ampere will represent the C, D, M and J segments. Since there are much more information available on the internet regarding the Chevrolet Volt than there are regarding the Opel Ampere They will be referred to as Chevrolet Volt. The vehicles are developed and produced by GM in North America and the production takes place at the GM Detroit-Hamtramck assembly plant in Hamtramck Michigan. Though the engine is from Opel's plant in Aspern, Austria and the individual battery-cells are from LG Chem, South Korea, then the public in the United States widely regards it as an American car. Even though there has so far only been sold 2.184 of this car (as of end of May 2011)[9] the marketing value and the resources that have been put into the development of these vehicles are immense and the importance for the General Motors Company therefore shouldn't be underestimated. The company General Electric has also announced that they will purchase 12.000 Chevrolet Volt until 2015, which will secure some volume production for Chevrolet Volt the coming years.[10] Furthermore GM is expanding the production capacity of Chevrolet Volt and Opel Ampere and production capacity will increase to 16,000 units in 2011. In 2012, global production capacity is expected to be 60,000 vehicles with an estimated 45,000 to be delivered in the United States.[11]

It has been defined that cars from the medium segment should be able to sustain a continuous speed of minimum 130 km/h. 130 km/h is the highest allowed speed on European – except for certain German motorways where there are no speed-limitations. For comparison it should be noted that the average speed on Danish motorways for 110 and 130 km/h allowances are 117 and 122 km/h respectively.[12] The minimum range is defined to be at least 600 km at 120 km/h and 550 km at 130 km/h. For further information see the box below.

[8] http://www.zeroemissionvehicles.eu/uploads/Power_trains_for_Europe.pdf p. 16
[9] http://media.gm.com/content/Pages/news/us/en/2011/Jun/chevsales/_jcr_content/rightpar/sectioncontainer_1/par/download_0/file.res/Deliveries%20May%202011.pdf
[10] http://gm-volt.com/2010/11/12/ge-to-buy-12000-chevy-volts-cruze-eco-gets-42-mpg-highway-rating-and-opel-ampera-priced/
[11] http://www.freep.com/article/201105190300/BUSINESS0101/105190632
[12] http://www.concito.dk/uploads/CO2ogfart.pdf

Assumptions regarding range as a function of speed

It is assumed that the vehicles will have a range of at least 600 km for NEDC and constant speed of up to 120 km/h. For constant speeds above 120 km/h the range drops – just like it is the case for all other kind of vehicles. A range of 400 km is assumed at a constant speed of 160 km/h. Our assumptions are seen in the figure below and so is the range for other drive trains and energy-carriers. In reality – if the vehicles can sustain 600 km or more at 120 km/h, then they will have a far longer range at lower speeds. Therefore in reality the range of our assumed vehicles will always be the same – or longer – than compared to BEVs and LTPEM powered FCEVs.

Figure 4 – Range for different kind of vehicles as a function of speed

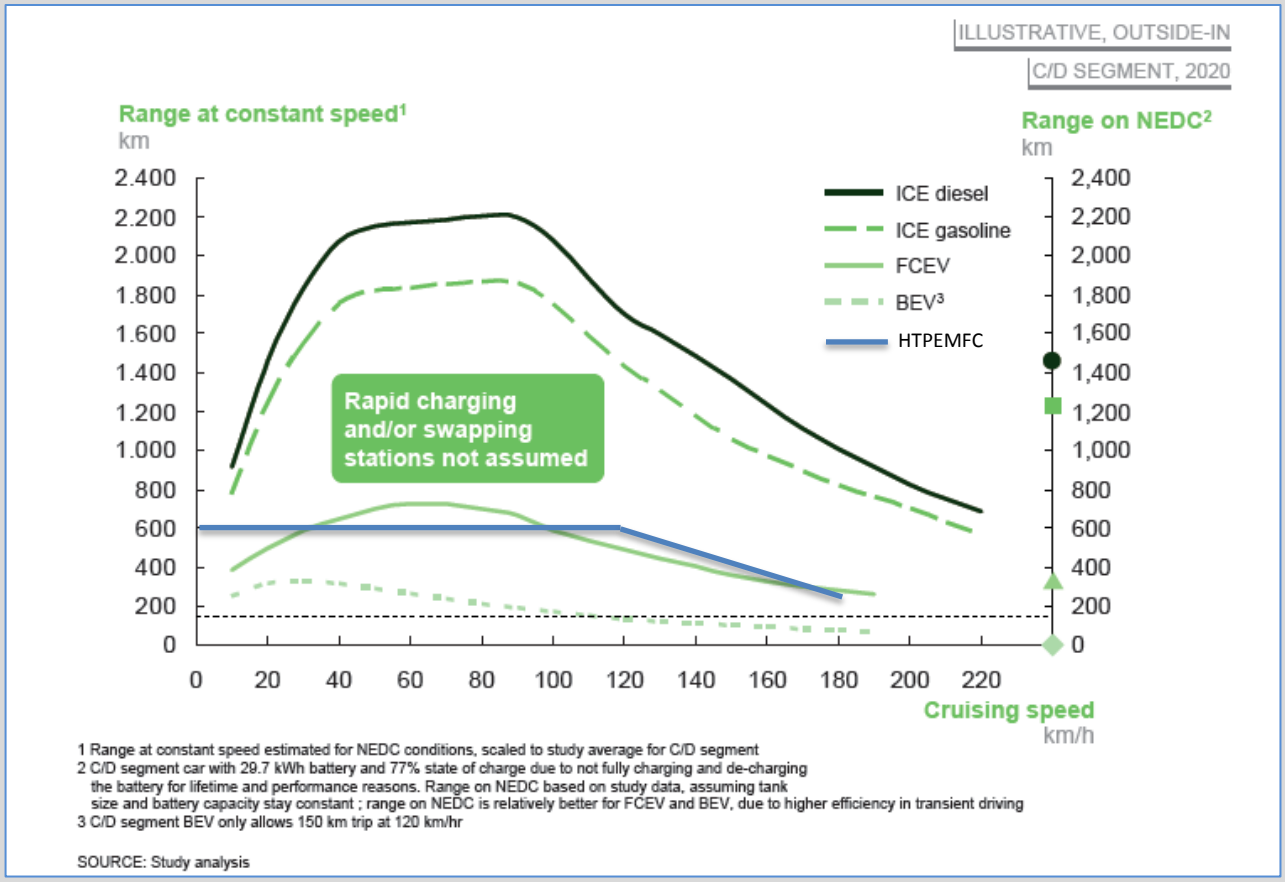

Source: http://www.zeroemissionvehicles.eu/uploads/Power_trains_for_Europe.pdf

The top speed of the Chevrolet Volt of 160 km/h (which is electronically limited) has been defined as the top speed of vehicles in the medium segment. The most important characteristics regarding the energy & power requirements for all-road cars are seen in the table below.

Table 4 – Minimum needed energy and power related features for a medium car

Description	SI unit	Number	Primarily energy/power from
Minimum continuous speed	- , km/h	NEDC, 130	Power from FC
Minimum range at continuous speed	km	550[13]	Energy from FC
Minimum top speed	km/h	160	Power from batteries
Minimum range at top speed	km	60	Energy from batteries

Cars with energy and power related features as listed in the table above is believed to satisfy the needs of more than 9 out of 10 customers.

Premium segment – Freeway driving

Segments E, F and S are in different ways at the very top of the market. Segment E is the most expensive segment where vehicles are still mass-produced. Segments F is a very small segment (less than 1 % of sales in Europe) which makes them even more expensive than they would be if they where produced in higher volumes. The S segment covers sport cars. This is from a technical point of view the most demanding segment since these cars are engineered for speed and acceleration meaning that they are normally small (2 seats is the norm), lightweight and are having a powerful engine (high kW/kg-ratio). It is however also often in this segment that radically new innovations are introduced from motorsport. In combination these three segments covers 2.5 % of the Danish market measured in sales numbers (2010) and 6 % of the European market (2008).[14]

In the premium segment the obvious choose for analysis is the electric vehicle that more or less re-ignited the global interest in electric cars – the Tesla Roadster. It is sexy, it is fast, it has superior acceleration and it has a long range compared to most other electric vehicles. The drawbacks are however immense and includes a heavy battery (450 kg), a long charge time of 4 to 30 hr depending on charger, a limited range – especially at high speeds and a relatively high price (compared to e.g. the Lotus Elise with which it share it's chassis).[15]

It has been decided that cars in the premium segment shall be able to sustain a continuous speed of minimum 160 km/h. It should be noted that driving 160 km/h is illegal in all European countries – except for certain German motorways. The minimum range is defined to be at least 600 km at speeds up to 120 km/h and 400 km at a continuous speed of 160 km/h. In order to have a decent acceleration even at high speeds a top speed of 200 km/h has been defined. This is also the top speed of the Tesla Roadster 2.5 which top speed is electronically limited. The most important characteristics regarding the energy & power requirements for all-road cars are seen in the table below.

[13] 600km-((600-400km)/(160-120km/h)*(130-120))=550.
[14] http://www.zeroemissionvehicles.eu/uploads/Power_trains_for_Europe.pdf p. 16
[15] http://www.teslamotors.com/blog/mythbusters-part-2-tesla-roadster-not-converted-lotus-elise

Table 5 – Minimum needed energy and power related features for a premium car

Description	SI unit	number	Primarily energy/power from
Minimum continuous speed	- , km/h	160	Power from FC
Minimum range at continuous speed	Km	400	Energy from FC
Minimum top speed	km/h	200	Power from batteries
Minimum range at top speed	Km	60	Energy from batteries

An overview of the market shares for the different segments and the vehicle that represent them is seen the figure below for Denmark (2010) and for Europe (2008). It is seen that the A and B class is hugely overrepresented in Denmark compared to the rest of Europe. It is also seen that the C, D, M and J class are under-represented in Denmark compared to rest of Europe. Finally it is seen that the sales of E, F and S class is app. 2.5 times lower for Denmark than for Europe as a whole.

Figure 5 – Car sales in Denmark, 2010 (left) and Europe, 2008 (right) grouped into segments

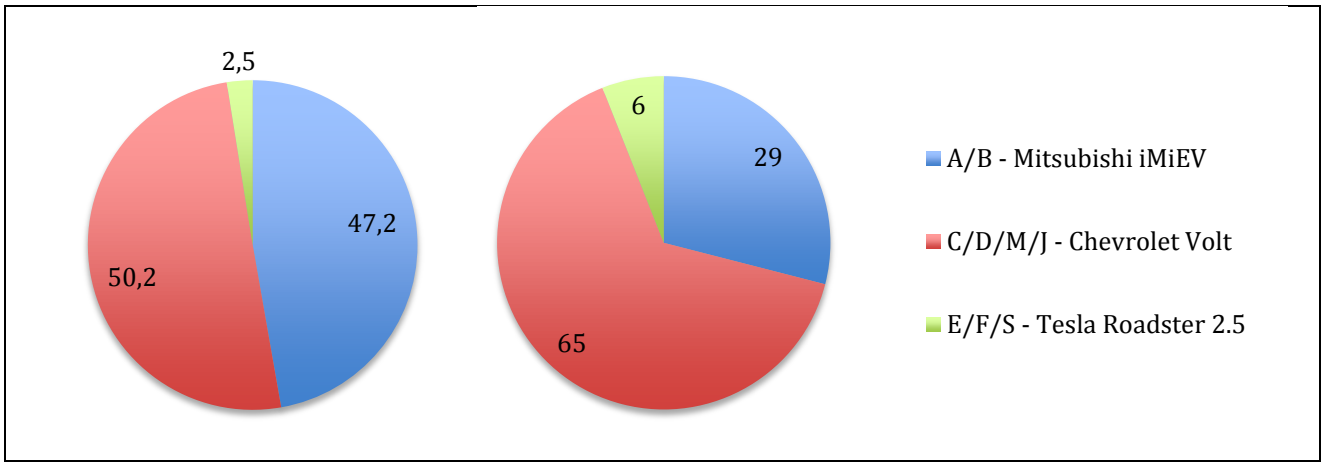

Source: http://www.zeroemissionvehicles.eu/uploads/Power_trains_for_Europe.pdf p. 16, http://www.bilimp.dk/press/content.asp?id=361

Technical assumptions

Key technical issues and assumptions regarding certain key technological issues are now described in more detail. "Technical assumptions" is divided into "Batteries", "Fuel cells", "Heat" and "Other".

Batteries

In this section the following issues will be discussed and defined:

- Voltage
- Battery-electric range
- Distance that the vehicle can sustain a certain drive-cycle
- State-of-Charge operating window
- State-of-Charge when starting up the FC.

Assumed battery performance

The manufacturers of electric vehicles disclose some, but not all relevant data for the battery-packs used in their electric vehicles. Since it has not been possible to obtain all the needed performance data for the batteries used in the vehicles that are analysed, a number of assumptions were made in this report. A data-sheet including all relevant data for the single cells has been found for some cells from the French battery-maker Saft.

Picture 1 – The Saft VL 37570 cell

These cells do however fall short on one important parameter – the c-rate. Since these cells only have a C-rate of 2. A C-rate of 4 – 10 is normally needed for different kinds of electric cars, then assumptions regarding the C-rates had to be made. There is a strong relationship between power density of a battery-cell (here expressed by the C-rate) and the energy density of a battery-cell (expressed by kWh/kg). It is assumed that the energy density of 174 Wh/kg[16] and the C-rate of 2 of the Saft cells is halved at a C-rate of 20. A linear relationship between these two points is assumed.

Battery voltage

There has been a clear trend towards higher and higher voltages the last couple of decades. In general the higher the voltage the higher the efficiency and the higher the voltage the smaller a diameter of the wiring is needed. The Mitsubishi iMiEV, Chrysler Volt and Tesla Roadster use voltages according to the following table.

Table 6 – Voltage of different vehicles

Vehicle	Voltage (V)
Mitsubishi iMiEV	330
Chrysler Volt	360
Tesla Roadster	375

Sources: http://www.mitsubishi-motors.com/special/ev/whatis/index.html, http://www.evsafetytraining.org/resources/auto-manufacturer-resources/~/media/Files/PDFs/VoltQuickRef3.pdf, http://webarchive.teslamotors.com/display_data/TeslaRoadsterBatterySystem.pdf

Battery electric range

Deciding on the size of a battery-pack (measured in km range and/or kWh energy) in an electric car with a range extender is very difficult indeed. For the time being no dominant design regarding

[16] (3.7V * 7 Ah/cell)/0.149 kg/cell.

pure BEV range exist. The optimum battery-electric range is among others a function of driving pattern and the marginal cost of a certain range.

According to data from Department of Transport at Technological University of Denmark most of the km driven in cars in Denmark is driven on relatively short trips.[17] The distribution is seen in the figure below.

Figure 6 – Distribution of km driven in cars in Denmark on a daily basis in 2006

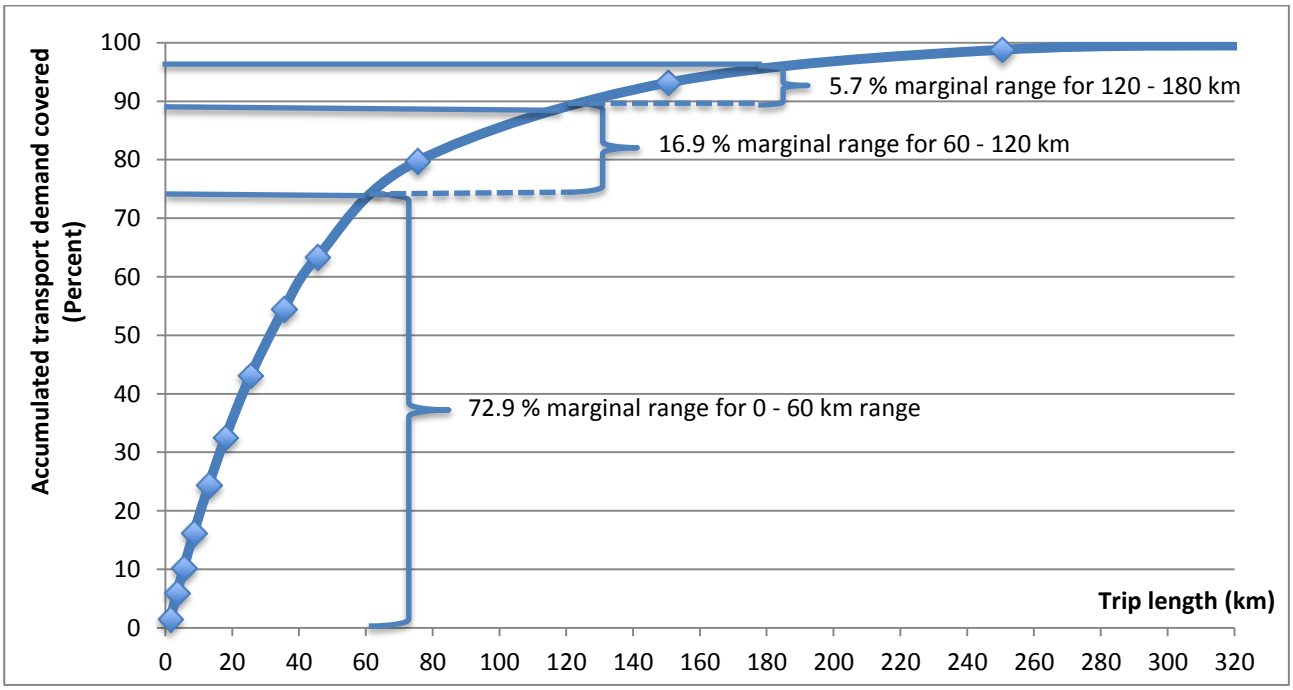

A relatively small battery-electric range can cover most of the km driven on a daily basis. It is seen that a battery with a range of just 60 km can cover 73 % of the km driven on a daily basis. If the battery-electric range is doubled then the accumulated transport demand covered on a daily basis increases by less than 17 %. Even though the cost of the batteries decrease as a function of battery-capacity (due to less restrains on power capacities), then it is clear that there is a diminishing return on investment on batteries.

If one assumes a certain (fixed) battery-price pr. kWh and a certain lifetime of the vehicle one can calculate the depreciation cost pr. added km battery-electric range. The following assumptions are made: A battery-price of 500 USD/kWh, a lifetime of 350.000 km[18], and energy use of 150 Wh/km and exchange rates of 5.5 DKK/USD and 7.45 DKK/€. In the figure below the depreciation costs measured in €cents/km battery range is seen.

[17] DTU – TU – Transport undersøgelsen, http://www.dtu.dk/centre/modelcenter/TU.aspx
[18] The 95% fractile lifetime for a gasoline car. Source: http://www.hydrogenlink.net/download/reports/power-balancing-fuelcells-hydrogen-denmark2009.pdf p. 45 -46 and own calculations.

Figure 7 – Battery depreciation cost (€cents/km battery range)

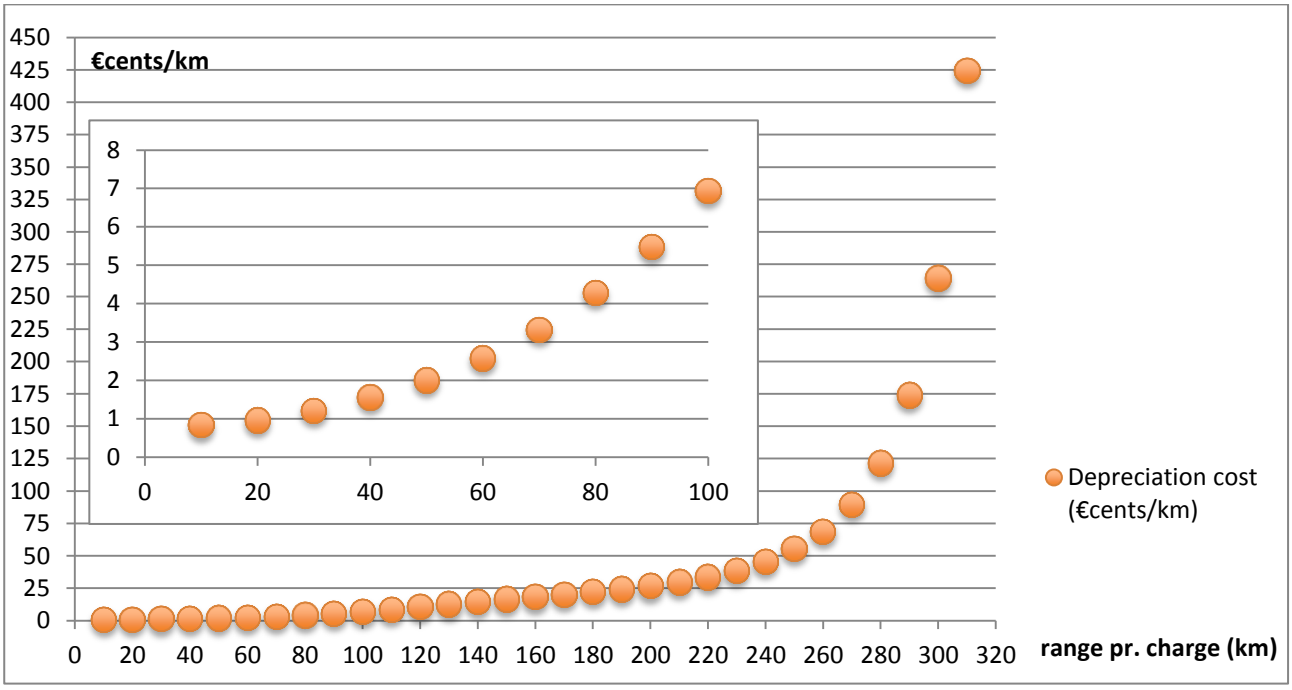

The Total Cost of Ownership pr. km (TCO/km) is a result of depreciation of the car pr. km, fuel cost pr. km and service & maintenance cost pr. km.

The service & maintenance cost is disregarded for a moment. In the figure below is seen the depreciation cost of the car pr. km and the fuel cost pr. km. Depreciation cost (€cents/km) is marked by red and the fuel cost (€cents/km) is marked by red in the figure below. It is seen that the depreciation cost varies between 4.4 and 23.2 €cents/km (at 350.000 km lifetime), that the fuel cost varies between 6.8 and 15.6 €cents/km (at 1.5 €/L) and that the combined depreciation and fuel cost varies between 11.1 and 39.0 €cents/km.

Figure 8 – Depreciation and fuel cost pr. km measured in €cents/km

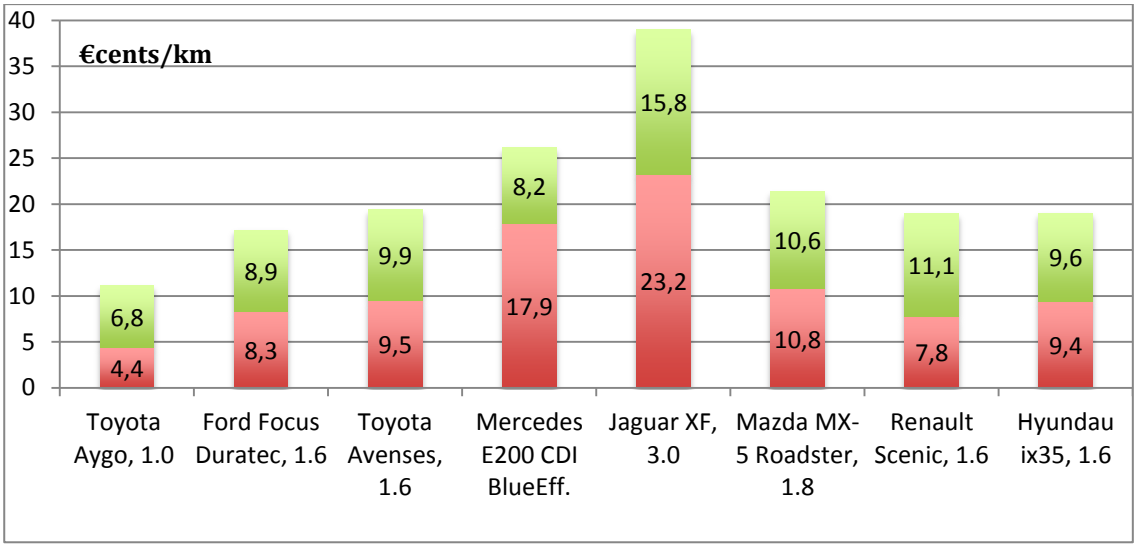

According to Figure 7 the marginal cost increase above the depreciation cost of 4.4 – 23.2 €cents/km (as seen in figure 8) at a pure battery-electric range of app. 80 to app. 150 km. Since the customer not only have to pay for batteries but also for electric motor(s) and for the fuel cells a pure battery-electric range of 60 km seems reasonable. This is equal to the pure battery electric range of the GM Volt. 9 kWh useful battery capacity for app. 60 km battery-electric range is necessary (California Air Resource Board, 2007 use 10 kWh, the Chevrolet Volt currently use 10.8 kWh pr. 60 km and GM estimate that number decreases to 8 kWh over time – primarily as a result of technological improvements and lower weight of vehicle).

State-of-Charge operating window

In order to run simulations we have to define a start State of Charge (SoC) and a minimum SoC. The start SoC minus the end SoC is known as the SoC operating window. There are no right or wrong answers to the questions about what the start and end SoC should be.

In general the larger the battery-pack (measured in km range of the battery-pack) the deeper a Depth-of-Discharge (DoD) is normally permitted. One is e.g. permitted to utilise all of the capacity in the Mitsubishi iMiEV, whereas one is only permitted to utilise 65 % of the capacity in the GM volt. Since one is only going to use the full range of Mitsubishi iMiEV now and then, the mere size of the battery-pack protects the individual cells. The opposite is the case for the GM Volt where General Motors have decided to take active steps in order to protect the battery by only allowing a 65 % SoC operating window.

From an economical point of view the depreciation cost measured in €cents/kWh has to be as low as possible. All battery-technologies have an operating window where the depreciation costs are the lowest. Most often the car manufacturers regard this as confidential information and data for e.g. Tesla are not obtainable from public accessible sources. It does however happen that the car

manufacturers disclose some information about the most economical SoC operating window.

General Motors has disclosed some information regarding this for the twin cars Chrysler Volt and Opel Ampere. The batteries used in these cars are normally charged to maximum 86 % of their capacity (SoC 0.86), the generator start up when one hits 45 % SoC in mountain driving and when SoC hits 35 % in normal driving. The SoC is allowed to drop to 21 % in normal conditions and one is however allowed to "limp home" until one hits 15 % SoC.[19] The Chrysler Volt and Opel Ampere are equipped with batteries with a voltage of 3.7 V/cell, 32 cells in series, 9 in parallel and a capacity of 15 Ah (1 h discharge rate). When multiplied with a 0.86 – 0.21 operating window the result is a useful capacity of 10.390 Wh. Using the batteries in the Chrysler Volt / Opel Ampere outside the 0.86 to 0.21 SoC operating window will result in a reduced lifetime (measured in both kWh and years) of the batteries.

It is assumed that one can operate the batteries in the HI-EPS in the same way as in the Mitsubishi iMiEv – that is from 100 to 0 % SoC. One will in order to maximise the lifetime of the batteries try to keep the SoC in a narrower band.

State-of-Charge when starting up the Fuel Cells

When the fuel cells shall start-up and when they shall not also depends on a number of factors. Some of the most important factors are;

- The distance that the vehicle has to cover and
- Whether one can recharge the battery when one arrives at the destination or not
- The need for cabin heat and thermal management of the batteries.

The vehicle itself obviously does not know whether it has to cover a long or a short distance. The driver therefore either have to manually start-up the fuel cell or let some kind of intelligence decide whether the fuel cell should start-up or not. GPS is already standard it most new cars and it assumed that this trend will continue the coming decades.

In the future all electric vehicles equipped with HTPEM fuel cell range extender systems are equipped with GPS systems. The GPS systems are voice controlled and each trip will start by the GPS system asking the driver of the destination. A highly sophisticated software system will then, based on a number of parameters, calculate the best energy-mix and thereby the best use of electricity from the batteries and electricity and heat from the fuel cell unit. Parameters among others include;

- SoC of battery
- Distance to destination
- Mix of allowed speeds on the roads chosen by the software
- Traffic situation on the roads chosen
- Vehicle parameters (fixed from the factory)
- Outside temperature
- Preferred cabin temperature

[19] http://gm-volt.com/2010/10/26/chevrolet-volt-will-utilize-10-4-kwh-of-battery-to-achieve-ev-range/, http://gm-volt.com/forum/showthread.php?7874-Diagnostic-tool-early-findings

- Auxiliary use
- Combined payload

Regarding the combined payload then sensors placed either at each of the four shock absorbers or in each seat and in the truck will weight or estimate the combined payload.[20]

Some parameters stay the same throughout the lifetime of the vehicle (e.g. curb weight and drag-coefficient), some changes over time (e.g. the efficiency of the batteries and the fuel cells) and other vary for each drive (e.g. the SoC and the payload). The software can take into account all of the parameters.

In the Chrysler Volt / Opel Ampere the gasoline range-extender start-up when the battery SoC drops to 35 % for normal driving and 45 % for mountain driving. In the Chrysler Volt that makes sense since the range extender is powerful enough to sustain the vehicles top speed of 161 km/h (100m mph) at all times. Furthermore the range extender is primarily intended for the delivery of kinetic energy.

For the HTPEM based fuel cells the case is quite different. First of all fuel cells will most often, due to weight, volume and cost issues (where cost issues is the most important factor in a pre mass commercialization stage) not be powerful enough to sustain the vehicles top speed. Secondly an internal combustion deliver a lot of waste heat, but most of the heat disappears as radiation from the motor block and is therefore very difficult to utilize. Normally one can utilize app. 20 % of the ICE's waste heat for cabin heating etc. For HTPEM fuel cells the heat comes at a high temperature (app. 150 ° C) and most of the waste heat (typically 80 - 90 %) can be reused for heating purposes. These two things in combination make it easy to utilize a high share of the waste heat. This is especially the case to liquid cooled HTPEM fuel cell systems, where a waste heat energy utilization of more than 80 % is achievable with relatively little effort. Since the waste heat energy utilization is app. four times higher for a HTPEM fuel cell system than for a gasoline ICE it can in certain cases make sense to use the HTPEM fuel cell system primarily for heating purposes and only secondly for the delivery of electricity.

The combination of a lower maximum power output than required for a high sustained top speed and the high waste-heat energy-utilization makes it clear that the operation of the fuel cells depends not only on the battery SoC but on algorithms where factors such as distance to destination, route, outside temperature and SoC for battery at beginning of the trip is important.

In a very simplified manner one can set up a two by two matrix with four different operating set points. On the X-axis we have outside temperature. The outside temperature defines to what extent the heater for the cabin as well as for keeping the batteries at a temperature at or above 15 °C has to be used or not. On the Y-axis we have the distance to the destination. It is assumed that the longer the distance the higher the average speed. In the matrix below there are the following use of the FC:

1) Outside temperature is low (e.g. -10 °C), the distance is long (e.g. 400 km)

[20] Sensors are already in place in the seats of most new cars in the form of so-called belt-alarms intended to remind the driver and passengers to use the seat-belt.

The FC will be used in its "power-mode" in order to deliver as much energy for the drive train as possible. The FC will have a high power output and an electric efficiency of app. 40 %. For fuel cell systems bigger than 5 – 6 kW only a part of the waste heat can be utilized. The more powerful the FC the lower the waste heat utilization. A combined efficiency of 45 to 50 % is however to be expected for most HTPEM FC range extenders.

2) Outside temperature is high (e.g. 20 °C), the distance is long (e.g. 400 km)

   The FC will be used in its "power-mode" in order to deliver as much energy for the drive train as possible. The FC will have a high power output but a low combined efficiency. The combined efficiency will be app. 40 %.

3) Outside temperature is low (e.g. -10 °C), the distance is long (e.g. 20 km)

   In order not to use high value electricity for heating the FC is turned on. The FC delivers the heat needed for heating of the cabin and for elevating and keeping the battery-temperature at 15 °C or higher. If for example 5 kW heat is needed and if the maximum power output from the FC is substantially higher, then the FC will be used on part-load. This is equal to a load-point to the left on each fuel cells polarization curve, which then again results in a high electric efficiency and a long lifetime of the FC. The combined electric and heating efficiency can depending on exact configurations be higher than 80 %.

4) Outside temperature is high (e.g. 20 °C), the distance is short (e.g. 20 km)

   There will be enough energy in the batteries to drive pure battery-electric (assuming a fully charged battery at beginning of trip) and the FC will therefore not be used at all.

Table 7 – Simplified operating set-points for HTPEM FC range extenders

Outside temp. / Distance & Speed	Cold (-10°)	Warm (20°)
Long, high speed	1) FC is run at full power and some waste heat is utilized	2) FC is run at full power. Waste heat is not utilized.
Short, low speed	3) FC is run to utilize heat, electricity is used for driving and for charging batteries	4) FC is not run. Pure battery electric driving.

Obviously countless combinations of the four above listed operating set point will exist in the real world. In a relatively cold climate the heater is on for more than half the year. Therefore in a climate like the Danish the FC will most often be started not as a function of SoC of the batteries, but as a function of temperature. In spring and autumn where the heat demand is relatively to a few kW (or less) the CHP efficiency of the FC will be very high.

Since the HI-EPS working group are interested in the capabilities of the vehicles when the FC is used, it is assumed that the FC is started whenever the SoC drops below 0.90. A SoC of 0.90 is chosen in order to be sure not to charge an already 100 % charged battery.

Distance that the vehicle can sustain a certain drive-cycle

For gasoline and diesel propelled vehicles the distance on a tank of fuel is measured in km. Older cars only have an analogue petrol or diesel gauge whereas never cars normally both have an

analogue and a digital gauge in the form of a driving computer showing the estimated distance to an empty tank based on the current driving pattern (see picture below).[21]

Picture 2 – Dashboard of a never car with both an analogue and a digital diesel gauge

Volvo S40D 2005 dashboard

Electronic diesel gauge showing the estimated range to empty tank based on current driving pattern

Analogue diesel gauge showing how many liters there is in the tank.

For BEV and fuel cell propelled vehicles it is however interesting to have a look at the distance measured in time. When driving long distances such as e.g. from Denmark to the Alps on skiing holiday a number of brakes are needed (for reasons such as going to the toilet, eating, drinking, stretching legs, refuelling, coffee, swopping drivers etc.). For each four hours (4 h) of continuous driving half an hour (0.5 h) brake is assumed. These brakes will be used for charging the batteries with the maximum charge rate possible from the FC. The driving computer will - based on the output from the FC, the battery SoC, the distance to the next brake and estimated duration of the next brake as well as information from the GPS, calculate the maximum speed the vehicle can sustain. The autopilot will then use this information to set a "maximum march speed". At all times there should be enough power to accelerate whenever the driver wants to do so or whenever it is needed. Obtaining and using the above listed information's will be cheap since all one needs is new software and a merge of the already existing driving computer and GPS system. In the picture below an example of how an updated dashboard can look like, including information about the output of the FC, SoC of batteries and recommended range to next brake, is seen.

Picture 3 – Possible layout of an updated dashboard for an electric vehicle with a HI-EPS

[21] http://www.redline.co.za/Volvo%20S40%20Diesel.htm

Examples

A trip from the town hall of Aarhus to the town hall of Copenhagen (Rådhuspladsen) is planned. According to www.viamichelin.com the trip is 305 km of which 293 km on motorways and is estimated to take 3 h and 5 minutes (of which 2 h and 42 minutes on motorways). On a trip like this brakes are normally very short (less than 10 minutes). The drive-pattern is estimated to look as shown in the table below.

Table 8 – Driving characteristic on trip from Aarhus to Copenhagen according to viamichelin

Road type	Distance (km)	Time (min)	Average speed (km/h)
Of motorways	12	23	31.3
On motorways	293	162	108.5
Sum	305	185	98.9

A trip from the city hall of Aarhus to 6580 Sankt Anton am Arlberg, which is one of the biggest skiing resorts of the Alps, is planned. According to www.viamichelin.com the trip is 1.238 km of which 1.215 km on motorways and is estimated to take 10 h and 57 minutes (of which 10 h and 32 minutes on motorways). On a trip like this longer brakes for eating etc. are normally needed. The first brake of half an hour will take place after 4 hour (240 min.) of driving. The second brake of half an hour will take place after 8.5 hours (510 min.) of driving. The drive-pattern is estimated to look as shown in the table below by www.viamichelin.com.

Table 9 – Driving characteristic on trip from Aarhus to Copenhagen according to viamichelin

Road type	Distance (km)	Time (min)		Average speed (km/h)	
		No brakes	2 brakes of 30 min.	No brakes	2 brakes of 30 min.
Of motorways	23	25	25	55.2	55.2
On motorways	1.215	632	692	115.3	105.3
Sum	1.238	657	717	113.1	103.6

From the above tables it is seen that the average speed is almost the same for a trip from Aarhus to Copenhagen as on a trip from Aarhus to the Alps (98.9 and 105.3 km/h respectively). Brakes of half an hour for each 4 hour of driving only reduce the average speed on motorways by 10 km/h (from 115.3 to 105.3 km/h).

The two examples indicate that a relatively low maximum continuous top-speed is needed. What the actual needs are should be discussed with car manufacturers as soon as possible.

Fuel cell system

In this subsection two issues regarding methanol and four issues regarding fuel cells are analysed. The following issues are analysed:

- Methanol tank
- Refuelling time
- Power density of fuel cells
- Start-up time
- Price
- Durability

Methanol tank

Currently the analysed fuel cells use a mix of 60 % methanol and 40 % water. The advantages include; a simpler system (since water do not have to be collected and re-used) and a safer energy-carrier. The downside is however that the fuel tank becomes bigger and more bulky. The bigger the system (measured in kW) and the more often it is used the more sense it makes to collect and reuse the water. It is assumed that water will be collected and reused.

According to the report "Well-To-Wheel analysis of future automotive fuels and powertrains in the European context" made for the European Commission the minimum range acceptable by customers is 600 km.[22] In the figure below the most sold car-model for each class and their range is listed. The range is a result of the tank capacity (L) multiplied by range pr. L according to NEDC.

Figure 9 – Range (according to NEDC) of the most sold cars in Denmark (2010) for each class

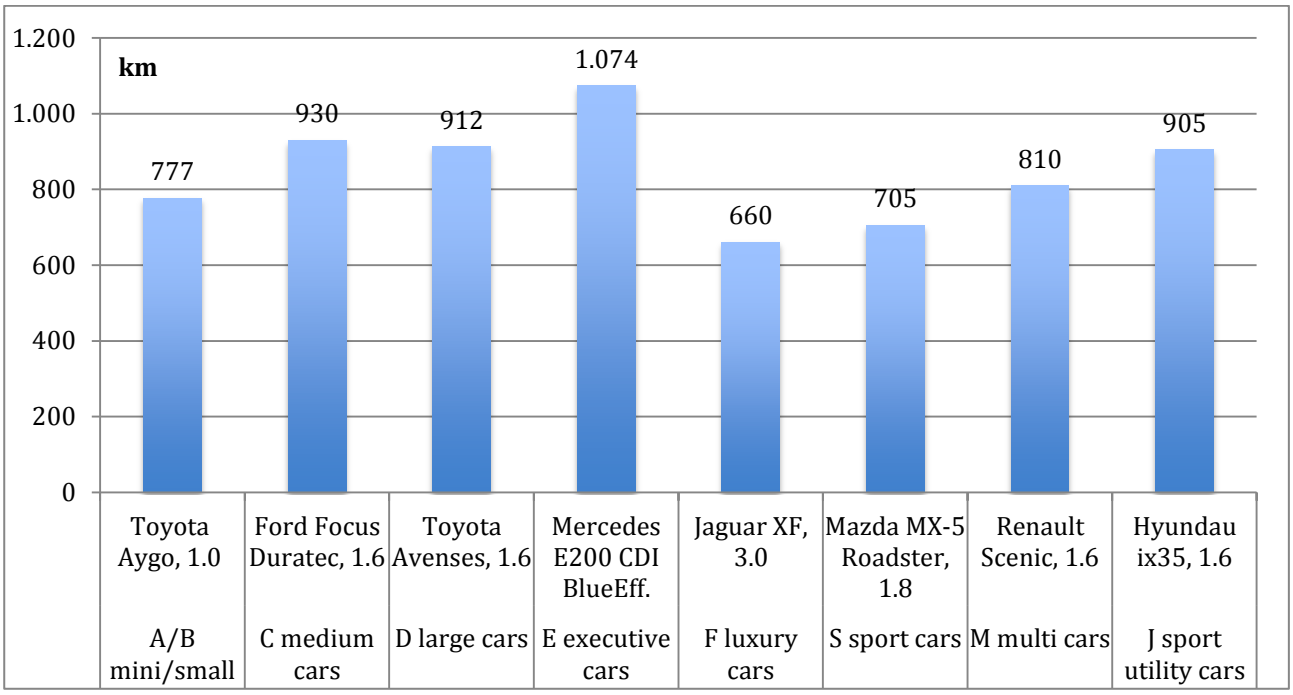

As seen the range varies from 660 km to more than 1.000 km pr. tank. Note that the listed cars are gasoline propelled. Diesel cars often have a better mileage and thereby a longer range. Some diesel cars have ranges of more than 1400 km. A minimum range of 600 km according NEDC has been defined earlier in this report.

Tank weight

The tank weight is assumed to be the weight of; (PVC coated steel straps + Steel shield) + Multi-layer HDPE tank.[23] The weight of the PVC coated steel straps and the Steel shield is assumed to be independent of the tank-volume whereas the weight of the Multi-layer HDPE tank is assumed to be a function of the internal tank-volume. 2.87 kg is assumed for the PVC coated steel straps and the Steel shield together and 11.2 kg is assumed for a 117.3 L (31 gallon) Multi-layer HDPE tank.

[22] http://www.europabio.org/Biofuels%20reports/well-to-wheel.pdf table 2.2.1 p. 18.
[23] http://css.snre.umich.edu/css_doc/CSS97-01.pdf

Based on analysis's it is found that the Mitsubishi iMiEV, GM Volt and Tesla Roadster needs 54, 92 and 88L methanol in order to sustain the drive-cycles defined earlier in this report. For further information see
The weights for the fuel tank systems for the three cars are seen in the table below.

Table 10 – Assumed weight of tank-systems for different cars

	L	kg
Mitsubishi iMiEV[24]	54	8.0
GM Volt	92	11.7
Tesla Roadster	88	11.3

Sources: http://css.snre.umich.edu/css_doc/CSS97-01.pdf P. 7.

Refuelling time

A refueling time similar to the refueling time of a gasoline car will require an energy input corresponding to a gas station that fuels a car with 40 L/minute corresponding to 200 kWh/min.

Power density of fuel cells

The 2015 fuel cell system performance.
The power-density (mW/cm2) MEA will increase from the current 250 mW/cm2 (0.5A/cm2 and 0.5 V) to minimum 400 mW/cm2 (0.8A/cm2 and 0.5 V). This is equal to an increase of 60%. This improvement is expected to be achieved no later than by the end of 2013. In 2025 the power density pr. cm/2 will probably as a minimum be double the 2015 number. Furthermore a new stack with significantly less mass is currently under development. A new weight-reduced stack will result in an improvement in power-density of more than 50 %. Combining the new MEA and the weight reduced stack will result in an improvement in power density of more than 150 %. In the table below the indexed power density of the old and new stack and old and new MEA is seen. The combination of the old stack and the old MEA is indexed at index 100.

[24] 2.87 kg + (11.2 kg/117.3 L*54L)= 8.0 kg.

Table 11 - Power-density of new stack with new MEA*

	Old stack	New stack
New MEA	158	254
Old MEA	100	161

*Numbers are based on reformate (0.7 % CO and 73-74 % H2).

Assumption
Dry reformate gas is assumed with maximum 0.85 % CO. The fuel cells will be running at 160° C.

Start-up time for HTPEM fuel cells

HTPEM fuel cells have a significantly higher operating temperature than LTPEM fuel cells (~ 160 Celsius versus ~ 75 Celsius), and thus also a higher start-up temperature. At an ambient temperature of – 20 degrees Celsius and where everything else is kept constant the Δt for the LTPEM fuel cell is 95 degrees Celsius whereas it for the HTPEM fuel cell is 180 degrees Celsius. The Δt is in other words app. two times higher for a HTPEM fuel cell system compared to a LTPEM fuel cell system at – 20 degrees Celsius. Therefore the start-up time of a HT-PEM fuel cell system is also, when everything else is kept constant and when HTPEM fuel cells are fully developed, expected to be app. 2 times longer than the start-up time for a LT-PEM fuel cell system.

In 2009 Toyota achieved at start up time of 30 seconds at -20°C, which they claimed was "the best cold start capability of any FCV in the world".[25] Therefore – in theory, if one only regards the thermal mass and assume the use of hydrogen as the energy-carrier – then a start up time of app. 1 minute should be possible when the HTPEM fuel cells are fully technological developed. Due to, a lot of work that still have to be done, some other limitations and the use of methanol as the energy-carrier (which has to be reformed) a realistic start up time of 5 minutes is assumed for the long run.

In the shorter run and in practical life the recommended start-up temperature for HTPEM fuel cells among others depends on the exact type of MEA, the producer and how clean the hydrogen is. A PBI MEA (from BASF fuel cells GmbH) and a new 5 - 8 kW liquid cooled stack from Serenergy is assumed. The cleaner the fuel, the lower the start-up temperature. The recommended minimum start-up temperature for Serenergy's fuel cells is 80°C and 120°C, for operation on pure hydrogen and reformate respectively. It is not recommended that the fuel cells are hibernated/stored at these temperatures, thus before start-up the modules must be preheated.

The fuel cell modules are preheated with the embedded electric heating element. The heating element is controlled by the integrated fuel cell controller. When the module is fully preheated, it

[25] http://www.cars21.com/files/papers/Kizaki-paper.pdf

will send the "ready for load" signal via the CAN interface. In the table below, start-up temperatures, energy consumption and other parameters intended for the system designer, are presented.

Table 12 – Start-up parameters for Serenergy's new liquid cooled stack

	Unit		
Fuel	-	Pure H2	Reformate
Start-up Temperature	°C	80	120
Start-up Time (from 25 °C to Start-up Temp.)	Min	<xx	<xx
Power Consumption (Heater)	W	Xxx	xxx
Energy Consumption (Heater)	Wh	<xx	<xx
Supply Potential (Heater)	VDC	Xx	xx
Min. stack temp. for achieving nominal power	°C	160	160*

* The nominal load point for reformate operation depend on reformate composition. A composition with max 0.7 % CO is assumed. Note: The nominal load point is defined for pure (99.9%) hydrogen operation.

The relative long start-up time is an issue that needs to be addresses if HTPEM fuel cells are to find general use as range extenders in vehicles.

Near term future (2013) expected start-up time

Different techniques for shortening start-up time are currently being investigated by the consortium. Fundamentally, there are three ways of doing this:

1. **Shortening the heat-up time.** This can be done in a number of ways, below a few of the most likely techniques are listed:
    a. Applying more powerful electrical heaters.
    b. Using the liquid cooling system in reverse. The liquid cooling system can be heated by burning fuel and/or by electrical heaters. The heat can for example be supplied from a reformer-burner, or another heat source in the system.
    c. Reducing the thermal mass of the fuel cell stack, and thereby reducing the energy and time needed for preheating the stack.
2. **Lowering operation/start-up temperature.** Lowering the start-up temperature means closing the time and energy gap between storage temperature and operation temperature. Operating a HT-PEM fuel cells at low temperatures can cause degradation. However, on-going R&D activities focuses on developing next generation control strategies and materials enabling low start-up temperature.
3. **Increasing hibernation/standby temperature.** Increasing the standby temperature also means closing the time and energy gap between standby and operating temperature, thus shortening the start-up time.

The three different ways to decrease the start-up time is shown in the figure below.

Figure 10 – Graphical overview of ways how to reduce start-up time

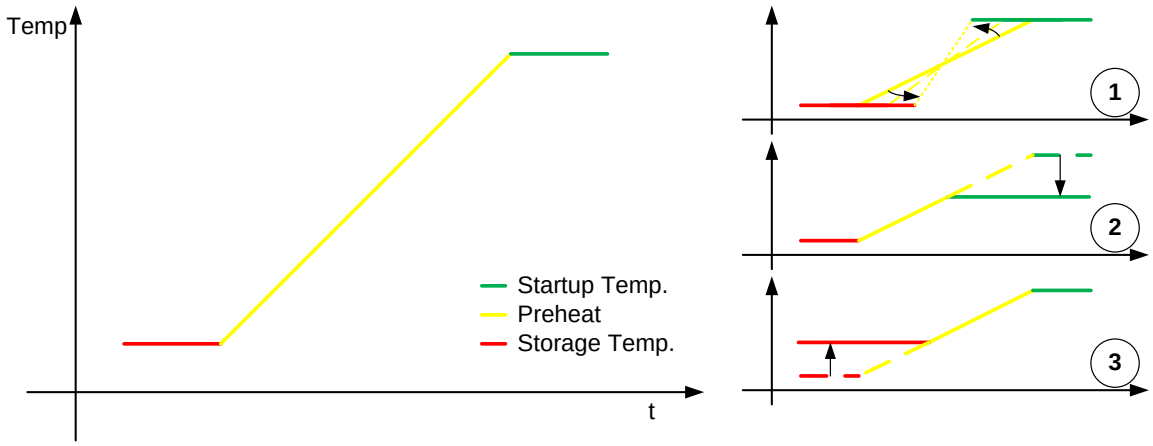

The implementation of point 1a, 1b, 1c in combination with 2 and/or 3 is expected to result in a greatly reduced start-up time. A future start-up time of 5 minutes or less, even from – 20 °C or colder is assumed in the long run whereas a start-up time of 15 minutes from – 20 °C is assumed for 2013. The long start-up time for a HTPEM fuel cell system compared to LTPEM fuel cell system as well as ICEs and batteries is a clear disadvantage of HTPEM fuel cells.

Start-up time for FC and turn-up / turn-down time

Currently (2011) we can only turn-up / turn-down by a ratio of 0.6A/min. We assume that the FC of the future can be turned up and down from 20 to 100 % in 10 – 15 sec. The target for 2013 is a turn up/down time from 20 to 100 % in less than 1 minute.

Electric heating-elements are currently used in order to heat up the fuel cells. By 2013 catalytically heating (by burning methanol) will be used. The start-up time target for 2015 is 10 minutes or less. In the long term the start-up time may be a s low as 5 minutes.

For 2015 we also assume that one can pre-heat the cabin, the battery and the fuel cell by sending a SMS to the car and telling it to be ready by a certain time, as fast a possible or in e.g. 1 hr. The software to take care of this will be rather simple.

Heat

Vehicles are designed to sustain the worst expected weather conditions experienced in the lifetime of the vehicle. If that were not the case vehicles would break down when such an expected weather extremes strokes. The night between January the 25th and the 26th 2010, Denmark experienced the coldest registered night in 23 years.[i] In Aars, North-Jutland a temperature of – 18 °C was measured.[ii] Falck and Dansk Autohjælp registered 2.400 – 2.500 people who experienced that their cars could start due to "flat" batteries from midnight the 26th till 11 o'clock on the morning of the 26th.[iii] Even though it sounds like a high number and even though Falck and Dansk Autohjælp certainly had a busy day it is still only app. 0.1 per cent of all cars in Denmark.

In this subsection the heat demand for keeping the batteries in their thermal sweet spot and for cabin heating is analysed.

Thermal management of batteries

It is the same for all batteries. From lead acid to lithium based batteries. The lower the temperature the more reluctant a battery is to release electrons and the higher the temperature the shorter the lifetime. Bill Wallace, General Motors director of Global Battery Systems has put it this way;

"Every battery has a temperature sweet spot where it provides the optimal blend of power output, energy capacity and long life… …Batteries that are too cold are reluctant to release electrons while batteries that run too hot can see a significantly shorter life."[26]

(Bill Wallace, General Motors director of Global Battery Systems)

There are basically two ways to deal with these facts. One can either choose to;

- Have a thermal system to keep the batteries in their best performing zone
- Not have a thermal system to keep the batteries in their best performing zone

In the Mitsubishi iMiEV the designers have decide not to have a thermal system to keep the batteries in their best performing zone whereas the designers of the Chevrolet Volt and the Tesla Roadster have decided to have a thermal management system. In this sub-section we will have a closer look at both the battery-system in the Mitsubishi iMiEV and in the Chevrolet Volt. Not all information is publically available for each of the systems, but by combining information about each cell and battery-system one can get a pretty good idea about pros. and cons. of not using vs. using thermal management of the batteries.

No thermal management of batteries – Case: Mitsubishi iMiEV

The Mitsubishi iMiEV use 88 LEV50 cells (see picture below).[27] At -25 Celsius only 119 Wh (2.75 V at 43.3Ah) is retainable versus 147 Wh (3.4V at 43.3Ah) at 25 Celsius. In other words the retainable capacity is reduced from index 100 at 25 Celsius to index 80.9 at -25 Celsius.[28] For the battery-pack the capacity is consequently reduced from 16.000 Wh to 12.941 Wh. In terms of range the range is reduced from 150 km to 121 km. If/when the heater is turned on the range drops further which will be discussed later in this report.

[26] http://media.gm.com/content/product/public/us/en/volt/home.detail.html/content/Pages/news/us/en/2011/Feb/0214_battery

[27] http://www.gsyuasa-lp.com/Products/GSYuasa-LEV50.pdf

[28] (119.075 Wh/147.22 Wh)* 100 = 80.9.

Figure 11 – Discharge curves for LEV50 cells at different temperatures

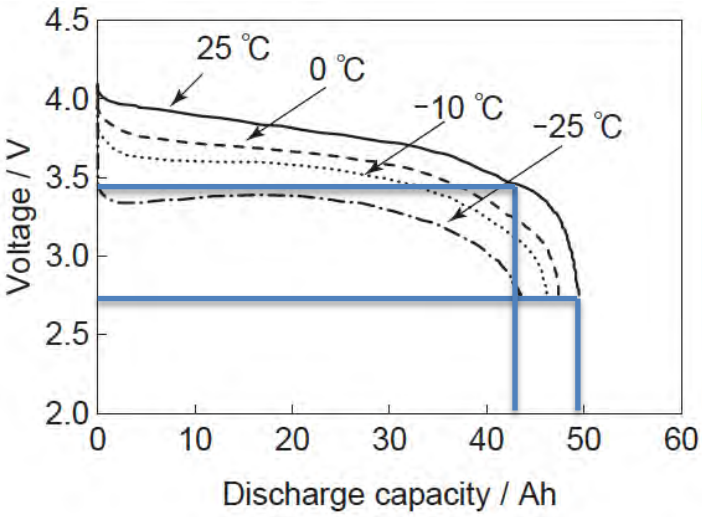

LEV50 cell, LiFePO4, 3.7V, 15 Ah/cell

The following is from an article regarding the Peugeot Ion, which was tested by the newspaper Nordjyske Stiftstidende September the 19th 2010.

"Hvis du bruger aircondition, kan det koste 5-25 procent på rækkevidden, mens varmeapparatet kan tage fra 5 og helt op til 45 procent, hvis de er rigtigt koldt.[29]*"*

"If you use air conditioning, it can cost 5-25 per cent of the range, while the heater can take from 5 to as much as 45 per cent if it is really cold."

At reduced range of 45 % is equal to a reduction from 150 km to a mere 82.5 km. It is concluded that the range of the Mitsubishi iMiEV and its sisters Citroen Zero and Peugeot Ion is sharply reduced in cold weather conditions.

Thermal management of batteries – Case: Chevrolet Volt

General Motors have revealed quite a bit of information about the thermal management of the batteries. GM own words about thermal management of the batteries is seen in the box below.

Textbox 1 – GM description of the thermal management system of the Chevrolet Volt batteries

- **Thermal management for durability and reliability:** Because batteries can be sensitive to temperature changes, the Volt pack is climate-controlled via an exclusive active liquid control system that continually monitors and maintains that battery pack temperatures for optimum performance and durability. Circulating liquid (consisting of coolant and distilled water) passes through a series of internal heat exchangers in the battery modules. The Volt features the only mass-produced battery that can be warmed or cooled. It is designed to provide reliable operation, when plugged in, at temperatures as low as -25 Celsius and as high as +50 Celsius.

[29] http://www.nordjyske.dk/artikel/10/5/2/3670663/3/buttet%20el%2Dcharmetrold

In cold weather, the battery is preheated during charging to provide full power capability. In hot weather – the most challenging environment for a battery – the Volt's battery can be chilled during charging. The Volt's thermal management system can also be powered during driving either by the battery or engine.

- **Energy management for durability:** Fully charging or fully depleting a battery shortens its life. The Volt's energy management system never fully charges or depletes the battery. The Volt battery is controlled, or buffered, so it operates within a safe state-of-charge window of 65 per cent. In demanding situations (such as driving in Mountain mode), the battery state of charge will raise the lower limit to ensure there is adequate power when needed. The battery's top and bottom "buffer zones" help ensure long life.

Source: http://ebookbrowse.com/10-chevrolet-volt-propulsion-121710-doc-d73975429

In the illustrations below the battery-pack for the Chevrolet Volt is seen. In the two upper illustrations one sees the overall distribution channels for coolant/heating media. In the two lower pictures one see one of the 144 thermal fins, including the flow channels and the overall heat management of the batterypack. There is one thermal fin for each two cells (144 thermal fins and 288 battery cells in total).

Picture 4 – View of the thermal management system of the Chevrolet Volt

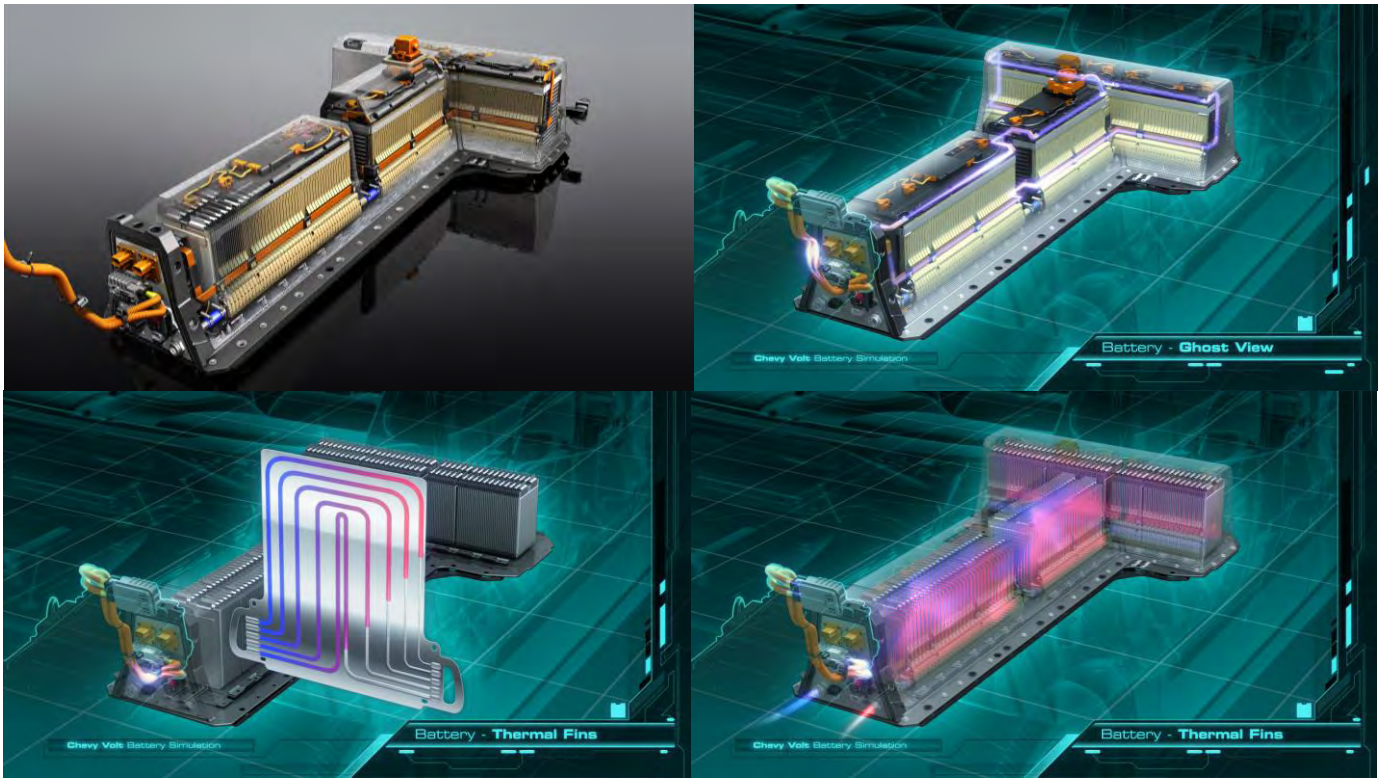

The most important drawbacks of thermal management of batteries are added weight and an increased price of the vehicle. Below the added weight and cost is estimated.

Weight of thermal management system

Each battery cell weighs 383 gram[30] and since there are 288 cells, all cells together weighs 110.3 kg. Since the battery-pack weighs 198 kg, then all other components weighs 87.7 kg. For each two battery-cells there are one cooling/warming plate. If one assumes that these plates weighs half as much as a battery-cell, then all 144 plates weighs 27.6 kg. There is 7 L of coolant liquids.[31] It is assumed that this amounts to app. 6 kg. Then there are the separator-plates which makes sure that the battery-cells and the coolant-plates are kept in the right spot. For the Mitsubishi iMiEV each of these pieces of plastic weighs 0.7 kg. Since there are 22 of these the total weight of these amounts to 15.4 kg. A similar weight for the Chevrolet Volt is assumed (15 kg.). Then there are cables, BMS, connectors etc. A total of 11 kg is assumed. Finally there is the outer casing and insulation. The total weight "overhead" from battery-module to battery-pack for the Mitsubishi iMiEV is 39 kg. The same weight overhead is assumed here and since cables etc. is assumed to weigh 11 kg, then there are 28 kg left for outer casing. In the table below the estimated weights of the different components are listed. In the column to the right the weight of the battery-pack in case there wasn't a coolant loop is estimated and listed. There are both direct effects (27.6 kg coolant plates and 6.1 kg coolant liquid) and 2nd order effects. The 2nd order effects are estimated at 3 kg due to thinner separator-plates, 3 kg due to coolant tubing, shorter cables etc. and 8 kg for a smaller and thereby lighter battery casing.

[30] http://ntrs.nasa.gov/archive/nasa/casi.ntrs.nasa.gov/20110011197_2011010830.pdf
[31] http://www.nxtbook.com/nxtbooks/sae/10EVSD1104/#/0

Table 13 – Estimated weight of the Chevrolet Volt battery pack

	Estimated/ Actual	Estimated weight with coolant loop (kg)	Estimated weight without coolant loop (kg)
Cells	Actual	110.3	110.3
Coolant plates	Estimated	27.6	0
Coolant liquid	Estimated	6.1	0
Separator plates	Estimated	15.0	12.0
Cables, BMS, connectors etc.	Estimated	11.0	8.0
Casing	Estimated	28.0	20.0
Sum	Actual	198	150.3

The weight factor from cells to battery pack is 1.80 (198/110.3 kg) and is estimated at 1.36 if there where no coolant loop (198/150.3 kg). Obviously the above listed weights are not correct. They do however give the reader an idea about the weight of the different components.

The weight factor from cells to battery-pack for Mitsubishi iMiEV and the Tesla Roadster is in comparison 1.36 and 1.48 respectively as seen in the table below.

Table 14 – Weight-factor from battery-cells to battery-pack

Car	g/cell (g)	no. of cells (no.)	Total cells weight (kg)	Total pack weight (kg)	Factor (factor)	Thermal management (yes/no)
Mitsubishi iMiEV	1.700	88	149.6	204	1.36	No
Chevrolet Volt	383	288	110.3	198	1.80	Yes
Tesla Roadster	44.5	6.831	304.0	451	1.48	Yes

Cost of thermal management system

On the 27th of May 2010 a GM executive finally admitted the total cost of the Volt's 16 kWh lithium-ion pack. According to Stracke the pack costs roughly $10,000. Since we also know that the cost of the battery-cells constitute app. 70 % of the overall cost of the battery (as of the 26th of March 2010)[32], it is assumed that the cells cost 7.000 USD. Since the battery-pack holds 16.632 Wh the cost in the spring of 2010 was 421 USD/kWh battery-cells. In the illustration below one sees that app. 70 % of the total cost for the battery-pack origins from the battery-cells and that GM also use the terms cells, modules and pack.

Picture 5 – GM use of terms and price of battery-cells as a fraction of battery-pack cost

[32] http://gm-volt.com/2010/03/26/gm-exec-gen-3-voltec-battery-to-have-shortened-lifespan-simpler-shape-and-be-offered-in-smaller-ranges/

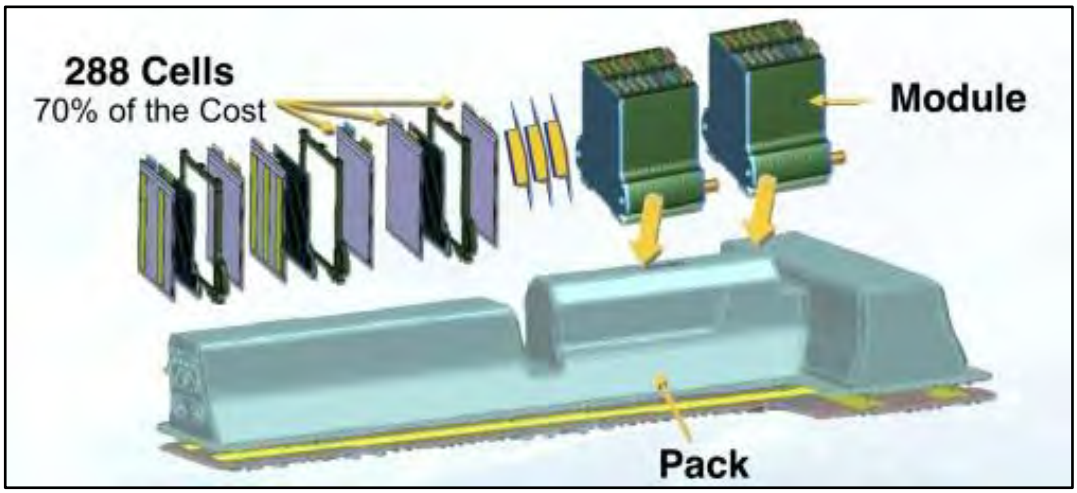

Source: [33]

Of the remaining app. 3.000 USD for the battery-pack it is assumed that app. 1/3 origins from the thermal management system and that the remaining 2/3 origins from the frame, BMS, cables etc. It is therefore assumed that the thermal management system costs app. 1.000 USD. With an assumed cost of 1/2 for the coolant plates and 1/2 for other components each coolant plate is estimated to cost app. 3.5 USD.

Closing remarks

From an engineering point of view it is highly interesting to note that while Mitsubishi have decided to go for a system without thermal management of the batteries, then GM and Tesla has decided to go for a system with thermal management. To use two so radical different approaches for the design of battery-packs is a sign that even the big car-manufacturers are not sure how best to design battery-packs. In other words it is a sign that no dominant design when it comes to the thermal management of batteries exists.

"When it comes to thermal management of batteries for electric cars it seems as if no Dominant Design exist yet.[34]"

When decent amounts of high quality waste-heat are available it is obviously that one should utilise the waste-heat for cabin heating as well as for thermal management of the batteries. It is the case since the cost (in terms of added weight and complexity of the vehicle) is relatively small (an estimated 45 - 50 kg plus radiator for the GM Volt) and the added battery capacity is relatively large (+ ~ 20 % for the Mitsubishi iMiEV) when one use thermal management of batteries.

Thermal management of cabin

Not only does the battery in a BEV have to sustain a cold day – the same counts for the heater. That is, the heater has to be designed for use in temperatures of at least – 18 °C and preferable colder, in order to keep the cabin warm. Below a graph denoting heat-requirements for different

[33] http://gm-volt.com/2010/03/26/gm-exec-gen-3-voltec-battery-to-have-shortened-lifespan-simpler-shape-and-be-offered-in-smaller-ranges/

[34] See Fast second by Markides and Geroski, 2005 for futher information about "Dominant Design".

temperatures for American cars is displayed. It is seen that app. 6 kW heat is needed at – 20 °C and at 0 % recirculated air.

Figure 12 – Heating/cooling thermal power as function of recirculated air & ambient conditions

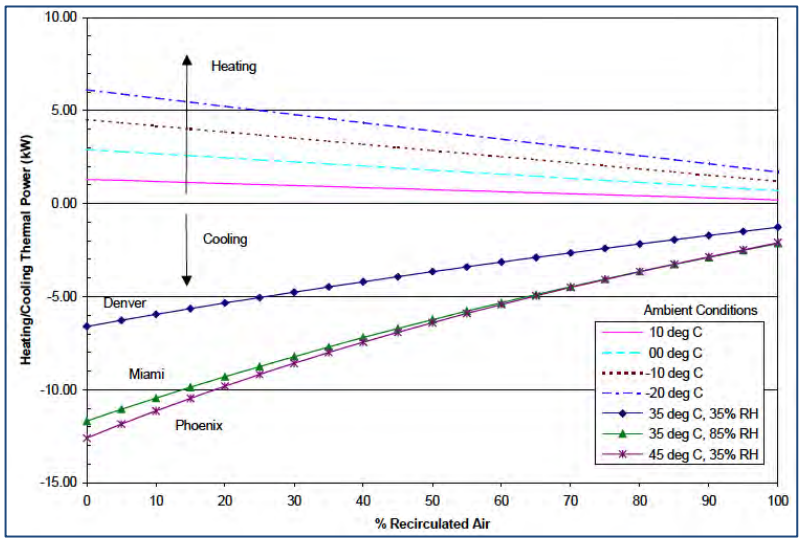

Source: http://www.nrel.gov/vehiclesandfuels/ancillary_loads/pdfs/vtmsfinalsent.pdf

The cabin heater with the biggest output from the company Webasto for cars has an output on 5.2 kW.[35] Therefore a maximum heat-demand for cabin heating of 5.2 kW is assumed. From the above figure one can also see that the maximum cooling effect required can be as high as 12 – 13 kW for a car driving in 45 °C and a humidity of 35 %. An efficient heat pump can reduce the demand to 5 – 6 kW or even less. One can also use heat from the fuel cells for cooling. Whether it is technically and economically feasible needs to be determined. Since the heat has a direction and a high quality (high temperature) there is however a high change that it is technical as well as economical feasible to do so.

Thermal management methods

Three different ways to heat up a cabin and batteries exists. One can either use electricity, burn fuel or utilise waste heat from different sources. The least attractive solution from a technical, economical and ecological point of view is to use electricity for heating. It is the least attractive solution since electricity can be transformed into heat but whereas heat only partly can be transformed into electricity. Of this reason electricity can be defined as more valuable than heat, and one should try to use the least valuable resource instead of the most valuable resource whenever possible. Using electricity for heating also greatly reduced the range of pure electric cars. The second best solution is to burn fuel. Since some of the energy in the fuel could have been used for producing electricity and/or motion it isn't the most attractive solution. The most attractive solution is to harness as much of the chemical bound energy as motion and/or electricity and then utilise some of the waste heat. The three primary ways to heat up a cabin is described below.

[35] http://www.standheizung.de/

Electrical heating

Some electric cars only use electrical heating. It is a cheap and simple solution. The disadvantage is however that one use high-value electricity from the batteries. By doing so one drains the batteries and thereby reduce the range of the electric car. That is a serious problem in cold climates such as the Danish. Both the Tesla Roadster and the Mitsubishi iMiEV use electrical heating.

Burner

The issue with a reduced range, when using electric heating, can be solved by installing a burner from e.g. Webasto or Eberspächer. Most electric cars in Denmark have installed some kind of burner. The disadvantage is that the electric car pollute the local as well as the global environment and that it still use some gasoline or diesel. Webasto have two kind of heaters for cars – Parking heaters and Auxiliary heaters. It hasn't been possible to find prices and specifications on auxiliary heaters of which reason the working group have decided to have a look at Parking heaters. In the table below some of the specs and prices of different Parking heaters from Webasto is listed. The data will later be used to estimate the value of the waste-heat from the HTPEM fuel cells.

Table 15 – Overview of specifications and prices of Webasto Parking heaters

Webasto terms (UK homepage)	Small and subcompact cars	Compact and middle-range cars	Luxury cars, off-road/van
HI-EPS terms (class)	A, B	C, D	E, F, S, M, J
Heater type	Thermo Top Evo 5 / Thermo Top E	Thermo Top Evo 5 / Thermo Top C	Thermo Top Evo 5+ / Thermo Top P
Max. heating period (min)	60	60	60
Fuel consumption (L) In a 20 min. heating phase at full load	ca. 0.17	Ca. 0.21	Ca. 0.21
Heater output (kW) Full/partial load	4.2/2.6	5.2/2.6	5.2/2.6
Price incl. VAT excl. mounting, Comfort preset timer, Germany (€)	733.37	966.96	1053.66
+ Mounting (€)	805.37	1038.96	1125.96
+ Telestart T91 (€)	1042.37	1275.96	1362.66
+ Telestart T100 HTM (€)	1122.37	1355.96	1442.66
+ Thermo Call (€)	1307.53	1541.12	1627.82

Sources: http://www.standheizung.de/, http://www.webasto.co.uk/home/en/html/homepage.html

Waste heat

The most economical and ecological way to heat up a cabin is to use heat that would otherwise be wasted.

If one use a range extender, which is the case in e.g. Chevrolet Volt the problem is that there is only waste heat available when the engine is actually running. When the engine is not running it is not known how they heat up the cabin. It is however assumed that he Chevrolet Volt use electric heating when the engine is not running.

All TDI engines from VW are so efficient that quite often there is not enough waste heat available for heating up the cabin. Of this reason they generate electricity via the generator and use the electricity generated to generate heat. The overall efficiency is obviously low of which reason this

is not the best way forward. It is like two steps forward and then one step backwards. The heating system in VW TDI cars is seen below.

Figure 13 – The heating system in VW TDI cars

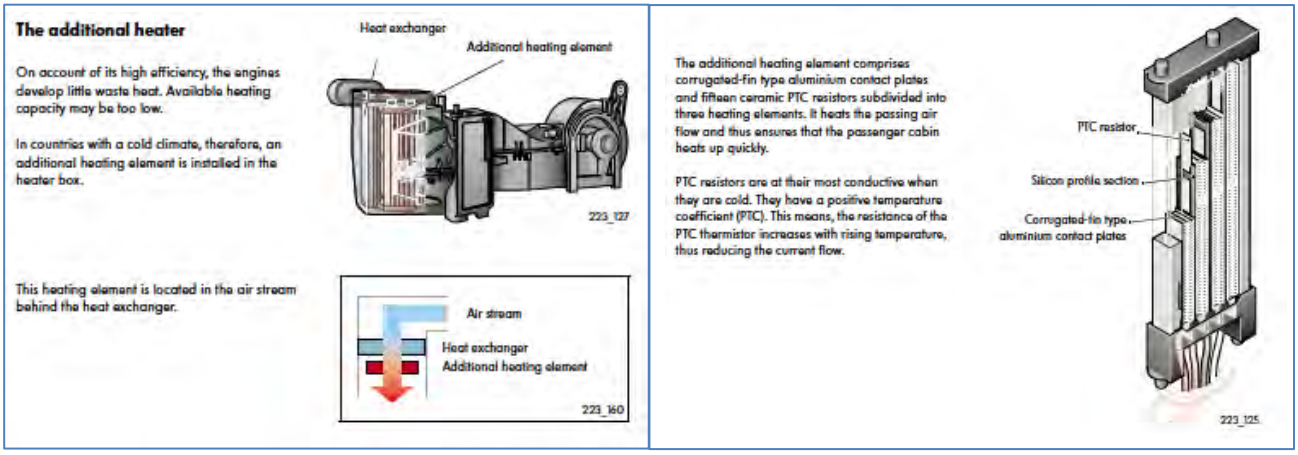

Source: http://www.volkspage.net/technik/ssp/ssp/SSP_223.pdf p. 69-70/88

The most common way to heat up the cabin in a car is to utilise the waste heat from the engine. It is simple, efficient, cheap and reliable to do this. The only drawback is that one can only use a part of the heat and that the Combined Heat and Power (CHP) efficiency from tank to wheel and cabin is low. Most of the waste heat occurs as radiation from the engine, which is difficult to utilise since the heat occurs as radiation (air-to-air) and since the heat doesn't have a direction.

The last way to utilise waste heat is to look for sources of heat where it is significantly easier to utilise the heat than from an ICE. Liquid cooled HTPEM fuel cells have excellent characteristics when it comes to utilizing waste heat since:

1) The heat comes at a high temperature (app. 150 ° C)
2) Most of the heat has a direction (via the cooling tubes vs. as radiation for an ICE)
3) It is easy to utilise since it comes in liquid form

Furthermore due to the high electric efficiency of the fuel cells the amount of waste (measured in kW heat) is also significantly lower than for an ICE. The contribution from utilising heat to the CHP efficiency is therefore also higher than for an ICE.

In the figures below the efficiency for a 10, a 20 and 40 kW HTPEM fuel cell unit with different degrees of heat-utilization are seen. An electric efficiency of 52 and 38 % is assumed at "no load" and "full load" respectively and a maximum heat-utilisation of 80 % of the available heat is assumed. Since at least 5 kW heat is needed for cabin heating in peak-situations the fuel cell has to produce at least 6.25 kW heat (5 kW/0.8). It hasn't been calculated how much energy is needed to heat up batteries in cold weather. If one assumes 5 kW, then the combined amount that has to be available is 12.5 kW before utilisation and 10 kW after utilisation (5 kW for cabin and 5 kW for batteries). It is strongly recommended that calculations be made in order to quantify the amount of heat needed to heat up batteries at different temperatures, masses, heat-up time etc.

At an electric load of 5 kW_{el} and 3 kW_{heat}, which can e.g. represent city driving at low speed in Copenhagen in the fall or spring in Denmark, where the heat is used both for cabin heating and for keeping the batteries at 20 – 25 °C, we see the following:

- The electric efficiency will be 45.0, 48.5 and 50.3 % for 10, 20 and 40 kW FC respectively
- The heat-efficiency will be 27.0, 29.1 and 30.1 % for 10, 20 and 40 kW units respectively
- The CHP efficiency will be 72.0, 77.6 and 80.4 % for 10, 20 and 40 kW units respectively.

Stars mark the CHP efficiency for the three different FC units.

Figure 14 – Combined Heat and Power efficiency map of a 10, a 20 and a 40 kW fuel cell system

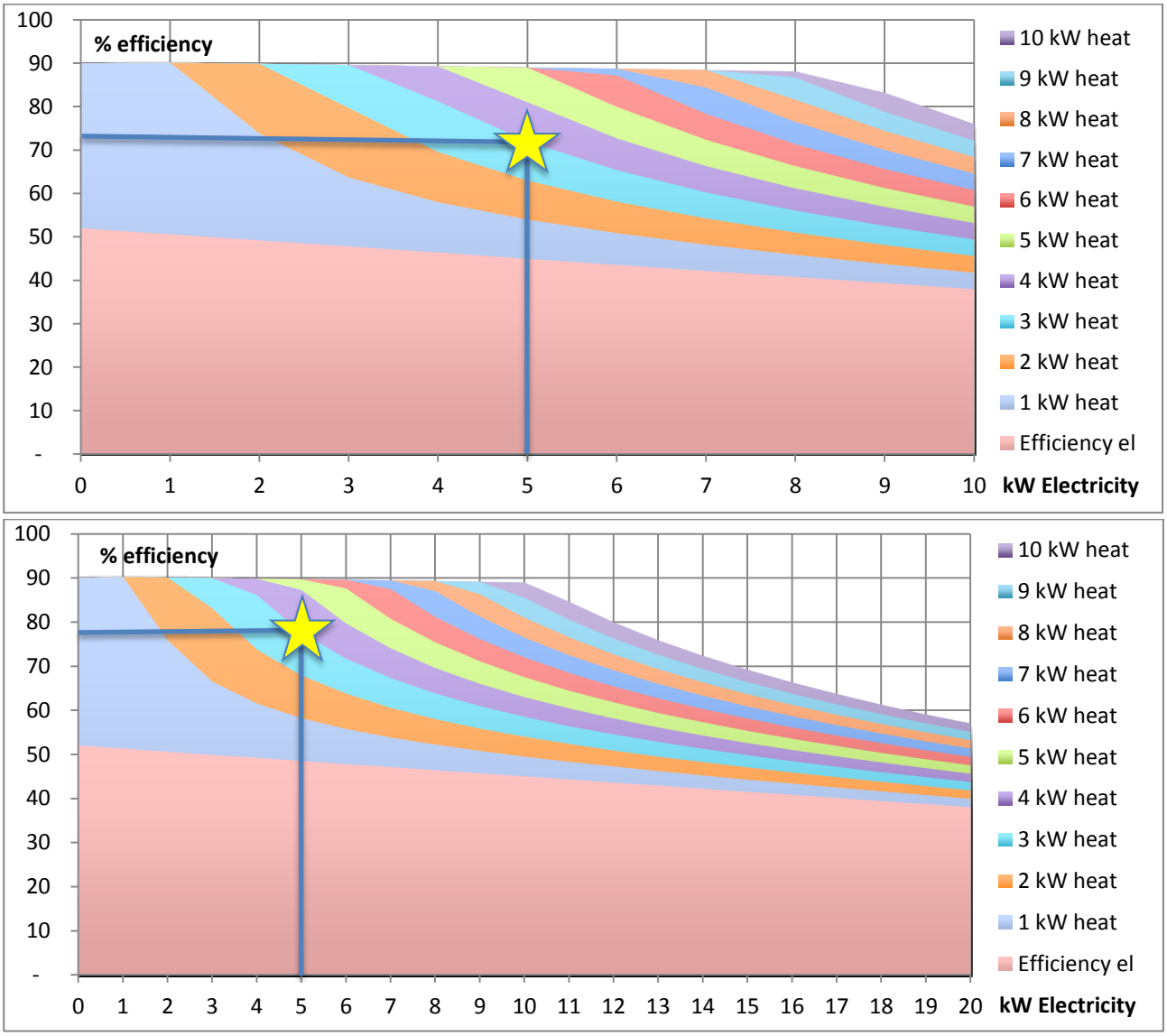

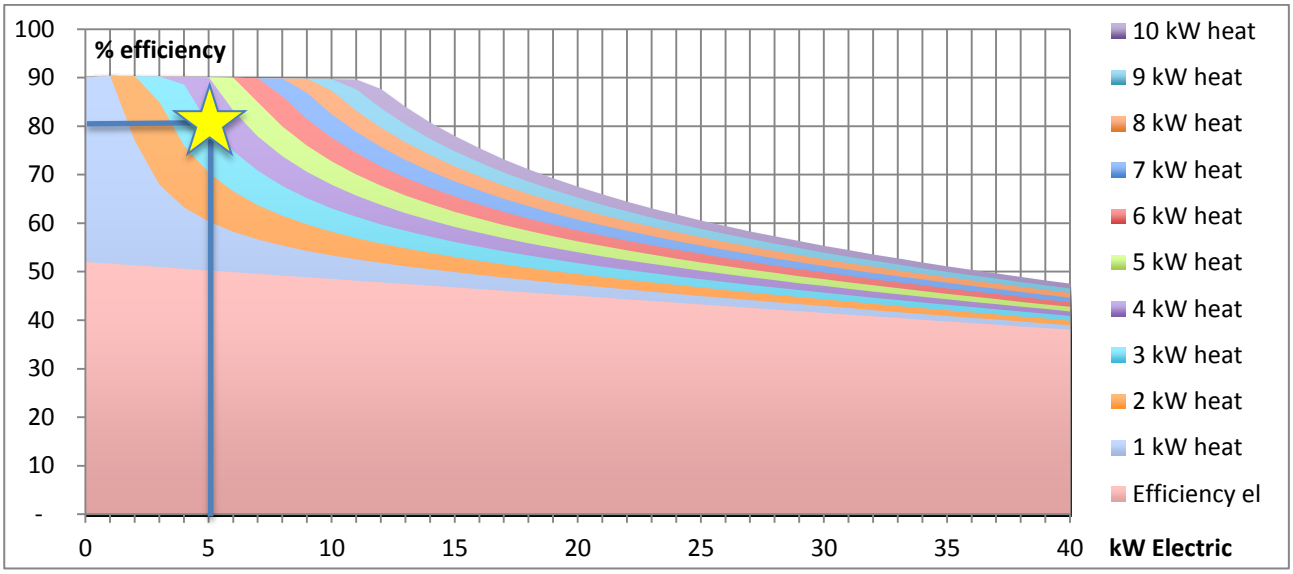

In the figures above it is furthermore seen that a 10 kW FC can barely produce enough heat for the peak-condition which is defined as – 20 °C and heat for both cabin and batteries.

In the table below the efficiency for a 10, a 20 and a 40 kW FC unit is seen when the load is 5 kW_{el} and 3 kW_{heat}.

Table 16 – CHP efficiency for a 10, 20 and 40 kW FC unit at 5 kW_{el} and 3 kW_{heat} load

Rank	Technology	Use of: *el, fuel, waste heat*	Examples

	Efficiency				
Max kWel	El (%)	Heat (%)	CHP (%)	Waste heat (%)	kWh fuel
10	45.0	27.0	72.0	28.0	11.11
20	48.5	29.1	77.6	22.4	10.31
40	50.3	30.1	80.4	19.6	9.95

As seen from the above figures and the above table not only does the electric efficiency increase with a decreased load of the FC – the heat-utilisation also increase. The combined effect is quite dramatic. The CHP efficiency in this example increases from 72.0 % to 80.4 %. The analysis is a bit simplified but it is however a decent representation of what happens in terms of efficiency.

In the table below the different overall heating technologies (electrical heating, burner and waste heat) are ranked from the least attractive to the most attractive solution.

6	**Electric heating** electricity from batteries	100 % el	Tesla, Mitsubishi iMiEV
5	**Burner** fuel	100 % fuel	Volvo C30
4	**Waste heat** from RX and electric heating	~ 50 % waste heat + ~ 50 % el	Chevrolet Volt
3	**Waste heat** from ICE and electric heating	~ 80 % waste heat + ~ 20 % el	VW with TDI engines
2	**Waste heat** from ICE	~ 100 % waste heat at low efficiency	Ordinary cars
1	**Waste heat** from FC	~ 100 % waste heat at high efficiency	FC vehicles

Table 17 – Heating technologies for vehicles ranked after their CO2 footprint

From a thermal management point of view it can be concluded that HTPEM fuel cells have excellent properties. For cabin heating at least 6.25 kW heat is needed and for batteries a roughly estimated 6.25 kW is needed. Therefore the thermal output of the FC has to be at least 12.5 kW.

Other

Curb weight

Different definitions of curb weight (also known as kerb weight) exist.[1] In the US the definition is the total weight of a vehicle with standard equipment, all necessary operating consumables (e.g. motor oil and coolant), a full tank of fuel, while not loaded with either passengers or cargo. This definition differs from definitions used by European Union manufacturers, which include the weight of a 75 kg and a 90 % filled tank.

"The mass of the driver is assessed at 75 kg (subdivided into 68 kg occupant mass and 7 kg luggage mass according to ISO Standard 2416 — 1992), the fuel tank is filled to 90 % and the other liquid containing systems (except those for used water) to 100 % of the capacity specified by the manufacturer."[2]

In the table below the differences are listed.

Table 2 – US and EU definitions of curb weight

	Operating consumables (L)	Fuel (L)	Passenger and cargo (kg)
USA	Full	100% full	0
EU	Full	90% full	75

Since all three vehicles do not follow the European standard for curb weight we have to adjust the curb weight of these vehicles so they represent the European curb standard. The curb weight of the;

- iMiEV, which is listed at 1.080 kg increases by 75 kg to 1.155 kg.
- Chevrolet Volt, which is listed at 1.715 kg decreases by 2.5 kg fuel[3] but increases by 75 kg person and luggage. The new curb weight is 1.788 kg.
- Tesla Roadster 2.5 increases by 75 kg to 1.310 kg.

[1] http://en.wikipedia.org/wiki/Curb_weight

[2] http://eur-lex.europa.eu/LexUriServ/LexUriServ.do?uri=OJ:L:1998:091:0001:0061:EN:PDF

[3] (35.2 L fuel tank * 0.72 kg/L gasoline * (1-0,1)).

Assumptions regarding the engine and the generator

Since GM do not disclose the weight of the motor and the generator we have to make some assumptions regarding the weight of these units. In the report "Well-to-whells analysis of future automotive fuels and powertrains in the European context" made for the European Commission it is stated that a 1.6 L PISI engine of 77 kW weighs 120 kg.[36] A linear relationship to other motor sizes measured in kW is assumed. Therefore the 63 kW engine of the Chevrolet Volt is assumed to weigh 98 kg.[37]

Eventhough Lotus do not state it anywhere one can from the pictures of the generator they use on their concept vehicle see that it is a generator from the company UQM that they use. Such a generator according to datasheets from UQMs homepage weighs 41 kg for a 50 kW generator.[38] The 85 kW generator from UQM weighs 50 kg.[39] If a linear relationship between the 50 kW and the 85 kW generator is assumed, then the 63 kW generator in the Chevrolet Volt weighs 44 kg.[40]

Auxiliary loads

The main purpose of the motor is to provide power for the wheels. However, a modern also car has other loads which the motor should supply. These loads are either due to safety, e.g. light, wipers, horn, etc. and/or comfort, e.g. radio, heating, air conditioning, etc. These loads are not constant, e.g. the power consumption of the air conditioning system strongly depends on the surrounding temperature. Even though some average values are suggested. These can be seen in Table 2.1. From the table it may be understood that the total average power consumption is *p*Aux = 957W.

Table 18 – The electric loads with the highest average consumption

Description	Average power [W]
Radio	52
Heating Ventilation Air Condition (HVAC)	489
Lights	316
Electric power steering	100
Total *p*AuX	957

[36] http://www.europabio.org/Biofuels%20reports/well-to-wheel.pdf table 4.2-1
[37] 63kW/77kW*120 kg = 98 kg.
[38] http://www.uqm.com/pdfs/HiTor%20spec%20sheet%203.30.11.pdf
[39] http://www.uqm.com/pdfs/PP145%20Spec%20Sheet%203.30.11.pdf
[40] 41 kg + (63-50 kW)/(85-50kW)*(50-41kg) = 44 kg.

[i] According to article: ”Thy fik den koldeste nat i 23 år” (Tv2.dk, 9.1.2010, Danny Høgsholt, http://vejret.tv2.dk/article.php/id-27684141.html?ss), Thy experienced the cooldest night in 23 years, when they the night to the 9th of January 2009 experienced – 15.9°C. Since – 18C is colder, that must be the coldest night for 23 years.

[ii] ”minus 18 i nat”, Lone Seir Carstensen, DMI.dk, http://www.dmi.dk/dmi/index/nyheder/nyheder-2/minus_18_i_nat.htm

[iii] Ekstrem kulde giver døde batterier, Jyllands Posten, Sarah Kott, 26.1.2010, http://jp.dk/indland/trafik/article1959252.ece

Appendix 4

Technical report

"CFD analysis of a 5kW methanol reformer"

CFD analysis of a 5kW methanol reformer

The report summarizes the computational fluid dynamics (CFD) analysis of a methanol reformer for a HTPEM fuel cell system with a rated electric power of 5 kW. Figure 1 shows an outline of the computational model. The overall reactor design is based on a shell and tube heat exchanger concept with the reforming process taking place in the tubes and the heat required for the endothermic reforming process being supplied from a heat transfer fluid flowing on the shell side.

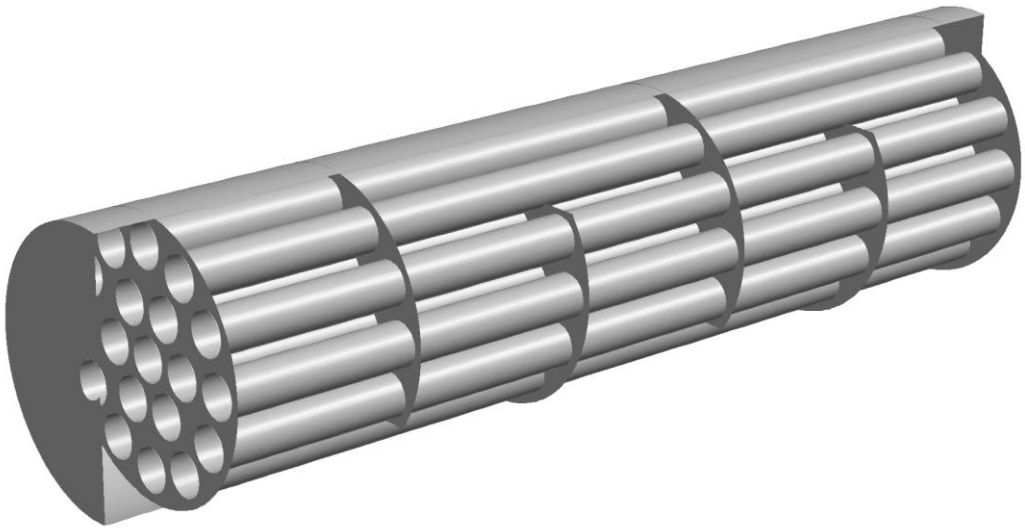

Figure 1 Outline of the computational fluid dynamics model of the methanol reformer.

The flows on both the tube side and the shell sides are assumed laminar. The model includes all species involved in the reforming process; CH_3OH, H_2O, H_2, CO_2 and CO. The catalyst pellet bed is modeled as a porous zone with an overall porosity of 0.5 and the associated pressure drop calculated from the Ergun equation. The thermal conductivity of the bed is modeled using the standard FLUENT approach for porous regions which uses a porosity weighted average of the solid and gas conductivities. Catalyst pellets are assumed to be present in the tubes as well as in the end caps of the reactor. The steam reforming process is modeled using a simplified reaction mechanism suggested by (Purnama et al. 2004) consisting of a methanol steam reforming step and the reverse water-gas-shift reaction.

$$CH_3OH + H_2O \rightleftarrows 3H_2 + CO_2 \qquad \text{Eq. 1}$$

$$CO_2 + H_2 \rightleftarrows H_2O + CO \qquad \text{Eq. 2}$$

The rates are calculated from relatively simple power laws with a slight adjustment to the rate expression for the steam reforming reaction compared to (Purnama et al. 2004).

$$r_{SR} = k_1 \, P_{CH3OH}^{m} \, P_{H2O}^{n} \qquad m = 0{,}8;\ n = 0{,}2 \qquad \text{Eq. 3}$$

$$E_a = 76\ kJmol^{-1}, \quad k_0 = 8{,}8 \times 10^8\ s^{-1} g_{cat}^{-1}$$

$$r_{RWGS} = k_2\, P_{CO2}\, P_{H2} - k_{-2} P_{H2O} P_{CO} \qquad \text{Eq. 4}$$

$$E_a = 108\ kJmol^{-1}, \quad k_0 = 6{,}5 \times 10^9\ bar^{-1}s^{-1}g_{cat}^{-1}$$

The tube walls are modeled using the 1-dimensional approach available in FLUENT with a wall thickness of 1 mm and stainless steel material properties.

The heat transfer fluid on the shell side of the reactor is assumed to be Paratherm NF. The oil flow rate has been set to ensure only 2-3 degrees temperature drop from the inlet to the outlet corresponding to the experimental conditions. Heat losses from the shell surface is modeled with a 1-dimensional heat transfer equation assuming an isulation layer thickness of 50 mm and a thermal conductivity of the insulation material of 0.05 W/mK.

For the baseline calculations a mixture of methanol and water vapor with a steam-to-carbon ratio of 1.5 flows into the catalyst bed with a temperature of 200°C. Figure 2 below shows predicted methanol vapor mole fraction in the center plane of the reactor. The fresh mixture enters from the left hand side in the figure and flows towards the right.

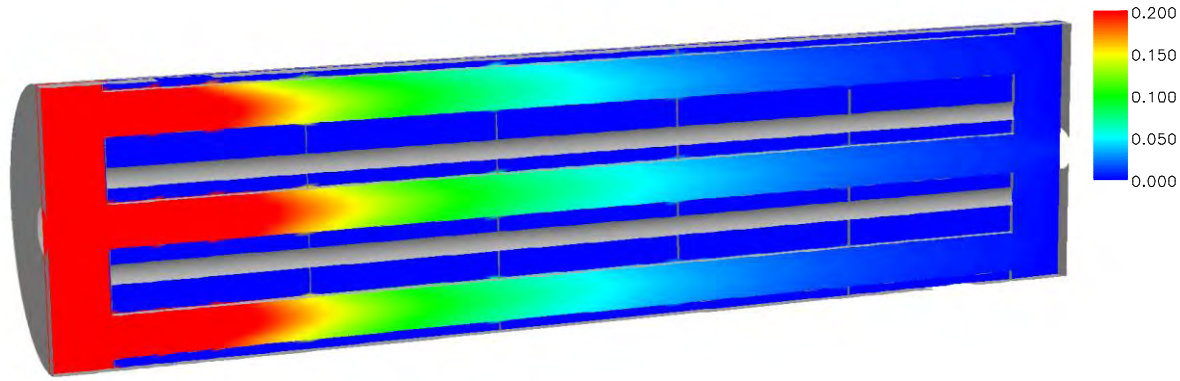

Figure 2 Methanol vapor mole fraction at the reactor center plane. The maximum value of the color scale has been reduced from 0.4 to 0.2 in the plot to better show the conversion in the last part of the reactor.

The main conversion is seen to take place in the first half of the reactor. For the CO formation the trend is the opposite with the main CO production occurring in the last half of the reactor. This is illustrated by Figure 3 showing the mole fraction of CO in the same cross section of the reactor. This is a typical trend that was observed in all simulation that when the methanol steam reforming is near completion the formation of carbon monoxide starts. At where high load where the steam reforming process occurs in the entire reactor very little carbon monoxides forms whereas the opposite is the case at low loads. This will be discussed in further detailed below.

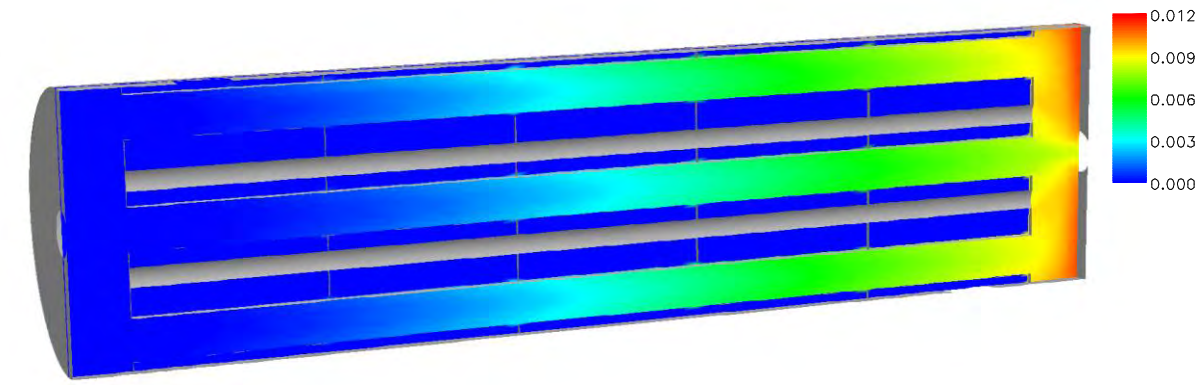

Figure 3 Mole fraction of carbon monoxide at the reactor center plane.

The corresponding temperature field is shown in Figure 4 at the same location in the reactor. The methanol-water mixture is heated to a temperature 5-10 degrees below the oil temperature when it enters the tubes. It is also noted that there is a 5-10 degrees radial temperature gradient through the catalyst pellet bed in the tubes. It is difficult to determine whether this radial gradient is accurately predicted as no measurements currently exist. The applied standard FLUENT thermal conductivity model in porous materials is relatively simple as mentioned in the beginning of this report. In addition, the model uses a lumped temperature for the gas and solid phases which may not accurately describe the region with fast steam reforming reaction rates due to the exothermic nature of this reaction that may cool the catalyst pellets below the gas temperature. Future temperature measurements inside the tubes are planned to investigate these issues.

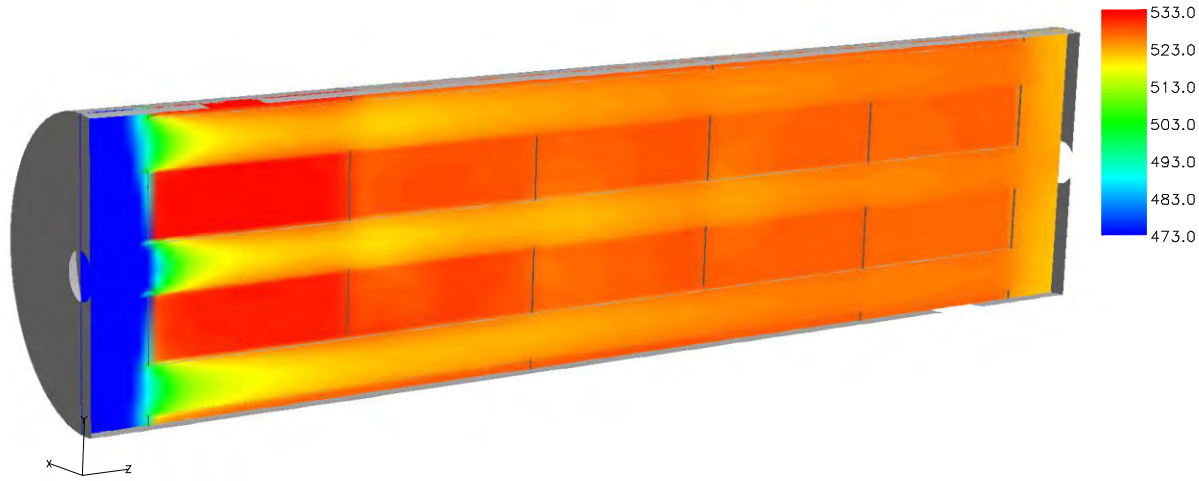

Figure 4 Temperature in the reactor center plane. Oil inlet temperature: 533 K. Methanol water mixture inlet temperature: 473 K.

Measurements were conducted by Serenergy mapping the exit gas composition versus the flow rate of methanol-water mixture at different temperatures. These measurements have formed the basis for a model validation study where a number of CFD calculations were performed at similar operating conditions to compare exit gas compositions.

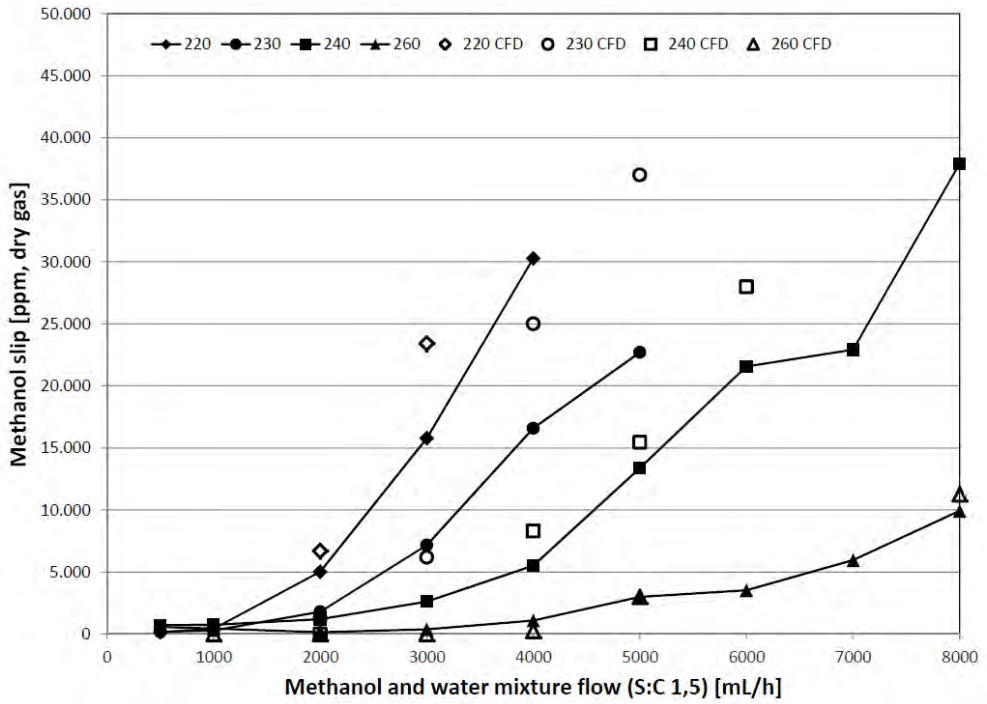

Figure 5 Methanol slip as a function of methanol-water mixture flow rate at different temperatures compared with CFD predictions.

The CFD based model captures the overall trend quite well. There is a tendency though for the CFD model to predict a stronger variation of the slip with increasing flow rate than seen in the measurements. A similar comparison is made for the carbon monoxide at the exit in Figure 6.

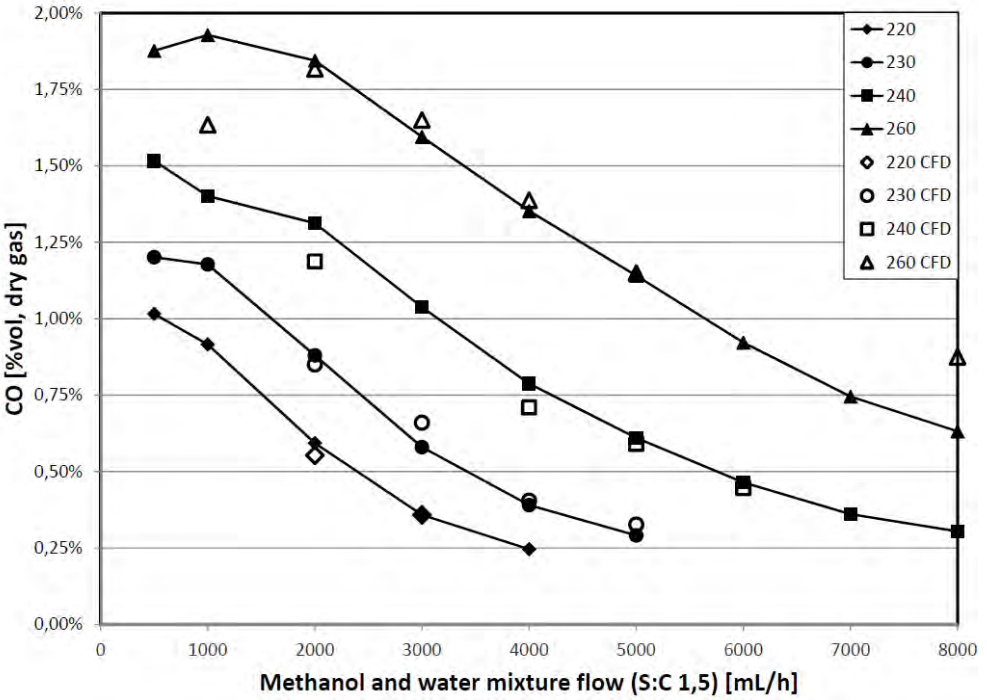

Figure 6 Carbon monoxide as a function of methanol-water mixture flow rate at different temperatures compared with CFD predictions.

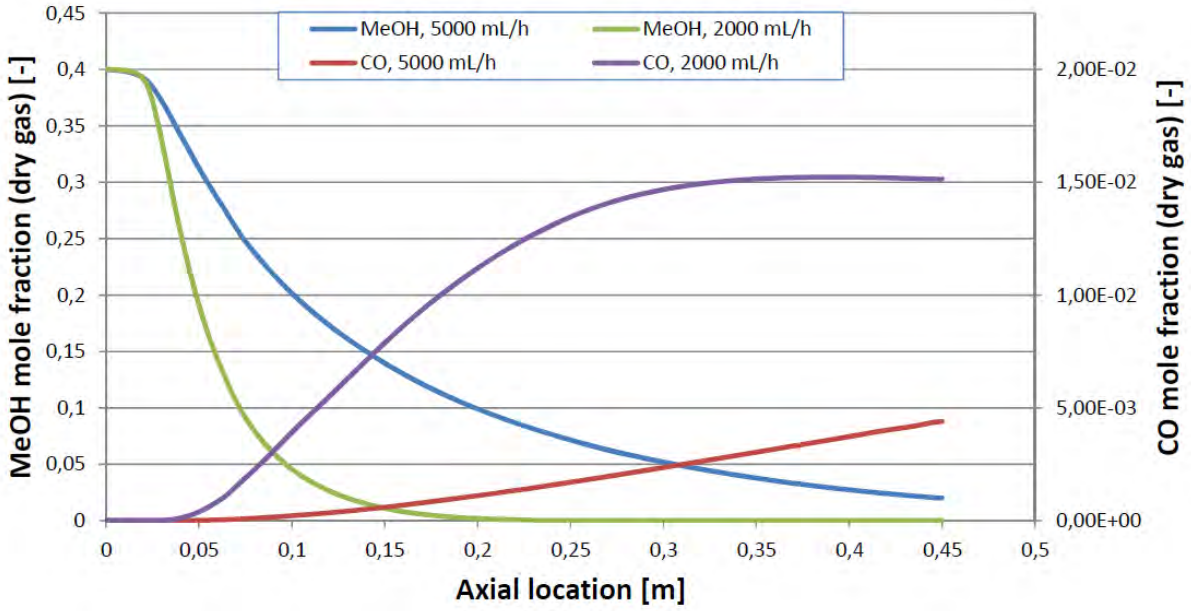
MeOH, 5000 mL/h
MeOH, 2000 mL/h
CO, 5000 mL/h
CO, 2000 mL/h
MeOH mole fraction (dry gas) [-]
CO mole fraction (dry gas) [-]
Axial location [m]
0,45
0,4
0,35
0,3
0,25
0,2
0,15
0,1
0,05
0
2,00E-02
1,50E-02
1,00E-02
5,00E-03
0,00E+00
0
0,05
0,1
0,15
0,2
0,25
0,3
0,35
0,4
0,45
0,5

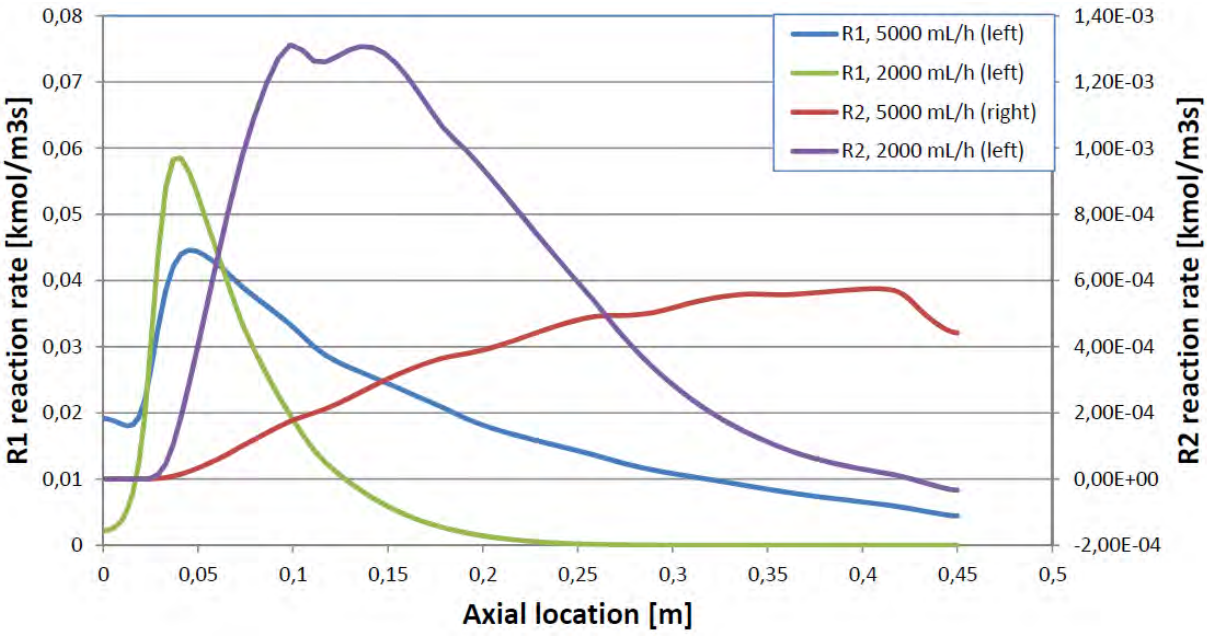
R1, 5000 mL/h (left)
R1, 2000 mL/h (left)
R2, 5000 mL/h (right)
R2, 2000 mL/h (left)
R1 reaction rate [kmol/m3s]
R2 reaction rate [kmol/m3s]
Axial location [m]
0,08
0,07
0,06
0,05
0,04
0,03
0,02
0,01
0
1,40E-03
1,20E-03
1,00E-03
8,00E-04
6,00E-04
4,00E-04
2,00E-04
0,00E+00
-2,00E-04
0
0,05
0,1
0,15
0,2
0,25
0,3
0,35
0,4
0,45
0,5

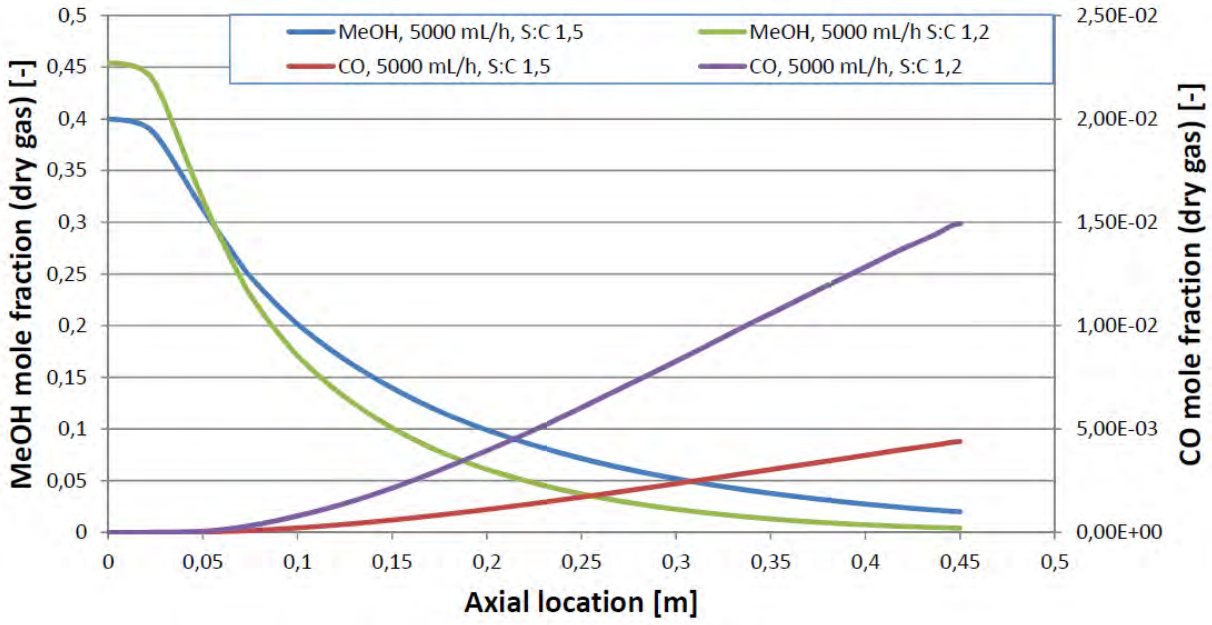
MeOH, 5000 mL/h, S:C 1,5
MeOH, 5000 mL/h S:C 1,2
CO, 5000 mL/h, S:C 1,5
CO, 5000 mL/h, S:C 1,2
MeOH mole fraction (dry gas) [-]
CO mole fraction (dry gas) [-]
Axial location [m]
0,5
0,45
0,4
0,35
0,3
0,25
0,2
0,15
0,1
0,05
0
2,50E-02
2,00E-02
1,50E-02
1,00E-02
5,00E-03
0,00E+00
0
0,05
0,1
0,15
0,2
0,25
0,3
0,35
0,4
0,45
0,5

Appendix 5

Technical report

"Fuel cell sealing concepts"

SCREENING REPORT - BIPOLAR PLATE MATERIALS

Serenergy A/S
Majsmarken 1
9500 Hobro

Key words: bipolar plates, fuel cells, BAC 2, PEAK, Aluminum, silver coating, BPP4, BMCI, Graftech

INTRODUCTION

In this report we present a survey of relevant plate materials for Serenergys high temperature PEM fuel cell stacks. The selection of plate material affects parameters like:

- Material cost
- Manufacturing method
- Fuel Cell stack performance
- Fuel Cell stack lifetime

The first two directly influences the cost of the final product, and the last two the customers experienced product value, hence the product price.

MATERIALS

Traditionally graphite based bipolar plates have been applied for PEM fuel cells. Graphite based plates have good properties with regards to low electrical resistance, high corrosion resistance and good thermal properties. However graphite plates can be difficult and expensive to manufacture within the necessary tolerances, furthermore they can in some cases have problems with low mechanical strength and high porosity. The latter is suspected to result in faster performance degradation of the fuel cell stack.

Because of the above mentioned problems it is relevant to do a survey of the current available plate materials for HTPEM fuel cell stacks. In the figure below a framework for material selection is presented. As it is seen two overall categories have been investigated; composite plates and metal plates. Composite plates are typically a combination of graphite and a polymer binder, but in some cases other materials can be added such as metal powder.

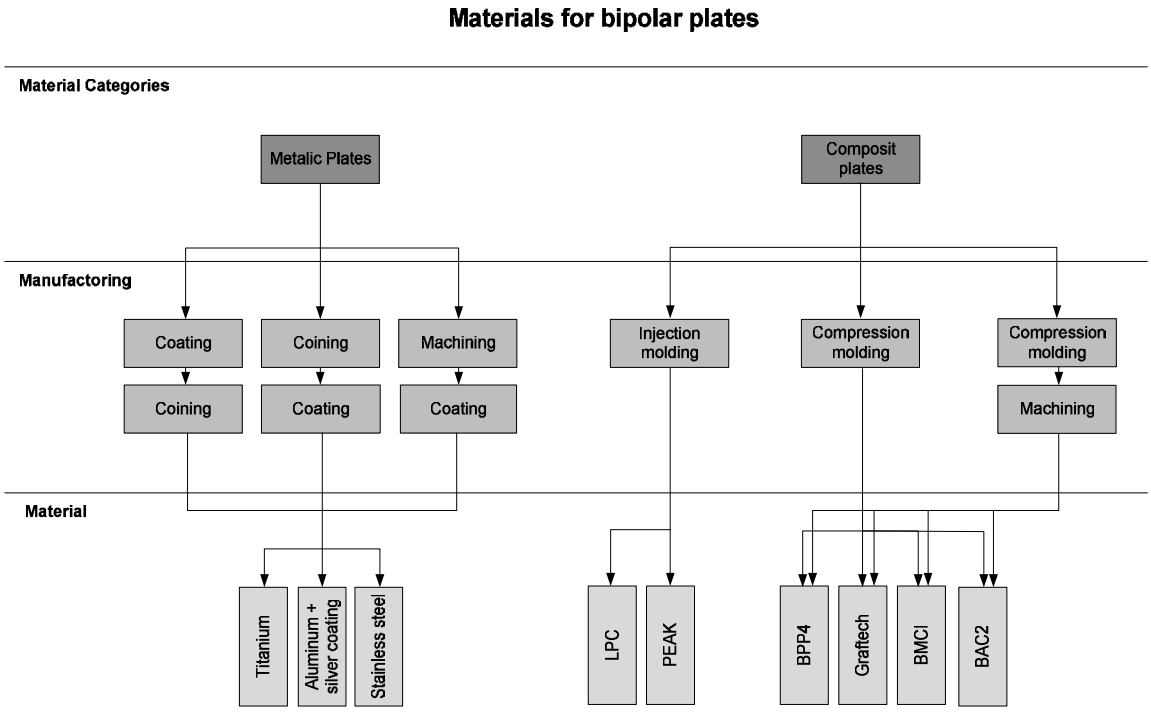

As mentioned above bipolar plate materials, need to excel with respect certain material properties. The reason for this is the fuel cell operating conditions which are defined below:

- Temperature: -20C to 180C
- Current densities: up to 2 A/cm2
- Humidity: High
- Chemical and acid compatibility:
    - High concentration of phosphoric acid
    - Coolant: Oil, Ester or Alcohol based

As it is seen these conditions are quit harsh, thus finding suitable plate material is challenging.

METAL PLATES

While metals generally are good engineering materials and are manufacturable by many different and effective methods, they typically suffer from corrosion problems. Especially in fuel cell environments, it has proven difficult to find long lasting metals, alloys, coating or combinations hereof. The typical issue is the combination of corrosive chemicals, high electrode potentials and the reducing atmosphere on the anode side and the oxidizing atmosphere on the cathode side. Making it inherently difficult to find protective surfaces for metals or alloys.

METAL PLATES - ALUMINUM WITH SILVER COATING

Aluminum has good thermal and electrical properties; furthermore it is fairly cheap and easy to machine or shape in e.g. a coining process. However a major drawback of aluminum is that it corrodes very easy in the harsh fuel cell environment, thus aluminum needs a coating in order to withstand the conditions in a HTPEM fuel cell. Coating with a silver layer could possibly protect the aluminum.

Besides from the coating process the metal plates needs to be shaped, either by a coining process or a machining process. Coining can possibly be performed before or after the coating process, whether the coating is done before or after can influence tolerances and costs.

If a coining process is used this can offer low costs in large/medium scale manufacturing, while machining is cost effective at small numbers.

At Serenergy aluminum plates with silver coating have been tested. The tests were conducted ex-situ in concentrated phosphoric acid. The tests have shown that even with the silver coating the plates have corrosion problems. Thus current coating technology needs further development.

METAL PLATES - BORIT

The Belgian company Borit offers production of bipolar plates in different metallic materials, e.g. stainless steel, aluminum, titanium.

More information on Borit can be found at: http://www.borit.be/Flow-Plates.html

The authors of this report have not found, or performed any tests of Borit's materials. Thus whether their technology is ready for the HTPEM technology is unknown.

THERMOSET COMPOSIT MATERIALS

A thermosetting plastic is polymer material that irreversibly cures. The cure may be done through heat, generally above 200 °C, or through a chemical reaction like the two-part epoxy.

Thermoset materials are usually liquid or formable prior to curing and designed to be molded into their final form. The following curing process transforms the resin into a plastic or rubber by a cross-linking process.

A Thermoset material mixed with graphite in the correct ratio can be used as bipolar plate molding compound.

The compound is typically granulate, dosed into a open mould, whereafter an upper part of the mould closes the mold and compresses at high pressure and temperature +200 C typically. This process is more difficult to control than that of e.g. injection molding, since both dosing, spreading of the material and time and pressure shall be controlled. However it the only really used process so far for graphite based HTPEM bipolar plates.

Typically thermo sets has a higher temperature resistant than thermoplastics.

COMPOSIT PLATES - BPP4

Sigracet - BPP4 is a thermoset polymer compound produced by SGL Carbon Groupe. This is the plate material typically used for Serenergys fuel cell stacks. The material consists of a phenolic polymer binder and graphite. The material is compression molded to form the plates for Serenergys stacks.

This material has successfully been used at Serenergy, however the material may have problems with respect to porosity.

More information on Sigracet – BPP4 can be found at:
http://www.sglgroup.com/cms/international/products/product-groups/eg/sigracet-bipolar-plates/index.html?__locale=en, and in the attached data sheet.

COMPOSIT PLATES – BMCI

The termoset polymer BMC 955 from Bulk Molding Compounds, inc. is also interesting. The polymer has similar characteristics as BPP4 with respect to electrical and thermal conductivity. However this material may have better characteristics with respect to porosity and mechanical strength, if compared to e.g. Sigracet BPP 4.

BMC 955 is interesting to test in future work.

More information in the attached datasheet

COMPOSIT PLATES – BAC2

Another termoset polymer is Elektrophen EP1109 from Bac2. EP1109 has a little low electrical conductivity than BMC 955 and BPP 4. The main advantages with this product are however, that it is easier to mold, according to the manufacturer.

More information about this material can be found at: http://bac2.co.uk/bipolar-plates, and in the attached datasheet.

COMPOSIT PLATES - GRAFTECH

Graftech's Grafcell components are unique because a natural graphite filler is used, compared with the synthetic fillers used in BPP 4 and BMC 955. Grafcell has very high inplane electrical and thermal conductivity, however though-plane the same properties are a little lower than BPP4 and BMC955.

Grafcell is quite expensive, though the above mentioned features make this material interesting for bipolar plates.

For more information see : http://www.graftechaet.com/GRAFCELL/GRAFCELL-Products/Flow-Field-Plates-(FFP).aspx, and the attached datasheet.

THERMOPLASTIC COMPOSIT MATERIALS

The principle of injection molding of plastic parts are widely used in the production industry. The main advantage in this process is the low cycle time and high consistency of the parts produced.

Injection molding of plastics are done with thermoplastics. Thermoplastics are elastic and flexible above a glass transition temperature Tg, specific for each one, in contrast to the sharp melting point of a pure crystalline substance. Thermoplastic polymers differ from thermosetting polymers in that they can be remelted and remolded.

Thermo plastic composite materials are interesting to examine due to the prospects of the relative fast and cheap production process it poses. Although these advantages are obvious and appealing. It has so far only been possible to produce thermoplastic composite bipolar plates for low temperature PEM fuel cells. Reason for this it the difficulty in finding the right compound for the challenging job. Especially the high demands on temperature stability is, in this context, something which rules many candidates out.

COMPOSIT PLATES – PEEK

PEEK is a performance Thermoplastic. It is an expensive but very stable and high performance plastic. It may be mixed with graphite powder to form an injection moldable compound. Potential draw back is its relative high melting point, and high viscosity, which may make it difficult to use in standard injection molding machines.

COMPOSIT PLATES – LPC

Another thermoplastic is LPC, this material is also possible to injection mold. The manufacturer Ticona. Updates can be found at: http://www.ticona.com/vectra

LCP is cheaper than e.x. PEEK and further has the advantage of a low viscosity during the injection molding process. This may in turn also be beneficial to produce bipolar plates with low porosity.

COMPARISON

Properties like electrical and thermal conductivity are important parameters for the fuel cell performance. In the table below, these properties are compared for some of the above mentioned materials.

	Electrical Conductivity [S/cm]		Thermal Conductivity [W/mk]	
	In-plane	Through-plane	In-plane	Through-plane
BPP 4	200	41.7	-	20
BMC 955	80	45	46,2	19,2
Grafcell	1429	33	275	5
Aluminum (pure)	≈375000	≈375000	≈230	≈230
Titanium (pure)	≈74000	≈74000	≈20	≈20
Stainless Steel (316)	≈13500	≈13500	≈15	≈15

CONCLUSIONS

In this review we have presented a survey of bipolar plate materials for HTPEM fuel cells. We have discussed two material categories; composites and metals. And their independent advantages with respect to material properties and manufacturing methods.

Finding the right materials can significantly reduce cost, and significantly improve lifetime and performance of fuel cell products, thus future work is important.

Future work will include ex-situ and in in-situ tests of plate-materials. This is currently planned at Serenergy, and at Serenergy's partners.

Fuel Cell Components

®SIGRACET - BPP

Bipolar Plate - BBP 4 (Phenolic Resin)

Physical Properties (Typical Values)
Physikalische Eigenschaften (Typische Werte)

Property	Unit	Value
Bulk Density Rohdichte	lbs/ft³ g/cm³	123 1,97
Flexural Strength Biegefestigkeit	psi N/mm²	5,800 40
Flexural Modulus E-Modul (aus Biegeversuch)	psi N/mm²	$2.0 \cdot 10^{6}$ 14.000
Compressive Strength Druckfestigkeit	psi N/mm²	11,000 76
Thermal Conductivity ⊥ Wärmeleitfähigkeit	btu/ft · h · °F W/m · K	12 20
Coefficient of Thermal Expansion ∥ Wärmeausdehnungskoeffizient	$1/°F \cdot 10^{-6}$ $1/K \cdot 10^{-6}$	1.8 3,2
Electrical Resistivity ∥ Spezifischer elektrischer Widerstand	µΩm	50
Electrical Resistivity ⊥ ■ Spezifischer elektrischer Widerstand	µΩm	240
Electrical Resistance ⊥ ● Elektrischer Widerstand	mΩcm²	5
Permeability Coefficient (Air) ⊥ ◆ Permeabilitätskoeffizient (Luft)	in²/s cm²/s	$0.775 \cdot 10^{-6}$ $5 \cdot 10^{-6}$
Recommended Max. Operating Temperature Empfohlene max. Betriebstemperatur	°F °C	≤ 355 ≤ 180

Addendum: is suitable for both compression molding and injection molding.

⊥ Through plane · Eigenschaft senkrecht zur Plattenebene
∥ In plane · Eigenschaft in der Plattenebene
■ Measured at 1,000 psi compaction pressure · mit 7,0 N/mm² gemessen
● Resistance of a 80 mil standard plate at 145 psi compaction pressure between two sheets of GDL (typical compaction pressure in an FC stack)
Durchgangswiderstand einer 2,0 mm Standardplatte gemessen mit 1,0 N/mm² Flächenpressung zwischen zwei Lagen GDL (Typische Flächenpressung in einem FC Stack)
◆ Measured at 77 °F using a vacuum experiment according to DIN 51935 and a 80 mil standard plate
Gemessen mit einer 2,0 mm Standardplatte bei 25 °C und 1 bar Druckdifferenz gemäß DIN 51935

DS FC 003 - BPP BBP 4 - Rev01

09 2004/1.5 3NÄ Printed in Germany

SGL CARBON GROUP

Fuel Cell Components

www.sglcarbon.com

Typical Data

BMC 955

Phenolic
Bipolar Plate Material

COMPRESSION MOLDING GRADE

Product Introduction

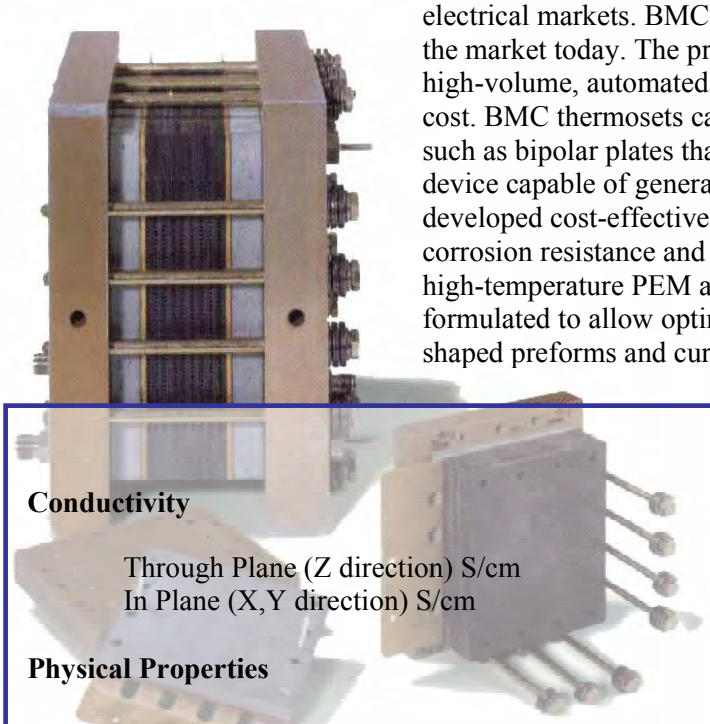

Bulk Molding Compounds, Inc. is the largest manufacturer of thermoset bulk molding compounds in North America, serving the automotive, appliance, and electrical markets. BMC thermosets are the most cost-effective plastic products on the market today. The process of manufacturing BMC thermosets is geared toward high-volume, automated systems to ensure the highest quality at the lowest possible cost. BMC thermosets can be designed to conduct electricity for use in applications such as bipolar plates that are used in fuel cells. A fuel cell is an electro-chemical device capable of generating electricity from oxygen and hydrogen. BMC has developed cost-effective products for use in bipolar plates having excellent corrosion resistance and enhanced performance at elevated temperatures. For use in high-temperature PEM applications (~ 180°C), BMC 955-17028 has been formulated to allow optimum ease of molding, without breathe cycles, using puck-shaped preforms and cure times only marginally longer than BMC 940 grades.

	BMC 955-17028	Test Method
Conductivity		
Through Plane (Z direction) S/cm	45	Vendor
In Plane (X,Y direction) S/cm	80	Vendor
Physical Properties		
Specific Gravity	1.90	ASTM D792
Mold Shrinkage before postbake, %	0.145	ASTM D955
Tensile Strength, MPa	35	ASTM D638
Tensile Modulus, Gpa	15	ASTM D638
Flexural Strength, MPa	49	ASTM D790
Flexural Modulus, Gpa	13	ASTM D790
Strain at Maximum Load, mm/mm	0.003	ASTM D790
Compressive Strength, through-plane, MPa	75	ASTM D695
Compressive Modulus, through-plane, GPa	0.3	ASTM D695
Compressive Strength, in-plane, MPa	59	ASTM D695
Compressive Modulus, in-plane, GPa	0.5	ASTM D695
Izod Impact, unnotched, J/m	67	ASTM D256
Compressive Creep, 200 psi		ASTM D2990
200 hr @ 180°C, %	TBD	
1000 hr @ 180°C, %	TBD	

Typical Data

BMC 955

Phenolic Bipolar Plate Material

COMPRESSION MOLDING GRADE

		Value	Test Method
Thermal			
DMA-Modulus, Gpa @	50°C	14.3	ASTM D4065
	100°C	13.1	
	150°C	12.1	
	200°C	11.6	
Glass Transition Temp (T_g peak in Tan-Delta), °C			>250
Thermal Expansion, µm/m °C, Through-plane		22	E831
In-plane (25 – 200°C)		5	
(200 – 250°C)		25	

Thermal Conductivity, W/m-K	In-Plane	Through-Plane	E1461-92
25°C	46.2	19.2	
85°C	43.7	18.5	

Diffusivity, cm^2/s			
25°C	0.302	0.125	E1461-92
85°C	0.231	0.098	

Specific Heat, J/g-K,	25°C	0.841
	85°C	1.04

Processing Information	
Cure time	60 – 90 seconds, 2.5 mm
Mold temperature	180ºC
Recommended tonnage	> 40 Mpa
Press close speed	3-4 seconds after material begins flowing

Important Notice:

The information and statements herein are believed to be reliable, but are not to be construed as a warranty or representation for which we assume legal responsibility. Users should undertake sufficient verification and testing to determine the suitability for their own particular purpose of any information or products referred to herein. **NO WARRANTY OF FITNESS FOR A PARTICULAR PURPOSE IS MADE**. Nothing herein is to be taken as permission, inducement or recommendation to practice any patented invention without a license.

Bulk Molding Compounds, Inc.
1600 Powis Court
West Chicago, IL 60185
Telephone: (630) 377-1065
Fax: (630) 377-7395
E-mail: bmc@bulkmolding.com

"The Fastest Growing Material Technology In The World Today."

09/22/08

Indicative Data Sheet

EP1109 for LTPEM & DMFC Bipolar Plates

ElectroPhen®

Conductive Composites for Bipolar Plates

Reduce Fuel Cell Stack Cost; Improve Stack Performance; Optimise Stack Design; Volume Production, Faster

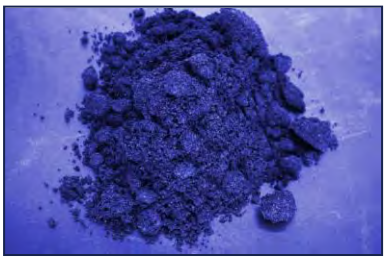

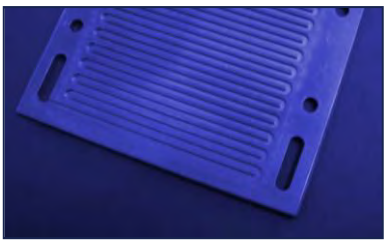

Bac2 has developed ElectroPhen®, a family of conductive composites based on its patented electrically conductive binder that has been optimised for bipolar plates used in LTPEM and DMFC Fuel Cells. The key benefits of ElectroPhen® are its low cost and ease of moulding, making scale-up to mass production rapid, predictable and economical. Bac2's development team can claim many years of experience in new material innovation, and fuel cell development & test, making ElectroPhen® bipolar plates the best choice for any new stack development.

What is ElectroPhen® ?

The key advantage of ElectroPhen® is that it uses Bac2's unique patented electrically conductive polymer as the binder for graphite particles…

- Low-cost raw materials and compression moulding process.
- Infinitely scalable for high volume production.
- No secondary processing required.
- Step-by-step route through evaluation and prototyping to mass production.
- Extensive in-situ fuel cell stack testing has been undertaken.

Property	Value	Units
Density	1.76	g cm^{-3}
Flexural strength	32	MPa
Shore "D" Hardness	71	
In-plane electrical conductivity	130	S/cm
Through-plane conductivity	34	S/cm
Temperature stability	180	^{o}C

In-house preliminary results for EP1109.

The absolute performance of this material is dependent on the form factor of the component moulded. The above results were achieved using a selection of moulded test pieces.

Evaluation:

Bac2 offers blank plates of varying dimensions to enable customers to evaluate the material in their own test facilities. Plates currently available in EP1109 formulation are:

BP1-3 – 300mm x 200mm x 3mm
BP2-1 – 150mm x 150mm x 1mm
BP2-2 – 150mm x 150mm x 2mm
BP2-3 – 150mm x 150mm x 3mm
BP2-4 – 150mm x 150mm x 4mm

Other plate sizes may be available on request.

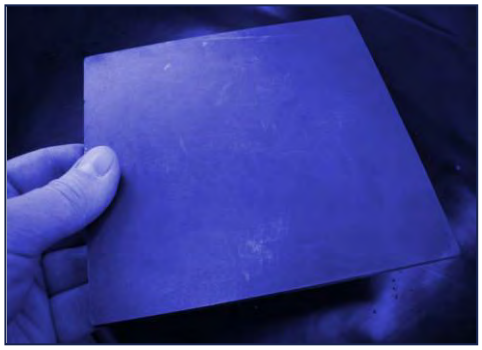

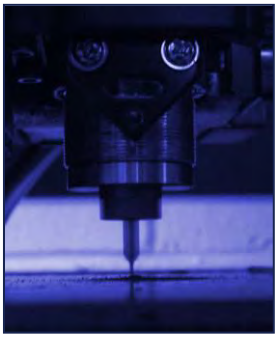

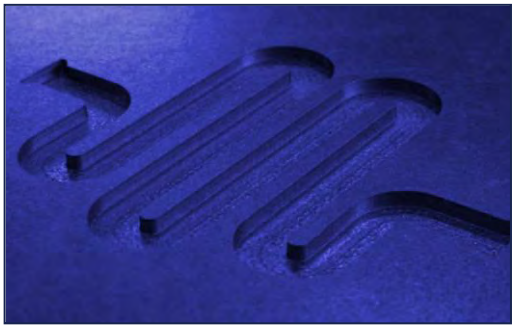

Prototyping:

Bac2 has in-house CNC machining facilities to rapidly provide customers with plates in accordance with their engineering drawings, enabling fully representative stacks to be assembled and tested.

Pilot Production:

Bac2 provides mould tools to its customers' specifications and moulds pilot run plates on its in-house compression mould facilities. Once these are approved and signed off by the customer, scale-up for volume production can commence.

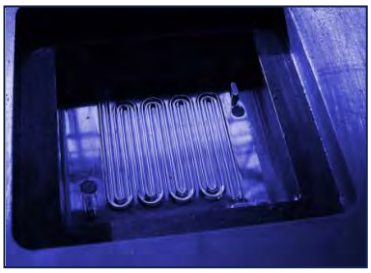

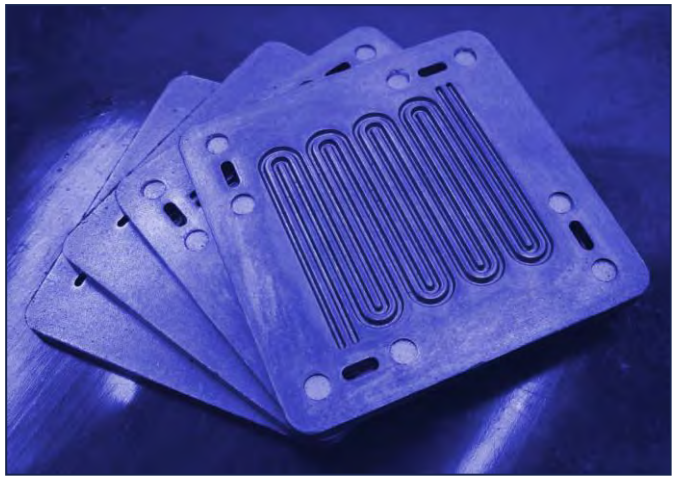

High Volume Production:

Bac2 uses 3rd party military and automotive approved moulding partners that have been audited for their quality systems and approved for mass production of ElectroPhen® bipolar plates. Shipments are made world-wide to customers' assembly facilities.

About Bac2:

Bac2 is a UK-based global supplier of components made from its unique ElectroPhen® family of advanced electrically conductive composites. At its laboratories in Southampton the company continues to develop its patented conductive polymer systems for a growing range of applications.

Bac2 Limited
Millbrook Technology Campus
Southampton SO15 0DJ
United Kingdom
www.bac2.co.uk
enquiries@bac2.co.uk

GRAFCELL®
FUEL CELL COMPONENTS

FFP SERIES

TECHNICAL BULLETIN 425

Manufactured from expanded natural graphite, GRAFCELL® Flow Field Plate (FFP) components retain a continuous graphitic phase. This unique phase continuity, combined with an extremely low contact resistance, provides superior electrical and thermal properties in comparison to both synthetic graphite composite and metallic fuel cell components. The thermal diffusivity of GRAFCELL FFP SERIES products is 8-12 times higher than composite materials and 33 times higher than stainless steel.

GRAFCELL FFP SERIES products have played a critical role in improving fuel cell power density and performance for over 10 years. With over two million kilometers of proven road experience car and bus applications annually, GRAFCELL FFP SERIES continuous phase flow field plates have replaced synthetic graphite as the premier material for PEM fuel cells.

Grade, Dimension and Coating Options

What types of GRAFCELL FFP components are available?

	FFP-100 SERIES	FFP-200 SERIES	FFP-300 SERIES
Fine Feature Formability	Better	Best	Good
Tensile Strength	Best	Better	Good
Minimum Web Thickness	100 µ	200 µ	300 µ
Thickness +/- 0.1 mm (0.004")	0.6-3 mm (0.024 - 0.118")		>3 mm (0.118")
Width +/- 1.0 mm (0.039")	Maximum Width: 254 mm (10")		
Length +/- 1.0 mm (0.039")	Maximum Length: 600 mm (23.62")		
Able to be Machined	Yes	Yes	Yes
Able to be Molded	Yes	Yes	Yes

Typical[1] Properties

What are the performance characteristics of GRAFCELL natural graphite FFP components?

- Nominal Density: 1.5 g/cc
- Thermal Conductivity (x-y): 275 W/m-K
- Thermal Conductivity (z): 5 W/m-K
- Electrical Resistivity (x-y)[2]: 7 µΩm
- Electrical Resistivity (z)[2]: 300 µΩm
- Coefficient of Thermal Expansion (x-y): 1-5 µm/m-K
- Coefficient of Thermal Expansion (z): 10 µm/m-K
- Tensile Strength: 30-50 MPa
- Flexural Strength: 50-70 Mpa
- Permeability (1 atm, 15 psi limit): <1 cc/min
- Tg: 125°C
- Contact Resistance: 8 µΩcm^2
- Thermal Diffusivity: 1.2 cm^2/sec

[1] Properties listed are typical and cannot be used as accept/reject specifications.
[2] ASTM C611. 4-Point Resistivity Test. The resistance of thin perforated flexible graphite at 0.4 MPa between gold platens.

For additional information, contact the GrafTech Sales Office: +1 (800) 253-8003 (Toll-Free in USA), +1 (216) 529-3777 (International), +1 (216) 529-3922 (Fax)

TB425-GC-FFP-TYP.doc Updated: 09/09/2007

GRAFTech International

Appendix 6

Technical report

"Fuel Cell Sealing Concepts"

WP 4.4: Fuel cell sealing concepts

Partner: Serenergy

Date: Feb 2012

Introduction

The stack concept being developed in this project has changed from being an air-cooled design to being a liquid cooled design. This gives advantages many areas but gives an extra challenge for the gasket/sealing concepts.

The liquid cooling is achieved by adding extra plates to the stack between every cell in which the cooling liquid flows. This gives the need for two different types of gaskets; one to seal the liquid plates and one to seal the gas (hydrogen and air) plates. The materials used for these seals could be the same or different. A large amount of time was spent identifying possible gasket materials. These are discussed later in the report.

In the stack environment the gaskets are exposed to a number of harsh environments. High temperature (approximately 170ºC) and pressure, phosphoric acid (released from the fuel cell membranes) and the chosen liquid coolant are the most likely candidates for causing material degradation of the gaskets. The gas gaskets should not come in contact with the cooling liquid so if a material that cannot hold to the liquid coolant but can hold the other parameters is found it could be considered here. The liquid gasket must be quickly degraded by any of the above mentioned as it will come in contact with them all.

This is the first liquid cooled stack designed by Serenergy and therefore the cooling liquid to be used was not yet decided. Due to this, the compatibility of a range of gasket materials is tested in conjunction with a range of cooling liquids.
A number of ex-situ and in-situ tests are completed. The results are presented below.

Table 1 shows a summary of the completed tests and their results. Following this a more detailed description is given of each test for the gasket materials tested.

Table 1: Summary of the completed tests.

Compatibility Test	Acryl	Flour Silicone	RAMP Silicone A (white)	RAMP Silicone B (black)	FKM (various grades)	Confidential liquid side gasket
TEG	Fair	n/a	Moderate	Moderate	Good-Fair	n/a
Paratherm NF	Poor	n/a	Poor	Poor	Good	n/a
DOW CAL 10 (EG w. Additive)	Poor	Good	n/a	n/a	n/a	n/a
Addinol XW15	Good	Good	n/a	n/a	n/a	n/a
Calflo AF	Poor	Good	n/a	n/a	n/a	n/a
MEG	Moderate	Good	n/a	n/a	n/a	n/a
DEG	Moderate	Good	n/a	n/a	n/a	n/a
H3PO4 (80%)	Poor	Poor	Poor	Poor	Good-Poor	n/a
Air (170ºC)	Poor	n/a	n/a	n/a	n/a	n/a
Operation in a stack	yes	no	no	no	yes	yes

Acryl tests

→ Cooling liquids

A piece of the acryl gaskets were tested in a number of different cooling liquids. TEG was tested in one round of testing and the other six liquids were tested in a separate round of testing. The results of the test with TEG are shown in Figure 1. After 20 hours at elevated temperatures the acryl was drying out and getting brittle when tested with TEG vapour and starting to dissolve when exposed to TEG liquid. The dark brown colour of the TEG in Figure 1 (b) is due to oxidation of the TEG which occurred so quickly because the container was open during testing.

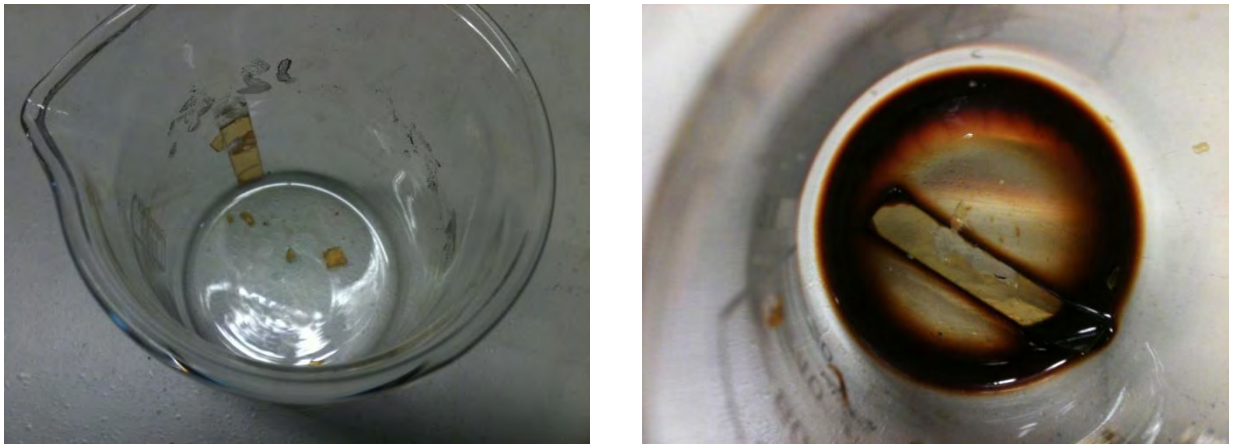

(a) Arcrly in TEG vapour. 200ºC, 20hr (b) Acryl in TEG liquid. 200ºC, 20hr

Figure 1: Results of acryl gasket material compatibility tests with liquid coolant, TEG.

Compatibility with the remaining cooling liquids was tested in bottles as illustrated below at 165ºC for 24 hours.

Filling level at the beginning of the test

The acryl began the test being transparent.

Table 2: Appearance change seen from submersing acryl in various cooling liquids at 165ºC for 24 hours.

Cooling Liquid	End appearance
MEG	Slightly yellow
DEG	Slightly yellow
DOWCAL 10	Opaque
Paratherm	Not tested. Known to be uncompatible.
Addinol XW15	No change
Calflo	Yellow

→ Air (170ºC)

To test the effect of heat on an acryl gasket one was mounted on a ~10 mm aluminum plate and placed in an oven at 240ºC for 2 hours. This is above the temperature that will be experienced in the fuel cell but was chosen because this is the temperature that the material is rated to.

When the block was removed from the oven the gasket had turned light brown (was initially transparent), and was less sticky. As the gasket cooled small cracks appeared as can be seen in Figure 2. Pressing on the gasket with a finger caused new cracks showing how brittle the gasket was getting.

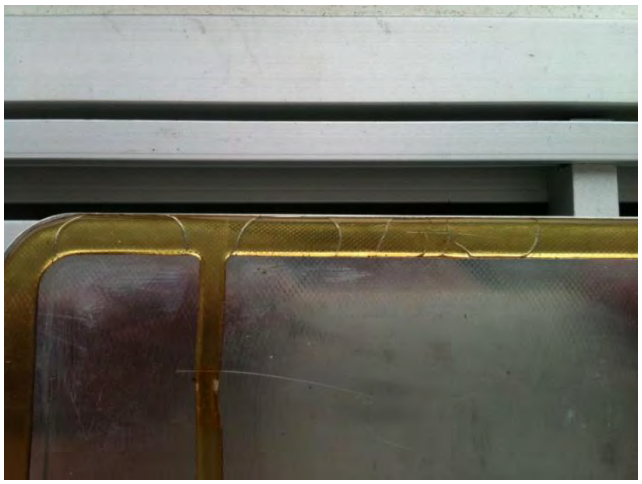

Figure 2: Acryl gasket after 2 hours in a oven at 240ºC.

→ In-situ test

A three cell stack test was performed with acryl gaskets used for both gas and liquid seals. The test lasted 1500 hours before beginning to leak cooling liquid and stopping.

At completion of the test the stack was disassembled. It was seen that the gasket was brittle, especially at the coolant in/outlet. The gasket looked dissolved in some areas and hardened in others.

Figure 3: Acryl gaskets after 1500hr of operation.

TEG was used as the cooling liquid in this test. It is known to polimerize when exposed to air and hot temperatures. It is believed that the test lasted so long because TEG polimerized in the cracks in the gasket on the liquid side. Without this effect it is believed that the acryl gaskets would have begun leaking earlier in the test.

Fluor silicone

→ Cooling liquids

Compatibility with the following cooling liquids was tested in bottles as illustrated below at 165ºC for 24 hours.

Filling level at the beginning of the test

The fluor silicone began the test being transparent.

Table 3: Appearance change seen from submersing fluor silicone in various cooling liquids at 165ºC for 24 hours.

Cooling Liquid	End appearance
MEG	No change
DEG	No change
DOWCAL 10	No change
Paratherm	No change
Addinol XW15	No change
Calflo	No change

→ Phosphoric acid

A sample was placed in a closed container with 80% phosphoric acid in an oven at 100ºC for 21 days.

At the end of the test significant loss of material was visible. Initially the sample was transparent and become more and more opaque as the test progressed.

Due to the poor performance in phosphoric acid testing with fluor silicone was discontinued.

Silicone A

Two silicone based samples were received from a supplier who thought the materials would be suitable but would not divulge their chemical make-up. They are therefore referred to in this report as silicone A and B.

→ Cooling liquids & phosphoric acid

The samples were submerged in TEG, phosphoric acid and paratherm in closed containers as indicated in Figure 4 (a). The containers were placed in an oven at 160ºC for 3 weeks and were inspected each week. The samples were removed from the liquid after completion of the tests and the results are shown in Figure 4 (b). The sample on the left is TEG which shows some discolouration. The sample in the middle was in phosphoric acid and has caused severe discolouration and material degradation. The sample on the right is paratherm which has also caused discolouration and material degradation.

(a) Test start. All liquids and samples had a similar appearance.

(b) Test completion.

Figure 4: Results of silicone A being heated to 160ºC in TEG, phosphoric acid and paratherm for 3 weeks.

Both gaskets will be in contact with phosphoric acid in the stack. Given the poor results of the first tests with phosphoric acid no further tests were carried out.

Silicone B

Two silicone based samples were received from a supplier who thought the materials would be suitable but would not divulge their chemical make-up. They are therefore referred to in this report as silicone A and B.

→ Cooling liquids & phosphoric acid

The samples were submerged in TEG, phosphoric acid and paratherm in closed containers as indicated in Figure 5 (a). The containers were placed in an oven at 160ºC for 3 weeks and were inspected each week. The samples were removed from the liquid after completion of the tests and the results are shown in Figure 5 (b). The sample on the left is paratherm which shows little change. The initial sample was in three pieces as shown here. The sample in the middle was in phosphoric acid and has caused severe material degradation. The sample on the right is TEG which shows little change.

(b) Test start. All liquids and samples had a similar appearance.

(b) Test completion.

Figure 5: Results of silicone A being heated to 160ºC in TEG, phosphoric acid and paratherm for 3 weeks.

Both gaskets will be in contact with phosphoric acid in the stack. Given the poor results of the first tests with phosphoric acid no further tests were carried out.

Fluoroelastomer (FKM)

Various FKM compounds from different suppliers have been tested and have shown promising results. This type of gasket is primarily being tested for use on the gas side of the cells.

→ Cooling liquids

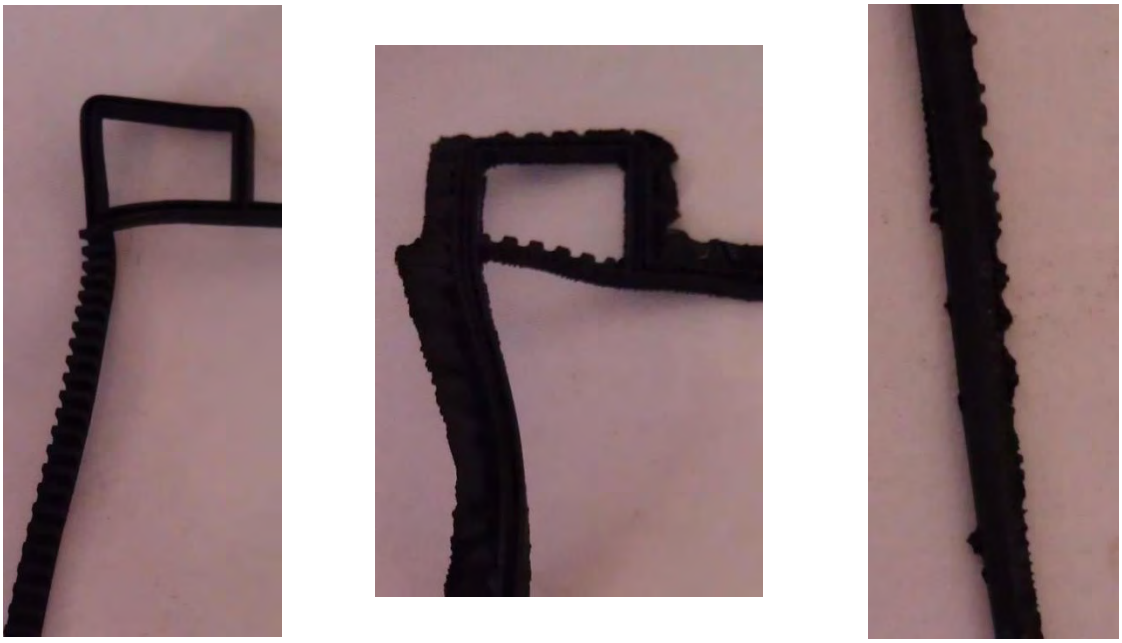

(a) (b) (c)

Figure 6: Results for 3 types of FKM after 14 days in phosphoric acid at 160°C.

Supplier (a) was found to be the most resistant to phosphoric acid. After completion of the test the surface of the gasket was found to be dry but no other obvious degradation was seen.

Supplier (b) gaskets were drier and more porous after the test. Little force was needed to break the gaskets.

Supplier (c) gaskets were also dry and brittle after the test. Pieces of the gasket material were found floating in the test beaker.

→ Phosphoric acid

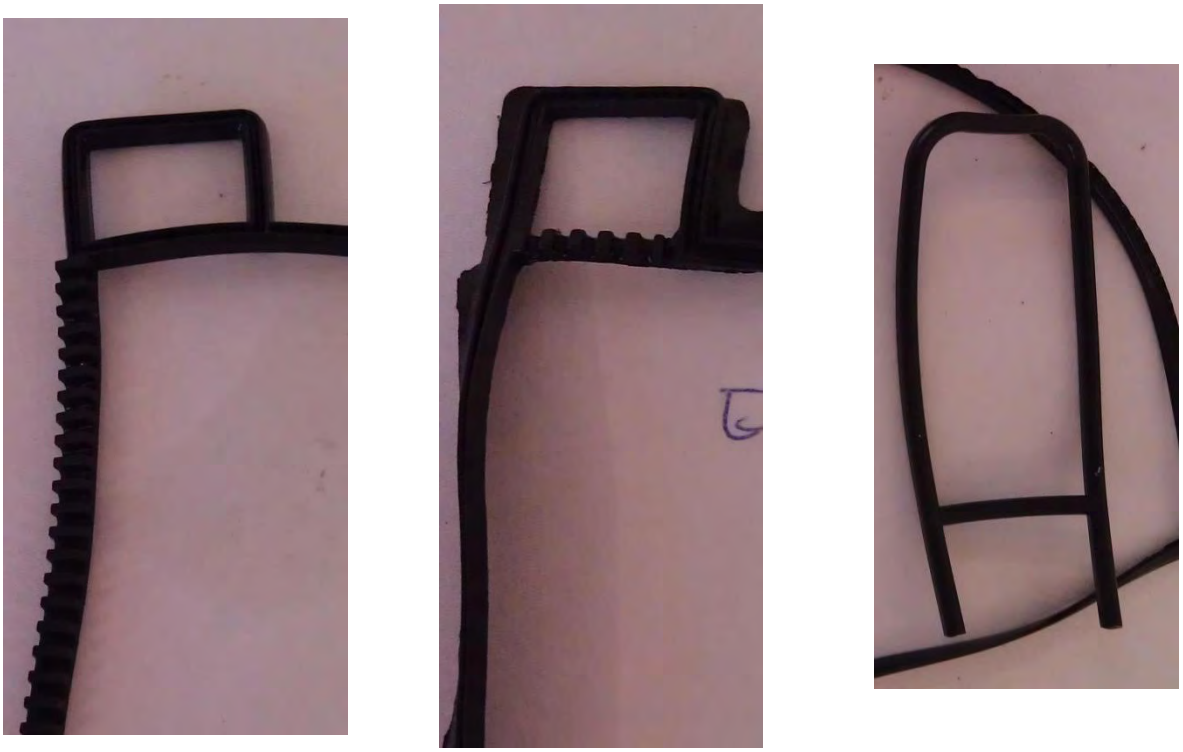

(a) (b) (c)

Figure 7: Results for 3 types of FKM after 14 days in TEG at 160°C.

Supplier (a) and (c) gaskets had no obvious change after the test, where as supplier (b) gaskets were easy to break when pulled and chunks of the gasket material were visible along the gaskets; they were no longer smooth.

→ Operation in a stack

A FKM gasket is currently being tested in a long term stack test. The stack has run for 500hr and is still tight.

Confidential liquid side gasket

→ Operation in a stack

A new gasket material for the liquid side of the cell is currently being tested in a long term stack test. The stack has run for 500hr and is still tight.

Due to the number of hours spent finding and testing gasket materials we do not wish to reveal the name of this promising, new, innovative solution.

Conclusion

The environment that the gasket material is exposed to in the fuel cell is harsh and requires a special material composition to continue functioning through the fuel cell's lifetime. After a long search promising gasket materials have been identified both on the gas and liquid sides of the cell and testing continues with them.

Current activities with gasket materials revolve around long term testing in a stack and improvement of production procedures with possible suppliers. Producing gaskets within our tolerances, with smooth surfaces has proven to be a challenge but the scrap rate on the received deliveries is falling so we believe we are nearing a quality solution.

Appendix 7

Technical report

"Charge and discharge algorithm"

HI-EPS

Charge and discharge algorithm

Contents

Figures

Revision history

Revision	Author	Comment
0.1	Karl Vestin	Prepared for review

Introduction

This document describes the charge and discharge algorithm for the HI-EPS battery/fuel cell pack. The intended audience is developed and designers working at Lithium balance A/S and Serenergy. The purpose is to describe an algorithm for controlling the fuel cell in order to utilize the fuel cell capacity to maximize the range of the vehicle while maintaining the battery within its voltage and current tolerances.

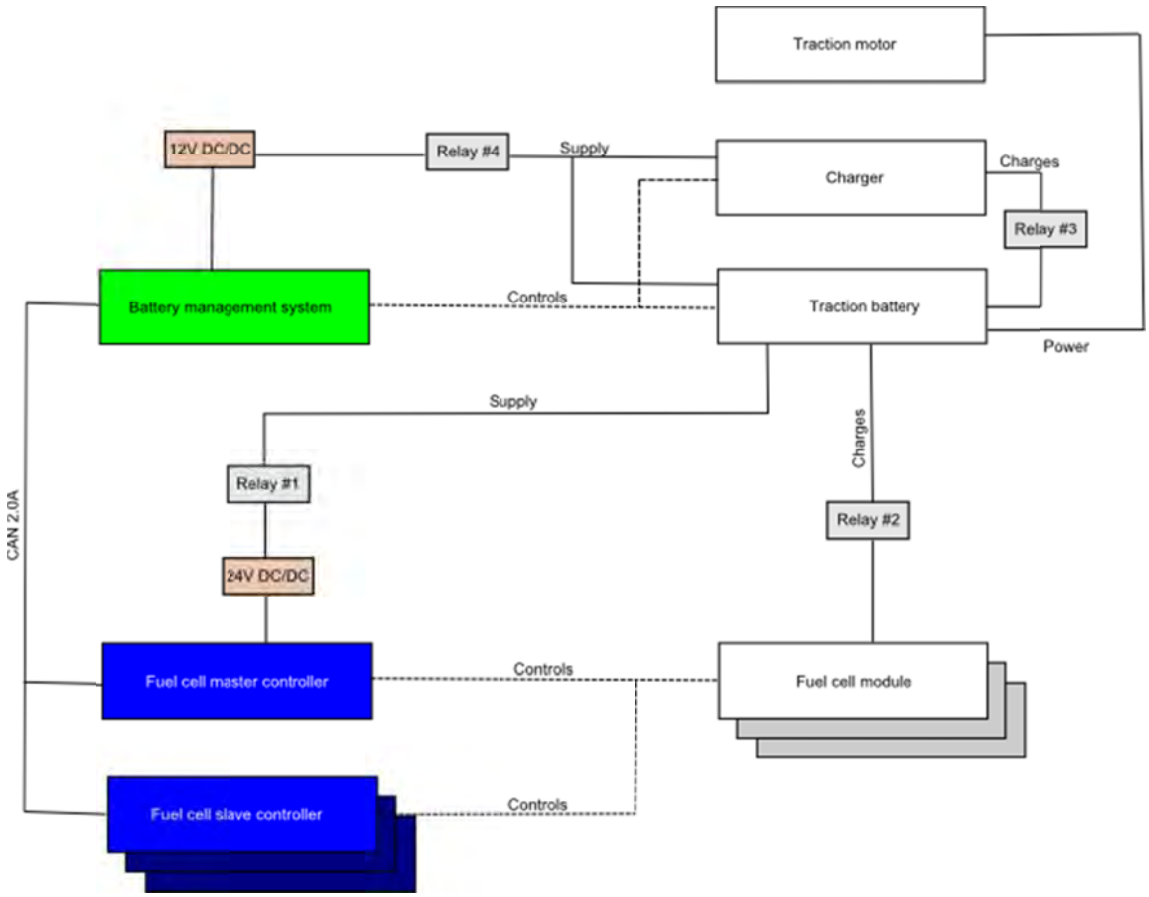

Figure 1: System overview

Conditions for charge

The fundamental problem for charging the HI-EPS pack can be summarized as follows:

1) The battery pack may never be over charged
2) While warming up the fuel cell consumes energy rather than producing it.
3) The fuel cell has a ramp down time from full operation during which the fuel cell must be able to deliver power into the battery.

To fulfill all these requirements the algorithm needs to take both fuel cell performance and battery capacity into account.

The conditions for charge using the range extender are defined as follows:

- All cell voltages are lower than 100mV below maximum.
- There is sufficient free capacity in the pack to allow 10 minutes of full fuel cell charging.
- Battery temperatures are at least 10 degrees within operational range (based on cell type).
- No errors in the BMS that prevent regular charge.
- Ignition key on.
- Sufficient capacity in pack to heat up fuel cells (estimated at 20% SOC)
- (Optional) The user has pressed the “Range Extension” button.

Operation

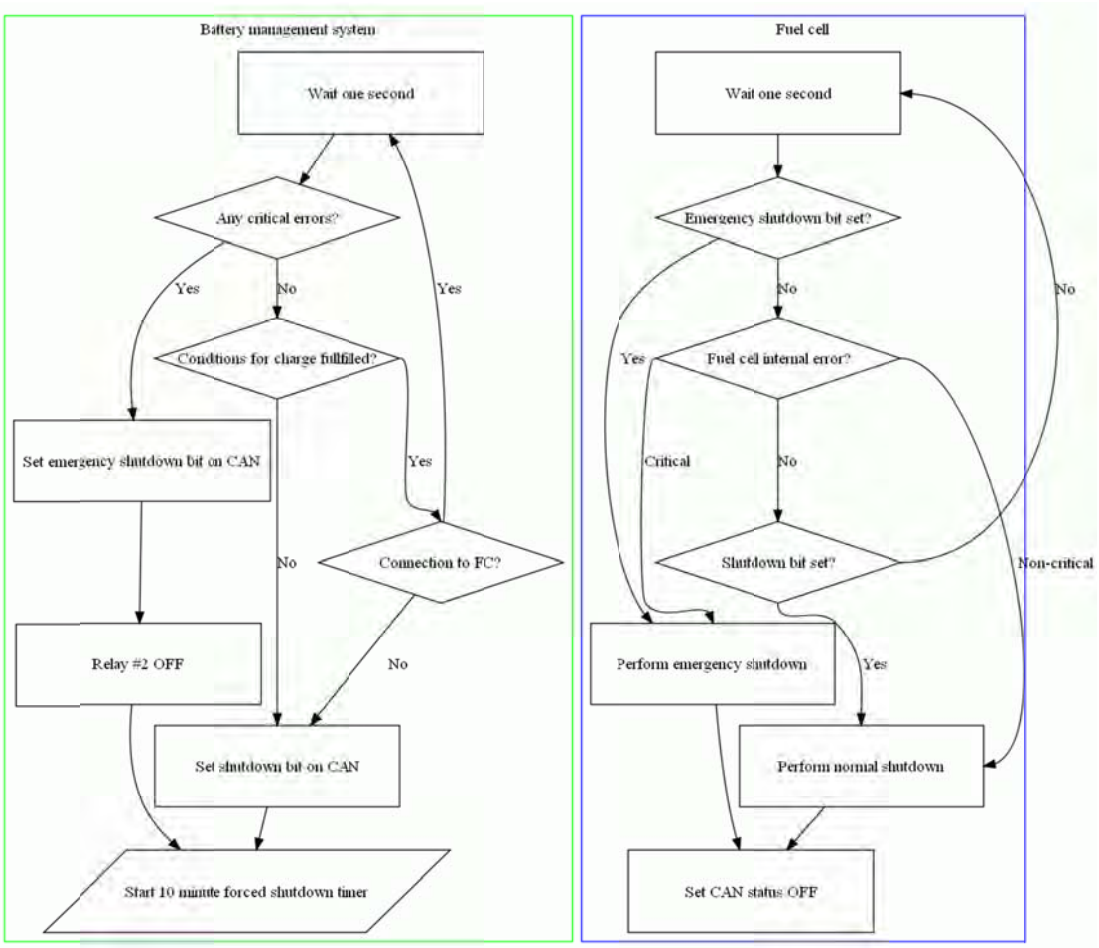

Figure 2: Operational sequence

Figure 2 shows the control flow diagram in operation. For further details see the system design document.

As shown in figure 2 the HI-EPS pack will support two shut down modes;

1) Normal shutdown. During this process the fuel cell is allowed to deliver power to the battery. This process must not damage the fuel cell or the battery.
2) Emergency shutdown. During this process the fuel cell cannot deliver power to the battery, but must shut down safely without any further current being delivered. Repairable damage to the fuel cell I acceptable in this case, but not danger to passengers in the vehicle.

Pack simulations

The simulations displayed in the figures below shows the charge and discharge algorithm with some sample pack and fuel cell configurations. The included Excel sheet is intended to help dimension pack and fuel cell to reach a required range with a given vehicle.

The samples below show cases how some different pack <-> fuel cell configurations can lead to varying vehicle ranges and the serious impact of even small changes in the warm up time of the fuel cell.

The included Excel sheets provides a simple tool for dimensioning pack and fuel cell towards a specific range target.

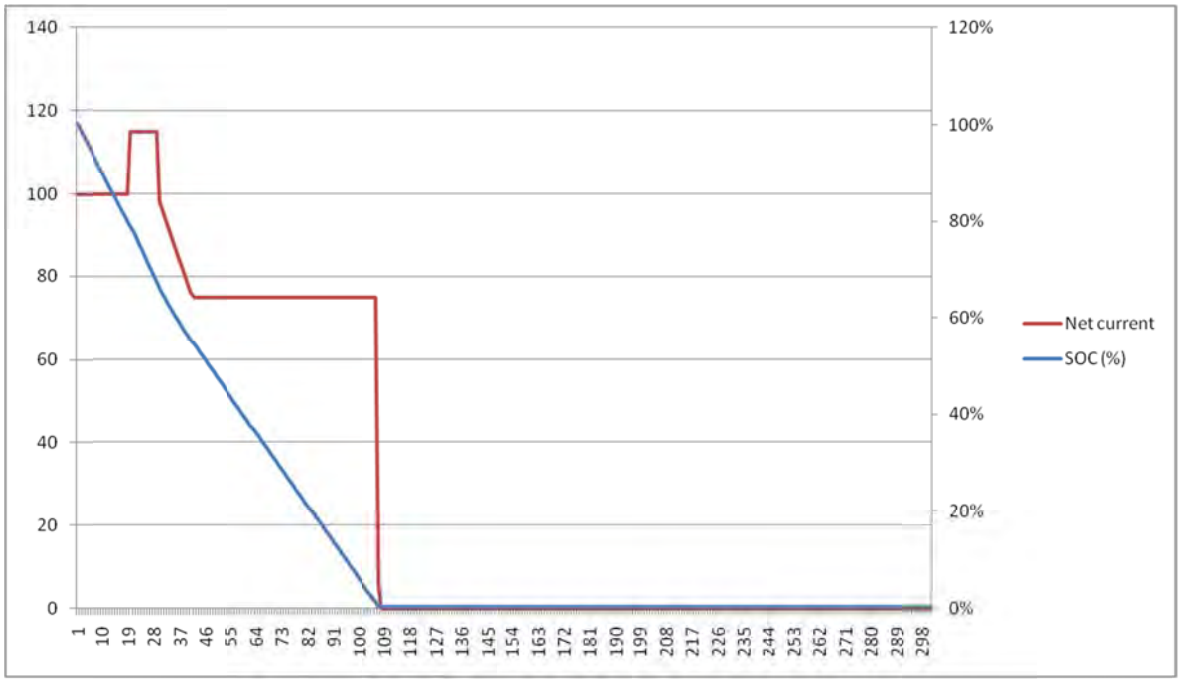

Figure 3: 150 Ah battery pack. 25A fuel cell with 10 minutes start up time

Simulation.xlsx

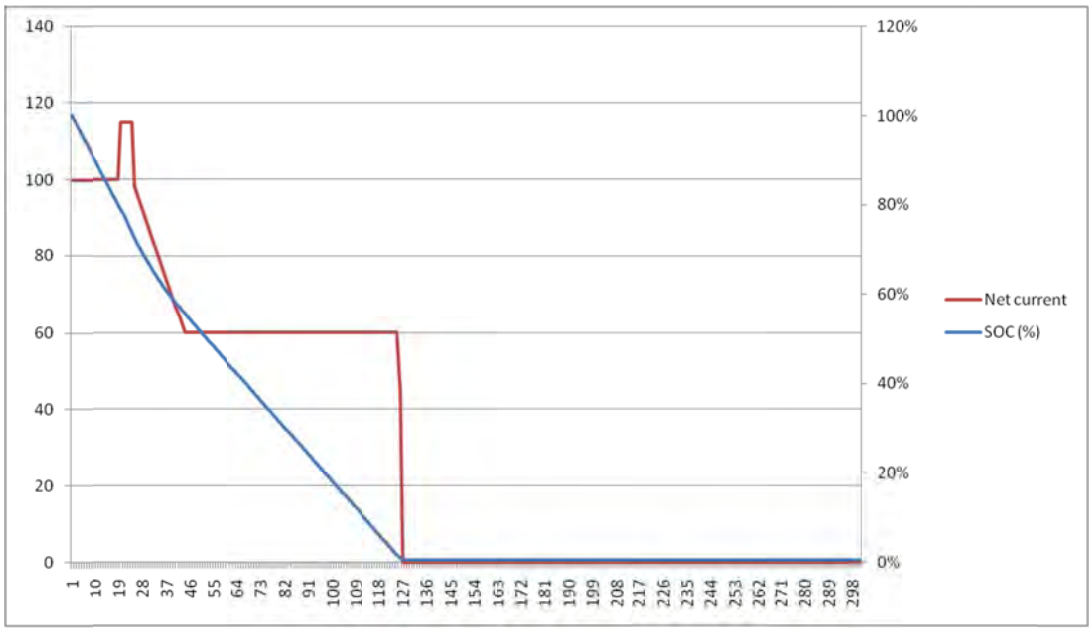

Figure 4: 150 Ah battery pack. 40A fuel cell with 5 minutes warm up time

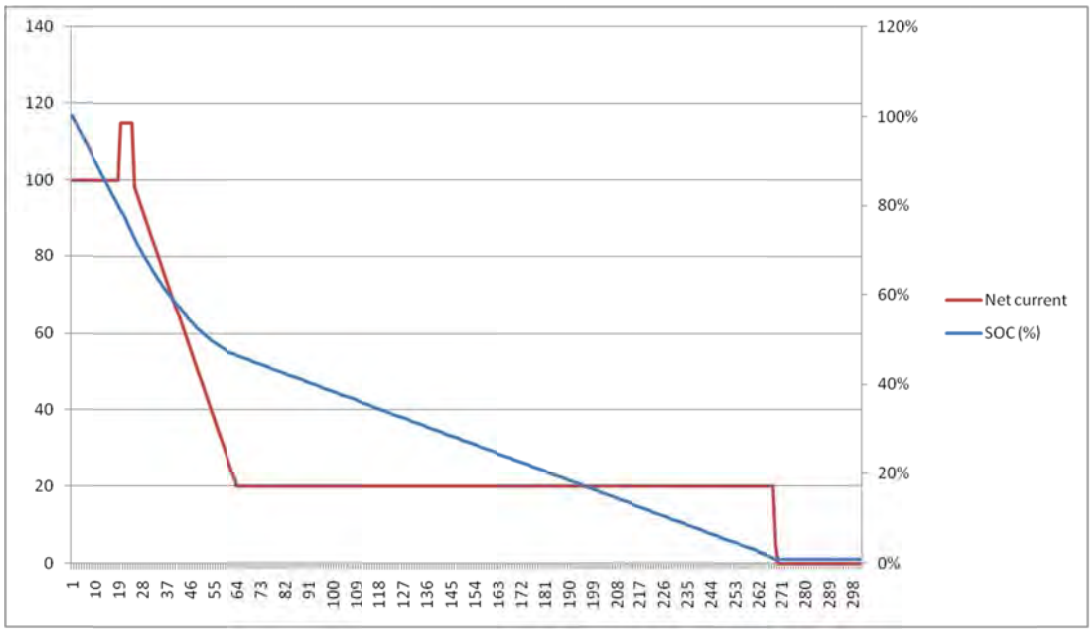

Figure 5: 150 Ah battery pack. 80 A fuel cell with 5 minutes start up time

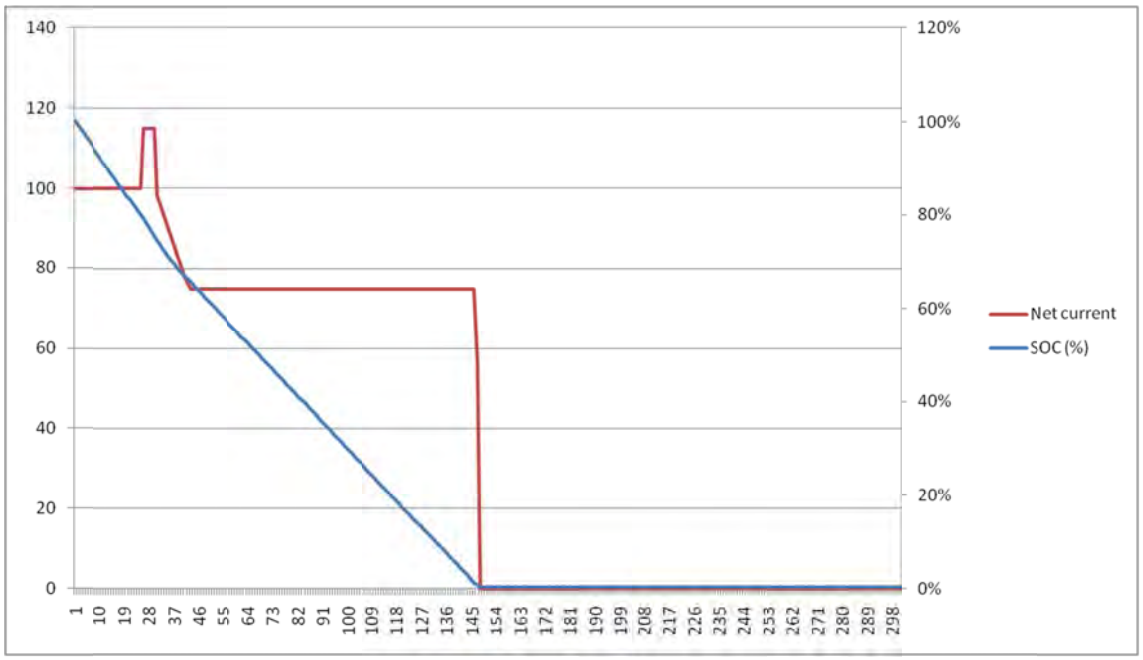

Figure 6: 200 Ah battery pack. 25A fuel cell with 5 minutes warm up time

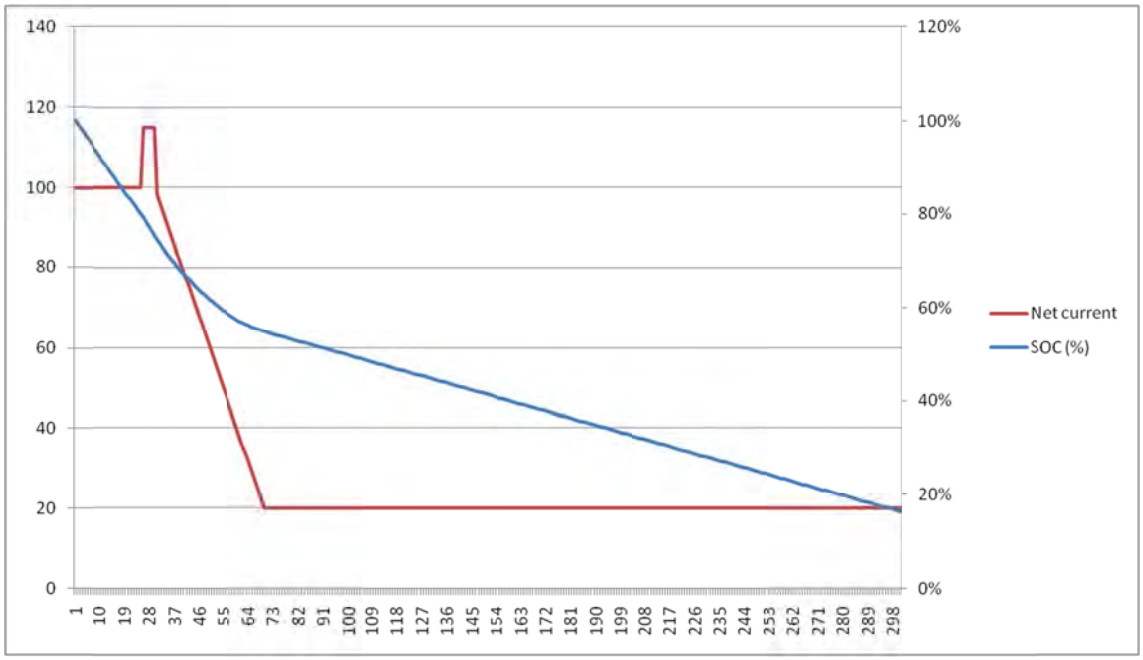

Figure 7: 200Ah battery pack. 80A fuel cell with 5 minutes warm up time

Conclusions

In order to drive a heavy vehicle (such as a Fiat Scudo) 600km using a 150 Ah pack the simulation sheet indicates that the range extender must be able to deliver 65A over the 300V battery pack (i.e. 19.5kW worth of fuel cell) with a tank large enough for approximately 8h.

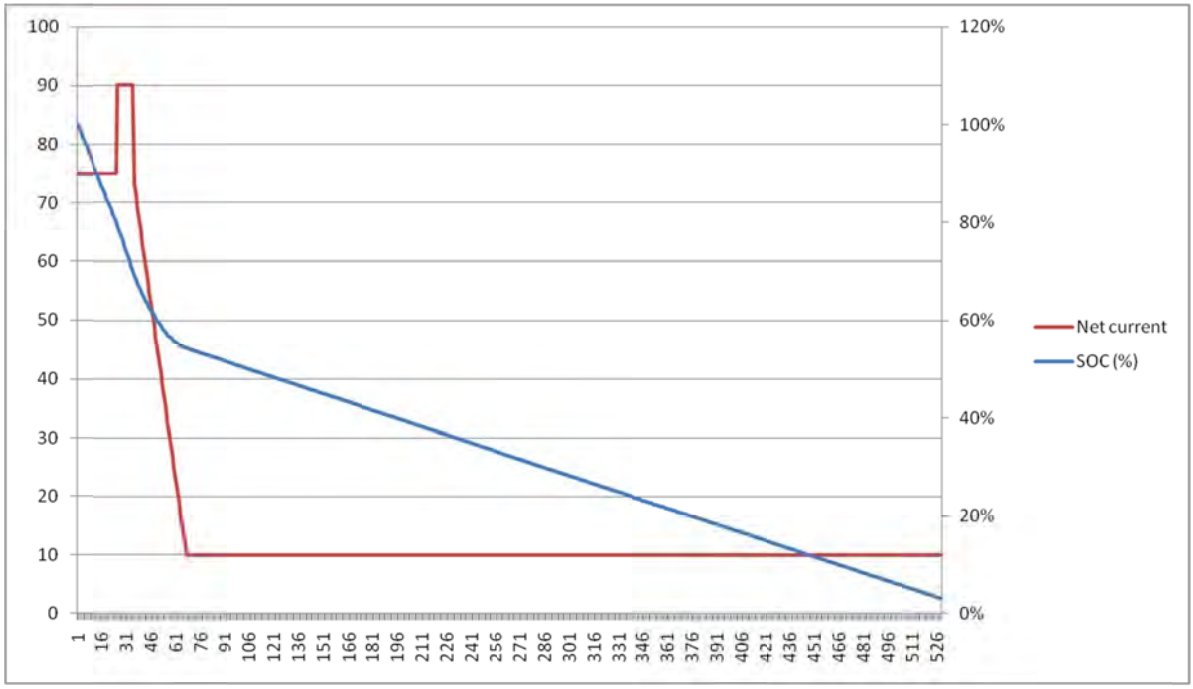

Figure 8: 600km drive of a heavy road vehicle

Simulation parameters

- Average current consumption 75A (this is approximately what is observed on the Scudo, and fits well with the measured 120km range of the vehicle without range extender)
- 150Ah battery pack
- Fuel cell warm up time: 10 minutes
- Fuel cell warm up current: 15A

Appendix 8

Power Point presentation

"The n-BMS – The Networked Battery Management System"

The *n*-BMS

The Networked Battery Management System

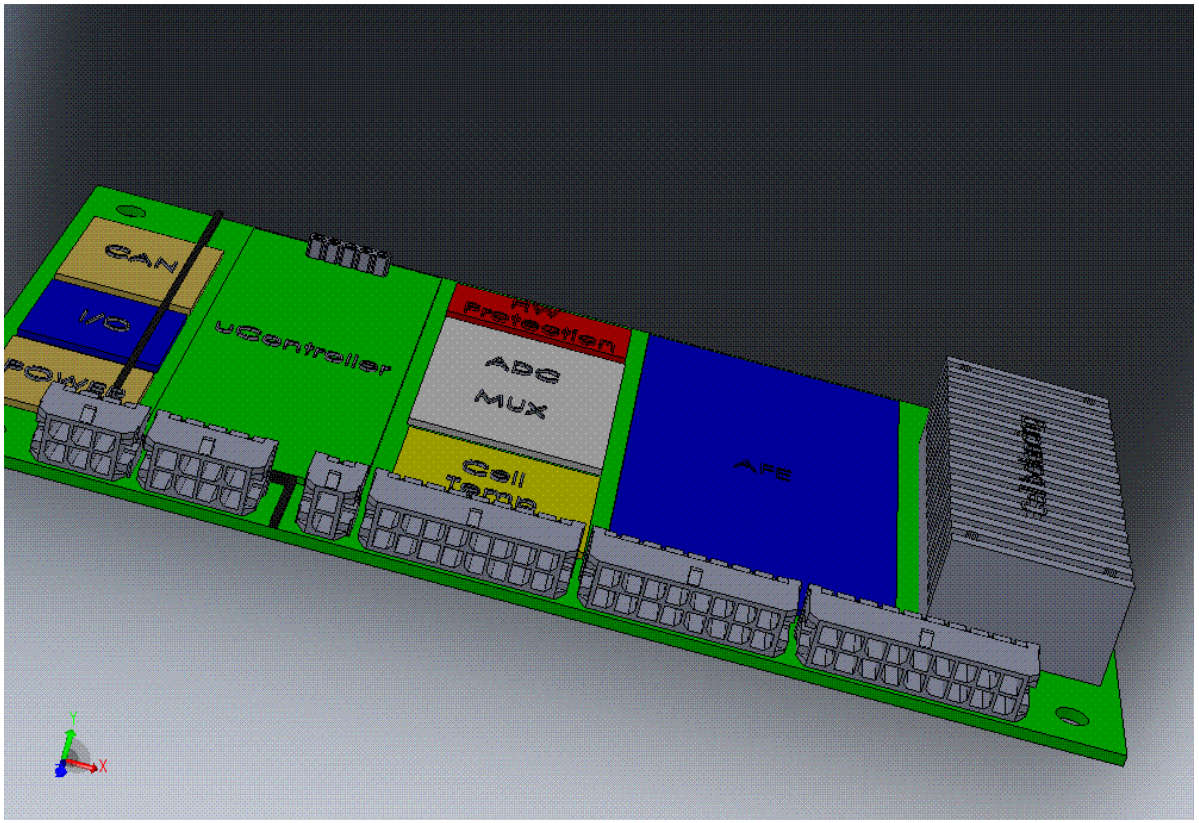

Automotive grade battery management

LiTHIUM BALANCE
BATTERY MANAGEMENT SYSTEMS

Battery management, explained

The collection of features and functions that enable the safe and reliable operation of battery cells or packs

- All battery types require some degree of management to optimise performance
- The larger the pack, the greater the need for management
- Lithium Ion batteries are relatively expensive and do not tolerate abuse – management is essential
- Lithium Ion batteries are inherently unsafe unless properly managed

BMS core features

PROTECTION

Safety and reliability
(Secure your investment)

Protection against:
Overcharging
Deep discharge
Overloading
Short-circuit
High/low Temperature
Isolation monitoring

PERFORMANCE

Raise capacity,
shorten charge time,
lengthen life

Cell balancing
Discharge/regen. rate control (power prediction)
Optimised charge algorithms

MANAGEMENT

Application interface and
diagnostics

Control outputs to switches or other systems
PC interface
Can-bus interface
History log

The basics

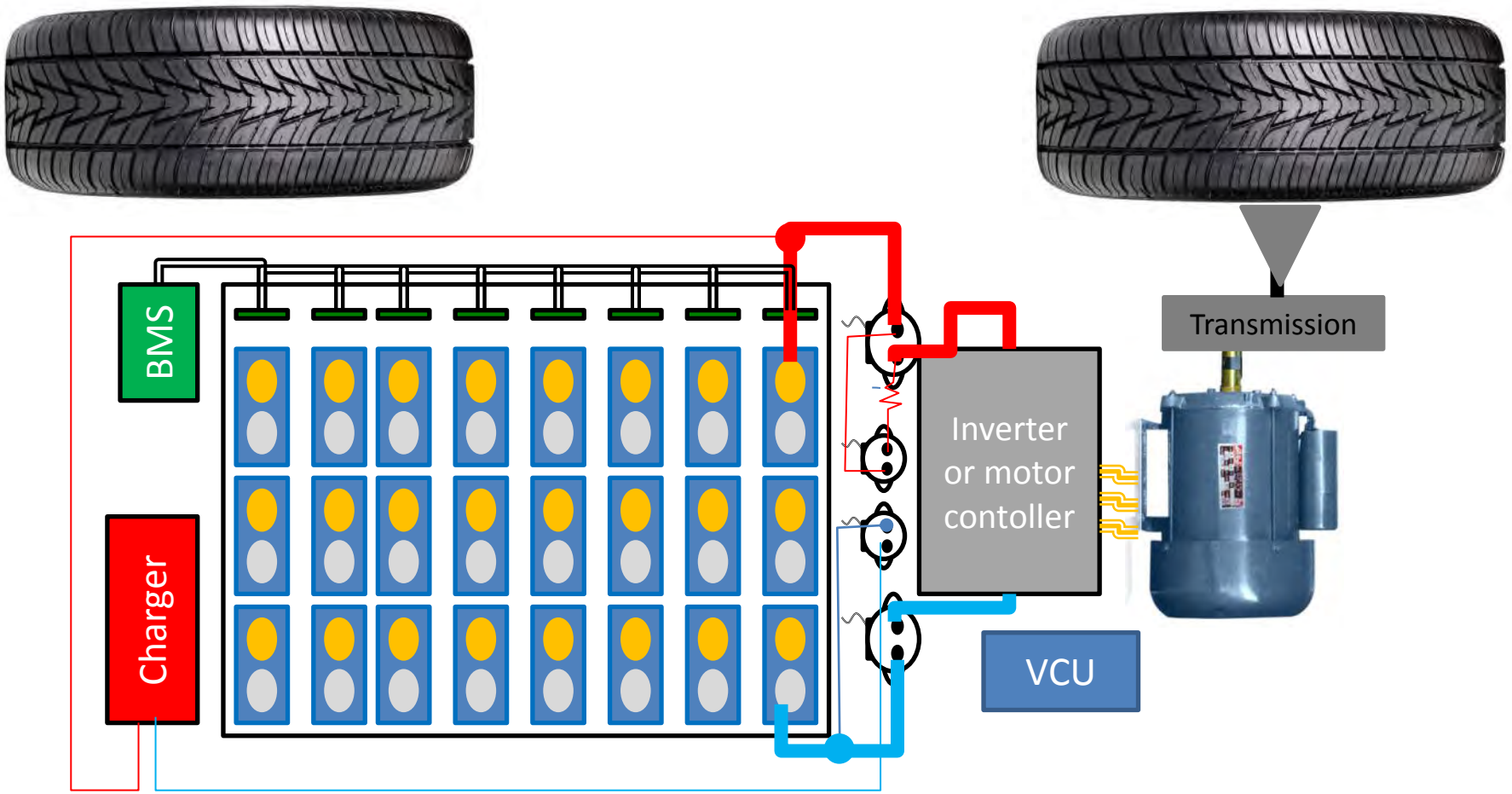

LiTHIUM BALANCE
BATTERY MANAGEMENT SYSTEMS

Generic BMS Elements

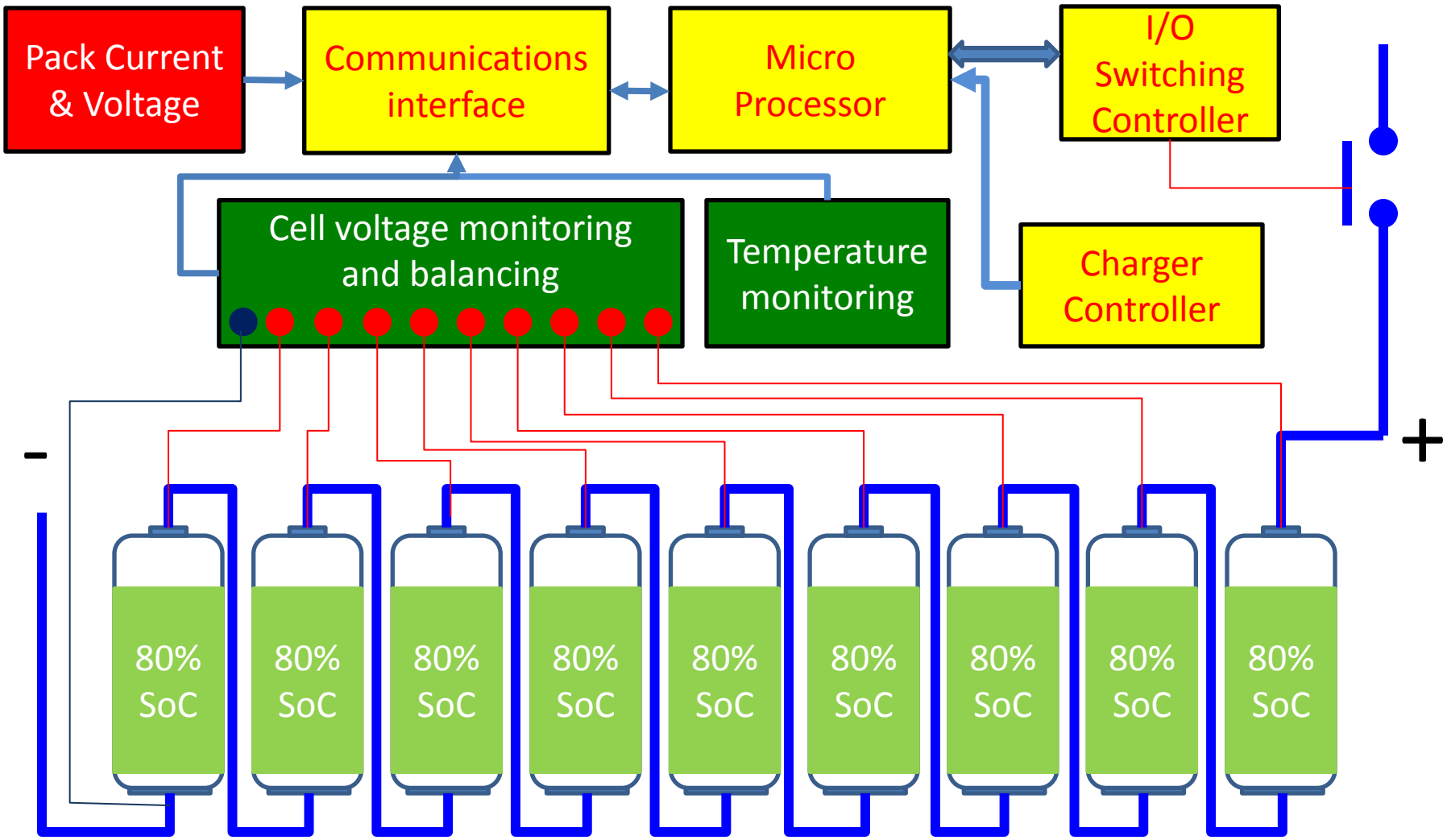

LiTHIUM BALANCE
BATTERY MANAGEMENT SYSTEMS

Communications (Comms.)

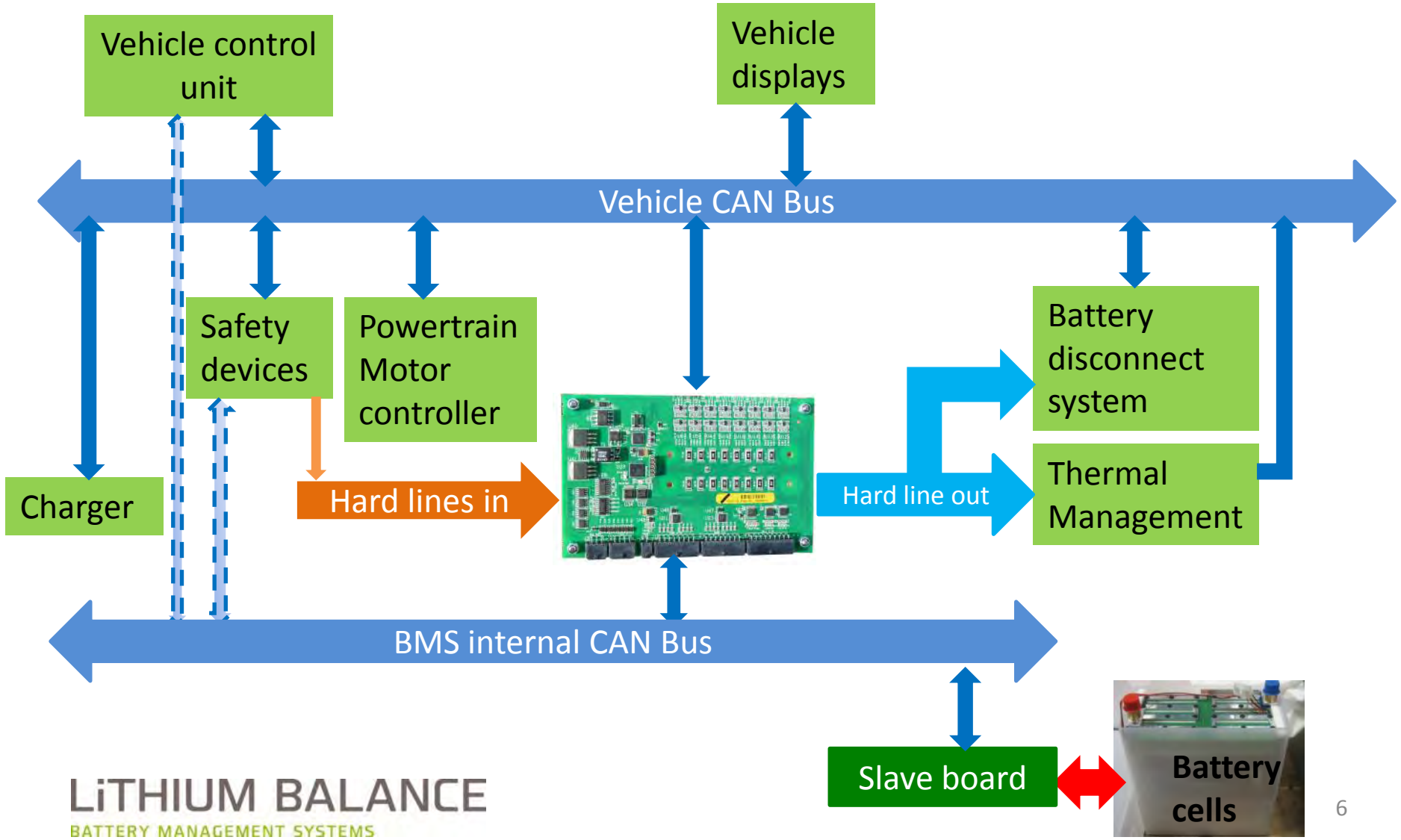

Architecture choices

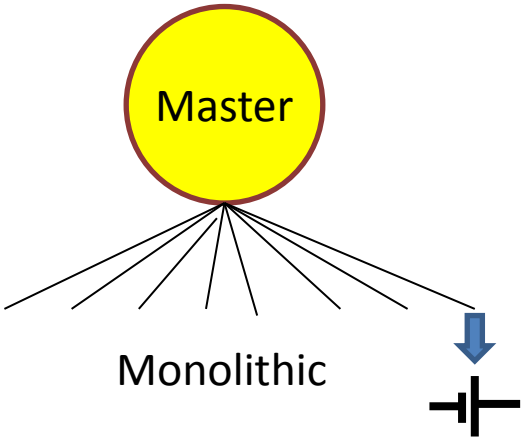

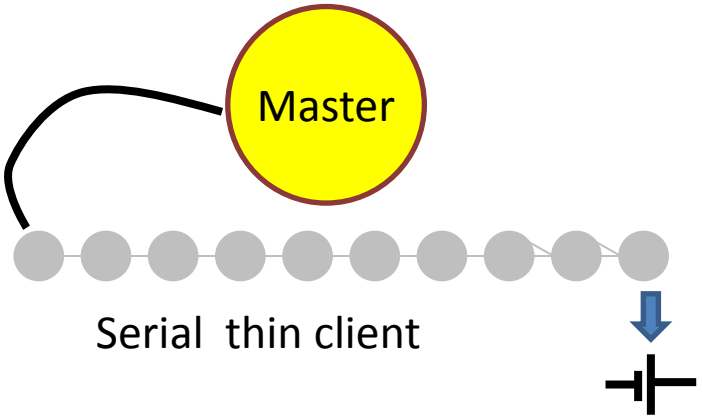

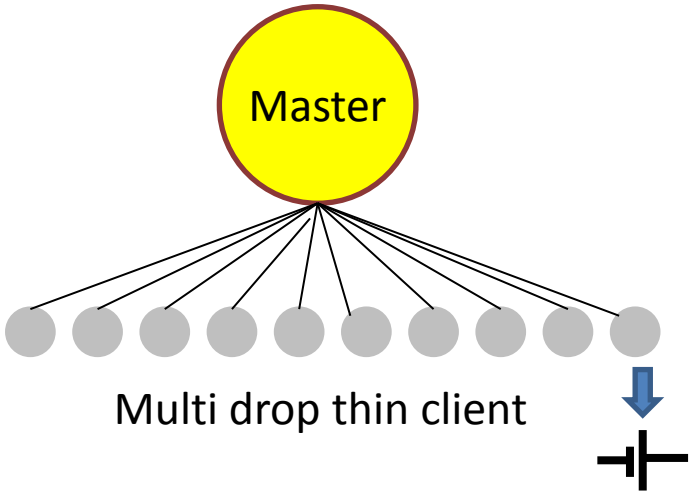

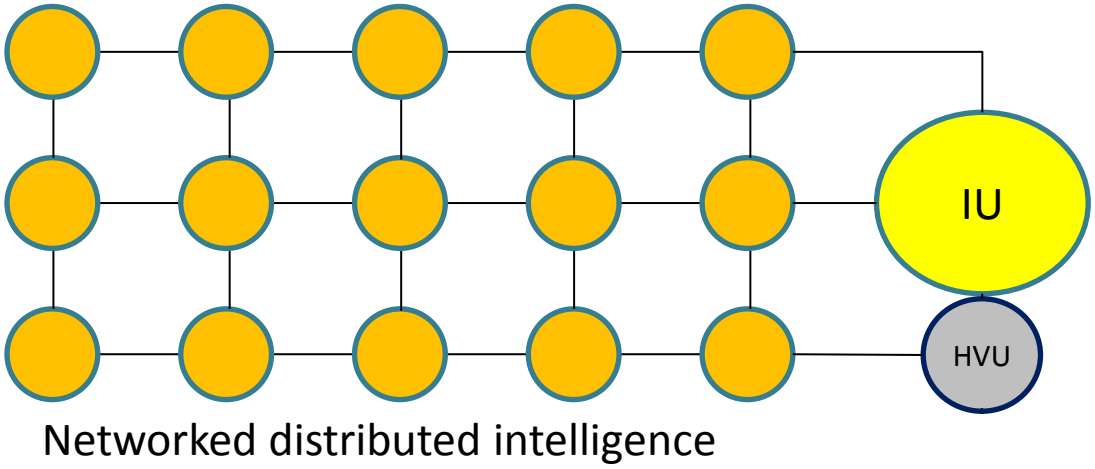

LiTHIUM BALANCE
BATTERY MANAGEMENT SYSTEMS

Introducing the *n*-BMS

- The networked BMS
- Scalable from 3 -1000v
- Manages up to 512 cells in series
- 3- principle elements
  - **IU** (Interface unit) – CAN interface to outside world contactor and charger control
  - **HVU** (High voltage unit) –pack level measurements of voltage and current
  - **CMU** (Cell monitoring unit) cell level measurements
- All communications over CAN

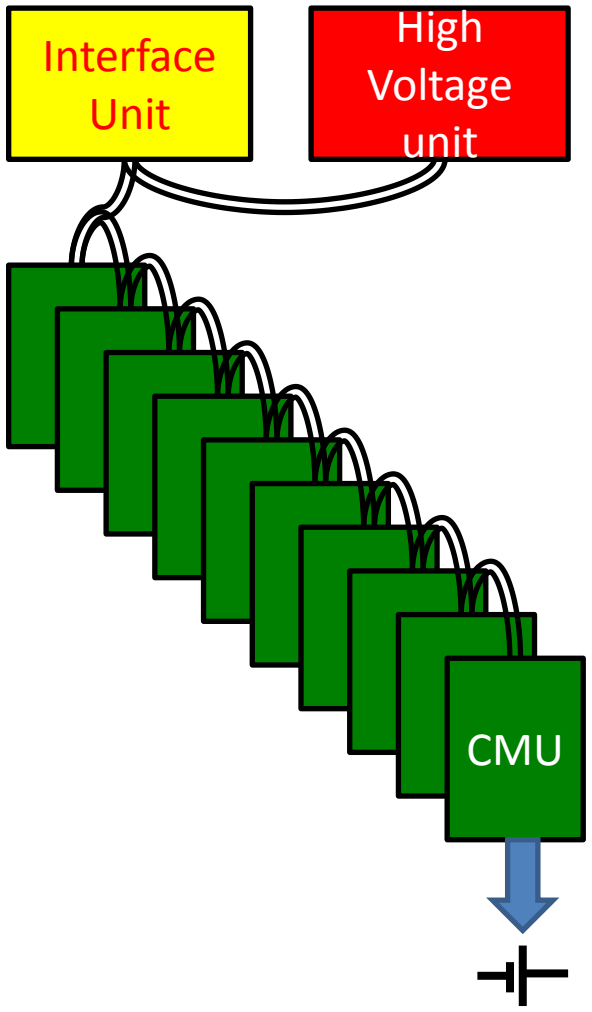

The n-BMS installed

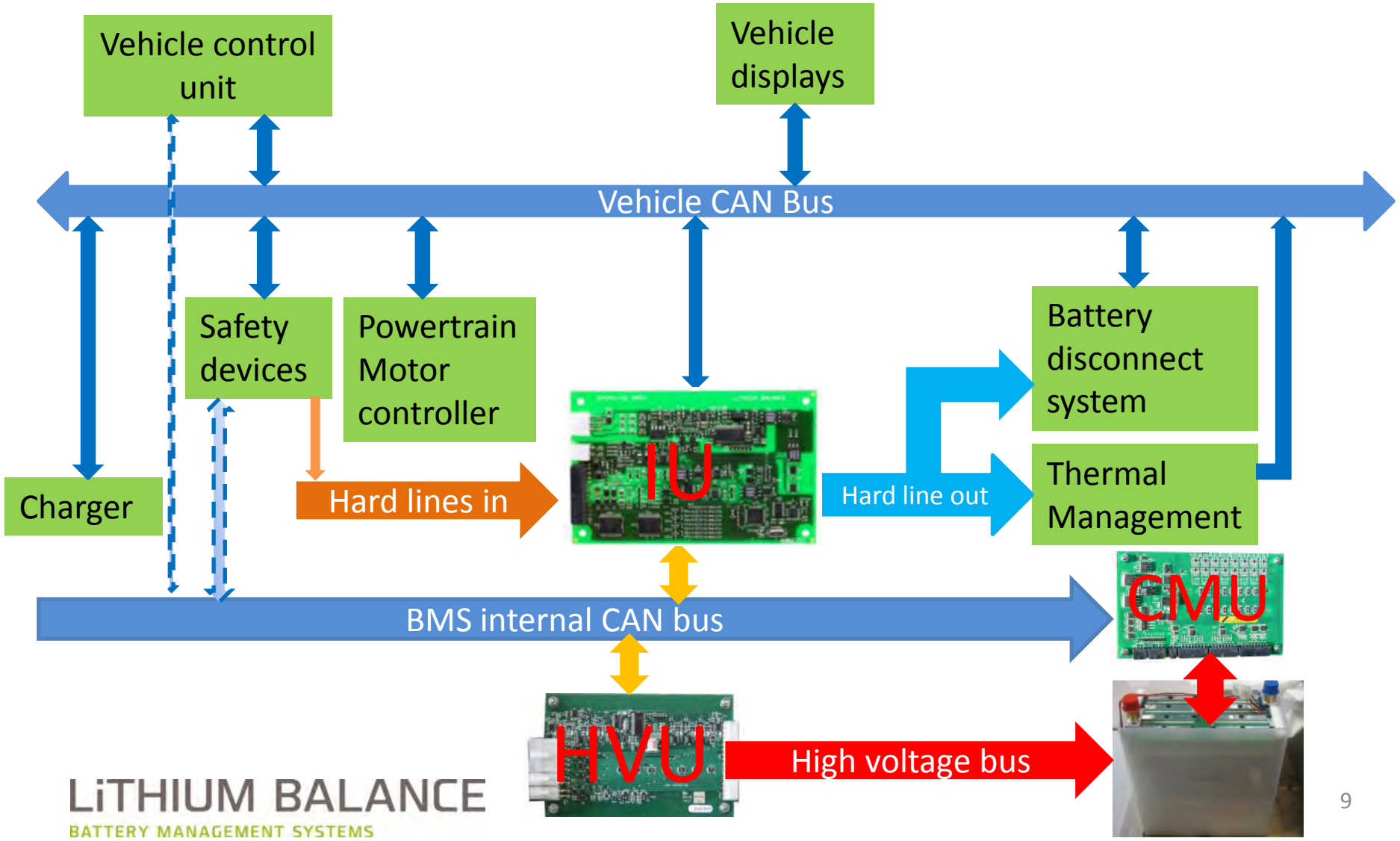

LiTHIUM BALANCE
BATTERY MANAGEMENT SYSTEMS

Distributed vs centralised intelligence

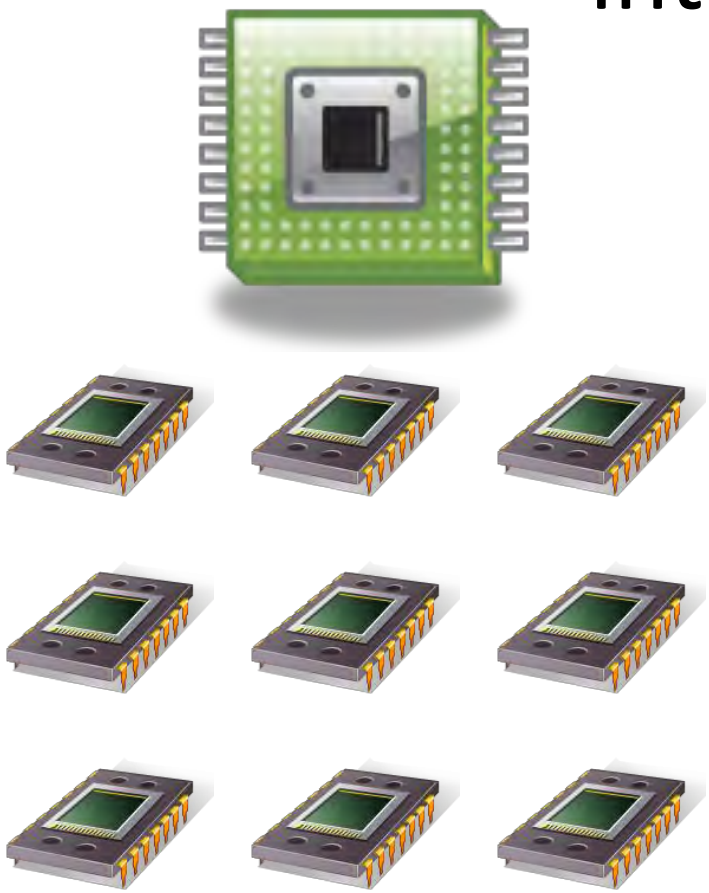

Multiple redundancy – just like the internet

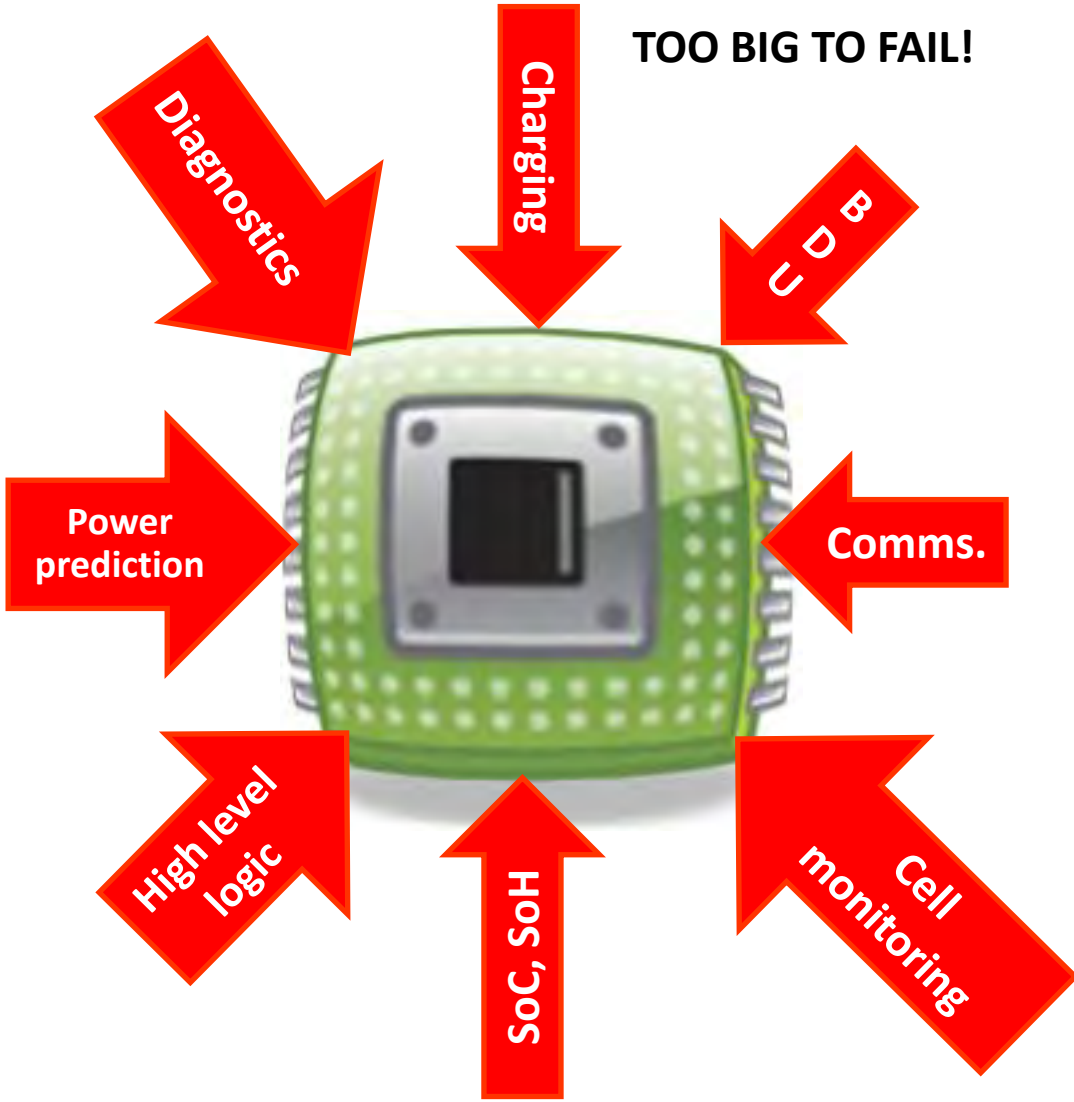

LiTHIUM BALANCE
BATTERY MANAGEMENT SYSTEMS

Taking it down to cell level

Simplify management by:

- Managing each cell individually
- Limiting pack performance according to the weakest cell
- Take individual cell SoH, temperature and cell voltage into account

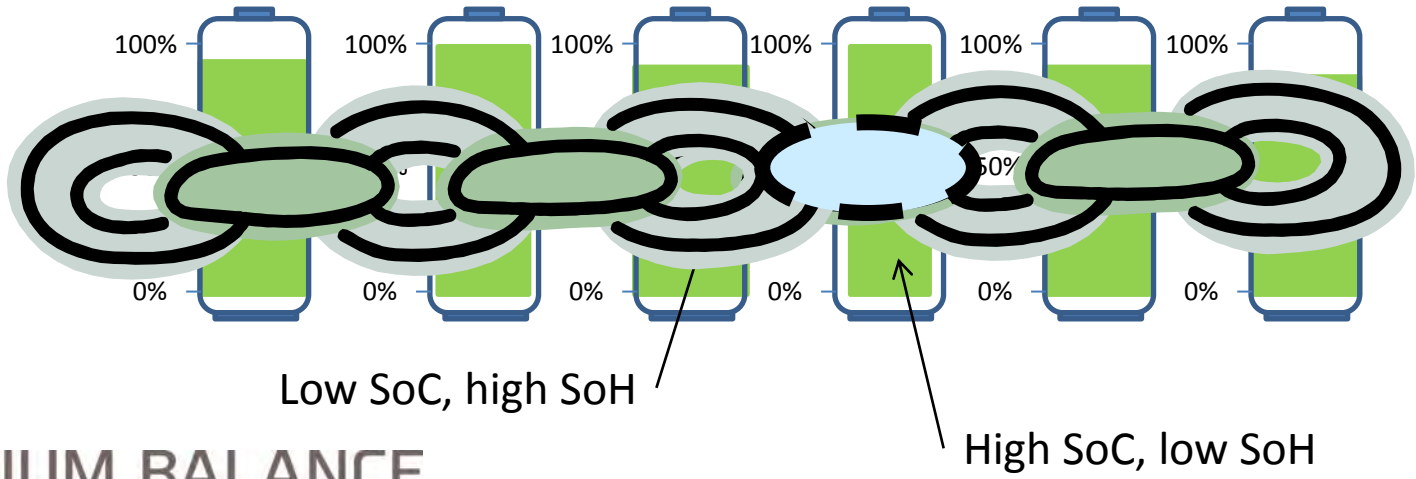

SoC calculation

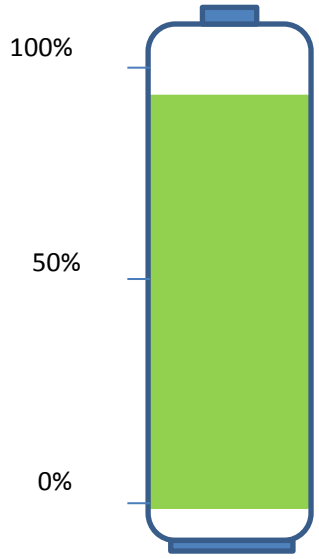

1. Integrate current
2. Adjust according to rate (Peukert effect)
3. Adjust according to cell temperature
4. Compensate for SoHc
5. SoC_{pack} is that of the weakest cell (may not start out being the lowest cell)
6. Use temperature corrected rest OCV to provide calibration points

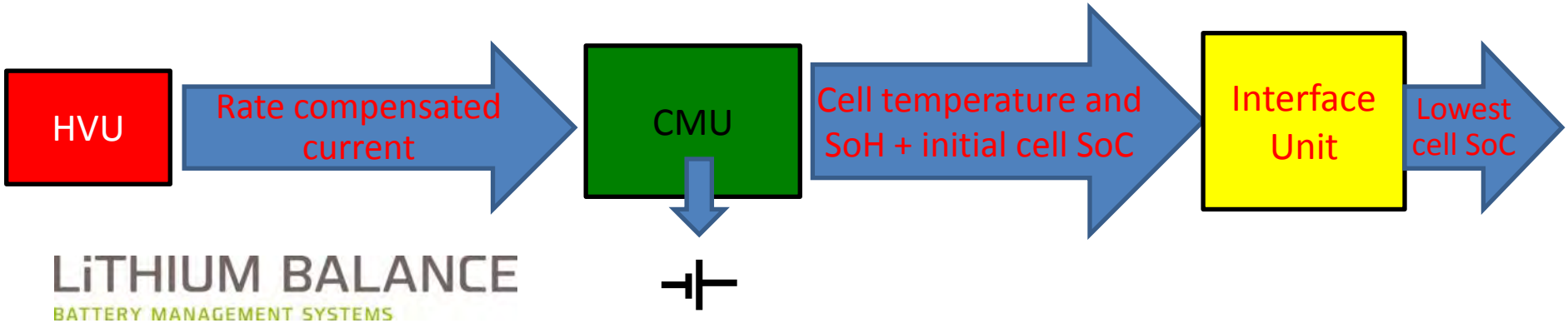

LiTHIUM BALANCE
BATTERY MANAGEMENT SYSTEMS

SoH calculation

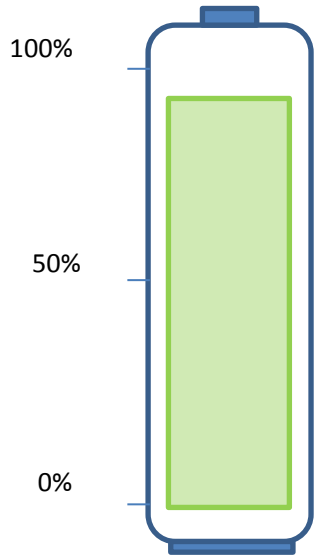

What is SoH (State of health)?

1. A measure of the loss in capacity from when the cell was new or the specified capacity
2. A measure of the loss of power performance from when the cell was new
3. A measure of how many operational cycles remain in the cell before is reaches its end of life

- *SoHc determined by comparing integrated current with change in OCV, corrected for temperature*
- *SoHp determined from cell DC resistance measured during the charging cycle*

The CMU

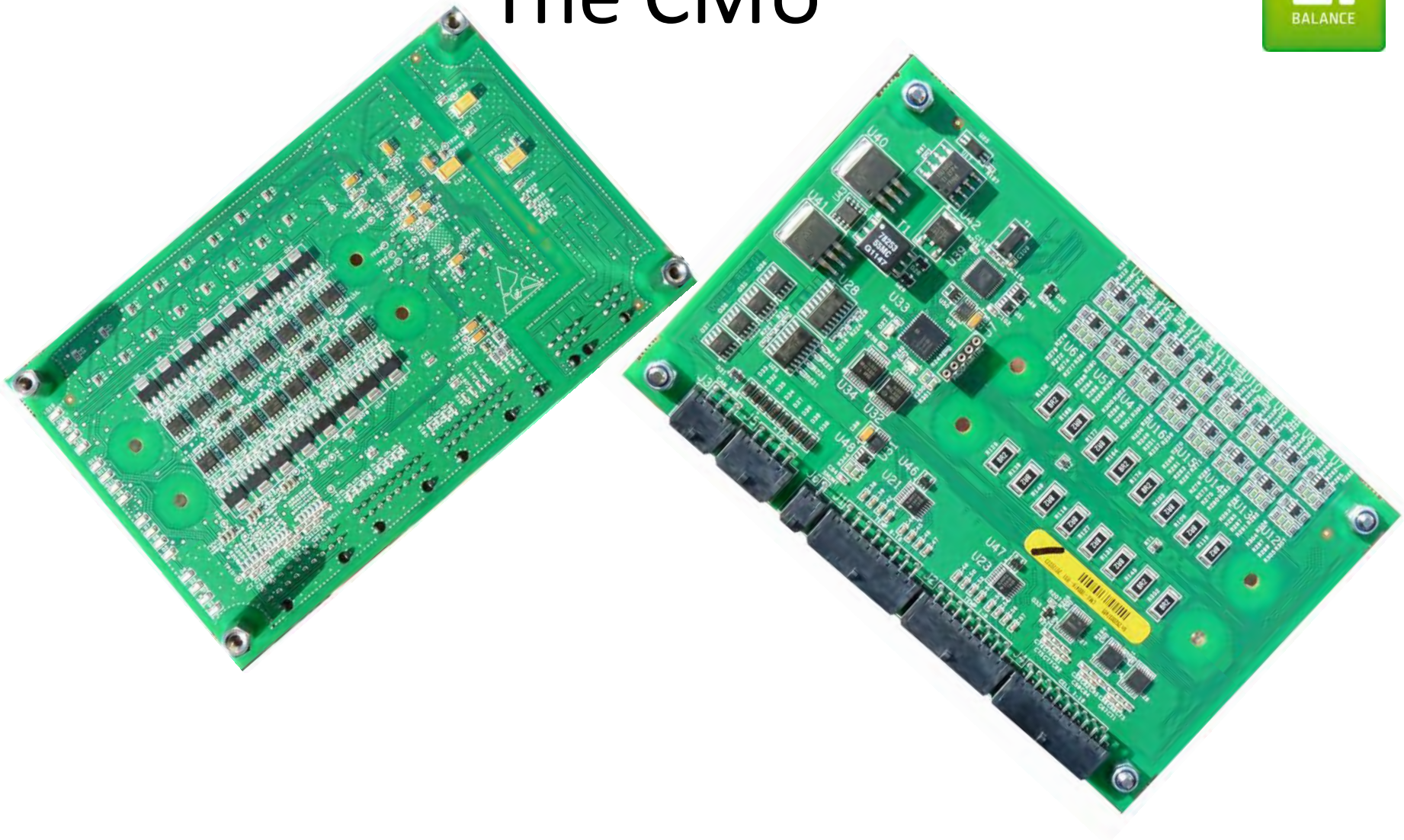

LiTHIUM BALANCE
BATTERY MANAGEMENT SYSTEMS

The **C**ell **M**onitoring **U**nits at a glance

- 16 cell monitoring unit made to automotive standards
- 0-4.6 volts measurement range
- CAN based communication
- High precision differential measurement engine with 1mV resolution
- High speed measurements reported at 20Hz
- 16 temperature measurement channels
- High impedance measurement circuit – doesn't unbalance cells
- Peer to peer monitoring of CMUs
- Automated board ID assignment
- High EMI / EMC resilience
- Fully redundant hardware overvoltage protection

Secondary hardware protection

- Overvoltage monitoring
- No processor intervention or delay
- Fast response (50ms debounce)
- Can be used with the BMS or with other safety systems
- Essential when working with volatile Li Ion chemistries

Balancing

- 500mA per cell, good heat dissipation
- Autonomous thermal management, precise cell voltages
- Continuous operation

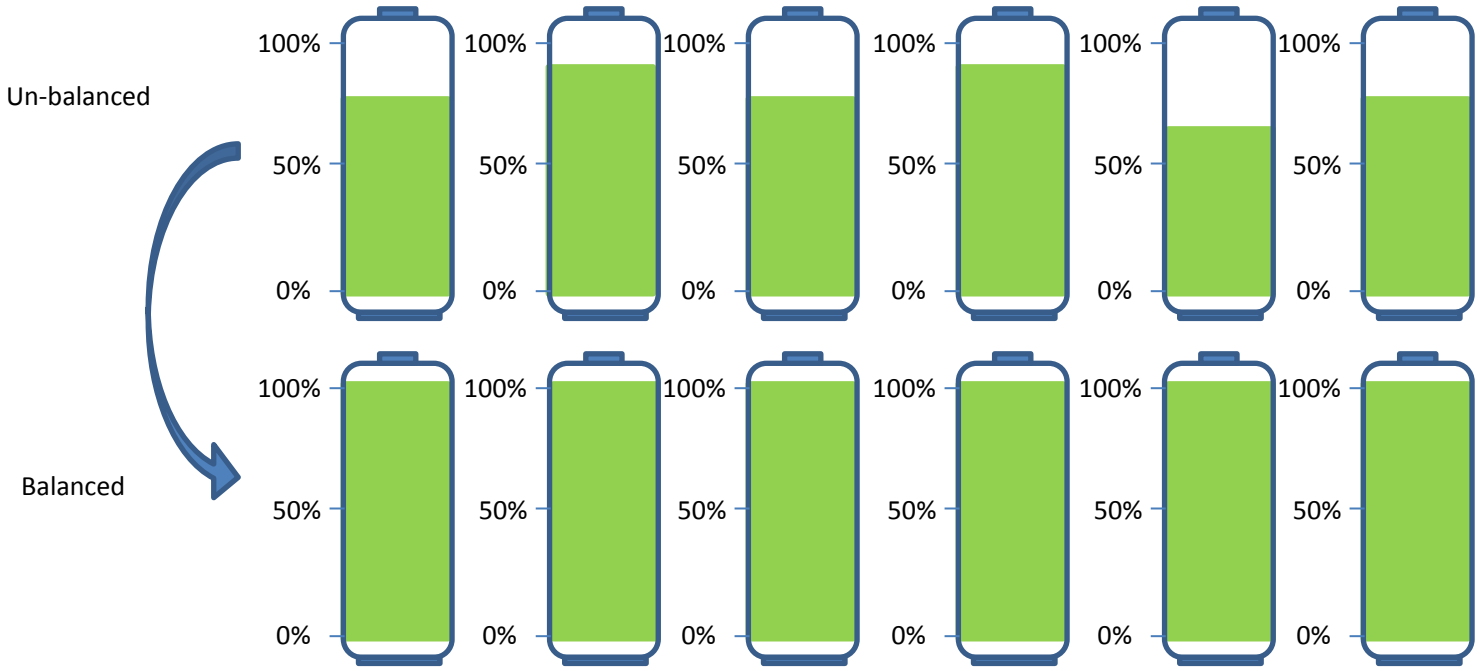

LiTHIUM BALANCE
BATTERY MANAGEMENT SYSTEMS

The **I**nterface **U**nit

- The interface to the rest of the vehicle such as the Vehicle control unit, charger, motor controller and thermal management system
- Controls contactors and handles any high level logic, includes contactor status monitoring
- Holds charging algorithms
- Diagnostic data

Isolated from the HV bus

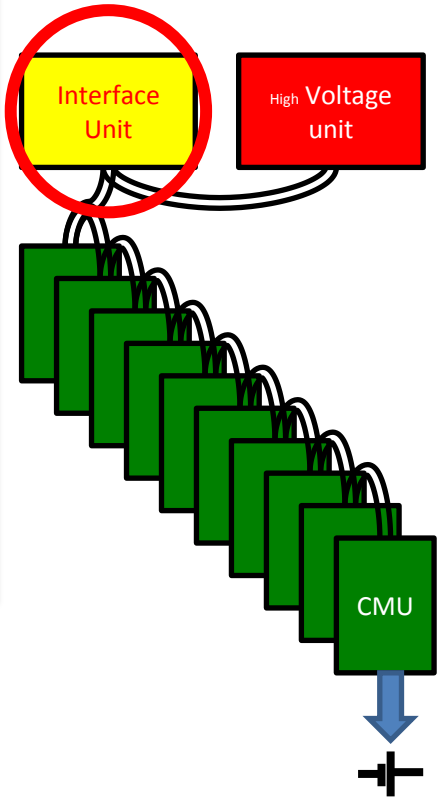

Easier to integrate

Modular architecture allows focus on:

- SAFETY
- Reliability (diagnostics)
- Warrantability (logging)
- Proprietary functionality
- Customer specific algorithms

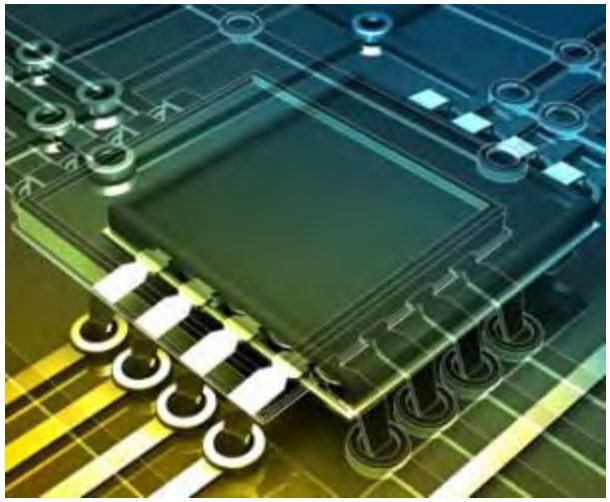

PROTECTION

Safety and reliability
(Secure your investment)

Protection against:
Overcharging
Deep discharge
Overloading
Short-circuit
High/low Temperature
Isolation monitoring

PERFORMANCE

Raise capacity, shorten charge time, lengthen life

Cell balancing
Discharge/regen. rate control (power prediction)
Optimised charge algorithms

MANAGEMENT

Application interface and diagnostics

Control outputs to switches or other systems
PC interface
Can-bus interface
History log

LiTHIUM BALANCE
BATTERY MANAGEMENT SYSTEMS

The **H**igh **V**oltage **U**nit

Performs the pack level measurements including:

- Current
- HV+ battery and load side
- Pack isolation
- Temperature of precharge resistor and shunt

Dedicated unit with safe architecture

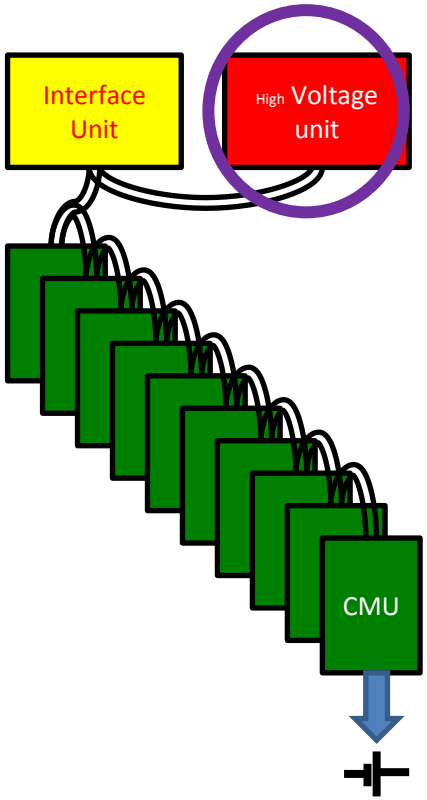

Investment where it counts...

In getting the price right!

- Careful selection of components
- Clever use of software
- EMS sourcing partners
- Mass produced
- Automotive grade but suitable for many other applications, leveraging volume across markets

If you can't afford it, it's not relevant

Summary

Why did we do it?

- Industry needs a well priced, high performance automotive grade BMS
- Enhance robustness and resilience by using a multi-node network architecture
- Improve performance through distributed parallel processing at source
- To open new possibilities for integration in automotive applications
- To explore new ways to better manage cells, improving reliability and reducing costs

Thank you for your attention

LiTHIUM BALANCE
BATTERY MANAGEMENT SYSTEMS

Appendix 9

Technical report

"Investigation test of CMU PCBA"

We help ideas meet the real world

DELTA Test Report

Investigation test of CMU PCBA

Performed for Lithium Balance A/S

Project no. T202080-1
Page 1 of 18

2012-04-04

DELTA
Venlighedsvej 4
2970 Hørsholm
Denmark

Tlf. +45 72 19 40 00
Fax +45 72 19 40 01
www.delta.dk
VAT No. 12275110

Title	Investigation test of CMU PCBA
Test object	CMU PCBA
Report no.	T202080-1
Project no.	T202080
Test period	28 Mar. 2012 to 30 Mar. 2012
Client	Lithium Balance A/S Baldershøj 26C, 1. Sal 2635 Ishøj Denmark Tel.: +45 58 51 51 04
Contact person	Mr. Karl Vestin E-mail: k.vestin@lithiumbalance.com
Manufacturer	Lithium Balance A/S
Specifications	Selected parts from several automotive EMC test standards
Results	The test object did not fulfil part(s) of the requirements, please refer to Section 1
Test personnel	Ms. Roa Salman Mr. Per Thåstrup Jensen
Test site(s)	DELTA, Venlighedsvej 4, 2970 Hørsholm

Date 2012-04-04

Project Manager **Investigatory test – report not signed**

Per Thåstrup Jensen
DELTA

Responsible **Investigatory test – report not signed**

Per Thåstrup Jensen
DELTA

Table of contents

1. Summary of tests

Tests	Test methods	Results
Immunity to fast transients	-	Failed
Immunity to UWB transients	-	Failed
Immunity to radio frequency electromagnetic fields	-	Failed
Immunity to LF magnetic field	-	Failed

The given result is based on a shared risk principle with respect to the measurement uncertainty.

Conclusion

The test object was subjected to an investigatory EMC test.

The test object did not meet the requirements.

The test object responded to fast transients, UWB pulses, radiated magnetic fields and RF electromagnetic fields. The test object responded by indicating cell overvoltage, indicating faulty (offset) cell voltages, and failing in CAN bus communication. In some cases the test object appeared to restart after CPU failure (HW watchdog activation). However, this was not investigated in detail.

The test results relate only to the object(s) tested.

2. Test object(s) and auxiliary equipment

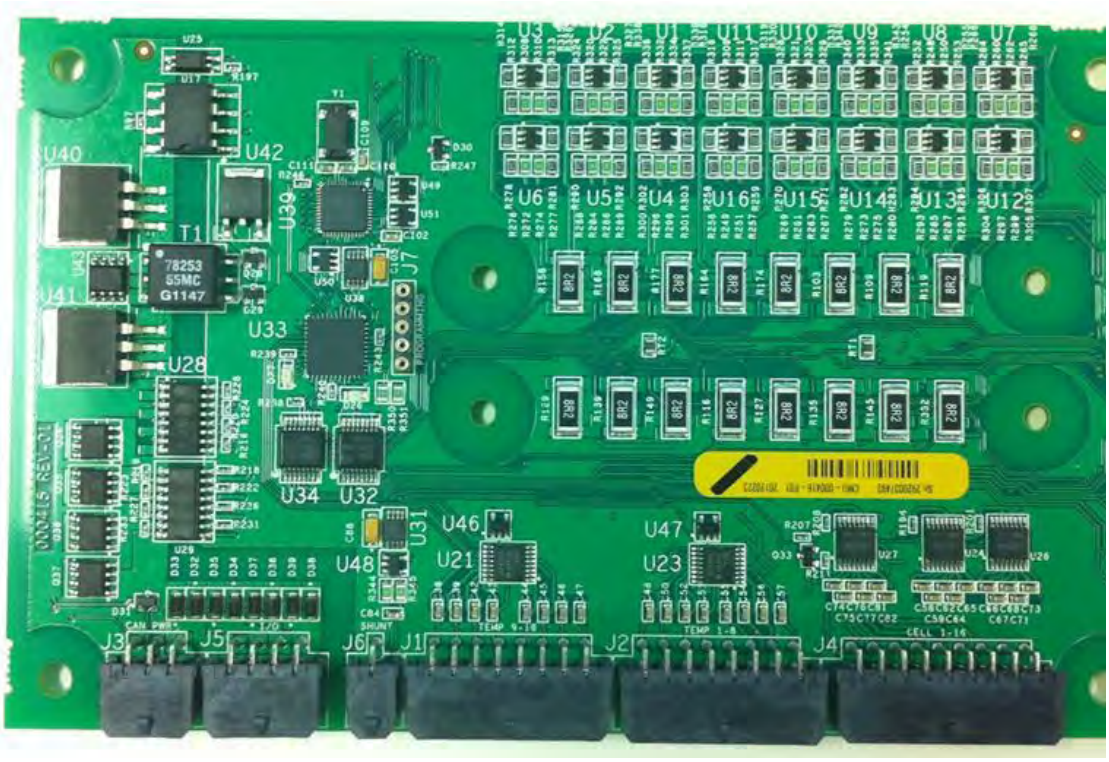

Photo 2.1.1 Test object PCB (heat sink above 8R2 Ohm resistors not fitted)

2.1 Test object(s)

Test object 2.1.1

Name of test object	CMU
Model / type	Prototype Rev. A
Part no.	00416
Serial no.	
FCC ID	
Manufacturer	Litium Balance
Supply voltage	12VDC
Software version	Prototype CMU.CAN_EXT_125
Hardware version	
Cycle time	50mSec
Highest frequency generated or used	8MHz
Comment	
Received	Date: 2012-03-28 Status:

2.2 Auxiliary equipment

Auxiliary equipment 2.2.1

Name of auxiliary equipment	16 pcs. Lithium cells and a test PCB containing associated LED lamps/switches
Model / type	-
Part no.	-
Serial no.	-
FCC ID	-
Manufacturer	Lithium Balance A/S
Supply voltage	-
Highest frequency generated or used	-
Comment	-

3. General test conditions

3.1 Test setup during test

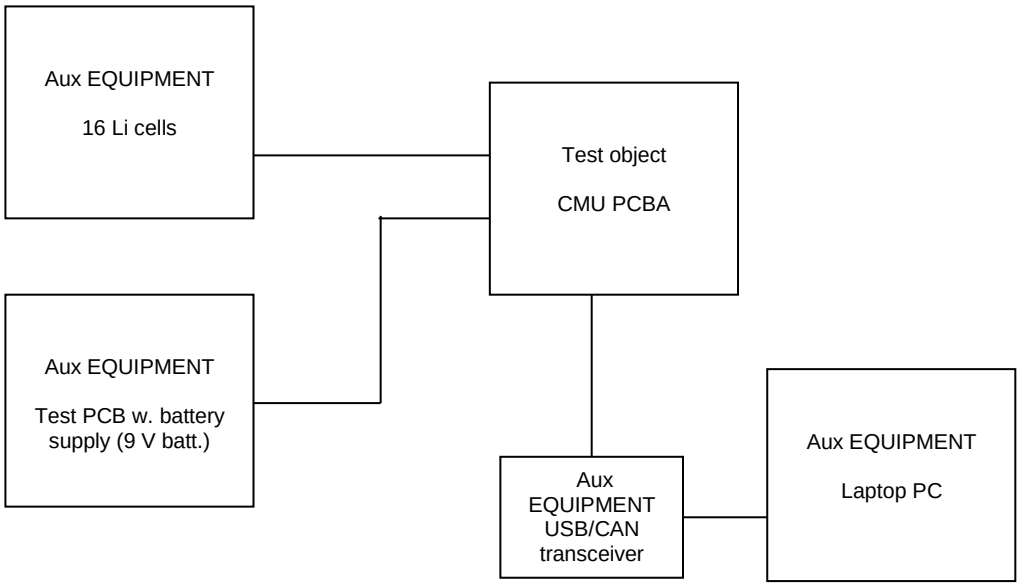

Figure 3.1.1 Block diagram of test object(s) with cables and auxiliary equipment.

3.1.1 Description and intended use of test object

The test object monitors the cell voltage on each of the 16 cells. During charging, the test object adds additional bleed resistor load to selected cells, if the cell voltage does not match the remaining cells, in order to balance the charging.

During the immunity test, the cells are not charged. The cell voltages are read via the CAN bus interface, and it is checked that no overvoltage- or other failure indications are activated.

3.1.2 Test modes during immunity tests

Voltage monitoring mode.

3.1.3 Test modes during emission tests

N/A

3.1.4 Nominal power consumption

N/A

3.2 Criteria for compliance during immunity test

Performance criteria according to corresponding standard were applied during immunity tests as follows:

General

The test object shall not become dangerous or unsafe as a result of the application of the tests.

Performance criterion A

The test object shall continue to operate as intended during the test.

The cell voltages on the 16 cells must remain stable at their initial voltage within max. +/- 1 mV.

No CAN bus transmission errors are allowed.

The red OVERVOLTAGE LED must remain OFF.

Performance criterion B

N/A.

Performance criterion C

N/A

3.3 Modifications of the test object

No	Modification
N/A	N/A

3.4 Test sequence

The tests described in this test report were performed in the following sequence:

1. Immunity to fast transients
2. Immunity to UWB pulses
3. Immunity to radio frequency electromagnetic field
4. Immunity to LF magnetic field

4. Test results

4.1 Immunity to fast transients (burst)

Test object	CMU	Sheet	Burst-1
Type	Prototype Rev. A	Project no.	T202080
Serial no.	N/A	Date	28 Mar 2012
Client	Lithium Balance A/S	Initials	PTJ
Specification	Selected parts from several automotive EMC test standards	Required Perf. criter.	A

Test method	EN/(IEC) 61000-4-4:2004+A1	Temperature	N/A °C
Characteristics	5 / 50 ns transients in 5 kHz bursts of 15 / 300 ms	Humidity	N/A % RH
Test equipm.	Midilab Hørsholm 29913	Uncertainty	N/A

Manufacturer's name of port	Test standard's name of port	Coupling	Amplitude [kV]	Passed	Remarks
+12VDC	DC power	L-GP	+/- 0.5	Yes	
+12 VDC	DC power	All leads-GP	+ 0.5	No	Note 1
+12 VDC	DC power	All leads-GP	- 0.5	Yes	Ok
+12 VDC	DC power	All leads-GP	- 1	Yes	Ok
+12 VDC	DC power	All leads-GP	+ 1	No	Note 1
Battery cable bundle	DC power	Cap.clamp-GP	+/- 0.5	Yes	
Battery cable bundle	DC power	Cap.clamp-GP	- 1	No	Note 1
Battery cable bundle	DC power	Cap.clamp-GP	+ 1	Yes	
Bundle, all other cables	Cable	Cap.clamp-GP	+ 0.5	Yes	
Bundle, all other cables	Cable	Cap.clamp-GP	- 0.5	No	Note 1
Bundle, all other cables	Cable	Cap.clamp-GP	- 1	No	Note 1
Bundle, all other cables	Cable	Cap.clamp-GP	+ 1	Yes	

Note 1: Red LED "Overvoltage" flashes during injection of each burst. Otherwise OK

Criteria for compliance See section 3.2

Test result The fast transients caused malfunctions

Compliant No

Test time 1 min/polarity

Comments	The transients caused the red overvoltage LED to flash during each transient event. The red LED is driven by the hardwired OVERVOLTAGE detectors U24, U26, U27.

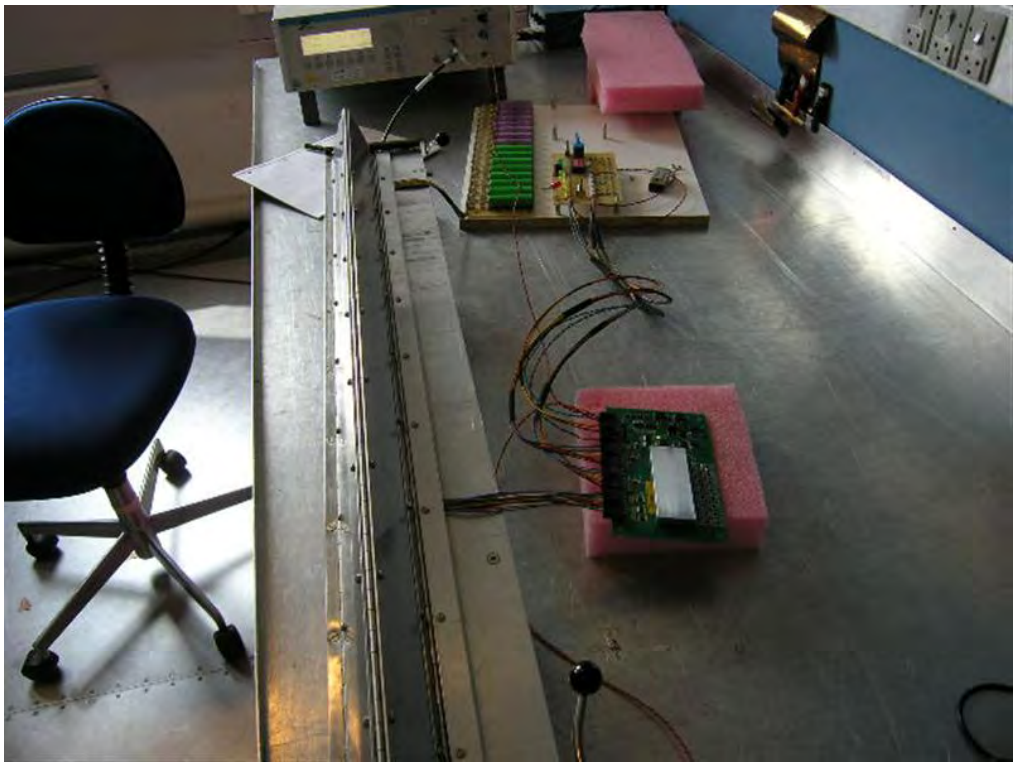

Photo 4.1.1 Test setup regarding immunity to fast transients on battery cable bundle.

4.2 Immunity to UWB transients

Test object	CMU	Sheet	blank-1
Type	Prototype Rev. A	Project no.	T202080
Serial no.	N/A	Date	28 Mar 2012
Client	Lithium Balance A/S	Initials	PTJ
Specification	Selected parts from several automotive EMC test standards	Required Perf. criter.	A

Test method Characteristics	EMC HALT 100 ps rise time pulses of amplitudes up to 20 kV injected via WBFC (WorkBench Faraday Cage, field injection)	Temperature Humidity	N/A °C N/A % RH
Test equipm.	Midilab Hørsholm EMC HALT generator and WBFC	Uncertainty	N/A

Test point	Test standard's name of port	Coupling	Amplitude [kV]	Passed	Remarks
Heatsink facing stripline in WBFC	WBFC	N/A	+ 20	No	Note 1
Heatsink facing away from stripline and placed near bottom of WBFC	WBFC	N/A	+/- 20	Yes	Ok
Heatsink facing stripline in WBFC, placed near WBFC bottom	WBFC	N/A	- 20	No	Note 2
Heatsink facing stripline in WBFC, placed near WBFC bottom	WBFC	N/A	+ 20	No	Note 3

Note 1: CAN bus interface fails, and must be restarteded (USB CAN device disconnected and connected again at PC). After the test, the CAN bus cable was extended so the USB device was placed >5 m from the WBFC.
Note 2: Red LED flashes and >100 mV measurement errors on cell voltages.
Note 3: CAN bus interface fails, and must be restarteded (USB CAN device disconnected and connected again at PC).

Criteria for compliance: See section 3.2

Compliant: The UWB pulses caused malfunction

Comments: The transients caused the red overvoltage LED to flash during each transient event. The red LED is driven by the hardwired OVERVOLTAGE detectors U24, U26, U27.

The UWB pulses caused the voltage measurement to fail. Voltage changes of up to 100 mV were observed during

some injections and amplitudes.

The UWB pulses furthermore caused the CAN bus communication to fail. From the observed response, it appeared as if the CMU processor stopped, and was restarted by the hardware watchdog circuit.

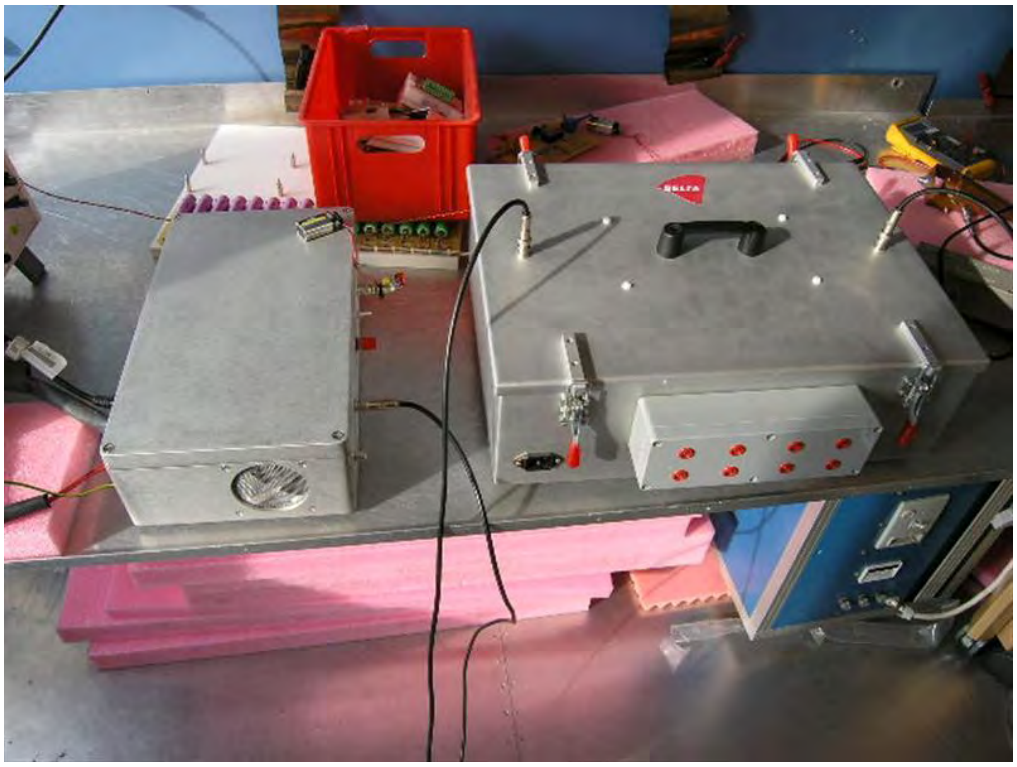

Photo 4.2.1 Test setup regarding UWB pulse injection into PCB using a WBFC (right) and a 100 ps rise time pulse generator (left).

4.3 Immunity to radio frequency electromagnetic field

Test object	CMU	Sheet	RF Field-1
Type	Prototype Rev. A	Project no.	T202080T202080
Serial no.	N/A	Date	30 Mar. 2012
Client	Lithium Balance A/S	Initials	RAS
Specification	EMC screening test for immunity to RF electromagnetic fields from an antenna placed 0.5 m from the test object.	Required Perf. criter.	A

Test method Characteristics	EN/(IEC) 61000-4-3:2006+A1+A2 16 point pre-Calibration	Temperature Humidity	N/A °C N/A % RH
Test equipm.	Test selv Room B	Uncertainty	N/A

Frequency range	Modulation	Field direction	Amplitude [V/m]	Passed	Remarks
80-1000 MHz	80 % AM 1 kHz	Horizontal	>10	Yes	Note 1,Note 2
80-1000 MHz	80 % AM 1 kHz	Vertical	>10	Yes	Note 1,Note 2
80-1000 MHz	80 % AM 1 kHz	Vertical	>10	Yes	Note 1,Note 3
80-1000 MHz	80 % AM 1 kHz	Horizontal	>10	No	Note 1,Note 3,Note 4

Note 1: EUT placed 0.5m from antenna, field strength unknown.>10V/m 80-100MHz, >22V/m 100-1000MHz
Note 2: EUT PCB facing antenna, cables in dipole position.
Note 3: EUT Side of PCB facing antenna
Note 4: 300mV offset on voltage measurement, measured at 700MHz

Criteria for compliance: See section 3.2

Test result: The radio frequency electromagnetic field caused malfunctions.

Compliant: No

Setup comments: Frequency step: 1 %, dwell time: 1 second

Comments: The measurement of the cell voltages was very much affected by the electromagnetic field. The measured offset was up to 300 mV. The measured voltages returned to normal values, when the RF field was switched off.

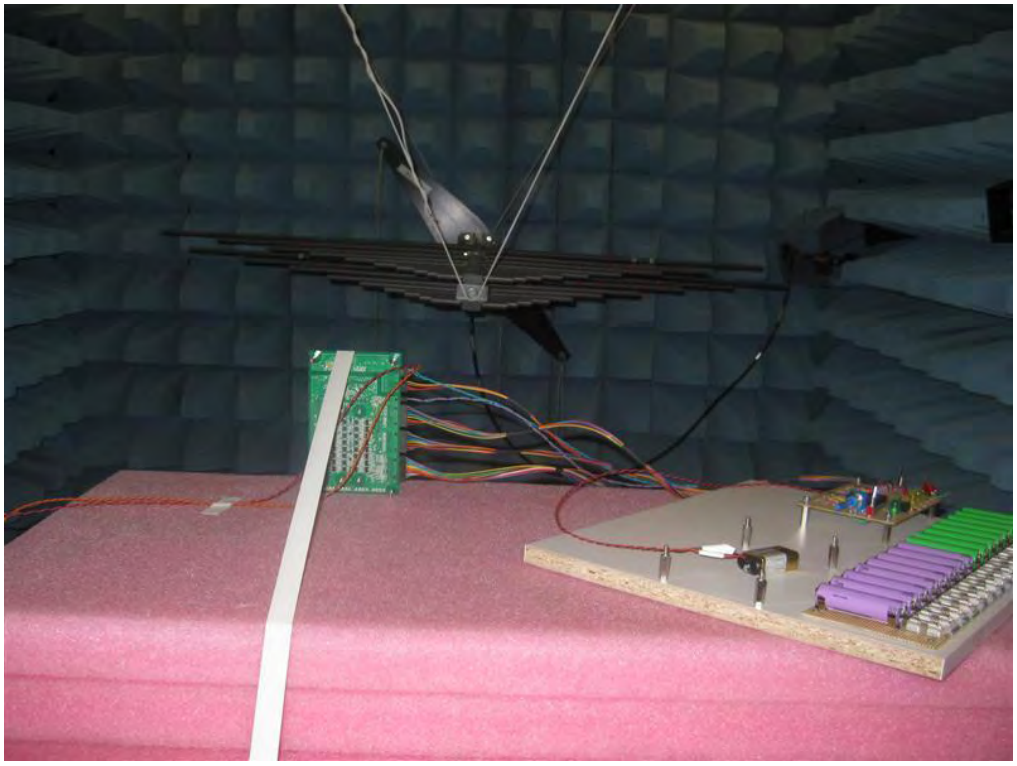

Photo 4.3.1 Test setup regarding immunity to radio frequency electromagnetic field.

4.4 Immunity to LF magnetic field

Test object	CMU	Sheet	blank-2
Type	Prototype Rev. A	Project no.	T202080
Serial no.	N/A	Date	28 Mar 2012
Client	Lithium Balance A/S	Initials	PTJ
Specification	Selected parts from several automotive EMC test standards	Required Perf. criter.	A

Test method Characteristics	MIL-STD 461E, test RS 101 Reduced frequency range	Temperature Humidity	N/A °C N/A % RH
Test equipm.	Midilab Hørsholm 29705, 29707, 49666, 49669, 29703, 49552	Uncertainty	N/A

Test point	Coupling	Coil current [A_{rms}]	Amplitude [A/m]	Passed	Remarks
CMU surface, 320 Hz	29705 coil	10	800	No	Note 1 3-4 mV
CMU surface, 500 Hz	29705 coil	10	800	No	Note 1 1 mV
CMU surface, 640 Hz	29705 coil	10	800	No	Note 1 2-3 mV
CMU surface, 1 kHz	29705 coil	10	800	No	Note 1 4-6 mV
CMU surface, 2 kHz	29705 coil	10	800	No	Note 1 2 mV
CMU surface, 3 kHz	29705 coil	10	800	No	Note 1 1-2 mV
CMU surface, 4 kHz	29705 coil	10	800	No	Note 1 1-2 mV
CMU surface, 5 kHz	29705 coil	10	800	No	Note 1 6-7 mV
CMU surface, 6 kHz	29705 coil	8	600	No	Note 1 1-2 mV
CMU surface, 7 kHz	29705 coil	8	600	No	Note 1 1-2 mV
CMU surface, 8 kHz	29705 coil	7	530	Yes	Ok
CMU surface, 9 kHz	29705 coil	6	450	Yes	Ok
CMU surface, 10 kHz	29705 coil	5	380	Yes	Ok

Note 1: The deviation in the observed cell voltages is noted for each frequency, and is in the range below 10 mV. The voltage deviations are slightly different when the radiating coil is placed near different parts of the CMU

Criteria for compliance See section 3.2

Compliant No

Comments

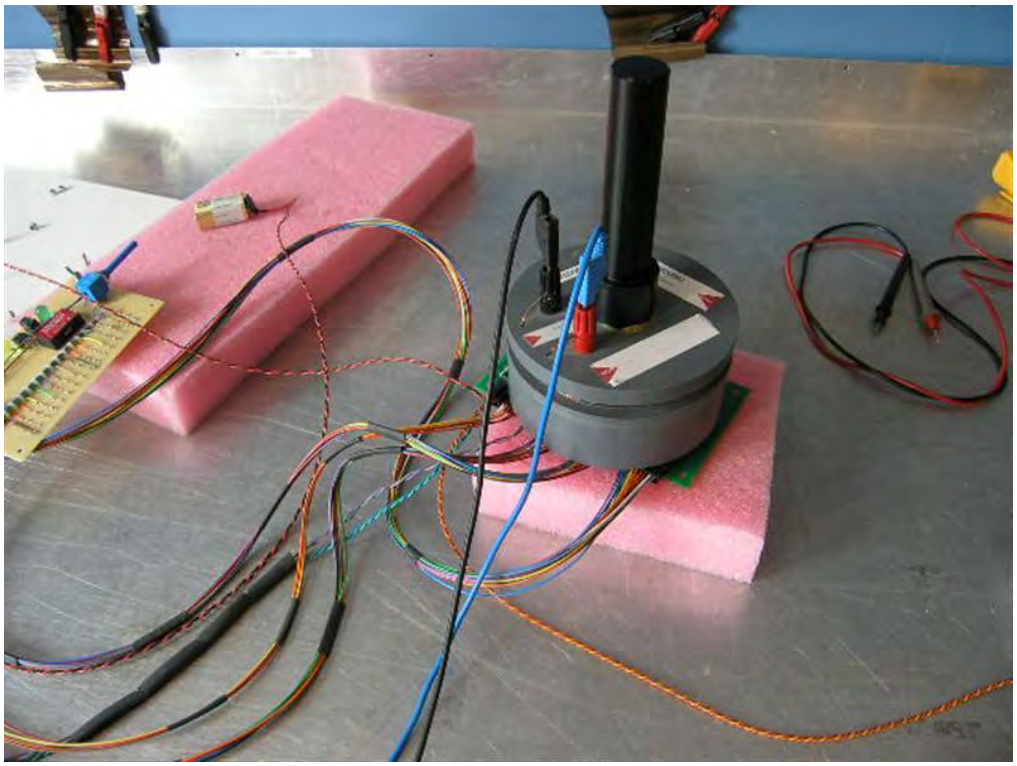

Photo 4.4.1 Test setup regarding immunity to radiated LF magnetic field. Radiating coil placed on CMU PCBA.